

Visualizing chemical transport from extracellular symbionts into squid host tissues using NanoSIMS

THÈSE N° 7909 (2017)

PRÉSENTÉE LE 20 JUILLET 2017

À LA FACULTÉ DE L'ENVIRONNEMENT NATUREL, ARCHITECTURAL ET CONSTRUIT

LABORATOIRE DE GÉOCHIMIE BIOLOGIQUE

PROGRAMME DOCTORAL EN GÉNIE CIVIL ET ENVIRONNEMENT

ÉCOLE POLYTECHNIQUE FÉDÉRALE DE LAUSANNE

POUR L'OBTENTION DU GRADE DE DOCTEUR ÈS SCIENCES

PAR

Stéphanie Kéren COHEN

acceptée sur proposition du jury:

Prof. R. Bernier-Latmani, présidente du jury
Prof. A. Meibom, Prof. M. J. McFall-Ngai, directeurs de thèse
Prof. Ph. Engel, rapporteur
Prof. S. Nyholm, rapporteur
Prof. M. Blokesch, rapporteuse



ÉCOLE POLYTECHNIQUE
FÉDÉRALE DE LAUSANNE

Suisse
2017

"I almost wish I hadn't gone down that rabbit-hole — and yet — and yet — it's rather curious, you know, this sort of life!"

-Alice in Wonderland

Acknowledgements

My PhD studies has been a period of intense learning for me, not only in the scientific field, but also on a personal level. I would like to thank the people who have supported and helped me throughout this period.

My deep gratitude goes first to my director, **Prof. Anders Meibom**, who provided me with the fantastic opportunity to do a PhD with him at EPFL. I would like to thank him for his continuous support and invaluable guidance throughout my PhD studies. His unwavering enthusiasm for research and original thinking always encouraged me to pursue my research. During my studies, he always engaged me in new ideas and kept motivating me even when things where not looking bright. I would like also to express my true gratitude for his patience in editing this thesis manuscript, I know it was not always easy.

My deep appreciation also extends to my co-director **Prof. Margaret McFall-Ngai**. I feel extremely fortunate to have work with Margaret and I would like to thank her for giving me the opportunity to work on this exciting and interesting system of the squid-vibrio symbiosis. I also thank both **Margaret and Prof. Ned Ruby** for sharing with me their immense knowledge and for the stimulating discussions we had along the years. Their drive and passion for this system specifically, and for science in general, have always inspired me.

I greatly appreciated the work done by **Prof. William E. Goldman** for providing us with the purified TCT molecules. I also would like to thank **Dr. Mahdi Belcaid** for providing us with the NLS sequences analysis.

I owe a depth of gratitude to **Marie-Steph** and **Jon L**, two post-doc colleagues from Ned lab. A big part described in this thesis was accomplished with the help and support of both. I would like to thank them for stimulating brain storming on the findings from this work and future directions. I also thank them for answering my numerous questions and for all the help in the experiments. I gained a lot from their scientific background. Without their support my research would have been undoubtedly impossible.

I am also deeply grateful to **my lab at EPFL**. My sincere gratitude goes to **Thomas**, for his intellectual insights and many fruitful discussions. More importantly, for his immense support during the writing of this thesis. I also wish to express my genuine thanks to **Emma** for her true friendship and enjoyable moments we spent together in the lab and the Suisse mountains. Her support and help, specifically through my mid-term thesis-writing crisis, was most appreciated. I would have gotten lost without her. Writing this dissertation would not have been possible without the support of Emma and Thomas. I would like to also thank **Louise** for her valued friendship and wise advices. **Charlotte** for her

positive energy and for always being up for beer at Sat. **Mustafa** for his support and friendship and for being the person he is! **Julia** for her tremendous help and support in sample preparation and analysis as well as IT issues. **Stephane and Florent** for their technical assistance in the NanoSIMS and Stephane for help in NanoSIMS imaging after my long nights spend at the lab. **Carole W**, for her administrative support and for being there for us. And for all the past and present LGB members, I thank all the lab for their unfailing assistance and for making my PhD life much more fun!

In addition, I thanks the present and former colleagues from **the lab of Margaret and Ned** who I had the pleasure to work with: **Sabrina, Sara, Tara, Silvia, Eric, Clotilde, Julia, Natacha, and Elizabeth**. I would like to express a special thanks to **Sabrina** for her great help with some of my experiments. **Sara** for her help in getting me settled when I first came to work at the lab in Hawaii. They all provided a friendly and cooperative atmosphere at the lab as well as insightful comments on my research.

I would like to thanks **Solenne M** for her great help with growing different bacteria strains for NanoSIMS analysis, when I could not.

I would like to thanks the **EMF team** at UNIL for interesting conversations and the nice company they provided me during the many months I spent sectioning and imaging my samples in their lab. In particular, I am grateful to **Jean** and **Céline** who patiently answered my endless questions and were always willing to help.

I thank the head of the CIME facility, **Graham Knott** and specifically **Mary C** for their important work in serial sectioning the squid and preparation of some squid samples for NanoSIMS to ease my workload, when I needed.

On a personal level, I am particularly grateful to my very good friends **Irit and Roy** and their wonderful kids who were my Israeli family here in Switzerland. For their amazing friendship, their wise advices and sympathetic ear. They gave me perspective on how to see things in life in general, and in my own research in particular. I thank them for all the tasty dinners, the evening at the balcony, and the many sleepovers. They were always there for me and without their support my PhD studies would not have been completed.

I would like to thank my closest friend **Melany**. Thank you for the continued faith in me and encouragement during my PhD studies. For all the joy, laughters and precious moments we shared these past few years and the ones we will continue to share in the years to come.

I would like to thank my dear friend **Agathe** for all the valued and fun times we shared together from the beginning of my PhD, at work and outside of work. I thank her for the good friendship through all those years and for her visits.

I am grateful to **Carole B** for her wonderful personality and good friendship and her vision of life that made me appreciate her greatly. Many thanks also for all the fabulous hikes we shared together.

I would like to thanks **my Israeli friends in Switzerland: Shachaf, Rotem and Gabi, Hadar and Horesh, Rachel and Ahai, Mor and Simone** for many dinners and memorable times we spend together. I thank them for always making me feel at home. A special thanks goes to **Shachaf** for always being there when I needed a friend and an ear to listen and for being my ski partner during the last winter season. This was a great break from the demanding writing.

To all my **good friends from Israel**, for their love and affection. For being there for me. Always.

Last but not least, my deepest appreciation goes to **my amazing family**: my parents and my sister for always believing in me and supporting me spiritually throughout this thesis work and for their endless and unconditional love throughout my life in general. I am who I am because of them. I greatly thank them for filling my life with happiness and joy. Without their ongoing support I would never have finish this thesis.

For all other people I met on the way and for being privilege to spend these years in the beautiful Switzerland!

Lausanne, 10 May 2017

Abstract

Chemical communication is the basis of host-microbe interaction. Insights into this communication will provide a deeper understanding of the mechanisms that govern these complex associations, in beneficial as well as pathogenic contexts. In this dissertation, we used the beneficial relationship between the Hawaiian bobtail squid *Euprymna scolopes* and its symbiont, bioluminescent bacterium *Vibrio fischeri* as a model system to investigate the molecular transfer from symbiont to host.

Using correlative transmission electron microscopy and quantitative ion microprobe isotopic imaging (NanoSIMS; nano-scale secondary ion mass spectrometry), the transfer and localization of ¹⁵N-labeled *V. fischeri*-derived molecules into tissues of newly-hatched squids were studied. Together, these data suggest that the squid is able to take up and incorporate bacterial products released from the symbiont and from other Gram-negative bacteria.

Inoculating squids with strongly ¹⁵N-labeled *V. fischeri* cells, or with outer membrane vesicles (OMVs) released by these cells, resulted in widespread ¹⁵N-enrichment inside the host light organ. ¹⁵N-enrichment was observed in the light-organ epithelia and in other squid tissues, such as the gills and gut. ¹⁵N-enrichment in light-organ tissues was most notable inside cell nuclei: preferentially in the euchromatin regions and the nucleoli. Squids exposed to a mixture of ¹⁵N-enriched amino acids showed comparable cellular ¹⁵N-distributions, suggesting that the majority of bacterial molecules were transferred to the host as part of a more general chemical transfer from the environment.

Inoculating squids with non-symbiotic Vibrionaceae cells (*Vibrio parahaemolyticus* and *Photobacterium leiognathi*) produced ¹⁵N-enrichment patterns similar and comparable to *V. fischeri*-induced patterns. It is likely that the similar host ¹⁵N-enrichment patterns between all bacterial treatments is induced by molecules that have shared structural and functional features and/or are processed by similar pathways within the host cells.

On the other hand, substantial differences in the host ¹⁵N-enrichment were observed when squids were exposed to OMVs derived from different bacteria; specifically, *V. fischeri*, *V. parahaemolyticus*, and *Escherichia coli*. These 'OMV ¹⁵N-enrichment patterns' were distinct, especially between the *Vibrio* strains and *E. coli*, demonstrating a clear host capacity for specific uptake of molecules derived from different bacteria.

This thesis provides new insights into the chemical transfer that might occur in the squid's natural habitat. The results indicate that, in addition to the highly specific molecular interactions *V. fischeri* is known to have with its host, a general molecular exchange takes place. Although the nature of this molecular uptake cannot be inferred from the observations presented here, the molecules involved

might have an essential role in interactions between the bacteria and their animal host. In broader terms, this work demonstrates the unique link between the spatial and functional information provided by the NanoSIMS imaging, which has the potential to open a new frontier for the study of communication between host and symbiont.

Keywords: symbiosis, chemical communication, *Euprymna scolopes*, *V. fischeri*, OMV, NanoSIMS

Résumé

La communication chimique est à la base de l'interaction hôte-microorganisme. Mieux étudier ces communications permettra une compréhension plus approfondie des mécanismes qui gouvernent ces associations complexes, que ce soit dans le contexte d'une relation bénéfique aux deux organismes ou d'une relation parasitaire. Dans cette thèse, nous avons pris comme modèle d'étude la relation bénéfique entre le seiche *Euprymna scolopes* et son symbionte, la bactérie bioluminescente *Vibrio fischeri* pour étudier le transfert de molécules du symbionte vers l'hôte.

En corrélant deux méthodes, la microscopie électronique à transmission et l'imagerie isotopique à haute résolution (NanoSIMS ; nano-scale secondary ion mass spectrometry), nous avons étudié le transfert et la localisation de molécules de *V. fischeri* marquées à l'azote 15 (^{15}N) dans les tissus de seiches récemment éclos. Nos résultats montrent que le seiche *Euprymna scolopes* est capable de capter et d'incorporer les produits bactériens libérés non seulement par ses symbiontes mais aussi par d'autres bactéries à Gram négatif.

L'inoculation de seiches soit avec des cellules de *V. fischeri* fortement marquées au ^{15}N soit avec les vésicules de la membrane externe (OMVs) elles aussi marquées au ^{15}N (obtenues après relargage par des bactéries marquées), a résulté en un enrichissement en ^{15}N de l'organe bioluminescent de l'hôte. Ces enrichissements en ^{15}N ont été observés au niveau de l'épithélium de l'organe bioluminescent ainsi que dans d'autres tissus de l'hôte tels que les branchies et l'intestin. Dans l'organe bioluminescent, les enrichissements en ^{15}N étaient principalement localisés dans le noyau: en particulier dans les régions de l'euchromatine et du nucléole. Les seiches exposées à un mélange d'acide aminés marqués au ^{15}N ont montré des distributions similaires, ce qui suggère que la majorité des molécules bactériennes utilisent un système de transfert général de molécules depuis l'environnement.

L'inoculation de seiches avec des cellules de Vibrionaceae non symbiotiques (*Vibrio parahaemolyticus* et *Photobacterium leiognathi*) a donné des patterns d'enrichissement en ^{15}N comparables à ceux obtenu par *V. fischeri*. Il est probable que cette similarité de pattern entre les différents traitements bactériens soit due à des molécules qui partagent des caractéristiques structurelles et fonctionnelles et/ou qui sont assimilées via des voies similaires au sein des cellules hôtes.

D'autre part, des différences substantielles ont été observées entre les enrichissements en ^{15}N de seiches exposés à des OMVs provenant de différentes bactéries ; en particulier entre *V. fischeri*, *V. parahaemolyticus*, et *Escherichia coli*. Les patterns d'enrichissement des OMVs en ^{15}N observés étaient différents, en particulier entre les deux souches de *Vibrio* et celle d'*E. coli*, ce qui démontre une capacité de l'hôte à assimiler spécifiquement les molécules dérivées de différentes bactéries.

Cette thèse apporte un nouvel éclairage sur les transferts chimiques qui peuvent avoir lieu au sein de l'habitat naturel du seiche. Les résultats indiquent que, en plus de des interactions moléculaires hautement spécifiques entre *V. fischeri* et son hôte, un échange moléculaire plus général existe. Bien que la nature exacte de cet échange ne puisse pas être déterminée à partir des observations présentées ici, les molécules impliquées ont potentiellement un rôle essentiel dans les interactions bactéries-hôte. De façon plus générale, ce travail démontre le lien entre l'information spatial et fonctionnelle donné par l'imagerie NanoSIMS, qui permet de franchir de nouvelles frontières dans l'étude des communications entre hôtes et symbiontes.

Mots-clefs : symbiose, communication chimique, *Euprymna scolopes*, *Vibrio fischeri*, OMVs, NanoSIMS

Contents

Acknowledgements.....	i
Abstract.....	v
Résumé.....	vii
Contents	ix
List of Figures.....	xiii
List of Tables.....	xv
List of Abbreviations	xvii
Literature review	1
I. Beneficial symbiosis as a model to study host-microbe cross-talk.....	1
II. The exclusive partnership between <i>Euprymna scolopes</i> and the bioluminescent bacterium <i>Vibrio fischeri</i>	3
A. The symbiotic partners.....	3
B. The structure of the light organ	5
C. Initiation of the symbiosis and symbiont-induced morphogenesis	6
D. Mechanism promoting specificity of <i>Vibrio fischeri</i>	10
E. <i>Vibrio fischeri</i> induces alteration in host genes expression	13
F. How do <i>Vibrio fischeri</i> deliver their signaling molecules into the host?	14
III. NanoSIMS as a tool to study animal-microbe association.....	16
A. Fundamentals of NanoSIMS	16
B. Basic requirements and limitation of the NanoSIMS technique	18
C. Exploring host-microbe associations with the NanoSIMS.....	19
D. NanoSIMS as an alternative method to visualize proteins and molecules in the cell	19
General procedure for NanoSIMS analysis	23
I. Samples preparation for TEM and NanoSIMS	23
I. NanoSIMS analysis	24

Chapter 1	Can we localize morphogen-induced signaling molecules in host tissues?	27
1.1	Detection of TCT in host cells.....	27
1.1.1	Materials and Methods	29
1.1.2	Results and discussion	30
1.2	Uptake of small organic molecules by juvenile squids	32
1.2.1	Material and Methods.....	33
1.2.2	Results and discussion	33
1.3	Supplementary information.....	39
Chapter 2	Tracking <i>V. fischeri</i>-derived molecules into squid host tissues during initiation of symbiosis	41
2.1	Introduction	41
2.2	Material and Methods	43
2.2.1	General procedures	43
2.2.2	Isolation of outer membrane vesicles (OMVs).....	44
2.2.3	Squid assays.....	45
2.2.4	Samples preparation for transmission electron microscopy and NanoSIMS.....	45
2.2.5	Prediction of NLS sequences in <i>V. fischeri</i>	46
2.2.6	Statistical analysis.....	46
2.3	Results.....	46
2.3.1	Juvenile squids inoculated with symbiont cells.....	46
2.3.2	Juvenile squids inoculated with <i>V. fischeri</i> -derived OMVs.....	55
2.4	Discussion	58
2.4.1	¹⁵ N-enrichment was observed inside host tissues early in symbiosis and does not require direct contact with <i>V. fischeri</i> cells	59
2.4.2	¹⁵ N-enrichment is systematically highest in the nucleolus.....	62
2.4.3	The squid response to OMVs was stronger than to whole bacteria	67
2.4.4	Conclusion and future directions	70

2.5	Supplementary information.....	71
Chapter 3	Tracking molecules from non-symbiotic bacteria into squid host tissues during the early hours after hatching	81
3.1	Introduction	81
3.2	Material and Methods	82
3.2.1	General procedures	82
3.2.2	Bacterial strains and growth conditions	83
3.2.3	Isolation of outer membrane vesicles (OMVs)	83
3.2.4	Squid assays	84
3.2.5	Sample preparation for transmission electron microscopy and NanoSIMS	85
3.2.6	Statistical analysis	85
3.3	Results	85
3.3.1	Juvenile squids inoculated with non-symbiotic bacterial cells	85
3.3.2	Juvenile squids inoculated with non-symbiont- derived OMVs	88
3.4	Discussion	93
3.4.1	¹⁵ N-enrichment patterns are not unique to the symbiotic partner	93
3.4.2	The differential response to <i>E. coli</i> OMVs might suggest a distinct mechanism of recognition and/or internalization into the host cells.....	94
3.4.3	OMVs from <i>V. parahaemolyticus</i> and <i>V. fischeri</i> colocalize with component of the secretory pathways	97
3.4.4	Conclusion and future directions	98
3.5	Supplementary information.....	100
	General discussion	105
A.	The nature of the molecular exchange	106
B.	OMVs colocalize with the Golgi apparatus: a specific pathway for OMVs delivery? ...	109
C.	Permissiveness of the light organ	109
D.	Concluding remarks and future perspective.....	110

Contents

References.....	113
Epilog	139
Curriculum Vitae	141

List of Figures

Fig. 1 <i>E. scolopes</i> light-organ system.....	5
Fig. 2 <i>V. fischeri</i> molecules induce light-organ morphogenesis.....	8
Fig. 1-1. ¹⁵ N-enrichment ($\delta^{15}\text{N}$) in epithelial cells lining the appendage, 3.5 h post exposure to ¹⁵ N-TCT.....	30
Fig. 1-2. ¹⁵ N-enrichment ($\delta^{15}\text{N}$) in squid epithelial cells of the light organ, 3.5 h post exposure to a mixture of ¹⁵ N-amino acids.	35
Fig. 2-1. Use of NanoSIMS to study transfer of chemical compounds from the wild-type <i>Vibrio fischeri</i> cells (ES114) into the squid tissues and cells.	48
Fig. 2-2. ¹⁵ N-enrichment (expressed as $\delta^{15}\text{N}$) in the juvenile squid light organ 2 h post inoculation with ¹⁵ N-labeled <i>V. fischeri</i> cells.....	50
Fig. 2-3. Intracellular distribution of ¹⁵ N-enrichment in the juvenile squid light organ 2 h and 3.5 h post inoculation with ¹⁵ N-labeled <i>V. fischeri</i> cells.....	51
Fig. 2-4. Distribution of ¹⁵ N-enrichment in a representative squid nucleus of an epithelial cell lining the appendage at 3.5 h post inoculation with ¹⁵ N-labeled <i>V. fischeri</i> cells.	51
Fig. 2-5. ¹⁵ N-enrichment along the surface of the appendage epithelium and the ‘shoulder’ area in juvenile squid light organ 6 h post inoculation with ¹⁵ N-labeled <i>V. fischeri</i> cells.	53
Fig. 2-6. ¹⁵ N-enrichment in nuclei and nucleoli (hotspots) in light-organ non-epithelial tissues (A-C) and in epithelial tissues in other squid organs (D-F) after 3.5 h inoculation with ¹⁵ N-labelled <i>V. fischeri</i> cells.....	54
Fig. 2-7. ¹⁵ N-enrichment in a juvenile squid light organ following 1 h and 3 h exposure to ¹⁵ N-labeled <i>V. fischeri</i> -derived OMVs.....	57
Fig. 2-S1. Differences in ¹⁵ N-enrichment in the nuclei of squid epithelial cells that are lining the medial appendage, 2 h post inoculation with ¹⁵ N- <i>V. fischeri</i> cells.....	69
Fig. 2-S2. Light micrographs of histological cross section (0.5 μm thick) of a juvenile <i>E. scolopes</i> showing the different organs that were analyzed in this study and their location in the squid.....	70
Fig. 2-S3. ¹⁵ N-enrichment in various epithelial tissues of the juvenile squid, 3.5 h post inoculation with ¹⁵ N-labelled <i>V. fischeri</i> cells.....	71

Fig. 2-S4. TEM micrographs of purified OMVs produced by wild-type <i>V. fischeri</i> (ES114).....	71
Fig. 2-S5. ¹⁵ N-enrichment in the connective tissue (A), gills (B) and reflector (C) after 3.5 h inoculation with ¹⁵ N-OMVs purified from <i>V. fischeri</i> cells.....	72
Fig. 3-1. ¹⁵ N-enrichment (expressed as $\delta^{15}\text{N}$) in the juvenile squid light organ 3.5 h post inoculation with ¹⁵ N-labeled non-symbiotic Vibrionaceae cells.	87
Fig. 3-2. ¹⁵ N-enrichment in nuclei and nucleoli (hotspots) in epithelial tissues in other squid organs after 3.5 h inoculation with ¹⁵ N-labelled <i>V. parahaemolyticus</i> cells.....	88
Fig. 3-3. ¹⁵ N-enrichment in squid epithelial cells exposed for 3 h to ¹⁵ N-labeled OMVs purified from <i>V. fischeri</i> , <i>V. parahaemolyticus</i> and <i>E. coli</i> , respectively.....	89
Fig. 3-4. ¹⁵ N-enrichment in the Golgi of squid epithelial cells exposed for 3 h to ¹⁵ N-labeled OMVs purified from <i>V. fischeri</i> and <i>V. parahaemolyticus</i>	90
Fig. 3-5. Correlation between the ¹⁵ N-enrichment in the nuclei and their corresponding nucleoli in squid epithelial cells after 3 h exposure to ¹⁵ N-labeled OMVs purified from <i>V. fischeri</i> , <i>V. parahaemolyticus</i> and <i>E. coli</i>	91
Fig. 3-6. ¹⁵ N-enrichment on the cell surface of the appendage epithelium in a juvenile squid light organ following 3 h exposure to ¹⁵ N-labeled OMVs purified from <i>V. fischeri</i> (A), <i>V. parahaemolyticus</i> (B) and <i>E. coli</i> (C).	92
Fig. 3-S1. Negative staining micrographs of OMVs that were isolated from <i>V. fischeri</i> , <i>V. parahaemolyticus</i> and <i>E. coli</i>	97
Fig. 3-S2. Light micrographs of histology cross section (0.5 μm thick) of a juvenile <i>E. scolopes</i> showing representative light organs that appeared to be abnormal.....	97

List of Tables

Table S 1-1 Statistical analysis of squids inoculated with amino acids mixture for 3.5 h post inoculation (3 animals).....	40
Table S 1-2 The chemical composition of Celtone base powder.	40
Table S 2-1 Statistical analysis of squids inoculated with <i>V. fischeri</i> cells for 2 h (3 animals) and 3.5 h (6 animals) post inoculation.....	75
Table S 2-2 Statistical analysis of squids inoculated with OMVs from <i>V. fischeri</i> cells for 1 h (5 animals) and 3 h (4 animals).....	77
Table S 2-3 <i>V. fischeri</i> ES114 proteins with NLS sequences.	78
Table S 3-1 Statistical analysis of squids inoculated with nonspecific environmental bacteria cells, <i>V. parahaemolyticus</i> (7 animals) and <i>P. leiognathi</i> (5 animals) for 3.5 h.....	101
Table S 3-2 Statistical analysis of squids inoculated with OMVs from <i>V. fischeri</i> (3 animals) and from nonspecific environmental bacteria, <i>V. parahaemolyticus</i> (5 animals) and <i>E. coli</i> (3 animals) for 3.5 h.	102

List of Abbreviations

AFM	atomic force microscopy	NLS	nuclear localization sequence
AMP	antimicrobial peptides	NO	nitric oxide
CFU	colony forming units	NoLS	nucleolar localization sequence
CO	carbon dioxide	NOS	NO synthase
CT	cholerae toxin	Nu	nucleolus
CYT	cytoplasm	OMP	outer membrane protein
DFAA	dissolved free amino acids	OMVs	outer membrane vesicles
DOM	dissolved organic matter	OsO₄	osmium tetroxide
dPBS	Dulbecco PBS	PAMPs	pathogen-associated molecular patterns
ER	endoplasmic reticulum	PBS	phosphate buffer saline
EsLBPs	<i>E. scolopes</i> LBPs	PGN	peptidoglycan
EsPGRPs	<i>E. scolopes</i> PGRPs	PGRPs	PGN recognition protein
EST	expressed sequence tag	PRRs	pattern recognition receptors
FISH	fluorescence in situ hybridization	PVDF	polyvinylidene difluoride
FMNH₂	flavin mononucleotide	QS	quorum sensing
FSIO	filter-sterilized (0.2 μm) Instant Ocean	RLI	Relative Labeling Index
FSW	filter-sterilized seawater	RNS	reactive nitrogen species
GA	Golgi apparatus	ROIs	Regions Of Interest
HPLC	high-performance liquid chromatography	ROS	reactive oxygen species
HPO	halide peroxidase	SEM	scanning electron microscopy
LBPs	LPS-binding proteins	TCT	tracheal cytotoxin
LPS	lipopolysaccharide	TEM	transmission electron microscopy
MAMPs	microbe-associated molecular patterns	TLRs	Toll-like receptors
MMD	minimal medium	TXSS	type X secretion system
mPBS	marine PBS	WT	wild-type
N	nucleus		
NanoSIMS	Nanoscale secondary-ion mass spectrometry		

Literature review

I. Beneficial symbiosis as a model to study host-microbe cross-talk

All animal species have associations with microorganisms. These partnerships are at the heart of animal biology. Whether beneficial or pathogenic, interactions between microbes and animals have profoundly influenced the evolution of life. However, for many years, descriptions of these symbiotic systems have mainly focused upon the features associated with pathogenesis, specifically in the context of human diseases. Biologists are now finding that many mutualistic interactions are imperative to normal ontogenesis and the life-span of their host. They can play a key role in such host processes as development, nutrient assimilation, reproduction, protection from potential pathogens, and stimulation of immune response(s) (reviewed in Bäckhed et al. 2005; Relman 2008; McFall-Ngai et al. 2013). Perhaps the best described system is the microbiome that lives in the human gastrointestinal tracts and is pivotal to the digestive physiology and to the development of the innate immune system.

Interdomain (bacteria:host) associations are possible because the microbes and their host can communicate efficiently with each other. This bi-directional communication, shaped by the dynamic coevolution between microbes and their host, is based upon exchanges at the molecular level that frequently involve ligand-receptor interactions. Bacteria produce a vast variety of chemical and nutritional compounds that mediate social behaviors between individual bacteria and participate in host-microbe interactions. Cross-talk between bacteria is mediated through chemical factors such as quorum sensing molecules (QS; Ng and Bassler 2009) that control gene expression as a function of population density, but lately their role in mediating communication with their animal host has been brought to light (Sperandio et al., 2003; Hughes and Sperandio, 2008; González and Venturi, 2013). In addition to QS molecules, bacteria also use cell-envelope components (i.e., LPS, PGN, outer membrane proteins), proteins, peptides, inorganic molecules, secondary metabolites, and short-chains fatty acids to communicate with their symbiotic partners (Rath and Dorrestein 2012; Sharon et al. 2014; Cleary et al. 2017). Conversely, different animal hosts are known to use hormones molecules (proteins, steroid and amino acid derivatives; Hughes and Sperandio 2008; Kendall and Sperandio 2016), hormone-like compounds, inorganic compounds, such as NO (nitric oxide) and CO (carbon monoxide), and nutritional signaling molecules (e.g., sugar and organosulfur compounds) to interact with the bacterial partners. These molecular exchanges can alter the activity of the partner: bacterial signals can modulate host cell-signal transduction pathways and affect gene-expression. Conversely, host molecules can modulate bacterial gene-expression, affect bacterial growth and/or help them gain competitive advantage, e.g., by creating an environment that only the symbionts can withstand (Davidson et al., 2004).

During the last decades, the development and application of genomic and transcriptomic analysis and the invention of new imaging methods, such as large-scale proteomics (e.g., Wang et al. 2016) and super-resolution microscopy (e.g., Li et al. 2015), respectively, have substantially increased our understanding of the complex reciprocal molecular dialogues that influence microbe-animal interactions. However, the precise nature of the molecular exchange between partners, i.e., how cells receive, process and respond to information from the environment, remains largely elusive.

There is now general acceptance of the fact that coevolved microbial symbionts play a key role in health and disease and result in shared cellular and molecular mechanism, such as the expression of specific colonization genes and effector molecules (including toxins), that are well conserved throughout the animal kingdom and characterize both beneficial and pathogenic associations (Hentschel et al., 2000; McFall-Ngai, 2008; McFall-Ngai et al., 2013). Importantly, it has become recognized that the host immune response to either harmful or benign microbial factors depends upon the context of the microbial signal (McFall-Ngai 2008; Vance et al. 2009; Casadevall and Pirofski 2015), such as the concentration and nature of the chemical cues and where and when they are perceived by the host (Vance et al., 2009). Therefore, symbiosis models can provide insights into evolutionary conserved differences between pathogenic and 'friendly' interactions.

Several natural models of microbial-host association exist. However, most of the models involve highly complex and variable microbial communities, such as the intestine tract, making it challenging to ascribe specific functions to specific symbionts. Relatively simple symbiotic relationships, like those established in many invertebrates, offer a better change of disentangling the complex molecular and cellular association between partners. The natural binary association between the Hawaiian bobtail squid *Euprymna scolopes* and the luminous bacterium *Vibrio fischeri* represents one such relatively simple symbiosis. Over the last 30 years, this squid-*Vibrio* symbiosis has been systematically studied, generating large amount of information about the physiological-, molecular-, and genetic-level host responses involved in the establishment of the association during the first days after hatching of the juvenile squid. This symbiosis therefore offers a compelling animal model for studies of the chemical dialogue between the host and its bacteria companion during animal development.

In the following, I review certain aspects of the initiation and establishment of the symbiosis between *V. fischeri* and the squid host, which contribute to the extreme specificity shown by the host squid towards *V. fischeri* during the establishment of the symbiosis. This short review is also intended to introduce the biological system that constitutes the experimental basis and motivation for the work carried out in this thesis.

II. The exclusive partnership between *Euprymna scolopes* and the bioluminescent bacterium *Vibrio fischeri*

A. The symbiotic partners

The marine bioluminescent *Vibrio* (now *Aliivibrio*) *fischeri* is a member of the *Vibrionaceae*, a large family of Gram-negative Gamma-proteobacteria (Fig. 1B). While most members of *Vibrionaceae* form beneficial alliances, a smaller group causes pathogenesis with both animals and humans (i.e., *Vibrio cholerae*, *Vibrio parahaemolyticus*). In its natural habitat of seawater, *V. fischeri* can be found either as motile free-living bacteria or as non-motile bacteria, engaged in beneficial associations with various marine squids (Boettcher and Ruby, 1990; Fidopiastis et al., 1998) and fishes (Nealson and Hastings, 1991). Its metabolic flexibility (Dunn, 2012) and genomic content (Ruby et al., 2005) enable *V. fischeri* to grow in diverse environmental conditions, including an animal host environment. Interestingly, although *V. fischeri* is known to be nonpathogenic, its genome carries homologs of *Vibrio* genes that may encode host-targeted virulence factors (Ruby et al., 2005).

V. fischeri produces luminescence when the luciferase enzyme, which is a mixed function oxidase, oxidizes reduced flavin mononucleotide (FMNH₂) and a long-chain aldehyde to FMN and the corresponding acid, a reaction that releases blue-green light (490 nm) as a byproduct. Light production is regulated by the *lux* operon (*luxCDABEG*) that encodes the luciferase and the enzymes that produce substrate for the reaction (Visick et al., 2000). The *lux* genes are tightly controlled, mainly through the LuxI and LuxR quorum-sensing system and are expressed when the high-density populations of *V. fischeri* are in symbiosis with the Hawaiian squid. LuxI synthesizes the autoinducer acyl homoserine-lactone, while LuxR synthesizes an autoinducer-dependent transcription factor (Visick et al., 2000). The autoinducer molecule is continually produced at low levels in the free-living *V. fischeri*. However, when the *V. fischeri* population reach a certain density inside the host, the autoinducer accumulates and begins to positively regulate the *lux* genes, and light is produced at the intensity level that is required for the animal host's use of the symbiont bioluminescence in its nocturnal behavior. The *lux* operon is a common feature among several host-associated bacteria and also participates in regulating genes involved in pathogenesis, biofilm formation, genetic competence and antibiotic production (Visick et al., 2000; Ruby et al., 2005).

The Hawaiian bobtail squid, *Euprymna scolopes*, is a small, sepiolid squid that lives in the sandy shallow reef areas of the Hawaiian archipelago (Fig. 1A; Berry 1912). Squid hatchlings are ~2-3 mm and as adults they can reach ~3-4 cm (Fig. 1C). For the most part of its life, this nocturnal predator stays buried in the sand and only emerges at dusk to feed on polychaetes and shrimps (Singley, 1982). To hide from predators, or stay unnoticed by its prey, the squid can either hide by covering itself with

sand, use of chromatophores to change their skin pattern and colors, or, during night, use bioluminescence produced by its symbiot *V. fischeri*. Production of bioluminescence is the functional basis of the squid-*Vibrio* symbiosis because it serves as counter-illumination to match star and moonlight thus 'camouflaging' the squid's silhouette (Jones and Nishiguchi, 2004). In exchange for *V. fischeri* luminescence, the squid provide *V. fischeri* cells with a protective niche and nutrients to support its rapid growth (Ruby and Asato, 1993).

A remarkable feature of this symbiosis is its extremely high specificity: *V. fischeri* is the sole bacterium that can form a permanent, extracellular symbiosis with the squid by occupying its light organ throughout the squid's lifetime (~9 months).

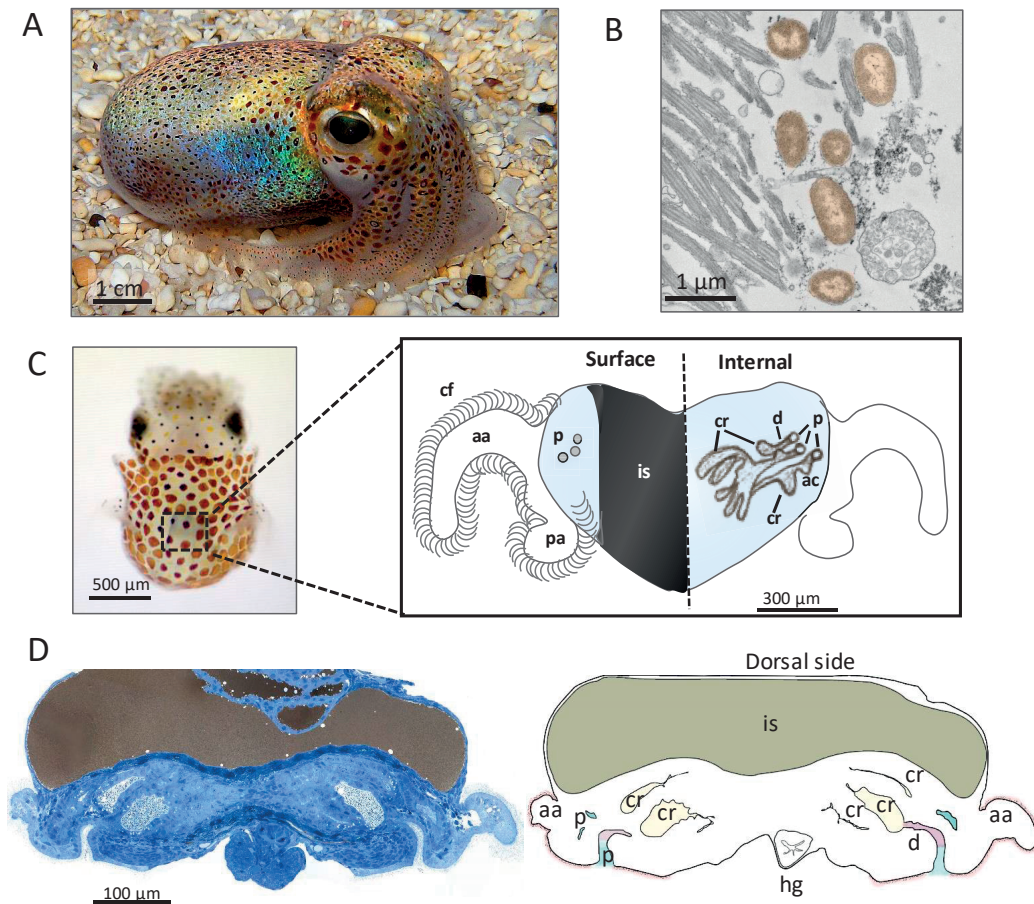


Fig. 1 *E. scolopes* light-organ system. (A) An adult animal. (B) A TEM micrograph of *V. fischeri* cells associating with the cilia of the squid epithelial cells; the bacterial cells have been false-colored to illustrate their relationships to host cells and distinguish them from other features in the image. (C) Left: A dorsal view of a juvenile animal. The approximate position of the light organ, within the mantle cavity, is indicated by the dashed box. Right: Enlargement of the bi-lobed light organ (ventral view), the tissue that contain the symbionts. The internal light organ occurs in the center of the mantle cavity, which is flushed with seawater during animal ventilation. Left half, the light organ surface that is in direct contact with the seawater. The light organ is surrounded by the ink sac (is) and its surface is covered by ciliated fields (cf). At the base of each ciliated appendage are three pores that form the entrance to the light organ. Right half, diagram showing the internal components of the light organ. After a period of 2–4 h in the aggregates on the appendages, the symbionts move through the pores, into the ducts, antechambers, and finally into the blind-ended crypt spaces where they colonize and induce bioluminescence (Nyholm and McFall Ngai 2004). Diagram adapted from Kremer et al. (2013). (D) Cross section through the light organ ~14 h post inoculation with *V. fischeri* cells. Left, a representative light micrograph of an 0.5 μm section; blue histological section, toluidine blue-borax staining. Right, diagram illustrating the different light-organ compartments as can be seen on the left. Each crypt is fully colonized by the symbionts. aa, anterior appendage; ac, antechamber; cr, deep crypts; d, duct; hg, hindgut; is, ink sac p, pore; pa, posterior appendage.

B. The structure of the light organ

The juvenile squid has a nascent light organ in the center of their mantle cavity (Fig. 1C). This bi-lobed structure consists of several host tissues: the epithelial appendages, crypts housing the symbionts, as well as accessory tissues: reflector and ink sac. In the adult light organ these accessory tissues, together with the muscle-derived lens (absent in juvenile squids), serve to modify the light

emitted by the bacteria (McFall-Ngai and Montgomery, 1990). Under the organ lies the hindgut (ventral view).

Each lobe on the light organ's lateral surface includes a posterior and an anterior ciliated epithelial appendage, which are single-layered epithelia covering a blood sinus. Cells of each appendage are covered by numerous cilia and each cilium is surrounded by several microvilli (Montgomery and McFall-Ngai, 1993). The ciliated fields are covered by a mucus matrix is shed from the epithelial cells comprising the appendages (Nyholm et al., 2002). At the base of the appendages, three pores occur on each side of the light organ, and each pore leads to a separate crypt (3 on each side) lined by a polarized, microvillus epithelium. The path of tissues through which the symbionts migrate includes several morphological regions: duct, antechamber, bottleneck (5-9 μm wide), and blind-ended, deep crypt (Sycuro et al., 2006). The three pairs of the deep crypts are different in size: the smallest crypt is located most anterior (crypt 3), the medium sized crypt is most posterior (crypt 2) and the largest crypt is situated in between (crypt 1; Montgomery and McFall-Ngai 1993). In the hatchling, the most developed crypt is crypt 1. Each of the six crypts becomes rapidly colonized by *V. fischeri* symbionts during the first few hours of after hatching. Inside the crypt the bacteria interact with the dense microvillous layer that covers the polarized crypt epithelium (Lamarcq and McFall-Ngai, 1998). Bacterial growth in the crypts is supported by nutrients, amino acids (Graf and Ruby, 1998), lipids, glycerophospholipids (Schwartzman et al., 2015), and chitin-derived sugars (Wier et al., 2010), which are provided by the host. The host also supplies oxygen to support the bioluminescence (Kremer et al., 2014).

C. Initiation of the symbiosis and symbiont-induced morphogenesis

Upon hatching, juvenile *E. scolopes* do not contain *V. fischeri* cells and need to acquire them from the surrounding seawater in a process referred to as 'winnowing' (Nyholm and McFall-Ngai, 2004). During the harvesting of *V. fischeri* from the bacterioplankton-rich environment (Lee and Ruby, 1994), the squid has two challenges: ventilate enough seawater to encounter *V. fischeri* and then specifically select *V. fischeri* cells from the millions of other bacteria present in the seawater to permit it to become the only symbiotic partner of the host squid.

V. fischeri cells first aggregate on ciliated fields above the pores for a period of 2-4 h in the mucus matrix secreted by the host. At a typical seawater concentration of ca. 5000 cells/mL, 3-5 cells of *V. fischeri* will attach to the cilia and form a small aggregate (Altura et al., 2013). Within a few hours *V. fischeri* cells become the dominant bacteria in the mucus (Nyholm and McFall-Ngai, 2003); they then travel through the pores into the ducts before finally colonizing the deep crypts (Nyholm et al., 2000). *V. fischeri* cells that fail to form this aggregate are not able to colonize the squid (Nyholm et al., 2000;

Millikan and Ruby, 2002; Yip et al., 2006). Importantly, although other Gram-negative bacteria (e.g., *Vibrio parahaemolyticus*) can associate with the superficial ciliated field and can even be found inside the light-organ pores, they cannot colonize the crypts even in the absence of *V. fischeri* cells (Nyholm et al., 2000).

Once inside the light-organ crypts, *V. fischeri* cells start to divide rapidly to a population of $\sim 10^6$ cells, (Ruby and Asato, 1993), filling the extracellular space (Nyholm and McFall-Ngai, 2003) and beginning to produce luminescence $\sim 8-12$ h after hatching of the squid (McFall-Ngai and Ruby, 1991). Each morning, sunlight signals the squid that it is time to vent 90-95% of its crypt contents (Graf and Ruby, 1998; Nyholm and McFall-Ngai, 1998; Nyholm and McFall-Ngai, 2004). The remaining 5-10% of the bacteria divides and repopulates the light organ during the coming day (Boettcher et al., 1996).

The presence of *V. fischeri* in the crypts induces developmental changes that are required for the life-long stability of the symbiosis (McFall-Ngai and Ruby, 1998). The most dramatic morphogenesis occurs following the first night of colonization (Fig. 2). At 12 h after inoculation, marking the beginning of *V. fischeri* populating the crypts spaces and concurrent with the first venting, an irreversible morphogenesis of the light organ is initiated: The superficial ciliated epithelium (i.e., the appendages) undergoes apoptosis and regression that culminates in the complete loss of the ciliated field, 4-5 days after the initial colonization (e.g., McFall-Ngai and Ruby 1991; Foster and McFall-Ngai 1998; Fig. 2B, C). The series of developmental events that take place during the first days of the symbiosis (Fig. 2D), transforms the light organ morphologically to efficiently `shut the door` and prevent further infection by non-performing *V. fischeri* or potential pathogens once the desired mutualistic association is obtained (McFall-Ngai and Ruby, 1998). Once the light organ is fully developed, the symbiosis is controlled by the host response to light cues as well as circadian rhythm. This includes the daily expulsion event, effacement of the crypts microvilli around dawn (Wier et al., 2010), circadian oscillation of cryptochromes clock genes in the host (Heath-Heckman et al., 2013), and changes in carbon metabolism to support the symbiont population in the crypts (Wier et al., 2010; Schwartzman et al., 2015).

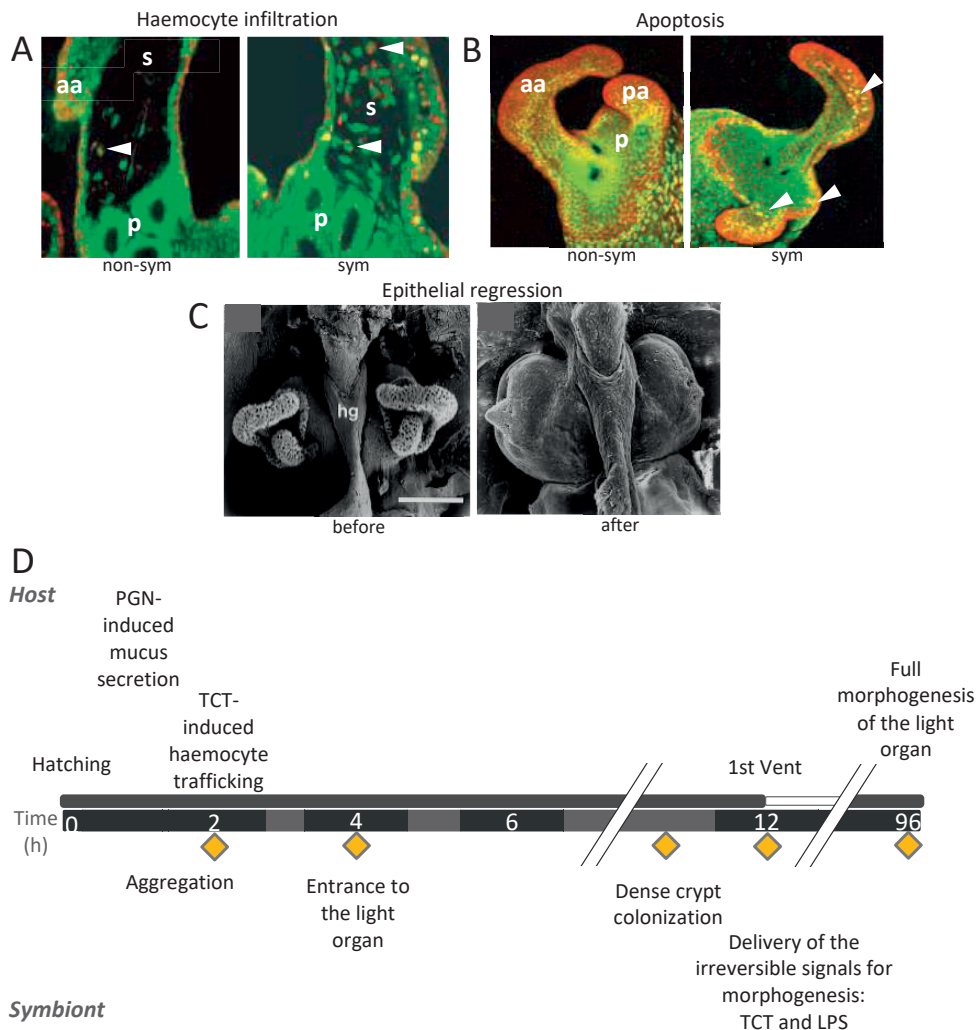


Fig. 2 *V. fischeri* molecules induce light-organ morphogenesis. (A) and (B) Confocal images of apo-symbiotic (apo, i.e., uninfected with *V. fischeri*) and symbiotic (sym) organ epithelial fields stained with acridine orange (green) and LysoTracker (red) (modified from Koropatnick et al. 2004). These stains are used to detect programmed cell death. (A) Haemocytes (arrowheads) within the appendage sinuses (s). (B) Apoptotic cells, yellow foci (arrowheads) (modified from Koropatnick et al. 2004). (C) Scanning electron microscopy (SEM) of epithelial fields before and after regression of the ciliated fields. Scale bar, 0.1 mm (modified from Foster and McFall-Ngai 1998). (D) Timeline illustrating relevant characteristics of the early symbiosis. *V. fischeri* cells aggregate near the ciliated epithelial fields and enter the light organ around 4–6 h post hatching. Within hours of successful colonization of the deep crypts of the light organ, the symbionts deliver an irreversible signal that triggers an extensive developmentally programmed tissue destruction (morphogenesis) of the light organ into a mature form lacking the ciliated epithelial fields. aa, anterior appendage; hg, hindgut; p, pores; pa, posterior appendage, s, sinus.

V. fischeri microbe-associated molecular patterns (MAMPs) orchestrate remotely, i.e., from the crypts, the events that lead to morphogenesis of the appendages. MAMPs are mostly thought to act as virulence factors by triggering inflammatory response (thus, named also pathogen-associated molecular patterns; e.g., Cookson et al. 1989; Pabst et al. 1999). However, in the squid-*Vibrio* mutualism these MAMPs have a benign function by inducing normal development in the host. Specifically, derivatives of lipopolysaccharide (LPS) and peptidoglycan (PGN), which are constituents of

the *V. fischeri* cell envelope, act as potent morphogens to induce normal light-organ morphogenesis in the squid host (e.g., Foster et al. 2000; Koropatnick et al. 2004; Nyholm and McFall-Ngai 2004; McFall-Ngai et al. 2012).

The role of MAMPs in host morphogenesis has been the focus of many studies in the last two decades. MAMP signaling starts already while the bacteria are outside of the host organism, i.e., free-living in seawater. Any PGN, or its molecular fragments in the surrounding seawater, broadly induces a non-specific mucus shedding (Nyholm et al., 2000). Interaction of *V. fischeri* cells with the host squid during aggregation triggers the infiltration of macrophage-like haemocytes (blood cells) into the blood sinuses of the ciliated epithelial fields (Koropatnick et al., 2004; Koropatnick et al., 2007; Fig. 2A). The PGN monomer, tracheal cytotoxin (TCT), is the molecule responsible for haemocyte trafficking (Koropatnick et al., 2004; Koropatnick et al., 2007). Secretion of the signals that cause irreversible apoptosis of cells in the ciliated appendages takes place in the crypts; the lipid A component of LPS alone can stimulate early-stage apoptosis (chromatin condensation) of the cells (Foster et al., 2000), while later-stage apoptosis (DNA fragmentation) and regression of these cells can be induced by the combined effects of TCT and the lipid A (Koropatnick et al. 2004; Troll et al. 2009; Fig. 2). The synergistic effects of TCT and LPS drive much of the light-organ morphogenesis but cannot bring it to completion. Studies have shown that symbiont-induced bioluminescence may act with TCT and LPS to induce full morphogenesis (Visick et al., 2000; Koropatnick et al., 2007; Chun et al., 2008; Troll et al., 2009; McFall-Ngai et al., 2010; McFall-Ngai et al., 2012) and can also induce other symbiont-mediated squid phenotypes (haemocyte trafficking, swelling of crypts cells; Visick et al. 2000; McFall-Ngai et al. 2012).

In addition to appendage morphogenesis, *V. fischeri* MAMPs induce other developmental events in the squid that include the irreversible attenuation of NO in the duct and crypts (Davidson et al., 2004; Altura et al., 2011) and some reversible changes, that require the continuous exposure to the *V. fischeri* to maintain these changes, such as cessation of mucus secretion at the surface epithelium (Nyholm et al., 2002), changes in microvillar density in the crypts (Lamarcq and McFall-Ngai, 1998) and narrowing of the ducts (Lamarcq and McFall-Ngai, 1998; Kimbell and McFall-Ngai, 2004).

Concurrent with host developmental changes, *V. fischeri* cells undergo changes in gene expression and morphology in order to adapt to its host environment. Bacterial features that are considered important for colonization include the ability to form a biofilm (Yip et al., 2006; Mandel et al., 2009; Brooks et al., 2014), to regulate motility (Millikan and Ruby, 2002; Altura et al., 2013), to follow a chemotaxis gradient (DeLoney-Marino et al., 2003; Mandel et al., 2012; Kremer et al., 2013) and to shift between glycerol and chitin catabolism (Wier et al., 2010).

D. Mechanism promoting specificity of *Vibrio fischeri*

Several mechanisms are known to increase specificity of selection of *V. fischeri* over other, non-performing or 'cheating' symbionts, as well as interlopers that would otherwise populate the light organ. This is a process that occurs in several steps and develops over the first few hours after inoculation of the squid host with its symbionts. This 'winnowing' process is achieved by combination of physical barriers, physiological constraints and, importantly, innate immune system. Remarkably, the juvenile squids are able to specifically sense and respond to the very few *V. fischeri* that initiate the close interaction with the ciliated epithelial cells and distinguish them among the myriad environmental bacteria present in the seawater. *V. fischeri* MAMPs play also a crucial role in shaping host physiology and biochemical environment to support a highly specific and stable colonization over the life of the squid.

i. Early permissiveness of the host light organ

Confocal microscopy studies have revealed that within the first hour after hatching, the crypts are permissive to entry of both *V. fischeri* symbionts and nonspecific bacteria (Gram-negative and Gram-positive, as well as particles with sizes less than 2 μm ; Nyholm et al. 2002). However, at ~ 2 h after hatching these initial bacterial 'intruders' are removed from the light organ by unknown mechanisms (Nyholm et al., 2002). The time window between 1 to 2 h after exposure to *V. fischeri* thus represents a 'nonpermissive phase', during which *V. fischeri* begins to aggregate on the surface light-organ (Nyholm et al., 2002). After this non-permissive phase, the crypts remove all cells other than those of *V. fischeri*.

ii. Navigating through morphologically and chemically distinct environments of the light organ

From the initial contact with the host to the colonization of the crypts, *V. fischeri* encounters multiple, complex environments to which its needs to adapt to successfully colonize the light organ. *V. fischeri* cells continuously interact with antimicrobial factors from the host and secrete MAMPs that help to shape the immediate environment (Ruby and McFall-Ngai, 1999; McFall-Ngai et al., 2010; Nyholm and Graf, 2012).

Shortly after hatching, the squid begins to ventilate seawater through their mantle cavity, bringing thousands of bacterioplankton species (Lee and Ruby, 1994) into the vicinity of appendages (Fig. 1C). The ciliated fields are covered by mucus matrix shed from the epithelial cells lining the appendage. The water current generated by the ciliated fields together with the ring-like shape created by each pair of appendages, are thought to promote the gathering and aggregation of the

symbionts within the mucus (Nyholm et al. 2000; Nawroth et al. in press) before bringing them towards pores that serve as the entrances to the light organ (McFall-Ngai and Ruby, 1998).

During the passage through the ciliated ducts, the symbiont encounters challenging environments that they need to overcome in order to progress to colonization: the cilia of the duct cells beat outward (towards the pores; McFall-Ngai and Ruby 1998) and high levels of oxidative stress is present in the ducts (Davidson et al., 2004; Altura et al., 2011). These morphological and chemical characteristics of the ducts together with symbiont-induced developmental changes in the ducts (i.e., increase in actin cytoskeleton and constriction of the duct; Kimbell and McFall-Ngai 2004) are thought to prevent non-symbiotic, Gram-negative bacteria from entering into the light organ and limit their opportunity for a subsequent colonization (Kimbell and McFall-Ngai, 2004). This indicate a key role for the duct in achieving specificity; once the symbiont is filling the crypts, there is shutdown of activities associated with the infection processes (i.e., mucus shedding; Nyholm et al. 2000).

Mucus chemistry plays a role in symbiont selection and is an essential feature in preparing the symbiont for events leading to colonization. In addition to creating an acidic environment in the mucus matrix (pH ~5.9-6.4; Kremer et al. 2013), the squid secretes antimicrobial peptides including NO (Davidson et al., 2004; Wang et al., 2010), hemocyanin (Kremer et al., 2014), and PGN recognition protein 2 (EsPGRP2; Troll et al. 2010). NO and hemocyanin are linked to oxidative activity while EsPGRP2 selects actively against Gram-positive PGN (Troll et al., 2010; Heath-Heckman et al., 2013). *V. fischeri* attaching to the cilia on the organ's surface also induces secretion of host enzymes into the mucus such as lipase, lysozyme, and chitotriosidase as part of the squid immune response (Kremer et al., 2013). The latter results in the accumulation of chitin derivatives in the mucus matrix. Remarkably, the presence of NO and chitin-derived sugar in the mucus primes *V. fischeri* cells for subsequent colonization (Kremer et al., 2013): (i) the symbiont migrates through the pores in response to chitobiose gradient (Mandel et al., 2012; Kremer et al., 2013), and (ii) the low NO concentration prepares them to the intense oxidative environment that exists in the ducts and antechamber (Davidson et al., 2004; Kremer et al., 2013).

iii. Immune system response

The host immune system plays an integral role not only in defending the host against pathogens but also in promoting the accommodation of benign symbiotic bacteria in the host and maintaining bacteria-host homeostasis (Cerf-Bensussan and Gaboriau-Routhiau, 2010). Interestingly, although the host innate immune system is continuously exposed to MAMP's from both mutualistic and pathogenic bacteria, it is able to distinguish between them (reviewed in Nyholm and Graf 2012; Chu and Mazmanian 2013). In the healthy human gut, for example, MAMP's released by commensal

bacteria do not stimulate inflammation but rather contribute to host development and enhanced immune function. The innate immune system uses conserved molecular structures named pattern recognition receptors (PRRs) to sense microbes. Binding of MAMPs to PRRs receptors will trigger downstream signaling pathway often through NF (nuclear factor)-kappa B (NF- κ B), a known regulator of apoptosis, which then can activate other immune response such as phagocytes and antimicrobial peptides (AMP) (Leulier and Lemaitre, 2008).

In the squid, host recognition of bacterial MAMPs have a central role in development of the light organ and in mediating host immune responses. Genetic and transcriptomic studies have characterized numerous PRRs in the squid: three members of the LBPs protein family (Chun et al., 2008; Krasity et al., 2011), five PGRPs (Goodson et al., 2005; Collins et al., 2012) and one TLR (Goodson et al., 2005). In addition, studies have demonstrated the presence of proteins that are members of the NF- κ B pathway (Goodson et al., 2005; Chun et al., 2008; Schleicher and Nyholm, 2011). To date, most studies have focused on *E. scolopes* PGRPs (EsPGRPs) and LBPs (EsLBPs). It was suggested that PGN and LPS activate a putative Toll/NF- κ B signaling pathway in the *E. scolopes* during early development of the light organ, through EsPGRP3 and EsPGRP4. These transcription factors then induce the synthesis of EsPGRP1 and EsPGRP2 (Goodson et al. 2005; reviewed in Royet et al. 2011). Transcripts encoding EsPGRP1 and EsPGRP2 were elevated predominantly within the crypts, where symbionts are in close association with the host (Nikolakakis et al., 2015). Immunocytochemistry of EsPGRP1, a nuclear protein, revealed that the loss of this protein from the nuclei of the superficial epithelium of the light organ correlates with the entry of these cells into late-stage apoptosis. Further, purified TCT alone was capable of inducing loss of EsPGRP1 in levels similar to the WT. EsPGRP2 localized to cytoplasmic areas of all epithelial cells that have direct contact with the seawater (i.e., gills, gut exterior, arms etc.; Troll et al. 2010). In the crypts, EsPGRP2 amidase activity is capable of breaking down TCT after the delivery of the irreversible signal for morphogenesis, which occurs at 12 h after initiation of the symbiosis (Troll et al., 2010). Transcriptomic analysis localized EsPGRP3, EsPGRP4 and EsPGRP5 transcripts in host haemocytes (Collins et al. 2012; Rader B and Nyholm SV unpublished), however, their role remains to be resolved. Among the LBPs family, EsLBP1 protein has been extensively studied (Chun et al., 2008; Krasity et al., 2015). In the light organ, this protein was found to be abundant on epithelial surfaces that directly interact with the symbiont and is thought to be important for PGN-LPS synergy (Krasity et al., 2015).

Antimicrobial peptides of the innate immune system have also been implicated in the *E. scolopes-V. fischeri* symbiosis. Analysis of host proteomics discovered numerous proteins that are involved in producing reactive oxygen species (ROS; e.g., hypohalous acid produced by light-organ halide peroxidase HPO) and reactive nitrogen species (RNS; e.g., NO) that contribute to the oxidative

environment in the light organ that the symbionts need to cope with (Small and McFall-Ngai, 1999; Schleicher and Nyholm, 2011). Symbiont cells produce proteins that are involved in protecting them from host ROS, such as catalase (KatA), a major scavenger of hydrogen peroxide (H₂O₂) and NO dioxygenase (Hmp; Schleicher and Nyholm 2011). As mentioned above, other antimicrobial peptides that have been suggested to have a role in the symbiosis include hemocyanin (Kremer et al., 2014) and EsPGRP2 (Troll et al., 2010).

Macrophage-like haemocytes are the only blood cell type of *E. scolopes* and they have the capability to attach, engulf, and kill bacterial cells. These immune cells are considered to play a key role in the host defense against microorganisms by maintaining the specificity of the interaction with *V. fischeri*. Migration of haemocytes into the blood sinuses of the superficial epithelium during infection with *V. fischeri* occurs such that within hours the haemocyte cells will fill the blood sinus. In the crypts, however, they are by comparison found only in very low numbers (Koropatnick et al., 2007). While, their function in the blood sinus of the appendage epithelium is not yet well understood, the irreversible signal for morphogenesis appears to induce transcriptional change in haemocyte genes suggesting their involvement in the developmental regression of the ciliated fields of the appendages (Koropatnick et al., 2007; McAnulty and Nyholm, 2017). In the mature symbiosis, unlike those in juvenile squids (Nyholm and McFall-Ngai, 1998), haemocytes found in the crypts have not been reported to contain *V. fischeri*. *Ex-vivo* studies with haemocytes from adults shown that through exposure to symbiont cells, haemocytes 'learn' to distinguish *V. fischeri* cells from other bacteria cells, and thus effectively avoid phagocytosis of the former (Nyholm et al., 2009). The ability of *V. fischeri* to resist adherence to host haemocytes may help in persistence of symbiont in the crypts spaces and contribute to the long-term specificity of this partnership.

E. *Vibrio fischeri* induces alteration in host genes expression

Several studies have reported on transcriptional changes in host light-organ tissues in response to the presence of the symbiont in the aggregate and/or colonization of the light organ. Differences in proteins profiles and transcript levels between symbiotic and aposymbiotic animals were recorded based on proteomic analysis (Doino and McFall-Ngai, 1995) and expressed sequence tag (EST) database (Chun et al., 2008; Wier et al., 2010), respectively. Wier et al. (2010) reported that differences in gene regulation are tied to the diel cycle, just before and after dawn (concomitantly with *V. fischeri* expulsion from the light organ).

One of the most striking observations made recently by Kremer et al. (2013) demonstrating that the intimate association of only 3-5 *V. fischeri* cells with the ciliated epithelial cells are sufficient to dramatically impact genes expression in the light-organ tissues during the first 3 h post hatching. The

most profound transcriptional change was in genes associated with protease activity and chitin metabolism. In contrast, in the presence 10^6 nonsymbiotic environmental bacteria, there was almost no change in host genes expression. Their data suggest that although the squids are exposed to a high background of nonspecific environmental bacteria, they are very sensitive to the presence of a few *V. fischeri* cells.

F. How do *Vibrio fischeri* deliver their signaling molecules into the host?

Signaling molecules, can travel as extracellular soluble compounds, through injection systems or packaged as cargo into vesicles. The way the molecules are trafficked will affect their distribution into and within target host tissues and cells. In the current work, I will focus on the delivery of molecular compounds from the symbionts into the host.

Pili, which are polymeric hair-like organelles protruding from the bacteria cell-surface, are involved in the adherence of bacteria to host cells (Pizarro-Cerdá and Cossart, 2006). *V. fischeri* has a variety of pili, including the putative type IV pili, the most common type of bacterial pilus (Ruby et al., 2005). Interestingly, in addition to aid in attachment to different kinds of surfaces, type IV pili is also important to the secretion of a variety of factors into the host (Lu et al. 1997; review in Pizarro-Cerdá and Cossart 2006), but their precise role in the squid- *Vibrio* symbiosis has yet to be understood.

Many Gram-negative bacteria utilize, needle-like, dedicated protein secretion systems to transport proteins into other places in the cells, the ambient environment, and other bacteria or eukaryotic cells. There are seven known secretion system of which three of them, the type-3 secretion system (T3SS), T4SS, and T6SS are capable of injecting secreted proteins from the bacterium directly into the cytosol of a target eukaryotic cell (reviewed in Tseng et al. 2009; Green and Mecsas 2016). These secretion systems are found both in pathogenic and beneficial bacteria (Galán and Wolf-Watz, 2006; Shen et al., 2012; Hickey et al., 2015). The model light-organ symbiont of the *E. scolopes*, *V. fischeri* strain ES114 (Boettcher and Ruby, 1990), carry a pES100 plasmid that encodes a putative T4SS (Ruby et al., 2005). In comparison to other secretion systems, T4SS has the ability to secrete bacterial DNA in addition to single proteins or protein complexes. The T4SS complex has a pivotal role in the pathogenesis of a wide-range of bacteria such as *Nisseria gonorrhoeae* (Hamilton and Dillard, 2006) and *Helicobacter pylori* (Backert and Meyer, 2006). The potential role of T4SS as a transport system of *V. fischeri* molecules into the squid remains to be elucidated.

Although the use of secretion system and pili are efficient mechanisms that ensure the access of a specific protein to the host cell, it requires a direct contact with recipient cell thus limit the physical range of action. However, bacteria can also excrete into the extracellular matrix either individual soluble compounds such as, cholera toxin, autoinducer, and PGN derivatives, that directly bind to host

receptor and hence facilitate their entry through the cell membrane, or deliver the molecules via bacterial-derived outer membrane vesicles (OMVs). In the following paragraph, I discuss selected details regarding secreted vesicles, which represent one important focus of this thesis.

Most Gram-negative bacteria produce outer membrane vesicles (OMVs) that contains molecules, which are typically associated with the outer membrane of bacteria: the insoluble outermost membrane component and soluble portions of the luminal periplasmic content. However, the content of OMVs is not identical to those in the outer membrane; Some molecules can be enriched whereas others are entirely excluded from the OMVs relative to their abundance in the bacteria cell. OMVs exhibit a diverse biological activity including regulation of microbial interactions within bacterial communities (e.g., in biofilms) and the promotion of bacterial survival and virulence within the community and inside an animal host (e.g., review in Kuehn and Kesty 2005; Schwechheimer and Kuehn 2015). It is now widely accepted that OMV synthesis is a regulated and controlled process that occurs during the active growth of the bacteria cells (Elhenawy et al., 2014). For many years, the study of OMVs has primarily focused on their role in pathogenic infection; through manipulation of the host immune system and establishment of a replicative niche (Amano et al. 2010; reviewed in Ellis and Kuehn 2010; MacDonald and Kuehn 2012). Only recently, studies have begun to investigate the function of OMVs in the establishment of beneficial associations (Shen et al., 2012; Elhenawy et al., 2014). Unlike secretion systems that require a direct contact with the host cells, OMVs allow long-distance transport of microbial factors (Bomberger et al., 2009; Ellis and Kuehn, 2010; Kulp and Kuehn, 2010; Shen et al., 2012).

Recently OMV function in the squid-*Vibrio* model was investigated and published in two sequential studies (Aschtgen et al., 2015; Aschtgen et al., 2016). *Vibrio fischeri* grown in culture has been reported to produce OMVs that are part of the symbiont's biofilm formation (Shibata and Visick, 2012). Aschtgen et al. (2015) demonstrated that addition of purified OMVs to the seawater containing juvenile squids is sufficient to induce haemocyte trafficking activity at levels to that induced by the WT bacteria. Further, the authors have identified PGN and LPS derivatives inside *V. fischeri* OMVs, but not TCT. In a subsequent study, purified OMVs induced late-stage apoptosis and regression of ciliated appendages; two developmental events that are known to be induced by the synergy effect of PGN and LPS (Aschtgen et al., 2016). They also determined that all LPS that is being secreted from *V. fischeri* is associate with OMVs.

Since purified *Vibrio fischeri* OMVs were shown to induce host phenotypes and that *Vibrio fischeri* cells are able to induce changes in host tissues in which they have either a direct association with (i.e., crypts epithelium) or are several cell layers away (i.e., superficial epithelium; for example, secretion of EsPGRP2 into the mucus shedding from these cells, suppressing mucus secretion, regression of the appendage etc.; McFall-Ngai and Ruby 1991; Nyholm et al. 2002; Troll et al. 2010), it has been speculated

that OMV secretion can become important in this symbiosis and might be used as vehicles to transport chemical compounds into the host.

Together, their findings indicate that *V. fischeri*-derived OMVs may play an important role in host developmental response to the symbiont.

III. NanoSIMS as a tool to study animal-microbe association

Nanoscale secondary-ion mass spectrometry (NanoSIMS) is an ion microprobe technique that combines high spatial resolution isotopic imaging with high mass resolution mass spectrometry to provide chemical and isotopic analyses of up to seven different isotopes simultaneously (multi-collection). The NanoSIMS is capable of mapping almost all elements in the periodic table (those that ionize efficiently from a given matrix) at high spatial resolution, even if present in very low concentrations, typically down to ppm-at% (review in Hoppe et al. 2013). In combination with experiments in which molecules (e.g., micronutrients, amino acids) enriched in otherwise low abundance stable isotopes (such as ^{13}C and ^{15}N) are introduced into an organism, the NanoSIMS can be used to image the uptake and/or transport of particular molecules, or their metabolic derivatives in tissue and cells.

Since its development in the 1990s, the NanoSIMS has found increasing use in the fields of material science (e.g., Valle et al. 2011), cosmochemistry (e.g., Floss et al. 2006; Hoppe 2006), and geochemistry (e.g., Stern et al. 2005; Wacey et al. 2011). In the last decades, the NanoSIMS has also been increasingly utilized in the field of biology to investigate a wide range of scientific questions. Biological NanoSIMS imaging of cells and tissues, ranging from bacteria to mammalian organs, include assimilation of ^{15}N -labeled ammonium and nitrate in corals and their symbiotic algae (Kopp et al., 2013), localization of ^{81}Br -labeled drugs in cancer cells (Lau et al., 2010), use of ^{15}N -labeled nucleic and amino acids to measure the turnover rates of proteins in hair-cell stereocilia (Zhang et al., 2012), incorporation of $^{15}\text{N}_2$ and $^{13}\text{CO}_2$ to measure phenotypic heterogeneity in bacterial populations (Zimmermann et al., 2015), and incorporation of ^{15}N -thymidine to understand cell renewal in mammalian heart tissue (Senyo et al., 2013), to give a few examples. Despite this increase in biological-oriented NanoSIMS studies in recent years, the NanoSIMS technology seems to be little known in the fields of biology and life science in general.

A. Fundamentals of NanoSIMS

The physical basis of the NanoSIMS ion microprobe is the sputtering and extraction of secondary ions from a sample surface due to the continuous impact of a beam of primary ions, focused to a spot-size (full width half maximum) around 100 nm. The process can be summarized as follows: A solid, flat

sample is introduced into the ultra-high-vacuum environment of the NanoSIMS analysis chamber. A 16 keV primary beam of ions (either a Cs^+ or O^-) sputters atoms and small molecules from the top few nanometers of the sample surface. In this process, a small fraction of the sputtered particles becomes ionized and can be extracted with an electrical field, forming a beam of ions originating from the sample; this beam is referred to as the secondary ion beam. The fraction of the sputtered particles largely depending on the chemical species and the composition of the sample that is ionized (Shimizu and Hart, 1982). The secondary ion beam passes through a magnetic field that physically separates ions according to their mass-to-charge ratio, before they are counted individually in electron multiplier detectors. The CAMECA NanoSIMS 50L, which is utilized in our lab, is equipped with seven electron multipliers, i.e., permitting simultaneous detection of 7 different isotopes from the same sputtered volume. By rastering the primary beam over the sample, seven isotope images can be acquired to create maps of the distribution of different isotopes in the analyzed area. From these images, isotopic ratio images can be then calculated.

A unique feature of the NanoSIMS, compared with other magnetic-sector SIMS instruments, is the coaxial electrostatic lens system. The primary beam hits the sample surface perpendicular, which permits to focus the beam onto an extremely small spot on the sample surface (~80-200nm). The secondary ion beam is extracted through the same coaxial lens system, and its optical elements can be used to extract and focus this beam as well. This geometry permits to reduce the distance between the sample surface and the optical elements ('working distance' ~400nm), and thus produce a much smaller beam size, compared with conventional ion probe instruments (beam size typically 5-30 micrometers, 'working distance' ~1.5 cm). A controlled raster of the highly focused primary beam across the sample surface allows secondary ion images to be produced with a spatial resolution that can clearly resolve structures larger than a few hundred nanometers in lateral, linear dimension. However, there is a trade-off for obtaining high spatial resolution; reducing the primary beam diameter (high resolution) reduces the primary beam current, and correspondingly fewer secondary ions are produced, limiting the analytical precision.

Mass resolving power is the capability to efficiently separate a specific secondary ion from other ions with very similar mass, which is a requirement for isotopic ratio measurements, such as $^{13}\text{C}/^{12}\text{C}$ or $^{15}\text{N}/^{14}\text{N}$. The mass resolving power of the NanoSIMS is easily capable of separation ions such as $^{13}\text{C}^-$ from nearby interferences like $^{12}\text{CH}^-$, or $^{15}\text{N}^{12}\text{C}^-$ from $^{14}\text{N}^{13}\text{C}^-$. The secondary beam consists essentially of individual, charged isotopes or small molecular ions, fragments of larger molecules, the identity of which is not known.

B. Basic requirements and limitation of the NanoSIMS technique

While NanoSIMS is a very powerful and versatile method, there are several practical issues and considerations to take into account when conducting NanoSIMS analyses on a biological sample. Sample preparation is crucial to successful NanoSIMS analysis of a biological sample. Due to the high vacuum (10^{-10} – 10^{-9} torr), only dehydrated samples can be analyzed; live samples thus cannot be analyzed. There are numerous ways to prepare a biological sample for these analysis conditions, e.g., chemical fixation, freeze drying, cryo-fixation. However, one should take into consideration the advantage and disadvantage of each preparation process and the artefacts caused by the process (review in Grovenor et al. 2006). For example, during chemical fixation followed by dehydration, diffusible mobile molecules are lost or massively redistributed within cells or tissues (Hayat, 1981; Grignon et al., 1997). Thus, chemical fixation methods are suitable for the analysis of elements bound to macromolecules that are not easily diffusible or that are incorporated into insoluble cell structures (e.g., mitochondria, DNA). Furthermore, C and N isotopic compositions can be modified by the different sample preparation treatments. For example, chemical fixation, resin-embedding, and/or different hybridization procedures; (Berry et al., 2013; Musat et al., 2014; Woebken et al., 2015) introduce large amounts of C into a biological tissue, which might dilute the original C isotopic signatures in the sample. In this case, the measured $^{13}\text{C}/^{12}\text{C}$ ratios of an isotopically enriched sample represent minimum values. However, C isotopic measurements are not the main topic of this dissertation, in which the focus was placed on N isotopic NanoSIMS imaging.

Sample topography can lead to edge- or surface charging effects; i.e., modify secondary ion extraction. Samples with relatively flat surfaces (surface roughness $< 2 \mu\text{m}$) are thus highly preferable. Polished or sectioned (i.e., with ultramicrotome) resin-embedded samples have been proven to not only be sufficiently flat, but also free of surface charging effects if coated by a thin (ca. 20 nm) layer of gold or other highly conductive metals prior to NanoSIMS analysis.

Despite the use of a highly focused and low-current primary beam, NanoSIMS is a destructive technique. The high energy employed by the primary beam is sputtering (and hence eroding) the sample surface during analysis. In general, however, it is possible to image a thin section (about 70 nm in thickness) for about an hour, long enough to obtain good quality isotopic images, before the primary beam penetrates through the section.

NanoSIMS imaging is often used in combination with light microscopy (current study), electron microscopy (TEM and SEM; Carpenter et al. 2013; Frisz et al. 2013; current study) and atomic force microscopy (AFM; Rakowska et al. 2013) in order to reveal cellular and sub-cellular structures that might be difficult to distinguish from NanoSIMS images alone, or to identify suitable area of interests in samples prior to NanoSIMS analysis.

C. Exploring host-microbe associations with the NanoSIMS

Although numerous studies have investigated the interactions between microbes and their animal or plant host, to the best of my knowledge these studies have focused on nutrient transfer and metabolic processes. Work in this area has included localization of ^{15}N -labeled nitrogen-fixing bacteria inside their coral larvae host (Lema et al., 2015), the transfer of fixed-nitrogen molecules from the bacteria to their marine shipworm host (Lechene et al., 2007), and the incorporation of labeled C- and N-containing photosynthates translocated from symbiotic algae to their coral host (Kopp et al., 2013; Kopp et al., 2015). Several studies have examined the transfer of molecules in the reverse direction, i.e., from the host to its symbionts. For example, Kaiser et al. (2015) studied the release of newly photoassimilated C and N from plant roots to support the nutrient demand of their associated soil microbes. Berry and coworkers (2013) combined FISH and NanoSIMS to characterize utilization of host proteins by the gut microbes. The intestinal microbial population was observed to forage on host-derived labeled proteins that are secreted into the mucin.

D. NanoSIMS as an alternative method to visualize proteins and molecules in the cell

Visualization of molecules in biological tissue can provide clues to their function and regulation and is, in general, central to understanding molecular and cellular biology. A widespread method to track molecules in biological systems is optical imaging of fluorescent probes. A vast array of different fluorescent probes exists, including fluorescent proteins (e.g., GFP, SNAP-tag), fluorescent dyes (e.g., Alexa), and fluorophore-labeled molecules (e.g., protein specific antibodies) (Crivat and Taraska, 2012). Fluorescence microscopy techniques allow to image molecules and proteins inside cells, tissue, and animals and to monitor binding and interaction between proteins. Although the development of new optical imaging probes and advanced imaging technologies based on fluorescence microscopy has rapidly advanced our understanding of the properties of biological molecules, fluorescent probes have some limitations. Fluorescent moieties may perturb the structure, size, and function of their molecular target and thus alter the (sub)cellular localization, or may be cleaved off by the metabolic activity of the cell before or during observation. Additional challenges include background fluorescence and the probe stability (Crivat and Taraska, 2012). A good illustration of some of these issues is provided by the study of Puckett and Barton (2009) who investigated the subcellular distribution of Ru-octaarginine conjugate with or without a fluorescent tag. Under the same incubation conditions, the fluorescent-labeled conjugate entered the nucleus whereas the non-labeled conjugate did not. Finally, it is noted that most of the conventional fluorescence microscopes are limited in resolution by the wavelength of light, typically 200-700 nm.

Unlike the fluorescent probes, the use of stable isotopes to label a specific molecule has little or no impact on their shape, or biological function, and such isotopic labeling raises the possibility to trace

these molecules, or their derivatives, with the NanoSIMS. With its high spatial resolution and high sensitivity, combined with the ability to correlate isotopic images with other sub-cellular or ultrastructure level imaging techniques, the NanoSIMS opens up exciting new opportunities to address complex scientific questions, such as the study of host-symbiont molecular exchange, the topic of this PhD thesis.

In this thesis work, NanoSIMS isotopic imaging was combined with transmission electron microscopy (TEM) imaging to investigate the chemical dialogue between the symbiont *V. fischeri* and its squid host *E. scolopes* during initiation of the symbiosis. More specifically, the spatio-temporal dynamics of transfer and localization of ^{15}N -labeled compounds from *V. fischeri* bacteria cells into the squid was determined. The key questions addressed were:

- 1) Can we visualize and localize *V. fischeri* morphogen-induced signaling molecules, specifically the PGN monomer, TCT, inside squid tissues using the NanoSIMS?
- 2) How are *V. fischeri*-derived compounds distributed within the light-organ compartments (e.g., appendage, pore and crypts) and in which cellular and sub-cellular organelles? Do they remain localized or do they travel through adjacent cells to distant sites of action? and where in the cells are they accumulating?
- 3) Is any potential molecular transfer that can be imaged with the NanoSIMS restricted to the light organ, where symbionts are in close association with host cells?
- 4) Is these transfer specific to squid inoculated with *V. fischeri* cells or do other non-symbiotic, Gram-negative bacteria (*Vibrios* and non-*Vibrios*) can induce similar enrichment patterns?

We used the exclusive symbiotic association between the squid and its bioluminescent bacteria to investigate molecular transfer underpinning host-microbe interaction.

This thesis manuscript is composed of the following chapters:

Chapter 1 presents an effort to detect and localize purified ^{15}N -TCT inside squid tissues. I then discuss the results and how these results led us to perform the subsequent experiment of exposing squids to ^{15}N -labeled small organic molecules. Finally, I discuss how the findings from both experiments led to the formulation of the experiments described in the next chapters.

Chapter 2 presents the distribution of ^{15}N -enrichment within the light-organ compartments and in other organ and tissue types inside juvenile squids that were exposed to ^{15}N -labeled *V. fischeri* cells and OMVs during the initiation of symbiosis. The intracellular localization of ^{15}N -enrichment in the light organ of the squid host is then described. In this Chapter, I focus on the shared ^{15}N -enrichment patterns that were observed in the whole-bacteria and OMVs treatments and discuss potential explanations for these results, whenever possible.

Chapter 3 presents the intracellular localization of ^{15}N -enrichment in the light organ of juvenile squids that were exposed to ^{15}N -labeled closely related *Vibrios* (*Vibrio parahaemolyticus* and *Photobacterium leiognathi*) and non-*Vibrio* (*Escherichia coli*) bacteria cells or their OMVs few hours after hatchings. Here I asked whether the ^{15}N -enrichment patterns that was observed in the squid in Chapter 2, is specific to the symbiotic partner.

General procedure for NanoSIMS analysis

Here, I outline the general procedures employed in this study for sample preparation prior to microscopy and NanoSIMS and provide details about the subsequent isotopic analysis of the samples in the NanoSIMS. These protocols were applied across all experiments presented in this thesis.

I. Samples preparation for TEM and NanoSIMS

Purified OMVs. Purified OMVs were visualized with TEM either by negative staining or ultrathin-sections of resin embedded material. For negative staining, 2-4 μL of sample were applied to glow-discharged carbon-coated copper grids (400-mesh; Electron Microscopy Sciences) and allowed to settle for ~ 1 min. Samples were then washed few times by floating grid sample-side down on drops of deionized water, followed by quick staining with 2% uranyl acetate. Grids were air-dried completely before visualization in the TEM. To assess the integrity of the OMVs after the chemical fixation procedure (see below for a detailed protocol), purified OMVs were fixed based on the fixation protocol that was used on the whole animal, with few modifications. The pelleted OMVs obtained after ultracentrifugation (2 h, $173,000 \times g$) were fixed in 2.5% glutaraldehyde and 1.5% potassium hexacyanoferrate (II) trihydrate prepared in dPBS. Samples were then post-fixed with 1% OsO_4 , dehydrated in ethanol (30%, 70% and 100%) and pure acetone before infiltration and embedding in Spurr's resin. OMV blocks were then sectioned and image in the TEM and NanoSIMS following the same procedure as for host tissue (see below).

Host tissue. Animals were fixed in a mixture of 2% paraformaldehyde and 2% glutaraldehyde prepared in marine phosphate-buffered saline (mPBS; 50 mM sodium phosphate buffer with 0.45 M NaCl; pH 7.4) at room temperature over 12 h. Rinsed animals were post-fixed for 1 h in 1% OsO_4 prepared in mPBS and dehydrated in ethanol series 30%, 50%, 60%, 70%, 80%, 90%, 95%, and 100%. Tissue were then infiltrated with a mix of 1:1 propylene oxide: unaccelerated Spurr's resin for 2 h followed by a mix of 1:9 propylene oxide: unaccelerated Spurr's resin for 48 h before transfer to fresh, unaccelerated Spurr's resin for one week. During each step of the fixation-infiltration procedure, samples were placed on a rotator at room temperature.

Samples were then embedded in 100% accelerated Spurr at 60°C for 48 h. Semi- and ultra-thin sections ($\sim 0.5 \mu\text{m}$ and $\sim 70 \text{ nm}$, respectively) were cut with an ultramicrotome (Reichert Ultracut S, Leica). Semi-thin sections were stained with Toluidine blue-Borax and imaged with a light microscope Leica DMRB equipped with AxioCam MRc5 camera (Zeiss, Germany) to aid in navigating around the squid tissues. Sections for NanoSIMS analysis were prepared in two different ways:

- (1) High resolution imaging for correlative TEM and NanoSIMS. Ultra-thin sections (~70 nm) were mounted on either formvar-coated alphanumeric grids (200 mesh) or oval slot grids with polystyrene coating. Grids were then counterstained with 4% uranyl acetate and Reynolds lead citrate, then observed at 80 kV with a TEM Philips CM100 (EMF, Unil). Prior to the NanoSIMS imaging of the slot grid samples, small holes defining the area of interest were punched in the section to mark the corners of the area to aid in navigating the sample. Subsequently, the formvar film with the section was carefully separated from the grid and mounted on a 10 mm coverslip (procedure done in collaboration with Jean Daraspe, EMF, Unil). This procedure allowed us to obtain better stability of the section under the NanoSIMS ion beam.
- (2) Large area coverage for statistical analysis. Semi-thin sections (~0.5 μm) were mounted on 10 mm coverslips and stained with Toluidine blue only (pH 9.5).

II. NanoSIMS analysis

Quantitative N isotopic imaging, correlated with either optical (tissue level) or TEM ultrastructural microscopy, was the focus of this thesis work. To image and quantify the distribution of ^{15}N -enrichment within juveniles *E. scolopes* at the cellular and sub-cellular levels, sample areas of interest were first selected by EM or optical microscopy observations and then analyzed with the LGB NanoSIMS 50L ion microprobe (CAMECA, France). Typically, ultrathin-sections sample on TEM grids were mounted on 10 mm aluminum stubs using copper tape, or semithin sections on glass cover slips. These were coated with a roughly 10 nm layer of gold to prevent surface charging. In the NanoSIMS the samples were bombarded with a 16 keV primary ion beam of (1-3 pA) Cs^+ focused to a spot size of about 100-150 nm on the sample surface. Secondary molecular ions of $^{12}\text{C}^{14}\text{N}^-$, $^{13}\text{C}^{14}\text{N}^-$ (to measure C isotopic compositions; rarely used) or $^{12}\text{C}^{14}\text{N}^-$, $^{12}\text{C}^{15}\text{N}^-$ (to obtain N isotopic compositions) were simultaneously collected in electron multipliers at a mass resolution ($M/\Delta M$) of about 9000, which is enough to resolve the $^{12}\text{C}^{15}\text{N}^-$ from $^{13}\text{C}^{14}\text{N}^-$ and $^{13}\text{C}^{14}\text{N}^-$ from $^{12}\text{C}^{14}\text{N}^-$, respectively. Charge compensation was not necessary. Typically images of $40\times 40\ \mu\text{m}$, $25\times 25\ \mu\text{m}$, or $15\times 15\ \mu\text{m}$ with 256×256 pixels were obtained for $^{12}\text{C}^{14}\text{N}^-$, $^{13}\text{C}^{14}\text{N}^-$ and $^{12}\text{C}^{14}\text{N}^-$, $^{12}\text{C}^{15}\text{N}^-$ by rastering the primary beam across the sample surface with a dwell-time of 5 milliseconds. Each isotope image consists of number of sequential sub-images (generally 5-10) acquired in order to minimized counting error on the isotopic ratios. These sub-images were corrected for machine drift and added together. The $^{15}\text{N}/^{14}\text{N}$ ratio distribution was obtained from the total count image by taking the ratio: $^{12}\text{C}^{15}\text{N}^-/^{12}\text{C}^{14}\text{N}^-$. ^{15}N -enrichment were expressed in the delta notation and given in units of permil as follows:

$$\delta^{15}\text{N} (\text{‰}) = \left(\frac{R_{\text{sample}}}{R_{\text{standard}}} - 1 \right) * 1000$$

Where R_{sample} is the measured $^{15}\text{N}/^{14}\text{N}$ ratio and R_{standard} is the natural $^{15}\text{N}/^{14}\text{N}$ ratio measured in non-labeled control samples prepared in identical manner. R_{standard} measurements were obtained on each new day of NanoSIMS analyses and varied very little from day to day (insignificantly compared with the observed isotopic enrichment). ^{15}N -enrichment was considered significantly labeled when above 3σ of the average $^{15}\text{N}/^{14}\text{N}$ ratio measured in similar areas of unlabeled control samples.

In experiments where the levels of ^{15}N -enrichment were compared among the light-organ compartments, ^{15}N -enrichment was expressed as a Relative Labeling Index (RLI), to compensate for the high variability among individual squids. RLI was defined as:

$$\text{RLI} = \frac{\text{^{15}N-enrichment of a nucleolus in a given light-organ compartment}}{\text{average ^{15}N-enrichment in nucleoli from all compartments of the specific squid light-organ.}}$$

NanoSIMS data processing and ROIs definition. Data were processed using the L'IMAGE® software. $^{15}\text{N}/^{14}\text{N}$ ratio images were constructed using a 3*3 pixel moving average smoothing algorithm. Regions Of Interest (ROIs) were defined from the $^{15}\text{N}/^{14}\text{N}$ ratio images, and the following ROIs were quantified:

- (1) ^{15}N -enrichment in the bacteria cells or the purified OMVs. Analysis was performed either on a drop of solution containing the cells or purified vesicles that were air-dried or on resin-embedded samples (cells or purified vesicles). ROIs were defined by drawing a contour around a single bacteria cell or around an area that integrated several cells or vesicles (OMVs are too small to be resolved as individual vesicles in the NanoSIMS).
- (2) Cytoplasm (excluding the nucleus), Golgi apparatus (specific to Chapter 3), nucleus (excluding nucleolus) and nucleolus (Fig. 2-1). In some cases, a line was drawn through a specific area in the cell and a $^{15}\text{N}/^{14}\text{N}$ profile was obtained for each point along the line (e.g., Fig. 2-1).

Chapter 1 Can we localize morphogen-induced signaling molecules in host tissues?

1.1 Detection of TCT in host cells

Chemical communication between microorganism and their eukaryotic host is the fundamental basis for forming and establishing a symbiosis. This chemical communication, referred to in the literature as signaling, is responsible for triggering highly specific cellular responses in both partners, and can determine whether a microbial infection causes disease or contributes to the healthy development of the host, e.g., through the establishment of a stable, symbiotic relationship. The molecules that are involved in this reciprocal dialogue are highly diverse, often very specific (i.e., are effective even at very low concentration, typically $\leq 10^{-8}$ M; Alberts et al. 2014), and might act in a localized manner via signal- (i.e., ligand) receptor interaction. Because of the great interest in understanding this molecular dialogue, much work has been done to help identify some of the molecules involved, mainly in pathogenic associations. However, at the subcellular level, information about uptake, distribution, and accumulation of such signaling molecules in symbiont host tissue is still largely absent. In this Chapter, I describe work to isotopically image, using the NanoSIMS ion microprobe, the transfer into host cells of the signaling molecule, PGN monomer (or 'tracheal cytotoxin', TCT), which is excreted by *V. fischeri* and is essential for the initiation and establishment of a stable symbiosis, (c.f. General Introduction). However, these results are preceded by a few paragraphs outlining the state-of-the-art knowledge about the role of these molecules in the establishment of the squid-*Vibrio* symbiosis.

In all Gram-negative and some Gram-positive bacteria, PGN is composed of repeated subunits of N-acetylglucosamine and N-acetylmuramic acid connected by a small number of amino acids including D-alanine, D-glutamic acid, *meso*-diaminopimelic acid, and L-alanine (Cloud-Hansen et al., 2006). PGN is a dynamic polymer that undergoes remodeling and recycling during bacterial growth. Lytic transglycosylases, LtgA1, LtgA2 and LtgD cleave the PGN into monomers. The permease AmpG then brings these monomers into the bacterial cell's cytoplasm (Jacobs et al., 1994), where they are recycled and ultimately re-incorporated into the remodeled cell wall (Goodell, 1985).

Only a few Gram-negative bacteria are known to release biologically active PGN monomers that have a profound effect on animal epithelial cells. Although bacterial cell lysis produces PGN derivatives that can elicit inflammatory responses of the immune system, this process is distinct from the active release of PGN in growing Gram-negative bacteria (Cloud-Hansen et al., 2006). This latter phenomenon was first described for the pathogens *Bordetella pertussis* and *Neisseria gonorrhoeae*, where release of

PGN monomers causes whooping cough (Rosenthal et al., 1987) and gonorrhoea (Sinha and Rosenthal, 1980), respectively. When released by *B. pertussis* the PGN monomer is referred to as TCT in the literature. In the following, the names 'PGN monomer' and 'TCT' will be used interchangeably. Although the mechanism of TCT production is not well understood, the lytic transglycosylase enzymes are thought to contribute to its production in some bacteria (Cloud-Hansen et al., 2006).

When released by *V. fischeri*, TCT acts as a potent morphogen to induce the normal morphogenesis of the squid light organ (Koropatnick et al., 2004). A TCT concentration as low as 10 nM induces a detectable morphogenic response and the host response is saturated at a TCT concentration of 1 μ M. TCT triggers the infiltration of macrophage-like haemocytes (blood cells) into the blood sinuses of the ciliated epithelial fields (Koropatnick et al., 2004; Koropatnick et al., 2007; Altura et al., 2013). Late-stage apoptosis (DNA fragmentation) and regression of these cells is induced by the synergistic effects of the PGN monomer and the lipid A component of LPS (Koropatnick et al., 2004; Troll et al., 2009). Although the PGN monomer alone is not able to induce apoptosis, it is necessary for the induction of late-stage apoptosis in the morphogenic program (Troll et al., 2009). These findings suggest that TCT plays a crucial role in the squid-*Vibrio* symbiosis (Koropatnick et al., 2004).

PGN recognition proteins (PGRPs) are innate immunity molecules, involved in sensing bacterial PGN in most animals. Five PGRPs have been characterized in *E. scolopes* (EsPGRPs), but the precise mechanism of TCT sensing by squid host cells is not understood. Immunocytochemistry of EsPGRP1, a nuclear protein that occurs in the nuclei of epithelial cells throughout the squid body, revealed that the loss of this protein from the nuclei of the superficial epithelium of the light organ correlates with the entry of these cells into late-stage apoptosis (Troll et al., 2009). Further, purified TCT alone (10 μ M) was capable of inducing loss of EsPGRP1 at a level similar to wild-type (WT) *V. fischeri* exposure. It is unclear whether the activity of the diffusible TCT is the result of a direct interaction with EsPGRP1, or works through a signal transduction pathway (Troll et al., 2009). In *Drosophila melanogaster*, the mechanism of TCT detection in the gut involves the extracellular PGRP-LC and intracellular PGRP-LE (Neyen et al., 2012), similar to the intracellular NOD1 receptor, which is used to detect bacterial PGN in epithelial cells (Magalhaes et al., 2005).

The mechanism of TCT delivery into host cells is also unknown. Purified *V. fischeri* outer membrane vesicles (OMV) induce haemocyte trafficking in the squid reminiscent of squids exposed to WT *V. fischeri* cells, but OMVs do not contain TCT (Aschtgen et al., 2015). Their data suggest that release of TCT and its delivery into host cells is independent of the process of OMV production.

Despite the importance of PGN, there is a lack of methods that enable real-time spatiotemporal imaging of PGN in live cells (Daniel and Errington, 2003; Olrichs et al., 2011; Kuru et al., 2012). Some of

the current methods limitations are due to toxic effects and poor membrane permeability of the probes. Therefore, stable-isotopic labeling of PGN molecules, where the molecular structure and function are not perturbed, combined with high spatial resolution isotopic imaging obtained, e.g., with the NanoSIMS instrument, might allow tracking PGN derivatives inside host cells. An initial effort to localize ^{15}N -labeled TCT within the light-organ epithelial cells using the NanoSIMS was conducted by Troll and co-workers (2009). In these experiments the juvenile squids were exposed to a concentration of $50\ \mu\text{M}$ ^{15}N -enriched TCT for durations ranging from 15 min to 24 h. However, the actual ^{15}N -enrichment level of the TCT was unknown and preliminary NanoSIMS imaging showed no traces of ^{15}N -enrichment in the squid light-organ tissues. Here, using different concentrations of TCT, incubation times, and correlated with detailed TEM observations, I present a more systematic attempt to use the NanoSIMS to localize ^{15}N -labeled TCT in squid tissues. These experiments are followed by a presentation of experiments designed to explore the sensitivity of the juvenile squids to small organic molecules, with the aim of understanding the broad chemical interaction that the squid might experience in its natural seawater habitat.

1.1.1 Materials and Methods

1.1.1.1 TCT purification

Isotopically labeled TCT was isolated from the supernatant of culture-grown *Bordetella pertussis* supplemented with ^{15}N -L-glutamic acid (98%; Cambridge Isotope Laboratories, Inc. MA, USA) as described previously (Cookson et al., 1989). *B. pertussis* TCT is structurally identical to that of *V. fischeri*. The Endotoxin concentration (20 EU/mL) in the purified TCT solution was considered negligible once it was diluted in the final seawater used to inoculate the squid (125 μL diluted in 20 mL FSIO). Purification of TCT by reversed-phase HPLC and endotoxin analysis were obtained in collaboration with Prof. William E. Goldman, Department of Microbiology and Immunology, University of North Carolina, USA). TCT was stored at 4°C until use. The ^{15}N -enrichment level in the purified TCT solution was a factor of about 300 times higher than the natural $^{15}\text{N}/^{14}\text{N}$ ratio as measured by the NanoSIMS.

1.1.1.2 Squid inoculation with purified TCT

Newly hatched animals were exposed to either $1\ \mu\text{M}$ ^{15}N -enriched TCT for 1 and 3.5 h, respectively. At this TCT concentration the response level of the squids to purified TCT is saturated (Koropatnick et al., 2004). At the end of the incubation, squid samples were fixed and prepared for observation by microscopy and were imaged with the NanoSIMS as previously described (see 'General procedure for NanoSIMS analysis').

1.1.2 Results and discussion

Consistent with the study by Troll et al. (2009), no detectable ^{15}N -enrichment was observed in the appendage and crypt epithelium in squids exposed to purified TCT molecules for 1 and 3.5 h ($n=2$ for each time point; Fig. 1-1). Therefore, these results do not provide verification that TCT molecules are indeed taken up into host epithelial cells of the light organ.

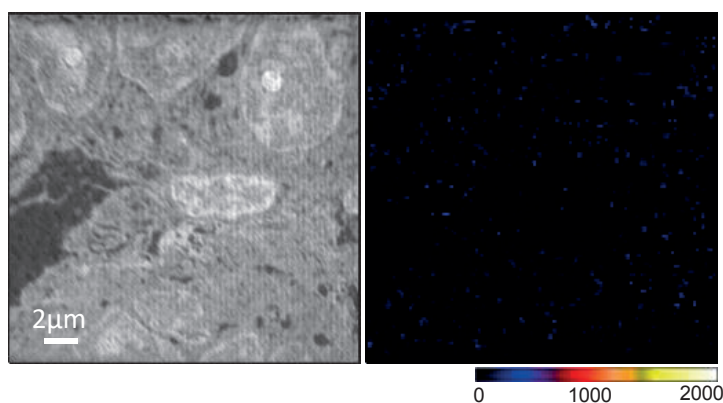


Fig. 1-1. ^{15}N -enrichment ($\delta^{15}\text{N}$) in epithelial cells lining the appendage, 3.5 h post exposure to ^{15}N -TCT. Left panel show tissue structure (NanoSIMS $^{12}\text{C}^{14}\text{N}$ image). Right panel show corresponding, quantified NanoSIMS $^{15}\text{N}/^{14}\text{N}$ ratio image. ^{15}N -enrichment inside host tissues and cells was not different from background levels. Values for the NanoSIMS scale are expressed in ‰ (see ‘General procedure for NanoSIMS analysis’).

Possible reasons for the absence of detectable ^{15}N -enrichment in any of the NanoSIMS images from this TCT experiment are discussed in the following. Throughout this discussion, it is assumed that the TCT molecules were effectively fixed, and hence not lost wholesale from the tissue, during the standard fixation-infiltration procedures employed in preparation for TEM and NanoSIMS imaging (Hayat, 1981). However, pervasive loss of TCT from the tissue cannot be ruled out with these methods (Hayat, 1981).

Based on its molecular mass (921 Daltons) and chemical characteristics (hydrophilic and polar; 3 carboxyl and 3 hydroxyl groups), it is unlikely that TCT, although a relatively small molecule, can passively diffuse through the host cell membrane (Alberts et al., 2014). Thus, to directly interact with a target cell, TCT needs to either bind to a cell-surface receptor (e.g., EsPGRP3, EsPGRP4) or get trafficked into the cell via the bacterial secretion system and then bind to an intracellular receptor (e.g., EsPGRP1) (Magalhaes et al., 2005). In some cases, more than one PGRP receptor is required to sense TCT, forming a homodimer or heterodimer complex with other PGRPs (e.g., TCT binding in *D. melanogaster*; Royet et al. 2011; Neyen et al. 2012). Either way, to be able to detect ^{15}N -enriched TCT with the NanoSIMS, it must accumulate either at the membrane or in specific sub-cellular structures inside the host tissues, in concentrations high enough that a $^{15}\text{N}/^{14}\text{N}$ ratio clearly distinguishably from surrounding, unlabeled tissue. In a typical NanoSIMS image, unambiguous detection of ^{15}N -enrichment requires an anomaly on

the order of 5% (50 ‰) relative to the natural $^{15}\text{N}/^{14}\text{N}$ ratio in an area several pixels large (i.e., 300 x 500 nm). Because the chemical composition in a given pixel is poorly constrained and can vary strongly as a function of, for example, the tissue to epoxy resin ratio, it is difficult to establish how many molecules of TCT are required within a given area for clear detection. The cell membrane is typically 7.5-10 nm thick (in a transversal cut), i.e., much smaller than the primary beam of the NanoSIMS (about 100 nm). Thus, if TCT accumulates exclusively on the exterior of the cell membrane, clear detection would be particularly difficult because the ^{15}N -enriched signal would be diluted by N from unlabeled material adjacent to the membrane within the same pixel.

Other characteristics of the PGRPs receptors can also contribute to the inability to visualize TCT with the NanoSIMS. PGRPs can be differentially expressed through the tissue and/or inhomogeneously distributed along and across the cells. For example, in the squid, transcripts of EsPGRP5 are found only in host haemocytes (Collins et al., 2012). In the Pacific oyster, a wide distribution of diverse PGRPs was found expressed across the oyster body. For instance, CgPGRP-S1S was expressed in the gills and mantle, -S2 in the haemocyte and -S3 in the digestive gland (Itoh and Takahashi, 2008). Tissue specific expression patterns are also known for other invertebrate (e.g., *D. melanogaster*) and vertebrates (*Danio rerio*, zebrafish; review in Royet et al. 2011). Because we do not know which of the EsPGRPs is the one that binds TCT and/or its localization in the squid tissue, it is possible that the wrong tissues were analyzed.

Furthermore, increasing evidence suggests that *V. fischeri* signaling molecules, including TCT, act locally on only few host cells and then affect other cells remotely through signal transduction pathways (e.g., transport of signals between neighboring cells). Exposed to an environmentally relevant concentration of *V. fischeri* (about 5000 cells/mL of seawater) during the first few hours after hatching, only 3-5 bacterial cells form an aggregate, which interacts intimately with two to three of the nearest host cells in the ciliated appendage (Altura et al., 2013). However, these few bacterial cells are able to induce a robust cell phenotype of TCT-triggered haemocyte trafficking (Altura et al., 2013) and changes in gene expression in the light-organ tissues (Kremer et al., 2013). Based on observed secretion rates of TCT by *V. fischeri* cells during log-phase growth cycle, ~5000 cells/mL would release only about 2 pM of TCT to the surrounding seawater. However, 2 pM of TCT is far below the concentration needed to trigger a morphogenic response in the host light organ (around 10 nM) (Koropatnick et al., 2004; Koropatnick et al., 2007; Altura et al., 2013). Thus, the fact that the juvenile squid light organ responds to an aggregation of only 3-5 *V. fischeri* cells on the appendage suggests at the same time a highly specific activity of TCT and that very locally delivered (and thus higher) concentrations of TCT are needed to trigger a host response – all of this argues against a high accumulation of TCT anywhere inside host tissues or on its external cell membranes.

Considering that this analysis did not detect any ^{15}N -enrichment in the squid light organ after exposure to purified TCT, and that this observation was consistent with earlier findings (Troll et al., 2009), I argue that localization of morphogen-induced signaling molecule TCT, inside the squid host tissue, cannot be resolved with the NanoSIMS under the specific experimental conditions used in this study. In order to enhance detection of TCT uptake by the host cells using NanoSIMS, an experiment in which cultures of haemocyte cells were exposed directly to high concentrations of ^{15}N -enriched TCT and subsequently imaged with the NanoSIMS should be considered.

At the same time, it is expected that other molecules, in addition to the highly specific PGN monomer, are exchanged between symbiont and host. The more general chemical 'conversation' between the symbiotic partners might very well include a wide spectrum of other small molecules, such as metabolites, amino acids, peptides etc., which would participate in numerous processes inside the host cells, including metabolism, protein synthesis, osmoregulation, etc. Experiments to investigate the broader molecular transfer from the environment to the host squid cells are presented in the following section.

1.2 Uptake of small organic molecules by juvenile squids

In their natural seawater habitat, marine organisms are continuously exposed to a myriad of particulate and dissolved organic matters. Particulate materials include small organisms such as plankton, bacteria, and smaller fragments of microbial biomass, whereas dissolved organic matters include metabolic products of different organisms, amino acids, carbohydrates, lipids, and macromolecules (Lee et al., 2004). From its first postembryonic ventilation, seawater harboring these organic substances are brought into the squid's body cavity at high rate. These materials then become accessible to squid tissues that are in direct contact with seawater, such as gills, the light organ, tentacles, and the digestive gland.

The ability to uptake dissolved organic matter (DOM; mainly amino acids and sugars) is a characteristic of most marine invertebrates (Thomson, 1874; Pütter, 1909; Stephens, 1988; Wright and Manahan, 1989; Manahan, 1990; Gomme, 2001). The total concentration of dissolved free amino acids (DFAA) in tropical reefs water are typically in the range of few nM to 1 μM (Ferrier, 1991; Schlichter and Liebezeit, 1991; Dove et al., 1997). Much work was carried out for over a century mainly focusing on the nutritional role of DFAA in adult invertebrates, such as molluscs (Thompson and Bayne, 1972; Stephens, 1988; Hoegh-Guldberg, 1999), annelids (O'Dell and Stephens, 1986; Stephens, 1988), and corals (Grover et al., 2008; Gori et al., 2014), where DFAA is an additional source of nutrients and energy, especially in tropical reef where particulate food is scarce. However, several studies on early developmental stages of marine invertebrate reported the great importance of DOM for non-feeding embryos and larvae (e.g.,

Shick 1975; Manahan et al. 1983, 1989; Jaeckle and Manahan 1992; Ben-David-Zaslow and Benayahu 2000) that were otherwise believed to depend entirely on endogenous reserves (e.g., Thorson 1946; Chia 1974). Genes supporting amino acids transport systems were characterized in embryos and larvae of echinoderm species demonstrating that some marine species have the ability to actively transport amino acids early in development (Allemand et al., 1985; Meyer and Manahan, 2009; Applebaum et al., 2013). The rate of amino acids uptake by marine invertebrate larvae that were exposed to a mixture of amino acids ranges between 0.8 to 8.8 pmol/h (Echiura, Manahan et al. 1989; Mollusca, Jaeckle and Manahan 1992; Echinodermata, Davis and Stephens 1984; Cnidarian, Ben-David-Zaslow and Benayahu 2000).

The experiments presented in the following had two main objectives: First, to determine the levels of ^{15}N -enrichment inside the light-organ tissues for a given extracellular concentration and second, to identify the intracellular localization of ^{15}N -enrichment in the epithelial cells of the appendages and crypts.

1.2.1 Material and Methods

A detailed procedure can be found in Supplementary information. Briefly, juvenile squids were incubated for 3.5 h in filter-sterilized (0.2 μm) Instant Ocean (FSIO) supplemented with $\sim 70\ \mu\text{M}$ of mainly ^{15}N -labeled amino acids and salts. At the end of incubation, squid samples were fixed and prepared for NanoSIMS analysis following the protocol described in 'General procedure for NanoSIMS analysis'. Sections of the light organs were imaged with TEM and/or light microscopy followed by NanoSIMS isotopic imaging to visualize and quantify the distribution of ^{15}N -enrichment within the epithelial cells of two light-organ compartments: appendages and crypts.

1.2.2 Results and discussion

After 3.5 h incubation with the ^{15}N -labeled amino acids mixture, ^{15}N -enrichment was heterogeneously distributed across the epithelial cells in the appendages and crypts (3 animals; Fig. 1-2). Overall, the appendage epithelia had higher ^{15}N -enrichment levels compared to the crypt epithelia; the subcellular enrichment patterns were, however, comparable (Fig. 1-2B; Table S 1-1). All cellular and subcellular compartments were highly enriched in ^{15}N ($> 500\text{‰}$). By correlating high resolution TEM and NanoSIMS images, it was possible to determine that the ^{15}N -hotspots were mainly co-localized with nucleoli and Golgi (Fig. 1-2). Smaller ^{15}N -hotspots were hard to identify ultrastructurally based on the TEM and NanoSIMS images, and were therefore not included in the following analysis. Strong ^{15}N -enrichment was also observed in the nuclei and cytoplasm. Note that although the ^{15}N -enrichment patterns were similar among individual squids, the levels of ^{15}N -enrichment were highly variable.

For statistical analysis, intracellular ^{15}N -enrichment was quantified for the entire cytoplasm, the nucleus, and the nucleolus, respectively. Systematically, the nucleoli exhibited the strongest

¹⁵N-enrichment among the organelles in these cells, with cytoplasm moderately labeled, and nuclei (excluding the nucleolus) with the lowest levels of ¹⁵N-enrichment. In the appendage, when compared to the cytoplasm, the nuclei were on average 22% less enriched ($p < 0.0001$) and nucleoli were 40% more enriched in ¹⁵N ($p = 0.006$) (Fig. 1-2B; Table S 1-1). In the crypts this pattern was less pronounced, with 13% less enrichment in ¹⁵N ($p = 0.02$) in the nuclei and 81% higher enrichment in the nucleoli ($p < 0.001$) (Fig. 1-2B; Table S 1-1) when compared to the cytoplasm.

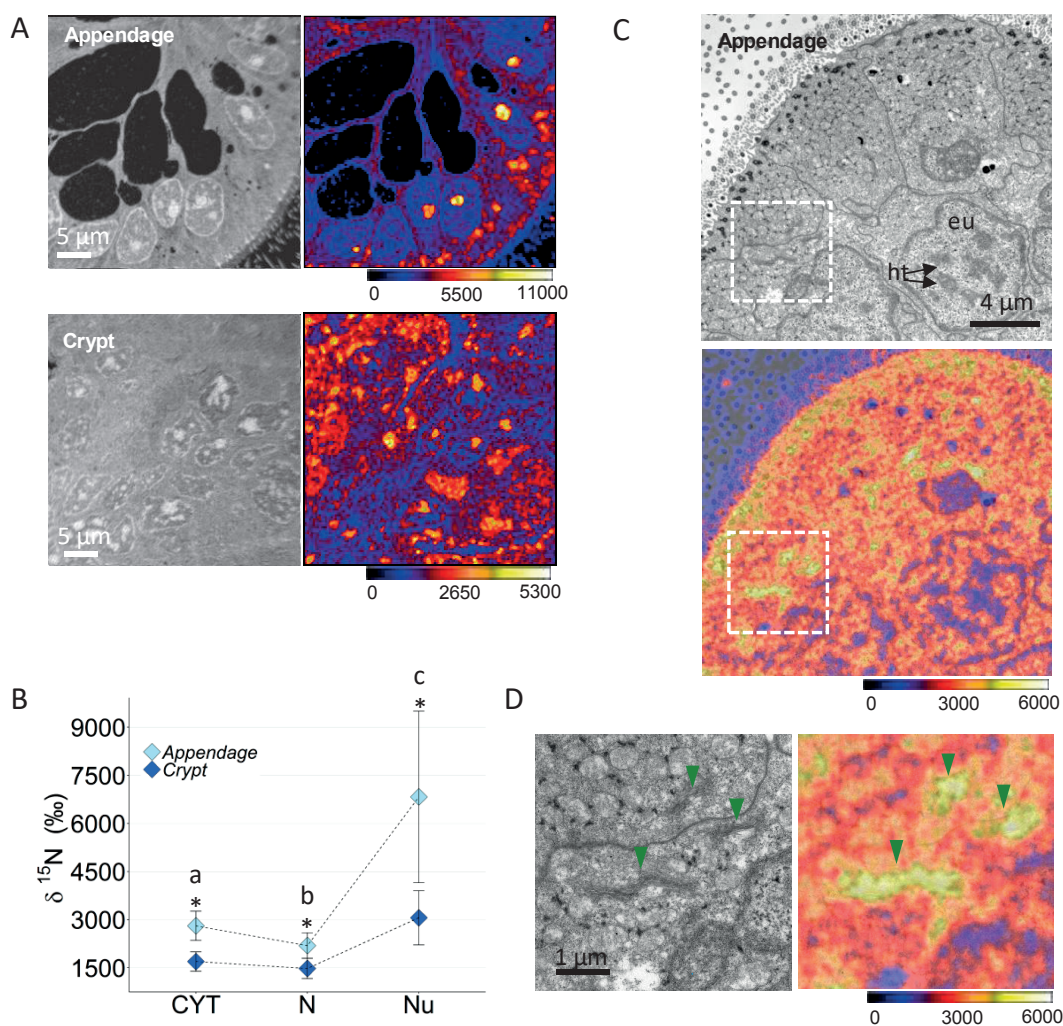


Fig. 1-2. ^{15}N -enrichment ($\delta^{15}\text{N}$) in squid epithelial cells of the light organ, 3.5 h post exposure to a mixture of ^{15}N -amino acids. (A) Left panel shows tissue structure (NanoSIMS $^{12}\text{C}^{14}\text{N}$: image). Right panel show corresponding, quantified NanoSIMS $^{15}\text{N}/^{14}\text{N}$ ratio image. (B) Distribution of ^{15}N -enrichment in cell organelles cytoplasm (CYT), nucleus (N), and nucleolus (Nu) in the appendage and crypt spaces (squids: 3 animals; cell organelles in each squid replicate: CYT: n=27-22; N: n=67-72; Nu: n=22-25, for appendage and crypt, respectively). Lower case letters indicate statistically significant differences between cell organelles (Table S 1-1). Asterisk indicate significant differences between compartments (Table S 1-1). Error bars represent one standard deviation. (C) Representative high resolution TEM (top) and NanoSIMS ratio image overlay (bottom) of the light-organ appendage. In the TEM image, euchromatin (eu; brighter grey) and the more condense chromatin, heterochromatin (ht; darker grey) are clearly visible. The high resolution images (n=2) allow for quantitative measurement of the ^{15}N -enrichment in specific organelles: nucleoli (12905 ± 318), euchromatin (2535 ± 211 , n=13) and heterochromatin (1968 ± 379 , n=13) in the nuclei and the Golgi apparatus (4204 ± 379 , n=8). Dashed boxes show representative locations of pictures zoomed in panel (D). (D) showing ^{15}N -hotspots colocalized with the Golgi apparatus (green arrowheads). Values for the NanoSIMS scale are expressed in ‰ (see 'General procedure for NanoSIMS analysis').

A previous study has examined the uptake of ^{15}N -aspartic acids ($20 \mu\text{M}$) by coral nubbins and found a ^{15}N -enrichment level of $\sim 75\%$ for the oral epidermis after 3.5 h incubation (Kopp et al., 2013), which is broadly consistent with the results on squids, after correction for the different concentration of amino acids used. These authors did not, however, provide information on the subcellular localization of

¹⁵N-enrichment inside the coral tissue. Another related study by Jiang et al. (2014) correlated scanning electron microscope (SEM) and NanoSIMS images to investigate the distribution of ¹⁵N in single MCF7 cancer cells exposed to ¹⁵N-glutamine (4 mM) for 24 h (Jiang et al., 2014). The general distribution pattern was comparable to this study, i.e., the relative ¹⁵N-enrichment factors in the different subcellular compartments were nucleoli> Golgi>nucleus (Fig. 1-2, current study).

How can we interpret the observed subcellular distribution of ¹⁵N-enrichment inside the squid cells? Amino acids are of fundamental biological importance for any cell. It is widely accepted that along with their pivotal role as building blocks of proteins and polypeptides, some amino acids also serve as regulators for key metabolic pathways and processes that are essential for the health, growth, development, reproduction, immunity, and homeostasis (Wu, 2009). Some examples include their involvement in regulation of gene expression (e.g., Kilberg et al. 2005), cell signaling (e.g., Ou et al. 2007), synthesis and secretion of low molecular weight hormones (e.g., Wu 2009), metabolism of nutrients (e.g., Meijer 2003) and oxidative stress (e.g., Brosnan 2001). Given their diverse physiological functions, it is not surprising that squid cells became quite strongly ¹⁵N-labeled as a result of exposure to ¹⁵N-enriched amino acids. Nonetheless, it was demonstrated that exposure of cells to amino acids primarily resulted in their participation in cell metabolism and synthesis of *de novo* proteins and for this reason they are broadly used in proteomics work. This concept will be elaborated in the following paragraphs.

Extensive efforts to visualize and quantify newly synthesized proteins were carried out over the last two decades with a variety of proteomics approaches, labeling techniques, and imaging methods. Such studies have revealed that the cell proteome is highly dynamic over very short time periods. Incubation of mammalian cells with labeled amino acids (fluorescence tagging or stable isotopes) over the course of few hours demonstrated a high protein turnover and distribution to various subcellular compartments (Beatty et al., 2006; Dieterich et al., 2006; Boisvert et al., 2012; Liu et al., 2012; Wei et al., 2013). Remarkably, proteins turnover in the cytoplasm and nucleus of HeLa cells is detected as short as 5 s after the pulse of the amino acids (Baboo et al., 2014). To confirm that the observed signal (fluorescence tagging or stable isotopes) is derived only from newly synthesis proteins and not from other processes in which the amino acids could participate, the cells (HeLa cells or human embryonic kidney cells) were treated with protein synthesis inhibitor (e.g., anisomycin), which resulted in a very low signal comparable to background levels (e.g., Wei et al. 2013; Baboo et al. 2014).

Among the subcellular compartments that have been visualized for *de novo* protein in such studies, the nucleoli have the highest percentage of nascent proteins (e.g., Wei et al. 2013). The nucleolus, which is the active site for ribosomal production, is also the most dense part of the cells and their proteins represent more than 80% of the nucleolus molecular mass (Birnstiel, 1967). Evidence for a high flux of nucleolar proteins (i.e., rapid import and degradation of proteins and rapid nucleolar

assembly within less than 1 h) has been observed with mass spectrometry-based stable isotope proteomics on nucleoli of HeLa cells (Andersen et al., 2005; Boisvert et al., 2012). Furthermore, nucleolin and nucleophosmin, which are abundant in the nucleolus, are among the 195 newly synthesized proteins identified in human embryonic kidney cells after a 2 h pulse *in vitro* with a methionine analog (AHA; Dieterich et al. 2006). Overall, the observation that the nucleoli in the squid appendage and crypt epithelia has the highest levels of ^{15}N is consistent with these reports.

What about the other cellular sub-compartments, i.e., nucleus (excluding the nucleolus) and cytoplasm? In a proteomic study by Boisvert et al. (2012), HeLa cells incubated with isotopically labeled arginine and lysine were subsequently processed to generate a separate cytoplasmic, nuclear and nucleolar fraction thereby allowing the quantification of protein abundance, synthesis, and turnover for each of these compartments. Interestingly, the relative protein turnover rates (the balance between protein synthesis and degradation) was demonstrated to be similar to this study in the sense that the fastest rates were recorded in the nucleoli, the lowest in the nuclei, and intermediate values in the cytoplasm after 3 h exposure to the amino acids (Boisvert et al., 2012).

Collectively these results indicate that a large fraction of the amino acids taken up by the squid cells were used in normal cell metabolism. This finding is consistent with the observation that Golgi complexes (a compartment of the secretory pathway) were also found enriched. This secretory pathway in eukaryotic cells is responsible for the synthesis, folding, and delivery of a wide range of cellular proteins to their final destinations, inside and outside of the cell via vesicular trafficking (e.g., Mellman and Warren 2000; Vázquez-Martínez et al. 2012). Proteins that are destined for the secretory pathway are synthesized by ribosomes that are bound to the endoplasmic reticulum (ER), which synthesizes more than 30% of the proteins in a typical eukaryote cell (Schubert et al., 2000). Nascent proteins are then undergoing post-translational modification, folding and assembling before being exported to the Golgi for further maturation and sorting. Once ready for forward trafficking, proteins are packaged into vesicles and transported to their final destination, where they exert their function. The secretory compartments are therefore highly active during the process of synthesizing new proteins, which is consistent with the high ^{15}N -enrichment that was observed in the Golgi apparatus of the squid light-organ epithelia. Future work should aim to quantify the level of ^{15}N -enrichment also in the ER compartments.

The high and easily detected levels of ^{15}N -enrichment following 3.5 h exposure to ^{15}N -enriched amino acids indicate that the juvenile squid light organ is receptive to broad spectrum of amino acids. This observation, together with the recognition that perhaps we are not able to detect very specific signaling molecules, such as TCT, inside the host squid cells, led to the formulation for a more general research question: Can we visualize and quantify a more general molecular transfer of bacterial-derived

molecules from the symbiotic *V. fischeri* into the squid light organ? To address this question we designed two sets of experiments, the results of which are outlined in the following chapters.

1.3 Supplementary information

To visualize the uptake of ^{15}N -labeled metabolites in light-organ tissues, juvenile squids (~4 h post hatching) were inoculated in FSIO supplemented with a mixture of mainly ^{15}N -labeled amino acids (Celtone base powder; ^{15}N , 98%; Cambridge Isotope Laboratories, Inc. MA, USA) for 3.5 h. Celtone base powder, which is derived from algal hydrolysates, comprising 70% amino acids, 20% sodium chloride and others sugars (Table. 1-S2).

Celtone base powder (^{15}N , 98%; Cambridge Isotope Laboratories, Inc. MA, USA) was dissolved in minimal salts media (MSM; Ruby and Nealson 1977) at 5 g/l supplemented with 11 mM ammonium chloride, 40 mM glycerol and 50 mM PIPES buffer (pH 7.2). Aliquots of 75 μL of this stock solution were added to 30 mL FSIO, to give 12.5 mg/l of Celtone. Because the exact composition of the amino acids in the powder was not known, we roughly estimated the concentration of amino acids in the final seawater solution to be 70 μM using a weighted-average of the molecular mass of each free amino acids (~125 g/mol) and the amino acids percentage in the powder (70%; according to the product information from the company; Table. 1-S2). Previous studies that investigated the uptake of dissolved amino acids by marine invertebrates traced the transport rate by doing a bulk measurement of the entire animal (followed the incorporation of radiolabeled amino acids; i.e., Manahan et al. 1982, 1983) and/or of the seawater (HPLC) in which the animal was incubated. As such, from these experiments it was not possible to speculate upon the amount of amino acids that will be taken up by the squids, and thus, the level of enrichment at a cellular and sub-cellular level. The decision to use 70 μM concentration was chosen in order to have a higher concentration than previously employed by Troll et al. (2009), in the case that their results were dose-dependent, while keeping in mind that an even higher concentration than 70 μM may affect the squid's health (E. Ruby, personal communication). Note however that this concentration was far from the concentrations used by previous studies, which were typically in the range of few μM (total amino acids concentration) and thus closer/comparable to the one prevailing in the natural seawater environment.

At the end of the 3.5 h incubation, squid samples were fixed and prepared for stable isotopes analysis in the NanoSIMS according to the protocol described in 'General procedure for NanoSIMS analysis'.

Data was analyzed using the non-parametric Kruskal-Wallis test followed by a pairwise Nemenyi test. Significance was associated with p values <0.05. Results are presented in Table S 1-1.

Table S 1-1 Statistical analysis of squids inoculated with amino acids mixture for 3.5 h post inoculation (3 animals).

Variables		N	Mean (%)	SD (%)	Statistics	P value
Tissue	Cell organelle					
Appendage	Cytoplasm	27	2806	457	Kruskal-Wallis test: $\chi^2 = 71.5$ df = 2	<0.0001
	Nucleus	67	2191	393		
	Nucleolus	22	6827	2675		
Crypt	Cytoplasm	21	1693	303	Kruskal-Wallis test: $\chi^2 = 61.6$ df = 2	<0.0001
	Nucleus	72	1476	314		
	Nucleolus	25	3058	845		
Comparing tissues type	<u>Cell</u> Kruskal-Wallis test: $p < 0.0001$ $\chi^2 = 32.5$ df = 1	<u>Nucleus</u> Kruskal-Wallis test: $p < 0.0001$ $\chi^2 = 78.5$ df = 1	<u>Nucleolus</u> Kruskal-Wallis test: $p < 0.0001$ $\chi^2 = 22.8$ df = 1			

Table S 1-2 The chemical composition of Celtone base powder.

CELTONE Powder Analytical Information	
APPROXIMATE COMPOSITION	
Amino Acids	70%
Sodium Chloride	20%
Moisture	10%
Glucose	<0.5%
Other Sugars	Trace

Following is a typical CELTONE amino acid profile table.

FREE AMINO ACID COMPOSITION				TOTAL AMINO ACID COMPOSITION			
Ala:	11.1%	Arg:	4.6%	Ala:	7.6%	Arg:	5.6%
Asp:	17.5%	Glu:	10.0%	Asp:	9.6%	Glu:	10.2%
Gly:	11.5%	His:	1.2%	Gly:	6.4%	His:	2.3%
Ile:	1.3%	Leu:	7.7%	Ile:	3.1%	Leu:	8.4%
Lys:	7.1%	Met:	1.7%	Lys:	12.0%	Met:	1.6%
Phe:	3.8%	Pro:	6.2%	Phe:	8.3%	Pro:	5.6%
Ser:	5.2%	Thr:	2.8%	Ser:	4.4%	Thr:	4.8%
Tyr:	3.7%	Val:	2.1%	Tyr:	3.8%	Val:	4.5%
Trp:	0.2%	Cys:	0.2%	Trp:	0.2%	Cys:	0.7%

Analytical data was obtained on a specific batch of ¹³C¹⁵N labeled CELTONE (CB0041).

Chapter 2 Tracking *V. fischeri*-derived molecules into squid host tissues during initiation of symbiosis

2.1 Introduction

Investigations of cross-kingdom signaling are central to increasing our understanding of host-microbe interactions. During the course of evolution, bacteria and their hosts have developed a common language comprised of small molecules, which enable the two partners to communicate. These molecules negotiate the complex relationship among pathogens, symbionts, and their animal host. Many of the bacterial molecules, referred to as microbe-associated molecular patterns (MAMPs; Koropatnick et al. 2004; Mackey and McFall 2006), are recognized by receptors of the host innate immune system termed pattern recognition receptors (PRRs; e.g., review in Akira et al. 2006; Medzhitov 2007). Most of the signaling is thought to occur on the cell surface *via* the binding of MAMPs, such as lipopolysaccharide (LPS) and peptidoglycan (PGN), to Toll-like receptors (TLRs) and peptidoglycan recognition proteins (PGRPs) on the host cell surface (e.g., review in Akira et al. 2006; Royet et al. 2011). Some MAMPs however, can be transported across the cell membrane (e.g., diffusion, bacterial secretion systems, bacterial extracellular vesicles) and recognized by cytosolic PRRs, such as endosomal TLRs (Ahmad-Nejad et al., 2002) and nucleotide-binding oligomerization domain (NOD) receptors (Viala et al., 2004). The received signal leads to the activation of downstream signaling cascades, mostly the nuclear factor-kappaB (NF- κ B) and mitogen-activated protein kinases (MAPKs) pathways, which ultimately affect gene regulation by the translocation of host proteins into the nucleus (e.g., Kawai and Akira 2007; Wells et al. 2010). In some instances, a single MAMP can be sensed by multiple receptors, the location of which (extra- versus intra-cellular), often leads to distinct signaling responses (reviewed in Vance et al. 2009; Vanaja et al. 2016). Although great progress has been made towards understanding these pathways, much remains unknown about the mechanisms that bacteria use to influence their host. How for example, are bacterial products presented to the host, and where are such signals sensed in the host cell?

The binary association between the Hawaiian bobtail squid *Euprymna scolopes* and the luminous bacterium *Vibrio fischeri* is an important and naturally-occurring model system for examining the molecular exchange responsible for the cellular interactions that occur between symbiotic partners. Upon hatching, juvenile *E. scolopes* have a nascent, bilobed organ in the center of their mantle cavity that does not contain any bacteria (Fig. 2-1A). However, immediately after hatching the squid begins to ventilate, bringing ambient seawater containing thousands of bacterioplankton species

(Lee and Ruby, 1994) to the vicinity of two protruding appendages, which comprise a single layer of epithelia overlying a blood sinus (Fig. 2-2A). Here, through extreme selectivity, *V. fischeri* cells aggregate for a period of 2-4 h in mucus secreted by the host epithelial cells located near the pores and become the dominant bacteria in the mucus aggregation (Nyholm and McFall-Ngai, 2003). During these first few hours, the intimate molecular interaction between *V. fischeri* cells and the squid begins, which results in the trafficking of macrophage-like haemocytes into the ciliated appendage and induces a rapid transcriptional response across the squid light organ (Kremer et al., 2013; Altura et al., 2013). Once the aggregate is formed, *V. fischeri* cells enter through the pores on either side of the light organ, travel down the ciliated ducts and the antechamber before finally colonizing the epithelium-lined crypts as a monospecific, extracellular symbiont, a partnership that will last for the lifetime of the squid (Nyholm et al., 2000). At 12 h, when the colonization is complete, MAMP molecules, specifically PGN (tracheal cytotoxin, TCT) and LPS, cause the complete and irreversible loss of the superficial ciliated epithelium (i.e., the appendages) and the full maturation of the light organ (e.g., McFall-Ngai and Ruby 1991; Foster and McFall-Ngai 1998; Koropatnick et al. 2004).

Our knowledge of how these MAMPs and other *V. fischeri* signaling molecules are delivered and recognized by the host is still limited. One possible mechanism is by the shedding of outer membrane vesicles (OMVs). OMVs, which are secreted continuously by Gram-negative bacteria, contain cell-envelope molecules such as LPS and PGN, outer membrane proteins and lipids, as well as periplasmic contents. It has become evident that these OMVs play an important role in both pathogenic and symbiotic associations (Kesty et al., 2004; Shen et al., 2012; Kaparakis-Liaskos and Ferrero, 2015). In the squid-*Vibrio* symbiosis, *V. fischeri* OMVs are known to induce squid phenotypes that are associated with host development and morphogenesis, including haemocyte trafficking and apoptosis at similar to levels those that are triggered by the whole bacteria (Aschtgen et al., 2015; Aschtgen et al., 2016). In fact, most of the morphogen-induced LPS molecules derived from *V. fischeri* are associated with the OMVs that it secretes (Aschtgen et al., 2016).

Here, the transfer and localization of *V. fischeri* molecular products into squid host cells during the initiation of symbiosis was studied. Juvenile squids were exposed to either ¹⁵N-labeled *V. fischeri* cells or ¹⁵N-labeled OMVs extracted from the bacteria. Host tissues were then analyzed using *state-of-the-art* correlative transmission electron microscopy (TEM) and quantitative ion microprobe isotopic imaging (NanoSIMS; nano-scale secondary ion mass spectrometry) techniques, which enabled us to visualize and quantify the incorporation and accumulation of ¹⁵N-enriched bacterial products within the squid host tissue at both tissue, cellular, and subcellular levels.

Various studies have used NanoSIMS as a tool to explore microbe-host association. However, these studies were aimed at examining the nutrient assimilation and metabolic processes (e.g., Lechene

et al. 2007; Berry et al. 2013; Kopp et al. 2013). This is the first study that visualizes the transport of bacterial-derived compounds into host tissue with NanoSIMS imaging in the context of the squid- *Vibrio* system (cf. review in the General introduction).

2.2 Material and Methods

2.2.1 General procedures

Adult Hawaiian bobtail squid (*E. scolopes*) were collected from shallow reef flats of Oahu, Hawaii and transported to the UW-Madison where they were maintained and bred in a recirculating artificial seawater system as described in Doino and McFall-Ngai (1995). All experiments conform to the relevant regulatory standards established by the University of Wisconsin-Madison.

2.2.2 Bacterial strains and growth conditions

V. fischeri wild-type strain, ES114, (Boettcher and Ruby, 1990) were grown overnight in LBS agar plates (LB agar containing 2% [wt/vol] NaCl; Graf et al. 1994). One colony of bacterial cells was diluted in 10 mL of minimal salts media (MSM; Ruby and Nealson 1977) supplemented with 11 mM [¹⁵N]-ammonium chloride (NH₄Cl; ¹⁵N, 99%; Cambridge Isotope Laboratories, Inc. MA, USA), 40 mM glycerol, 50mM PIPES buffer (pH 7.2) and 5 g/L of Celtone base powder (¹⁵N, 98%; Cambridge Isotope Laboratories, Inc. MA, USA). Celtone is a mixture of ¹⁵N-labeled amino acids, nucleic acids, peptides, vitamins, salts and essential nutrients, a combination of substances that had been proven efficient to gain enhanced growth rates in minimal media. The medium was filtered through a 0.2 μm membrane. For unlabeled bacterial cells, isotopically normal ammonium chloride and Celtone base powder were added. Cells were grown in 10 mL of medium that were added to the 125 mL flask to ensure gas exchange occurred between the culture and the air, and to reduce the chances of the media becoming hypoxic. Cells were incubated in an orbital shaking incubator at 220 rpm and 28°C. A series of sub-culturing (initial OD_{600nm} of ~0.0025) was carried out to obtain maximum ¹⁵N-bacteria enrichment (30-40 generations). Cells from the last passage (OD_{600nm} of 0.2-0.5) were washed twice in filter-sterilized (0.2 μm) instant ocean (FSIO) (Aquarium Systems, Mentor, OH) by centrifugation (2 min, 8000 rpm) before using them to inoculate the squid.

An experiment to examine potential carry-over effects from the washing of the bacteria cells grown in the labelled medium was carried out. The methods and results of this experiment is described in details in the Epilog section.

To determine the ¹⁵N- enrichment of bacteria in the culture, a drop of the washed bacteria was put on an aluminum stub and left to dry before NanoSIMS analysis was performed (details of the

NanoSIMS analysis described in 'General procedure for NanoSIMS analysis'). ^{15}N -enrichment in the bacteria varied between 60,000% to 70,000% above the natural $^{15}\text{N}/^{14}\text{N}$ ratio.

2.2.3 Isolation of outer membrane vesicles (OMVs)

OMV extraction was conducted as outlined in Aschtgen et al. (2015). Bacteria cells were grown to an $\text{OD}_{600\text{nm}}$ of ~ 2 in 200 mL MSM supplemented with ^{15}N -Celtone base powder, as described before. The culture supernatants were centrifuge at $4,500 \times g$ for 15 min at 4°C . The resulting supernatant was collected and filtered through $0.45 \mu\text{m}$ and $0.22 \mu\text{m}$ pore-size polyvinylidene difluoride (PVDF) membrane filters (Millipore Corp., Billerica, MA) to remove remaining bacterial cells. The supernatant that contained the OMVs was separated from other extracellular bacterial products by ultracentrifugation at $173,000 \times g$ for 2 h at 4°C in a 90 Ti rotor (Beckman Coulter, Inc., Brea, CA) to remove cell debris. The supernatant was discarded and the pellet, containing OMVs, was rinsed 3 times in 15 mL Dulbecco's phosphate buffered saline (dPBS; 0.2 g KCl, 0.2 g KH_2PO_4 , 11.7 g NaCl, 1.1 g Na_2HPO_4 , 0.1 g $\text{MgCl}_2 \cdot 6\text{H}_2\text{O}$, and 0.1 g CaCl_2 per liter deionized water supplemented with an additional 11.7 g NaCl/L, and filter-sterilized; Aschtgen et al. 2015) and the ultracentrifugation step was repeated after each wash. The vesicle pellet was then resuspended in 1 mL dPBS. The protein concentration of the OMVs was estimated using the Qubit 2.0 fluorometer (470 nm excitation/570 nm emission) (Life Technologies, Grand Island, NY). The fluorometer was first calibrated using proteins standards (0, 200 and 400 $\mu\text{g}/\text{mL}$) supplied by the company. After calibration, OMV samples (2 μL) were diluted into a working solution of buffer-fluorescent dye mixture to a final volume of 200 μL . Samples were then vortexed and incubated in the dark for 15 min at room temperature. The intensity of the fluorescent dye was measured following the manufacturer's instructions. The relative concentration of vesicles in each sample was also determined using the lipophilic dye FM4-64 (535 nm excitation/670 nm emission; Molecular Probes), as described previously (Aschtgen et al., 2015). OMVs were incubated at a concentration of 3.3 $\mu\text{g}/\text{mL}$ of dPBS at 37°C for 10 min and were then quantified using a Tecan Genios Pro plate-reader fluorometer (Tecan group, Männedorf, Switzerland). Control samples were FM4-64 probe alone and vesicles alone. Vesicles were visualized by electron microscopy (see protocol in 'General procedure for NanoSIMS analysis'; Fig 2-S4). Purified OMVs were then stored at -20°C until use. OMV concentrations (50 μg protein/mL) for subsequent experiments were chosen to be similar to previous studies in which such exposure produced haemocyte trafficking, a characteristics of normal light-organ development (Aschtgen et al., 2015) similar to the level triggered by the symbionts when symbiont population fills the crypts. Levels of ^{15}N -enrichment as measured in a sample of purified vesicles (left to air dry before the NanoSIMS analysis) were similar to the ^{15}N - enrichment of bacterial cells from the growth medium (see above).

2.2.4 Squid assays

Within ~4 h of hatching, juveniles *E. scolopes* were placed in FSIO, containing either ¹⁵N-labeled *V. fischeri* cells or ¹⁵N-labeled purified OMVs. To investigate how *V. fischeri* compounds interact with squid cells in early-stage symbiosis, animals exposed to *V. fischeri* (10⁶ CFU/mL) were kept in the vials for 2, 3.5, 6 and 14 h (n=3-6), respectively, whereas animals exposed to OMVs were kept for 1 and 3 h (n=4-5), respectively. Note that squids were exposed to a much larger inoculum than what occurs in a natural seawater environment (~5000 cells/mL). It has been shown that with increase inoculum size there is an increase in the numbers of bacteria in the aggregate as well as an increase in the squid response to the presence of the bacteria (i.e., haemocytes trafficking) (Altura et al., 2013). Because I did not know whether differently-sized aggregates would influence the enrichment patterns, it was decided to use a higher concentration of *V. fischeri* cells. Another reason for using such a large concentration of *V. fischeri* cells was to minimize the risk of being under the detection limit of the NanoSIMS. In a preliminary experiment, squids exposed to natural seawater concentration of *V. fischeri*, showed either no ¹⁵N-enrichment or very low amount of ¹⁵N-enrichment. Control samples were squids inoculated with unlabeled bacteria.

To determine the concentration of bacteria (CFU/mL) in the incubation seawater, 5 µL were plated on LBS medium (LB agar containing 2% [wt/vol] NaCl), and the colonies that grew were counted on the following day. Control samples were squids inoculated with unlabeled bacteria. After 2 and 3.5 h incubation, bacteria were observed either in the form of aggregates in the mucus above the pores, inside the pores, and/or inside the duct. No bacteria were observed in the crypt spaces at these time points. After 6 h incubation, few bacterial cells were observed in the crypts, and after 14 h the crypts were fully populated by *V. fischeri*. Colonization of the symbiotic juvenile squid was validated by measuring the luminescence output of the juveniles using a TD 20/20 luminometer (Turner Designs, Sunnyvale, CA, USA). To confirm that the bacteria had aggregated along the appendages and near the pore at 2 h post inoculation, a few individuals (n=5) were inoculated with GFP-labeled bacteria and subsequently visualized for the location of the bacteria on/in the light organ using Zeiss LSM 510 confocal microscope. At the end of incubation time, squids were anesthetized in a solution of 2% ethanol in FSIO containing 0.001% CellTracker Orange (Molecular Probes, Eugene, OR). The mantle and funnel tissues were then dissected to expose the underlying light organ and the tissues were fixed.

2.2.5 Samples preparation for transmission electron microscopy and NanoSIMS

For details please refer to 'General procedure for NanoSIMS analysis'.

2.2.6 Prediction of NLS sequences in *V. fischeri*

The amino acid sequences of *V. fischeri* ES114 strain were obtained from the BioCyc (<https://biocyc.org/>) data repository. The software PredictNLS that was used in this study is one of the most commonly used to predict a nuclear localization sequence (NLS; Cokol et al. 2000). Analysis using PredictNLS was carried out using a Linux-based server. The Emboss software (Rice et al., 2000), in conjunction with custom Python scripts (written and run by Dr. Mahdi Belcaid, HI, USA) were used for processing the protein sequences and for parsing the results. The subcellular localization of *V. fischeri* proteins with the putative NLS sequences was predicted using PSORTb v3.0.2 (Psort, 1997).

2.2.7 Statistical analysis

Differences in RLI between the light-organ compartments (appendage, pore, and crypt) at both time points were tested using a two-way factorial ANOVA test after log transformations of the data followed by the Tukey HSD test for multi-group comparison (Table S 2-1B and Table S 2-2). When no significant differences were found, data were pooled. Data from experiments comparing the differences in the levels ¹⁵N-enrichment among squid tissue types and cell organelles did not meet the assumptions of the parametric test, and therefore were compared by the non-parametric Kruskal-Wallis ranked test, followed by a Nemenyi *post hoc* test. All statistical analyses were performed using the statistical program R (Maxwell and Delaney, 2004), version 3.2.0. Data are expressed as means \pm 1 standard deviation (SD). *P* values of <0.05 were considered as statistically significant for all testing. Tables 2-S1 and 2-S2 provide a summary of tests for statistical significance for all experiments presented in this study.

2.3 Results

2.3.1 Juvenile squids inoculated with symbiont cells

To investigate how *V. fischeri* interacts with squid cells in early-stage symbiosis, newly hatched animals were inoculated with live, ¹⁵N-labeled *V. fischeri* cells (ES114) and sampled at 2 h, 3.5 h, 6 h and 14 h post-hatching. Sections of the light organs were imaged with TEM and/or light microscopy followed by NanoSIMS isotopic imaging to visualize the distribution of ¹⁵N-enrichment due to assimilation of bacterial molecular compounds (Fig. 2-1). After 2 h, only 3 out of 6 squids were labeled; the remaining samples were either completely unlabeled, or had very low levels of enrichment so these were omitted from further analysis. In squids with detectable ¹⁵N-enrichment, heterogeneously distributed but ubiquitous ¹⁵N-enrichment was detected across the epithelial cells of the light organ as early as 2 h post inoculation (Fig. 2-1 C and E, 2-2B). At 2 h, bacterial cells were still aggregating above the pores and in few cases individual cells began to be visible within the ducts, located in the interior of the pores (Fig. 2-1B-D). Nevertheless, enhanced levels of ¹⁵N were also detected in epithelial tissues physically distant

from the pores, notably in the crypts (~100 μm ; Fig. 2-2B), where TEM observations indicated that no symbionts were present.

2.3.1.1 Intracellular distribution of ^{15}N -enrichment in light-organ epithelia

We first sought to determine the relative abundance of ^{15}N inside the epithelial cells of the light organ. Typically, ^{15}N -enrichment was associated with the host cell cytoplasm and nuclei, with strong hotspots localized in the nucleoli (data obtained from the mosaic in Fig. 2-2B and 2-3A; Fig. 2-1E; Table S 2-1B). Levels of ^{15}N -enrichment were significantly different between cellular organelles, where cytoplasm displayed the lowest levels of ^{15}N and nucleoli the highest (Fig. 2-3A; Table S 2-1B). In fact, levels of enrichment in the nucleoli were more pronounced than in nuclei and cytoplasm. This pattern, although more notable in the appendage, was observed in all light-organ compartments (Fig. 2-3A). Note that in the following analysis, the comparisons between host tissues, cell types and treatments are based solely on the differences in the observed average levels of ^{15}N -enrichment in nuclei and/or nucleoli, unless stated otherwise.

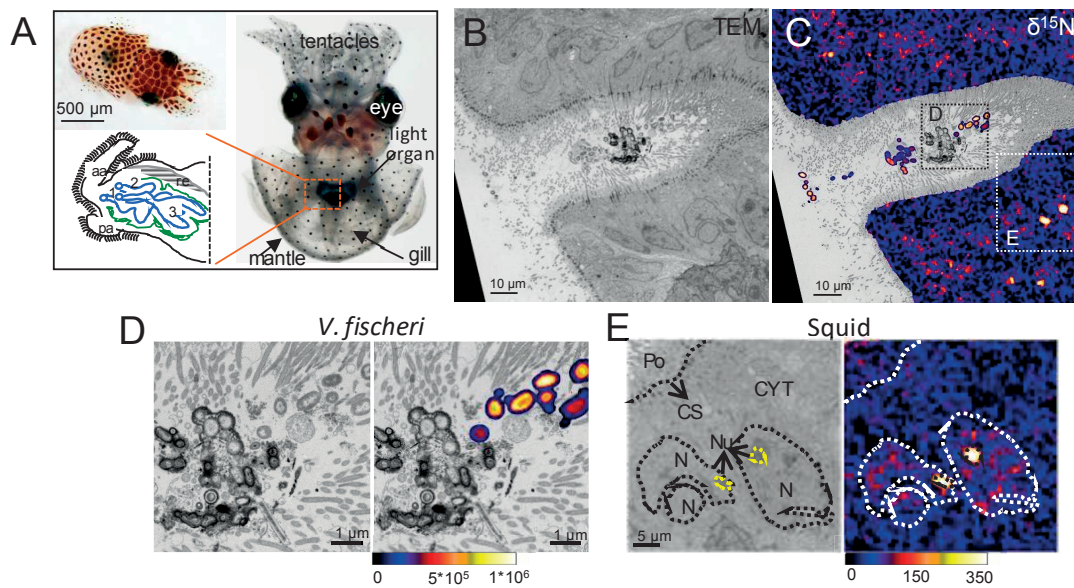


Fig. 2-1. Use of NanoSIMS to study transfer of chemical compounds from the wild-type *Vibrio fischeri* cells (ES114) into the squid tissues and cells. (A) Top left: Juvenile squid at hatching. Right: Ventral view of the squid showing the location of the light organ in the mantle cavity of the squid. Bottom left: schematic presentation of one half of the light organ depicting the surface of the ciliated epithelial appendages (aa, anterior appendage; pa posterior appendage) that are in direct contact with the seawater and the three pores through which the symbionts migrate to their final residence, the crypt spaces (crypts labeled as 1, 2, and 3). (B) mosaic TEM micrograph showing an aggregate of *Vibrio fischeri* cells in the pore associated with the ciliated epithelium of the squid, 2 h after inoculation. (C) Corresponding NanoSIMS $^{15}\text{N}/^{14}\text{N}$ ratio images (superimposed on the mosaic TEM). Colored boxes in (C) show representative locations of pictures zoomed in panels (D) and (E). (D) Strongly ^{15}N -labeled *V. fischeri* cells in the pore together with unlabeled, non-symbiotic environmental bacteria (Left: TEM image; right correlated NanoSIMS and TEM images). Note the black layer surrounding the non-symbiotic bacteria observed in the TEM micrograph suggesting a host immune-system defensive reaction against interlopers. (E) A close-up TEM image of squid epithelial cells. Dotted lines surrounding organelles illustrate typical regions of interest (ROI; here cytoplasm (CYT), nucleus (N) and nucleolus (Nu) used in the sub-cellular NanoSIMS image analysis. CS, cell surface; Po, pore space. Values for the NanoSIMS scale are expressed in ‰ (see ‘General procedure for NanoSIMS analysis’).

NanoSIMS analyses revealed a characteristic pattern of ^{15}N incorporation into the nuclei of epithelial cells of the light organ (Fig. 2-4). The ^{15}N -profile across the two forms of nuclear chromatin, euchromatin and heterochromatin, showed that ^{15}N accumulated preferentially into regions of euchromatin, which are regions typically engaged in active transcription of DNA (Fig. 2-4B and C). Systematic differentiation of euchromatin from heterochromatin was not systematically possible in NanoSIMS images. ^{15}N -enrichment of nuclei was therefore reported as the average for the entire nucleus, excluding the nucleolus, when this structure was observed in the plane of the section.

In the nucleoli, substructures in the ^{15}N -enrichment were correlated with areas that were highly condensed (i.e., relatively darker grey). Such regions had significantly higher ^{15}N -enrichment when compared with less dense nucleoli regions (Fig. 2-4B); the latter is thought to be involved in nuclear organization (Lechene et al., 2006).

Intriguingly, some euchromatin regions exhibited high levels of ^{15}N -enrichment that were comparable to the nucleoli enrichment of either the specific cell or other cells in the same compartment.

However, these observations were rare and were only observed in the 'shoulder' area of the appendage (2 animals, 4 cells; Fig. 2-S1). This intriguing observation suggests that these cells may have functions or characteristics that distinguish them from the majority of other epithelial cells.

Finally, ^{15}N -enrichment at later time points during the initiation of symbiosis, i.e., at 6 h and 14 h, respectively, was investigated. At these stages, the symbiont cells have reached (6 h) and colonized (14 h) the crypt spaces. The subcellular distribution of ^{15}N -enrichment at 6 h was similar to the patterns observed at both the 2 h and 3.5 h time points, however, with apparent higher levels of ^{15}N -enrichment (data not shown). At this time point small hotspots were detected along both, the apical surfaces of the ciliated field and the microvilli lining the cells in the 'shoulder' area (Fig. 2-5), which were absent before. A closer examination of these ^{15}N -hotspots, showed that they correlated with the fibrous material found in between the cilia and microvilli, which cover the epithelial cells of the appendages and the 'shoulder' area (Fig. 2-5B and C). The fibrous matrix is speculated to be mucus that is secreted by the epithelial cells of the light organ. At the 14 h time-point, no ^{15}N -enrichment was observed inside squid cells ($n=5$; data not shown). This finding is perhaps not surprising because, after 14 h bacteria cells occupy the crypt space at densities of up to 10^6 . This population descends from one or two ^{15}N -labeled cells, and cell division have diluted this ^{15}N -enrichment to the point where transfer of molecules from the bacteria to the squid becomes impossible to detect. It is important to note that by stating this, it is assumed the animals were able to take up molecules only from the bacteria population in the crypts and not from the ^{15}N -labeled bacteria that are in the surrounding seawater. For subsequent analysis, ^{15}N -enrichment patterns were only investigated at 2 h and 3.5 h.

2.3.1.2 Distribution of ^{15}N -enrichment within the light-organ compartments

After 2 h of incubation with symbiont cells, ^{15}N -enrichment in the light-organ nuclei was the highest in the appendage epithelium and the lowest in the duct (appendage >> pore > crypt >> duct; Fig. 2-2B, inset, data were obtained from the mosaic in 2-2B; Table S 2-1A). Similar to the pattern that was observed for nuclei enrichment, nucleoli of light-organ epithelial cells, display a systematic trend both at 2 h and 3.5 h post-inoculation with the highest relative ^{15}N -enrichment levels recorded in the appendage, intermediate levels in the pores, and lowest levels in crypts (Fig 2-3B; Table S 2-1C). The overall relative enrichment in the light organ was indistinguishable between the time points. Nucleoli enrichment is not presented for the duct, because not sufficient data for statistical analysis was obtained. Note that ^{15}N -enrichment levels in nucleoli were variable within a single animal and showed even greater variability between animals. To account for this 'between animal' biological variability, ^{15}N -enrichment was expressed as a Relative Labeling Index (RLI; see Materials and Methods) (Fig 2-3B; Table S 2-1C).

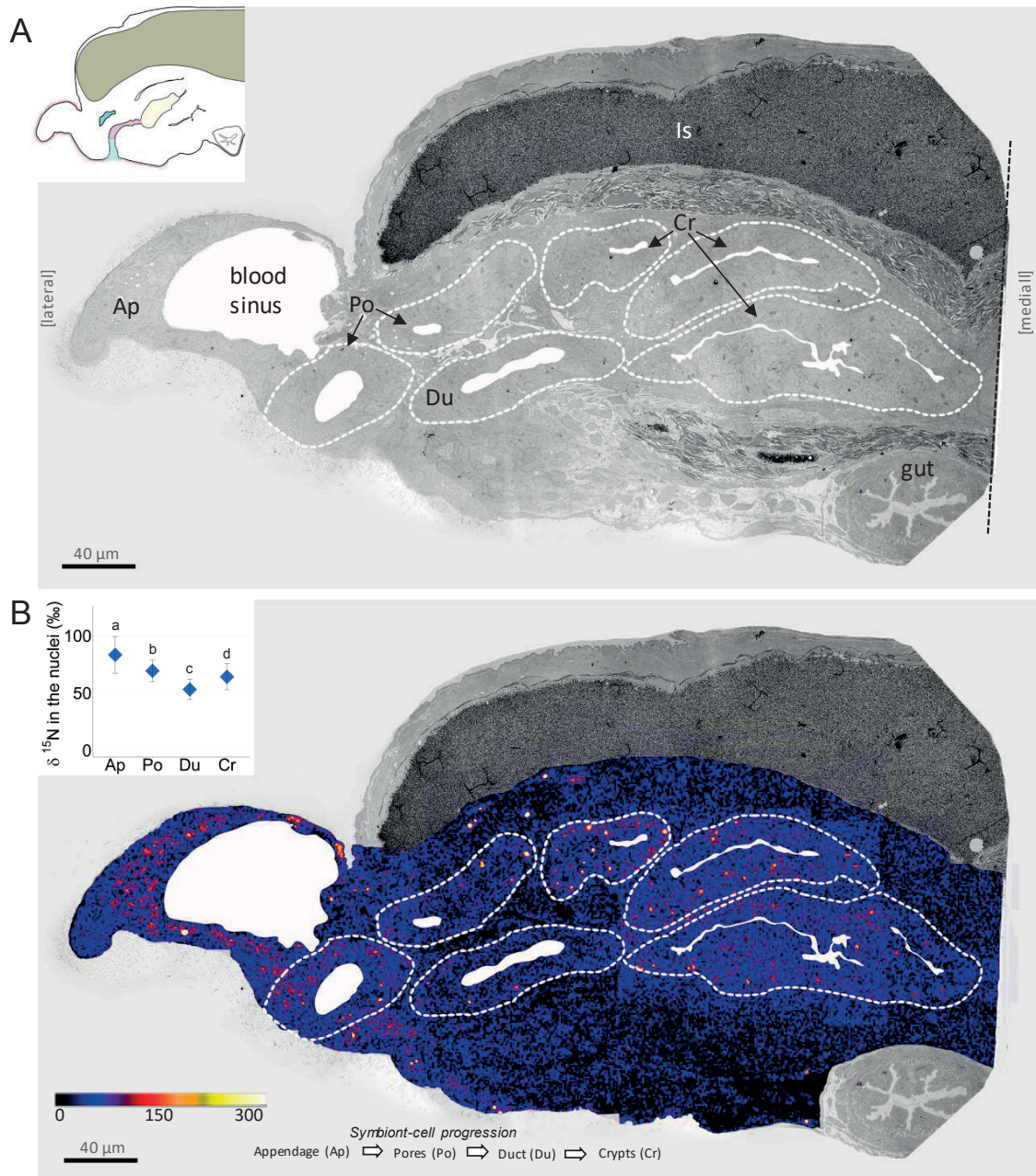


Fig. 2-2. ^{15}N -enrichment (expressed as $\delta^{15}\text{N}$) in the juvenile squid light organ 2 h post inoculation with ^{15}N -labeled *V. fischeri* cells. A TEM micrograph (A) and the corresponding mosaic of 65 individual high resolution NanoSIMS images (B) covering half the light organ of the juvenile squid. (A) The different light-organ compartments are depicted in the TEM micrograph. The inset is a diagram, illustrating half of the light organ. (B) The nucleoli are systematically visible as strong ^{15}N -hotspots. Inset shows the average level of ^{15}N -enrichment in the nuclei of cells in different compartments (data obtained from the mosaic; Ap, appendage (n=46); Po, pore (n=45); Du, duct (n=36); Cr, crypt (n=126)). Values for the NanoSIMS scale are expressed in ‰ (see 'General procedure for NanoSIMS analysis').

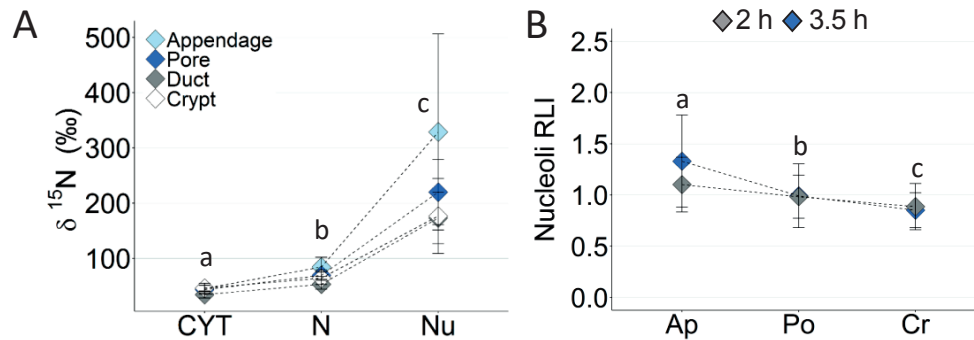


Fig. 2-3. Intracellular distribution of ^{15}N -enrichment in the juvenile squid light organ 2 h and 3.5 h post inoculation with ^{15}N -labeled *V. fischeri* cells. (A) Comparison of ^{15}N -enrichment in the cytoplasm (CYT), nuclei (N) and nucleoli (Nu) of the light-organ epithelial cells were obtained from high-resolution NanoSIMS mosaics (illustrated in Fig. 2). (B) RLI (c.f. M&M) of nucleoli in squid epithelial cells 2 h and 3.5 h post inoculation, respectively (squids: 2 h, 3 animals; 3.5 h, 6 animals; 6-10 nucleoli per compartment). Lower case letters indicate statistically significant differences between the light-organ compartments (Table 2-S1A and 2-S1B). Note that 2 out of 6 squids were unlabeled in the 2 h inoculation experiments with *V. fischeri* cells and thus were not included in the analysis. Error bars represent 1 standard deviation. Ap, appendage; Cr, crypt; Du, duct; Po, pore.

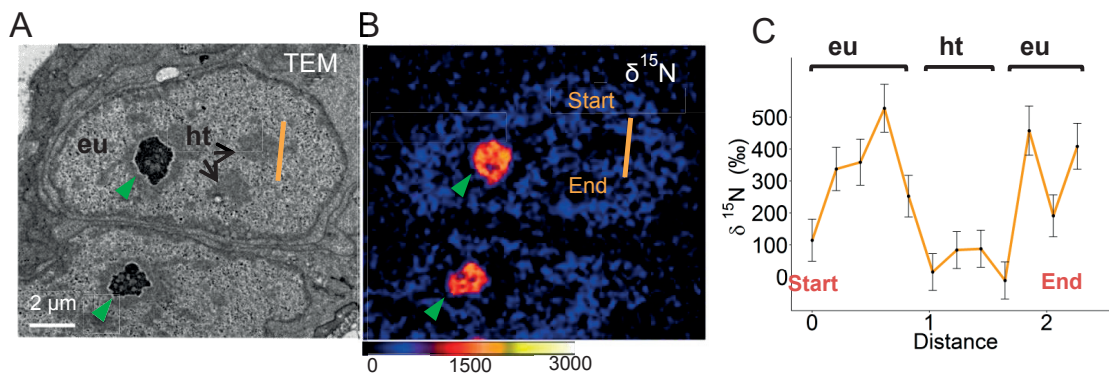


Fig. 2-4. Distribution of ^{15}N -enrichment in a representative squid nucleus of an epithelial cell lining the appendage at 3.5 h post inoculation with ^{15}N -labeled *V. fischeri* cells. (A) High magnification TEM micrograph and (B) corresponding NanoSIMS $^{15}\text{N}/^{14}\text{N}$ ratio image of two cell nuclei. The nucleolus (green arrowheads), euchromatin (eu; brighter grey) and the more condense chromatin, heterochromatin (ht; darker grey), regions are clearly visible. The nucleoli are strongly enriched in ^{15}N . Values for the NanoSIMS scale are expressed in ‰ (see 'General procedure for NanoSIMS analysis'). (C) Variations of ^{15}N -enrichment along the line-profile indicated in A and B (orange line) passing through the euchromatin and heterochromatin regions of the nucleus. Euchromatin is more labeled than heterochromatin.

2.3.1.3 Distribution of ^{15}N -enrichment in other squid organs and cell types

To determine whether the ^{15}N -enrichment is specific to the light-organ epithelia, other non-epithelial squid tissues inside the light organ and in other organs were also analysed (Fig. 2-6, 2-S2 and 2-S3; Table 2-S1D). Significant ^{15}N -enrichment in the nuclei and, in some cases, also in the nucleoli was observed. The latter was evident in the following tissues: (i) non-epithelial tissues inside the light organ, including macrophage-like haemocytes in the appendage sinus ($n=4$), reflector (data not shown) and connective tissue and (ii) epithelial tissues outside of the light organ, including the gut, endothelial cells, gills, and digestive gland ($p<0.0001$; Fig. 2-6). Interestingly, while haemocyte cells in the appendage sinus appear to have comparable enrichment to the appendage epithelium, haemocytes in the gill sinuses

were unlabeled. Comparison between different organs revealed that the light-organ appendage was clearly the tissue with the strongest enrichment levels. In direct comparison with nuclei of epithelial cells in all light-organ compartments (pooled together), cell nuclei in the connective tissue were on average 63% less enriched in ^{15}N ($p = 0.004$), the gut 68% less ($p < 0.0001$), the gills 31% less ($p < 0.0001$), the endothelial cells 52% less ($p < 0.0001$), and the digestive gland 45% less ($p < 0.0001$) (data obtained from one animal; Fig. 2-6G; Table S 2-1D). Note that, unlike the epithelium of the light organ and the gills, in which all cells were significantly ^{15}N -enriched, not all cell nuclei and nucleoli in the connective tissue, gut, digestive gland, and endothelial cells were enriched above control background. No ^{15}N -enrichment was detected in the brain, retina, epithelium supporting the statoliths, tentacles, optic lobe, white body, mantle muscle, and mucus cells (Fig. 2-S3). These data suggest that the ^{15}N -enriched molecules from the symbiont bacteria were not randomly distributed in the squid body but targeted several organs, among which the light organ had the highest enrichment.

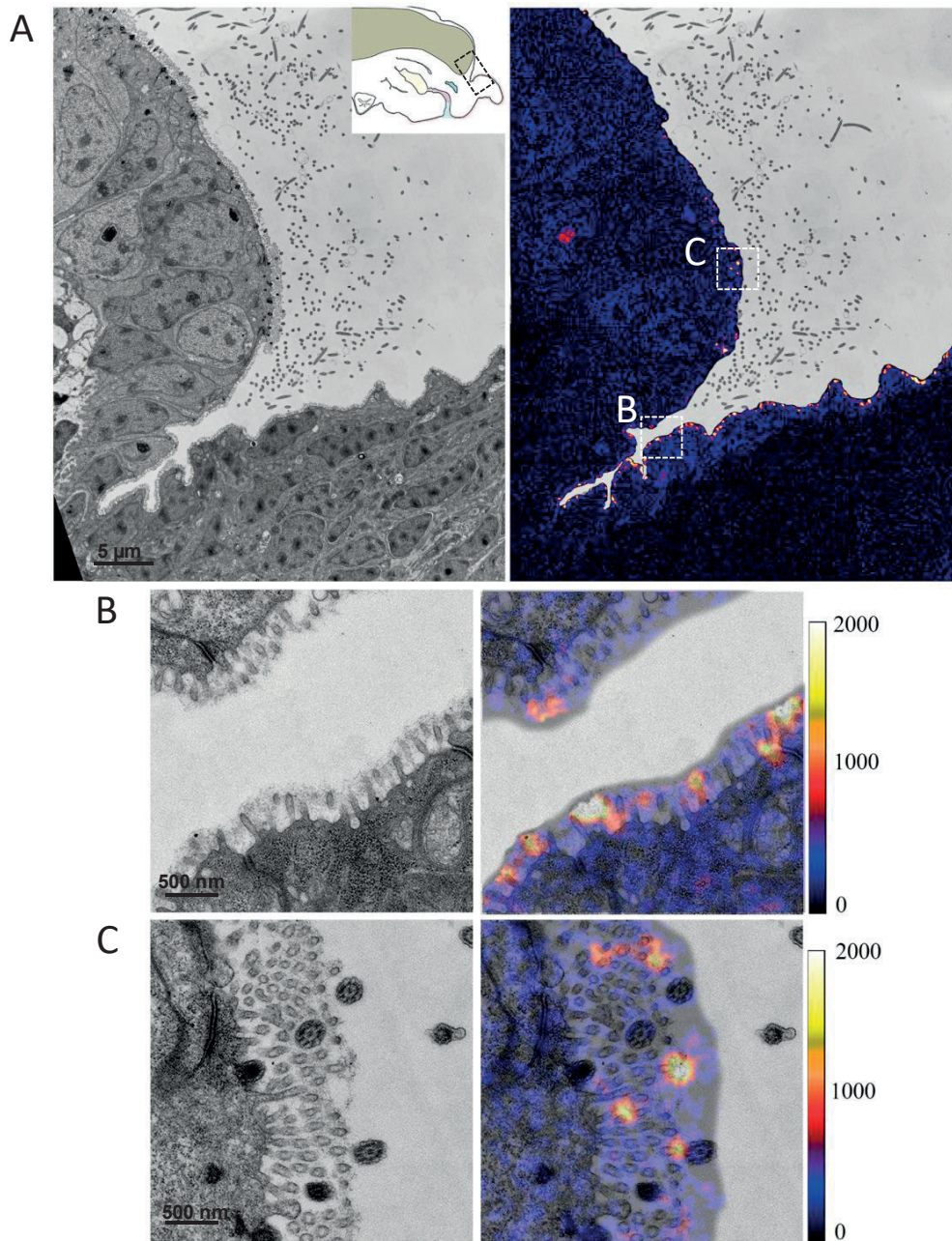


Fig. 2-5. ^{15}N -enrichment along the surface of the appendage epithelium and the 'shoulder' area in juvenile squid light organ 6 h post inoculation with ^{15}N -labeled *V. fischeri* cells. (A) TEM micrograph (left) and the corresponding mosaic of high resolution NanoSIMS $^{15}\text{N}/^{14}\text{N}$ ratio images. Inset illustrates the area in which the imaged where taken. Dashed boxes show representative locations of pictures zoomed in panels (B) and (C). (B) and (C) A representative TEM (left) and NanoSIMS ratio image overlay (right) showing ^{15}N -hotspots along on the ciliated surface of the appendage epithelium (B) and along the microvilli lining the cells in the 'shoulder' area. Note that most of the hotspots co-localized with fibrous materials that I speculated to be the mucus matrix that is secreted by the squid epithelial cells. Values for the NanoSIMS scale are expressed in ‰ (see 'General procedure for NanoSIMS analysis').

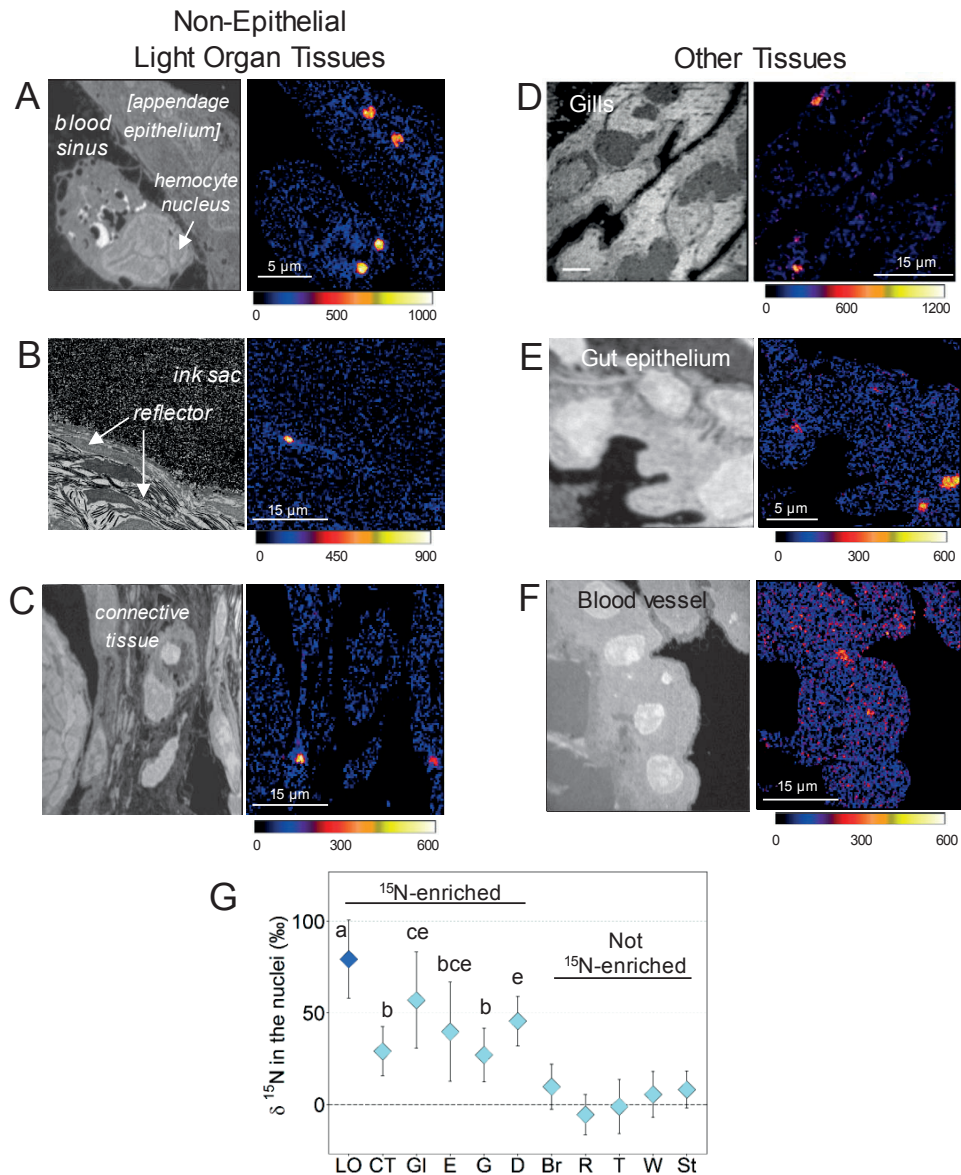


Fig. 2-6. ^{15}N -enrichment in nuclei and nucleoli (hotspots) in light-organ non-epithelial tissues (A-C) and in epithelial tissues in other squid organs (D-F) after 3.5 h inoculation with ^{15}N -labelled *V. fischeri* cells. Left panels show tissue structure (NanoSIMS $^{12}\text{C}^{14}\text{N}$ image). Right panels show corresponding, quantified NanoSIMS $^{15}\text{N}/^{14}\text{N}$ ratio image. Values for the NanoSIMS scale are expressed in ‰ (see ‘General procedure for NanoSIMS analysis’). (G) Representative (1 animal) ^{15}N -enrichment in nuclei (excluding the nucleolus when visible) in different tissues. Non-epithelial tissue inside the light organ (LO; n=72): connective tissue (CT; n=59), and epithelial tissues outside of the light organ: brain (Br; n=16); digestive gland (D; n=31), endothelial cells (E; n=48), epithelium supporting the statolith (St; n=27), gills (GI; n=34), gut (G; n=100), retina (R; n=11), tentacles (T; n=29) and white body (W; n=27). Only enriched tissues were considered in the statistical analysis (indicated by lower case letters for significant differences Table S 2-1C). Error bars represent 1 standard deviation.

2.3.2 Juvenile squids inoculated with *V. fischeri*-derived OMVs

Juvenile squids were inoculated with purified ^{15}N -labeled *V. fischeri*-derived OMVs for 1h and 3h to determine whether the observed enrichment inside host tissues incubated with ^{15}N -bacteria cells can be also induced by the bacteria-derived OMVs (Fig. 2-7; Table S 2-2). In general, ^{15}N -enrichment patterns in host tissues and cells were similar to squids inoculated with bacteria cells; however, ^{15}N -enrichment levels were much higher following OMV exposure (Fig. 2-7; Table S 2-2). This time though, levels of ^{15}N -enrichment were affected by incubation time and were higher after 3 h exposure to OMVs, compared to the 1 h of exposure. The relatively high levels of enrichment could be partially attributed to the high concentration of OMVs used in this study (50 μg protein/mL). This concentration was chosen so that these results would be comparable with those of former studies, which showed that such exposures were sufficient to induce haemocyte trafficking and apoptosis of cells in the appendage, both of which are characteristics of normal light-organ development (Aschtgen et al., 2015; Aschtgen et al., 2016).

Squids exposed to *V. fischeri* OMVs showed very similar subcellular ^{15}N -enrichment patterns compared with *V. fischeri* exposed to ^{15}N -labeled bacteria (Fig. 2-7). This was particularly pronounced in the epithelial cells of the light organ where the lowest levels of enrichment were observed in the cytoplasm, intermediate levels were localized to the nuclei, specifically, as before in euchromatin regions, and the highest levels appeared as hotspots in the nucleoli (compare Fig. 2-7A and D; Table S 2-2A). However, the difference in ^{15}N -enrichment among cell organelles appeared lower for OMV-treated squids (Table S 2-2A; data presented only for the appendages).

The relative ^{15}N -enrichment pattern within the light-organ compartments after exposure to OMVs, at both time points, was also comparable with the pattern induced by symbiotic cells, although differences between light-organ tissues were slightly accentuated, in the order appendage > pore > crypt (Fig. 2-7E; Table S 2-2B). Note that nucleoli data are expressed as RLI, to enable comparison with the results of the previous experiment. OMVs also produced qualitatively similar ^{15}N -enrichment patterns in other organs (e.g., gills, reflector, connective tissue; Fig. 2-S5) as in the *V. fischeri* inoculation experiment. The main difference being that essentially all host cells nuclei and nucleoli had detectable ^{15}N -enrichment after exposure to OMVs.

Small hotspots of ^{15}N -enrichment were observed along the apical surfaces of the ciliated field and the gills and along the microvilli lining the cells in the `shoulder` area (Fig. 2-7B and C, respectively). These enrichment patterns resembled the enrichment that was detected 6 h after exposure to symbiont cells (Fig. 2-5) and was also correlated with fibrous material in host-secreted mucus covering the epithelial cells (Fig. 2-7B and C, inset). Surprisingly, no vesicles could be observed to be associated with these hotspots. To validate that the chemical fixation and dehydration procedures did not affect the integrity of the vesicles membrane, purified vesicles were fixed and embedded using a protocol similar to

that used for the animal tissue sample preparation. As demonstrated by the TEM images (Fig. 2-S4), vesicle membranes remained largely intact, indicating that sample processing cannot explain the absence of vesicles associated with these ^{15}N - hotspots.

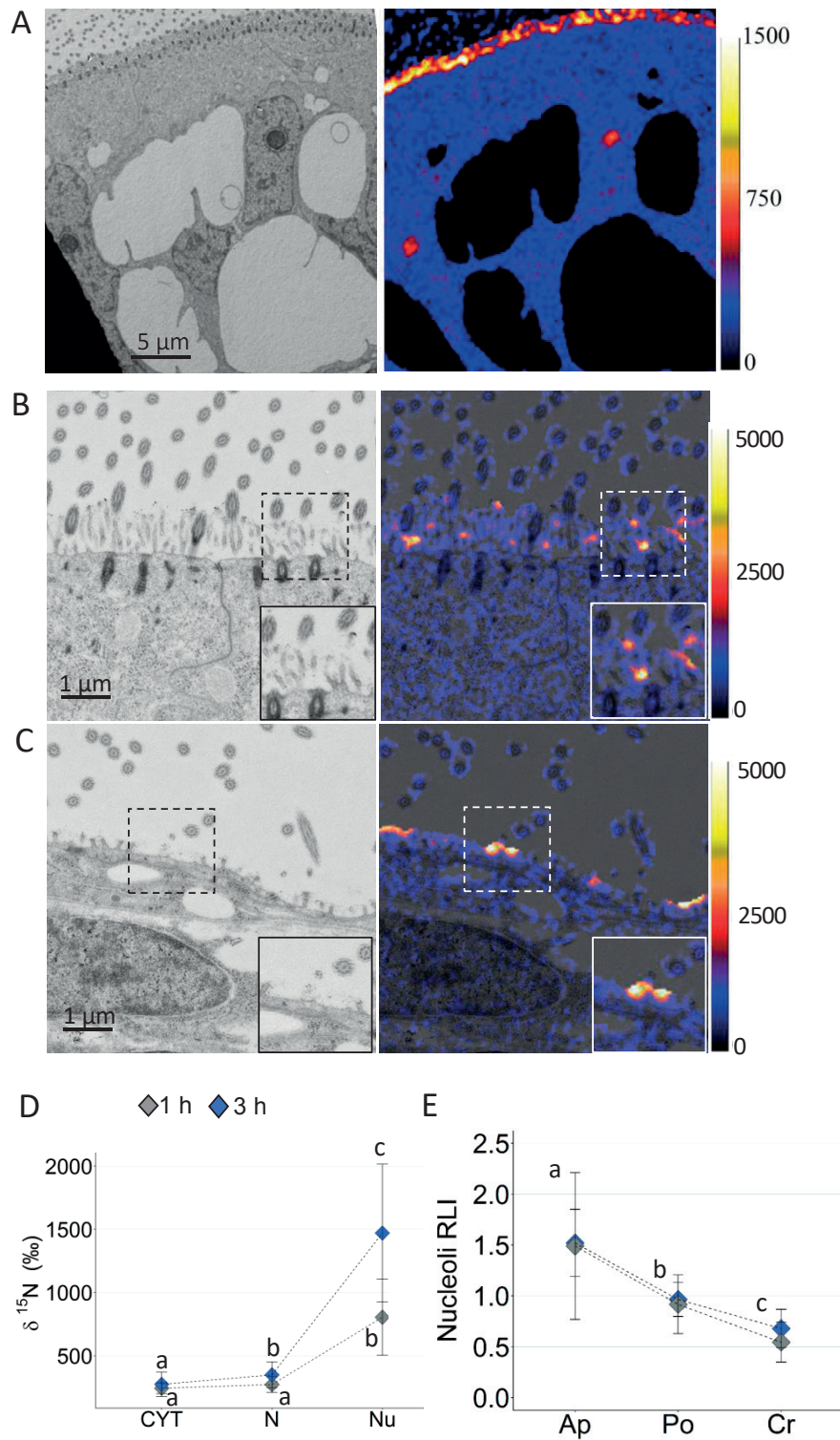


Fig. 2-7. ^{15}N -enrichment in a juvenile squid light organ following 1 h and 3 h exposure to ^{15}N -labeled *V. fischeri*-derived OMVs. (A) A TEM micrograph (left) and the corresponding NanoSIMS $^{15}\text{N}/^{14}\text{N}$ ratio image (right) of an appendage 1 h post inoculation with OMVs. NanoSIMS image shows the ^{15}N -enrichment on the cell surface of the appendage epithelium. The nucleoli are visible

as strong ^{15}N -hotspots. (B) and (C) are representative high resolution TEM (left) and NanoSIMS ratio image overlay (right) of the ^{15}N - hotspots on the cell surface of the epithelial cells. Inset is high magnification of the region highlighted in the dashed box. (B) The ^{15}N -hotspot along the surface of the ciliated field. (C) The ^{15}N -hotspot along the microvilli lining the cells in the 'shoulder area'. Note that most of the hotspots co-localized with fibrous materials that I speculated to be the mucus matrix that is secreted by the squid epithelial cells. (D) ^{15}N -enrichment in the cytoplasm (CYT), nuclei (N) and nucleoli (Nu) of the epithelial cells lining the appendage. (E) RLI of nucleoli in the different light-organ compartments (squids: 1 h, 5 animals; 3 h, 4 animals; 6-10 nucleoli per compartment). Ap, appendage; Cr, crypt; Du, duct; Po, pore. Error bars represent 1 standard deviation. Lower case letters indicate statistically significant differences between cell organelles and light-organ compartments (Table 2-S2).

Considered together, these findings indicate that OMV derivatives induce intracellular ^{15}N -enrichment patterns very similar to those observed in *V. fischeri* inoculation experiments, which suggests that the OMV-derived molecular cargo delivered to the host nucleus is similar to the products secreted by whole bacterial cells.

2.4 Discussion

Using the squid-*Vibrio* animal model, the transfer of bacteria-derived molecular compounds into host tissues and cells during the onset of symbiosis has been investigated. In this study, I demonstrate that when juvenile squids were inoculated with live, ^{15}N -labeled *V. fischeri* cells: (i) ^{15}N -enrichment was detected inside the host light-organ epithelia as early as 2 h post inoculation, even in deep tissues (up to $\sim 100\ \mu\text{m}$ from the surface) where no symbionts were present; (ii) The level of ^{15}N -enrichment within light-organ compartments was highest in the appendage epithelium and lowest in the duct; (iii) Intracellular distribution of ^{15}N -enrichment in light-organ tissues was most notable inside cell nuclei, corresponding to areas dominated by euchromatin and nucleoli; and (iv) ^{15}N -enrichment was not restricted to light organ epithelia. When juvenile squids were inoculated with *V. fischeri*-derived OMVs, I observed similar ^{15}N -enrichment patterns as those in squids that were exposed to whole bacteria, although higher levels of ^{15}N -enrichment were recorded in the OMV treatment. These data indicate that there was a transfer and incorporation of *V. fischeri*-derived molecules into squid tissues and cells. Furthermore, I show that the squid responded in a similar fashion to molecules secreted from the whole bacteria and to the molecular cargo carried by their OMVs, suggesting that at least some of the molecules that induced the ^{15}N -enrichment in the squids are shared between the whole cells and their OMVs. Supporting this conclusion is recent evidence showing that *V. fischeri* OMVs can induce similar squid phenotypes as can whole bacteria (Aschtgen et al., 2015; Aschtgen et al., 2016). Considering the high degree of similarity in the ^{15}N -enrichment patterns induced by inoculation with both the OMVs and the whole bacterial treatments, I will describe the general patterns that were shared between both experiments from the level of the organism to the subcellular scale, outlining potential explanations for these findings, wherever possible. Note that NanoSIMS analysis does not permit identification of the molecules that are enriched in ^{15}N , but it does provide quantitative information about the transfer of bacterial-derived materials during the onset of the symbiosis.

2.4.1 ¹⁵N-enrichment was observed inside host tissues early in symbiosis and does not require direct contact with *V. fischeri* cells

During the early stages of symbiosis (2-3 h following inoculation), *V. fischeri* cells were primarily localized to the epithelial surfaces of the appendage and pores. However, ¹⁵N-enrichment was evident in tissue layers physically distant where *V. fischeri* cells do not interact directly at this time (e.g., crypt, digestive gland; Fig. 2-2B) or are not accessible to the *V. fischeri* cells (e.g., connective tissue, reflector, endothelial cells; Fig. 2-6). This observation indicates that direct contact between the bacteria cells and their host is not necessary to transfer bacterial-derived ¹⁵N-compounds into the host tissues. More importantly, these data illustrate that direct contact with bacterial secretion systems and flagella are not necessary for the observed host ¹⁵N-enrichment. The similarity in enrichment patterns between OMVs and whole bacteria cells suggests that at least some of the products secreted by *V. fischeri* cells may have been packed into OMVs before they were up taken by the host. OMVs are small in size (~30-60 nm for *V. fischeri*; Fig. 2-S4A) and readily diffuse to deep tissues so they can be quickly internalized into host cells (Wai et al., 2003; Bomberger et al., 2009). In fact, the secretion of OMVs has been suggested to be one strategy that pathogens use to cover larger areas and to reach distant tissues, which would otherwise be inaccessible to their toxins (Bomberger et al., 2009; Kaparakis-Liaskos and Ferrero, 2015). Additionally, OMVs were suggested as a mechanism by which molecules secreted from extracellular bacteria can gain access to the cytosol of host cells (Vanaja et al., 2016).

Considering the notable patterns across the light-organ compartments and that the ¹⁵N-enrichment were primarily associated with specific subcellular compartments, these data also suggest that the squid exhibit a selective response to *V. fischeri*-derived molecules.

2.4.1.1 Differential enrichment in the light-organ epithelia

While many different epithelial and non-epithelial tissues had detectable levels of enrichment, the light-organ epithelia clearly had the highest enrichment levels (Fig. 2-6G). This finding is not particularly surprising, since the light-organ epithelia is the area that the symbionts eventually colonize and therefore can interact directly with some of the light-organ compartments during the onset of symbiosis. As such, the light-organ epithelia may be more permissive and receptive to *V. fischeri* molecules. Several studies have provided insights into the molecular interactions that occur between *V. fischeri* and host cells in the light organ that do not entail a close association between both partners. During the initial hours of symbiosis (2-3 h), squids are able to sense and respond specifically to only a few *V. fischeri* cells in an environment that contains millions of other non-symbiotic bacteria (Kremer et al., 2013; Altura et al., 2013). Within 3 h, of exposure to natural inoculum (~5000 cells/mL), 3-5 viable cells were observed to aggregate on the light-organ surface (Altura et al., 2013). During this time, the cells interact intimately with the ciliated field and secrete a PGN monomer that induces the migration of

macrophage-like haemocytes into the blood sinus underlying the host appendage (Koropatnick et al., 2007; Altura et al., 2013). These few attaching cells are also responsible for the induction of robust gene expression in host cells of the light organ, changes that promote their subsequent colonization of the deep crypts (Kremer et al., 2013). It remains unclear whether these signals affect solely the 2-3 host cells in direct contact with the colonizing *V. fischeri*, or whether the molecules induce transcriptional changes throughout the light organ. *V. fischeri* cells were found to induce non-localized changes in the squid *via* signal molecules when the bacteria are occupying the deep crypts. The presence of *V. fischeri* cells in the crypts, induces changes in gene expression in the duct epithelium (Nikolakakis et al., 2015) and the irreversible morphogenesis of the light-organ appendages (McFall-Ngai and Ruby, 1991; Foster and McFall-Ngai, 1998). Collectively, these studies suggest that the light-organ tissues are highly sensitive to the presence of symbionts and can elicit host responses even in locations where the symbionts are absent. These findings provide further evidence for the light organ sensitivity to soluble *V. fischeri* compounds that are present in the seawater.

2.4.1.2 ¹⁵N-signature in the duct is exclusive

The deep crypts are connected to the external seawater through pores that are located on the light-organ surface, allowing molecules to be transported in the incoming seawater and to diffuse to the site of action. The ducts, located immediately in the interior of the pores, are thus exposed to more bacterial products than the crypt epithelia. As such, one could expect to observe higher ¹⁵N-enrichment in the ducts compared to the epithelia of the crypt. However, this was not the case. In fact, the epithelial cells lining the ducts exhibited the lowest levels of ¹⁵N-enrichment when compared to epithelial cells from other compartments within the light organ (Fig. 2-2B, inset; Fig. 2-3), suggesting that cells in the ducts respond differently to the bacterial molecules.

During the early events that lead to colonization, the epithelia of both the appendage and the crypts interact closely with the symbiont cells, and thus one would expect them to be more susceptible to their presence. Indeed, it is this intimate association that induces the transcriptional, morphological and chemical alterations that are ultimately responsible for the distinct developmental fates of these two compartments (e.g., McFall-Ngai and Ruby 1991; Montgomery and McFall-Ngai 1994; Lamarcq and McFall-Ngai 1998; Koropatnick et al. 2014; Schwartzman and Ruby 2016). The duct epithelia, however, have only brief direct contact with the bacteria cells when they migrate from the pores into the deep crypts. Yet, despite this fact, by 12 h the symbionts elicit specific developmental modifications and changes in gene expression that add to the unique environment that is known to prevail in the duct (McFall-Ngai and Ruby, 1998; Kimbell and McFall-Ngai, 2004; Nikolakakis et al., 2015). These include changes in the synthesis of actin cytoskeleton, which is accompanied by the constriction of the duct that

limits further entry of bacteria (Kimbell and McFall-Ngai, 2004). Whether such distinct developmental modifications are induced in those experiment by the short encounter with the bacteria or by signal molecules secreted by the bacterial population in the crypts, is unclear. Nevertheless, considering the low levels of ^{15}N -enrichment observed in this region and the distinct chemical environment that prevails in the duct, it is conceivable that the duct epithelium senses and responds differently to the bacteria compared with other structures in the light-organ epithelia.

2.4.1.3 Enrichment in other organs and tissue types

Apart from the light-organ epithelia, ^{15}N -enrichment were observed in non-epithelial tissues inside the light organ, such as the macrophage-like haemocytes observed in the appendage sinus, reflector and connective tissue and in epithelial tissues outside of the light organ including the gut, the gills, and the digestive gland (Fig. 2-6G). The patchiness of the labeling between tissue types, and the absence of labeling in some of the tissues examined, highlights the differential nature of the uptake of bacteria-derived molecules. Among these tissues and cell types, haemocytes (Fig. 2-6A) and gills (Fig. 2-6D) appeared to be the most receptive to *V. fischeri* ^{15}N -enriched molecules. It is interesting that both gills and haemocytes are cell types that are affected by the bacteria presence. At the onset of symbiosis, haemocytes migrate into the appendage sinus in response to signaling by TCT (which could not be detected in the host tissue; cf. Chapter 1) and OMVs (Koropatnick et al., 2007; Aschtgen et al., 2015). After colonization, *V. fischeri* is able to alter the haemocyte cytoskeleton (Schleicher et al., 2014). It is not clear how haemocytes sense *V. fischeri*-derived molecules, but together with the presented results, the findings to date suggest that haemocytes are more susceptible to bacterial products, early in the development of the symbiosis. Alternatively, the labeling could be as a result of bacterial degradation. Haemocytes cells from juvenile squids have been shown to possess the ability to engulf bacteria cells during early symbiosis (Nyholm and McFall-Ngai, 1998), including *V. fischeri*.

The gills have been shown to respond to bacterial presence with robust changes in gene expression at 72 h post colonization (S. Moriano-Gutierrez, unpublished data) and changes in production of a host pattern-recognition receptor, EsLBP1 (*E. scolopes* lipopolysaccharide-binding protein 1) at 18 h (Krasity et al. 2015; Fig. 2-6G). However, similar post-colonization changes were also observed in the eyes and the tentacles (for the EsLBP1) in these studies, whereas no ^{15}N -enrichment in these tissues was found here. Gills are also involved in controlling bacteria populations in cephalopods. If the animal is septic, gills concentrate and sequester invading bacteria into nodules (Bayne, 1973). In this study, the brief association that the gills have with the bacteria cells or the continuous flow of bacteria products from the seawater during each ventilation seems sufficient to enrich these cells. Direct contact with seawater might also explain the ^{15}N -enrichment observed in the digestive gland, but not the ^{15}N -

enrichment in the gut and endothelial cells, which are localized deep inside the squid (Fig. 2-6G). It is possible that the high inoculum of *V. fischeri* in the seawater resulted in some bacteria being digested by the squid and that ^{15}N -enriched metabolites were directly incorporated into the gut cells and the endothelial cells surrounding the blood sinus. In one case, I found bacteria-sized spots in the gut lumen that were highly enriched in ^{15}N and thus likely to be bacteria (data not shown). More studies are required to better understand the variation in enrichment between these tissues and the light-organ epithelia.

2.4.2 ^{15}N -enrichment is systematically highest in the nucleolus

The nucleus systematically had the highest enrichment among the cellular organelles (Fig. 2-3A and 7D). Closer examination of the sub-nuclear structures revealed that enhanced ^{15}N -enrichment corresponded with euchromatin regions rather than those dominated by heterochromatin, while the nucleolus was systematically the most ^{15}N -enriched structure in all experiments and across all exposure times.

In eukaryotes, nuclear DNA is packaged into chromatin and is constantly undergoing remodeling to enable replication, transcription, repair, and/or cell division to take place (Tremethick, 2007). The nucleosome, the basic unit of chromatin composed of DNA wrapped around core histone proteins, is a highly organized structure that maintains the stability and accessibility of the DNA genome. Interphase DNA is organized into two chromatin states— the heterochromatin and the euchromatin, which differ in their level of condensation. It is well established that the level of condensation defines the expression state of the DNA. Heterochromatin is highly condensed, gene-poor, and transcriptionally silent, while euchromatin is less condensed, gene-rich, and more easily transcribed (Huisinga et al., 2006). Chromatin dynamic, i.e., gene regulation, is achieved by post translation modifications (PTMs) on histones (i.e., acetylation, methylation, phosphorylation etc.) and multi-proteins complexes that associate with chromatin (Strahl and Allis, 2000; Gardner et al., 2011). In the nucleus, the rDNA region of the chromosome is termed the nucleolus; the most prominent sub-nuclear structure. The nucleolus is a multifunctional organelle involved primarily in ribosome biosynthesis; it plays a role in the storage and transcription of rDNA and the assembly and maturation of ribosomes. In addition to its main role in the production of ribosome subunits, the nucleolus also functions as a central hub in the coordination of key cellular processes, such as cell-cycle progression, apoptosis, DNA replication and repair, and stress responses (Boulon et al., 2010; Audas et al., 2012a; Audas et al., 2012b).

It is not surprising, therefore, that some pathogenic bacteria exploit the nucleus for their own benefit. Besides their ability to interfere with cytosolic signaling pathways, there is growing evidence that some pathogenic bacteria can target the host nucleus and nucleolus as a strategy to suppress immune

response and take control of essential cellular functions, such as the cell cycle and transcriptional program to promote their own survival. Bacterial molecules and secreted effectors that enter the nucleus can modulate the host epigenome by both direct and indirect mechanisms (reviewed in Hamon and Cossart 2008; Escoll et al. 2016). Host histones can be directly targeted by secreting effectors that mimic the function of eukaryotic proteins. For example, *Chlamydia trachomatis*, *Legionella pneumophila* and *Bacillus anthracis* release proteins that contain a SET domain into the host (Alvarez-Venegas, 2014). The SET domain is an evolutionarily well-conserved sequence that methylates lysine residues in the histones and thus influences gene expression (Dillon et al., 2005). Furthermore, other bacteria proteins that contain a SET domain, such as the one released by *Burkholderia thailandensis*, directly target the nucleolus, activating rDNA gene expression (Li et al., 2013). Such changes in rDNA transcription have been hypothesized to be a mechanism that facilitates pathogen replication by controlling their host's ribosome machinery. Indirect post-translation modifications of chromatin are induced by effectors secreted from *Listeria monocytogenes*, *Escherichia coli*, and *Shigella flexneri* through changing the levels of chromatin-binding proteins or interfering with the access of transcription factors at specific genes (Lebreton et al., 2011; Shames et al., 2011; Harouz et al., 2014).

Until now, the strategy of influencing host nuclear physiology was reported mostly in intracellular bacterial pathogens and a few extracellular bacteria (review in Bierne and Cossart 2012; Escoll et al. 2016). To the best of our knowledge, the use of such strategies in beneficial symbiosis interactions has not yet been reported. It is therefore intriguing to consider the possibility that some of the observed ¹⁵N-enrichment inside the sub-nuclear components was induced by secreted bacterial molecules that specifically target the nucleus, and more notably the nucleolus. This observation raises the question whether targeting the nucleus is a means of communication between the squid and its symbiotic partner, during the early stages of symbiosis? More specifically, could the widespread transcriptional changes in the light-organ epithelia (Kremer et al., 2013) be a result of a direct interaction of bacterial molecules with host nucleus? If so, this may be one reason why such high ¹⁵N-enrichment in the nucleus and the nucleolus was observed. In the following paragraphs, I will outline the requirements for a specific molecule to be able to target the nucleus and nucleolus and discuss whether this possibility exists in the squid-*Vibrio* symbiosis and consider these issues in the context of the presented results.

In eukaryotic cells, transport between the cytoplasm and the nucleus occurs through membrane structures termed nuclear pore complexes. While proteins and macromolecules that are smaller than about 60 kDa or have a diameter of less than 9 nm can passively diffuse across the nuclear envelope (Paine et al., 1975; Talcott and Moore, 1999; Lusk et al., 2007), most molecules with functions in the nucleus are actively transported *via* these nuclear pore complexes (Lange et al., 2007; Marfori et al., 2011). The main determinants that localize a molecule to the nucleus are specialized signals comprised of

6-10 basic positively charged amino acids (mainly lysine and arginine), which are termed nuclear localization sequences (NLS; Paine et al. 1975; Bickmore and Sutherland 2002; Gorski et al. 2006) and which are recognized by karyopherins transporters (Lange et al., 2007; Marfori et al., 2011). The best described sorting signal for nuclear import is the classical NLS (cNLS), which consists of either one (monopartite) or two (bipartite) stretches of basic amino acids separated by 10-12 amino acids residues (Boulikas, 1992). Few consensus sequences of NLS have been identified (Dingwall and Laskey, 1991) however many cNLS appear to be more complex and cannot be inferred only from these consensus sequences (Christophe-Hobertus et al., 1999; Cokol et al., 2000) and some of the cNLS motif can be also found in non-nuclear proteins (Boulikas, 1992). Many factors, such as the location of the signal inside the protein (protein context), flanking sequences (Roberts et al., 1987; Fontes et al., 2003), and the affinity and concentration of the import transporters have limited the reliability of prediction of nuclear-localized proteins (review in Lange et al. 2007; Marfori et al. 2011).

Once imported or diffused into the nucleus, some proteins are uniformly distributed throughout the nucleoplasm, whereas others are targeted to specific nuclear compartments such as the nucleolus. As opposed to the nucleus, there are no known mechanisms of active transport into the nucleolus and many molecules traverse rapidly through this component (Phair and Misteli, 2000; Grünwald et al., 2008). Some NLS also serve as nucleolar localization sequences (NoLS), which are required for the nucleolar localization of peptides and proteins (Dang and Lee, 1989; Hatanaka, 1990; Scott et al., 2010). However, a molecule can also have a separate NoLS sequence independent of the NLS motif (Scott et al., 2010). NoLS transport signals, which are localized closest to the protein termini, contain a high abundance of basic (have a basic side chain at neutral pH), positively charged amino acids, which have a high isoelectric point (ca. 12.7), and are generally rich in arginine with some lysine residues (Scott et al., 2010; Martin et al., 2015). The shortest peptides found to accumulate in the nucleolus are either 6 arginine residues or 4 arginines in combination with NLS motif (Martin et al., 2015). However, although these features are common to all NLS motifs, they are not the sole requirement for nucleolar localization. The strong positively charged amino acid sequences need to be distributed over a certain molecular surface to have the potential to accumulate in the nucleoli. For example, two molecules with the same isoelectric points but with different amounts (5 vs. 15 amino acids) and compositions of amino acids (lysine and arginine) can differ in their nuclear distribution, with the former displaying a homogenous distribution in the nucleus while the latter will display a distinct nucleolar localization (Martin et al., 2015). The strong, positively charged amino acids should be mediated by a counter-charge in the nucleolar compartment. These molecules are likely to interact with the negatively charged nucleic acids, which, stored in the form of rRNA, are highly abundant inside the relatively acidic environment of the nucleolus (pH<7.2) compared to the nucleoplasm (pH=7.2; Martin et al. 2015). Indeed, it was reported

that some proteins can be captured and immobilized in the nucleolus by a family of non-coding nucleolar RNA using nucleolar detention sequences (NoDS; Audas et al. 2012a, 2012b). In fact, of 4500 nucleolar proteins discovered, only ~30% have been directly linked to ribosome biogenesis (Ahmad et al., 2009; Boulon et al., 2010). It was later proposed that the nucleolar proteome can be subdivided into two protein populations: (i) resident proteins that have an active function in ribosomal biosynthesis and (ii) immobilized proteins, which under normal conditions are in constant flux in and out of the nucleolus (Phair and Misteli, 2000). However, in response to certain environmental and cellular stimuli, such as nutritional state and stress signaling, these immobilized molecules are detained in the nucleolus away from their site of action. By doing so, the nucleolus can inhibit basic cellular processes and thus play a central role in their regulation (Audas et al., 2012a; Audas et al., 2012b). These nucleolar proteins have been shown to play a crucial role in modulating cell cycle, cell growth, cell death, DNA replication, and stress response (Boulon et al., 2010). The strict requirements and regulations for targeting the nucleus and nucleolus emphasizes the crucial role that these components play in cells, and suggests that molecules that do not have a nuclear or nucleolar function will either be maintained at low background concentrations or be completely excluded from those regions, especially from the nucleolus.

2.4.2.1 Searching for NLS in *V. fischeri* proteins

Bioinformatics analysis was performed to identify which *V. fischeri* proteins contain NLS motifs and can therefore be considered as potential candidates for targeting the nucleus. Out of a total 3,819 protein sequences of *V. fischeri* ES114 strain, 58 proteins were found to carry a putative NLS sequence (Table S 2-3). The 58 *V. fischeri* proteins were predicted to localize in the cytoplasm (n=27), inner membrane (n=12), periplasmic space (n=1) and outer membrane (n=1), while the location of some remained unknown (n=17). It still remains to be determined whether some of *V. fischeri* proteins that possess the putative NLSs are able to target the nuclei of squid cells. Recent proteome profiling of *V. fischeri* OMVs (J. Lynch, personal communication) showed that 3 out of 243 OMV proteins matched the NLS-containing proteins of *V. fischeri* (Table S 2-3, marked in bold). In the future, it will be important to determine whether these proteins target the host nucleus by, for example, tagging these specific proteins with a fluorescent molecule such as GFP and visualizing their subcellular localization, or deleting the predicted NLS sequence and disabling the import machinery, which should disrupt its transportation into the nucleus. Nonetheless, even if one or more proteins target the nucleus and the nucleolus, our data suggest that they need to accumulate in high proportions inside these two compartments to induce the high ¹⁵N-enrichment that was observed.

An alternative explanation is that *V. fischeri* have proteins with NLS sequences that have not yet been defined as NLS motifs. Despite the great progress that has been made in recent years, the list of

NLS motifs (experimental and homologues) is not complete (Marfori et al., 2011). Proline-tyrosine NLS (PY-NLS) in particular, are not well defined (Lee et al., 2006). Unlike cNLS, PY-NLS sequences are more variable and complex in their structural and biochemical properties, making it more difficult to predict such signals (Xu et al., 2010). Another way to target the nucleus is using small or intermediate-sized molecules (<40-60 kDa), which can either diffuse passively across the nuclear pores, contain cNLSs (Grünwald et al., 2008; Martin et al., 2015), or form stable interactions with a nuclear element, such as chromatin, chromatin-associated proteins, or nascent transcripts (reviewed in Gama-Carvalho and Carmo-Fonseca 2001). An example of this was described in early studies conducted on the heterogeneous nuclear ribonucleoprotein (hnRNP) A1, which showed that, despite its small molecular size (36 kDa), this protein was retained in the nucleus following transcriptional activity, by binding to newly synthesized RNAs (Vautier et al., 2001). This protein was later described to contain the PY-NLS. In *E. scolopes*, an EsPGRP1, a small 23.5 kD PRR protein, does not have a cNLS, and is exclusively observed in the nucleus under normal conditions in the aposymbiotic animal (Troll et al., 2009). *V. fischeri* molecules that mediate the morphogenesis of the squid light organ, TCT and LPS, are small enough (0.92 and ca. 20 kDa, respectively) to diffuse through the nuclear pores. Troll et al. (2009) showed that the loss of the nuclear protein EsPGRP1 in apoptotic cells is induced by purified TCT, which raises the question: is this caused by the direct interaction of TCT with the protein, or through signal transduction? To investigate this hypothesis, previous studies exposed juvenile squids to isotopically labeled ¹⁵N-TCT and subsequently analyzed them with NanoSIMS to visualize the subcellular localization of TCT (Troll et al. 2009; this study, Chapter 1). However, no ¹⁵N-enrichment statistically significant from the natural ratio was observed and therefore there was no evidence to support the sub-cellular or sub-nuclear localization of TCT. Indeed, even if TCT is able to enter the nucleus, it is doubtful whether these concentrations are sufficient to cause the high nucleoli ¹⁵N-enrichment observed in the current study. (For a more detailed discussion on the TCT results please see Chapter 1).

We cannot rule out the possibility that none or only a small amount of bacterial molecules is able to target the sub-nuclear compartments. If this is the case, then the metabolism of ¹⁵N-bacterial products by host cells can provide another possible explanation for the high ¹⁵N-enrichment in the sub-nuclear compartments. Secreted bacterial products can include macromolecules (e.g., LPS, PGN and flagella), metabolic byproducts, and signaling molecules. Bacterial products that are taken up by host cells can be used directly in cell metabolism or be broken down into smaller molecules, which could subsequently act as building blocks for other cellular processes. Because the nucleolus has high metabolic activity, in addition to ribosome biosynthesis (Olson 2004; Pederson and Tsai 2009; reviewed in Boulon et al. 2010), it is not unreasonable to expect high ¹⁵N-enrichment in the nucleoli. Indeed, large-scale proteomic studies reported that within a short period (1-5 h) of exposure to a mixture of amino acids, the nucleoli

undergo the highest protein turnover compared to the nucleus and cytoplasm (Beatty et al., 2006; Boisvert et al., 2012; Wei et al., 2013). The observations that the signaling molecules that are used for communication between symbiotic partners generally function at very low concentrations ($\leq 10^{-8}$ M), and in a highly localized manner, cannot provide an explanation for the relative high enrichment in the nucleoli and the widespread ^{15}N -enrichment patterns and thus further support to this metabolic hypothesis. To try to understand how much of the enrichment is derived from the metabolism of bacterial products in host cells, future studies should investigate, for example, whether the presence *V. fischeri* cells in the seawater affect host-cell metabolism. This could be conducted by inoculating squids with non-labeled *V. fischeri* cells (or their OMVs) together with ^{15}N -labeled amino acids, that can be used in metabolic processes in the host cells, and compare these results to squids that are exposed only to the latter.

2.4.3 The squid response to OMVs was stronger than to whole bacteria

Squids exposed to OMVs had higher levels of ^{15}N -enrichment than those exposed to whole bacteria (Table S 2-1C and S 2-2B). These differences were significant as early as 1 h after inoculation. Interestingly, this phenomenon was not confined to the light-organ epithelia, but was also observed in other organs and tissue types, such as gills, connective tissue and gut, where most cells and their sub-nuclear components were enriched. Our results agree with the findings of Aschtgen et al. (2015, 2016) who also observed a more accentuated response (i.e., haemocyte trafficking, apoptosis and regression of the light-organ appendages) in squid cells following exposure to OMVs compared to whole bacteria. Exposure to OMVs, resulted in maximum levels of haemocyte trafficking as early as 3 h post-colonization, whereas exposure to bacteria cells took 18-24 h to attain comparable levels (Aschtgen et al., 2015). Levels of appendage apoptosis were similarly high within 10 h (Aschtgen et al. 2016). The authors argued that *V. fischeri* OMVs reach the deep crypts (the place from where the irreversible signal of morphogenesis is delivered) more quickly, compared to bacterial cells, which must first migrate and then colonize the crypts space before they can trigger this response. Alternatively, the high concentration of OMVs that was added to the seawater may enhance the supply of bacterial products to the squid cells to levels that are higher than those secreted by the bacteria cells, resulting in stronger ^{15}N -enrichment being observed in the OMV treatment. In addition, some molecules can be present at higher quantities inside the vesicles (Kulp and Kuehn, 2010). At 3 h exposure to OMVs, ^{15}N -enrichment inside the host cells was more evident than 1 h. Studies showed an increase with time in OMVs association with host epithelial cells which they explained as either binding of vesicles to receptors induce upregulation of the OMVs receptors or recycling back of these receptors to the cell surface after internalization of their content (Bauman and Kuehn, 2009; Parker et al., 2010). The higher enrichment that was observed at 6 h post inoculation with *V. fischeri* cells further suggests a dose-dependent response in which a cumulative

response to bacterial-derived molecules over time was observed. If true, then this would raise questions about the lack of detectable ^{15}N -enrichment at 14 h post inoculation with *V. fischeri* cells. I suggest that the host cells have reduced or completely stopped the uptake of bacterial products from the seawater and the ^{15}N -enrichment that was already incorporated into the cells has been diluted by normal cell metabolism and respiration to background levels. At 14 h, bacteria have fully colonized the crypts and the irreversible signal for regression of the appendage has already been delivered. It is conceivable that, after the successful colonization of the crypts and the delivery of the morphogenesis signal, the squid is less receptive to diffusible or secreted symbiont molecules in the surrounding seawater. This hypothesis was suggested as a possible explanation for the decrease in host-secreted mucus along the ciliated epithelial appendages, after *V. fischeri* permanently colonized the crypts (Nyholm et al., 2002). Once colonization is established, mucus secretion is suppressed, preventing bacteria from forming normal aggregates and further colonizing the squid. One possibility is that *V. fischeri* cells alter the activity or density of the receptors to PGN at these surfaces, resulting in a decreased sensitivity to PGN derivatives (Nyholm et al., 2002). The high variability in ^{15}N -enrichment that exists between squid individuals makes it difficult to conclusively prove or disprove this hypothesis, but this is an interesting topic for future experiments.

Small ^{15}N -hotspots that appear to be associated with the mucus matrix coating the ciliated fields and microvilli surface of the cells in the `shoulder` and the gills were observed in squid that were exposed to OMVs, as early as 1 h (Fig. 2-7B and C). Surprisingly, correlative TEM-NanoSIMS analysis revealed that these hotspots do not correspond to OMVs (Fig. 2-7B and C, inset). To verify that the integrity of the vesicle membranes was not impaired by the protocol, the purified vesicles were embedded in resin and observed using TEM. These images showed intact vesicles membrane, suggesting that the integrity of these structures was not compromised by the sample preparation. This finding raises two main questions: (i) how does ^{15}N -enrichment occur without observing vesicles, and (ii) why is ^{15}N -hotspot enrichment restricted to these regions? To the best of our knowledge, no study has investigated the accumulation of OMVs or their content on the surface of host cells. However, most if not all research that used epithelial cells to study OMVs were conducted on cell cultures that are devoid of cilia and microvilli, which are otherwise normal characteristics of the apical surface of epithelial cells in intact animal tissues. Additionally, accumulation of *V. fischeri* vesicles has never been observed on the squid apical surface of the appendage or anywhere else in the light organ (M.S. Aschtgen personal communication). One can speculate that vesicles do not aggregate on the surface because the mucus contains LPS degradative enzymes, such as lipases (Kremer et al., 2013) and acyloxyacyl hydrolase (AOAH) (Munford and Hunter, 1992; Weinrauch et al., 1999), which can degrade OMVs caught in the sticky and thick mucus layer before they are internalized into the cells. To understand whether the ^{15}N -

enrichment on the cell surface is due to the presence of enzymes that degrade the vesicles, future work should involve inhibitors to the actin cytoskeleton polymerization of host cells that will disrupt vesicle association and internalization into the host cells. If the ^{15}N -enrichment still occurs in the presence of this inhibitor, it will provide evidence that the vesicles are enriching these areas before they enter the cells. Another possibility is that some of the OMV content that is internalized by the host cells is trafficked back outside of the cells *via* endocytic recycling. The main routes by which OMVs enter non-phagocytic host cells is through endocytosis pathways. Indeed, in the squid, the internalization of *V. fischeri* OMVs into squid epithelial cells and haemocytes is known to be a pre-requisite for inducing the squid response (Aschtgen et al., 2015).

Endocytosis occurs by a number of diverse mechanisms including clathrin-dependent endocytosis, and clathrin-independent pathways such as macropinocytosis, caveolin-mediated uptake, and lipid raft-mediated internalization (O'Donoghue and Krachler, 2016). Regardless of the mode of entry, transport vesicles are usually fused with each other to form an early endosome, where sorting occurs. From these early endosomes, the cargo is either trafficked to the late endosomes and the lysosomes for degradation, delivered to the Golgi apparatus-ER network, or recycled back to the plasma membrane (e.g., Doherty and McMahon 2009; Grant and Donaldson 2009). Recycling can also occur at later steps, *via* the perinuclear endocytic recycling compartment and subsequent transportation to the plasma membrane. Some of the earliest evidence for the existence of endocytic recycling comes from bacterial toxins, such as the plant toxin ricin (Iversen et al., 2001) and Shiga toxin (Mallard et al., 1998). It is not clear, however, how many molecules are recycled in the plasma membrane and whether or not they stay bound to the plasma membrane or are exported back to the extracellular matrix. It is possible that a fraction of ^{15}N -enriched cargo produced by the OMVs is recycled back to the cell surface; this phenomenon is what was observed in form of hotspots that were associated with the cilia and microvilli. To my knowledge, there is no literature observing such a mechanism operating after OMV internalization.

Interestingly, I observed the same small hotspots at the 'shoulder' region 6 h after exposure to whole bacteria. It is therefore possible that the symbiont-induced ^{15}N -enrichment on the cell surfaces is due to of OMVs secretion by the whole bacteria. But, why do we see ^{15}N -enrichment localized in these regions? One theory is that the strong current that is generated by the cilia along the apical surface of the appendage, which helps in concentrating bacterial in aggregates above the pores (Nyholm et al. 2000; Nawroth et al. in press), is weak or completely stagnant in this 'shoulder' area and thus molecules and small particles get stalled in the thick mucus layer coating these regions. Indeed, if the activity of cilia is stopped, particles and debris adhere to the mucus along the appendages (Nawroth et al. in press). Differences in the structural and biochemical characteristics of the epithelial cells along these surfaces

might cause these differences. Koropatnick et al. (2014) showed that the appendage epithelium is comprised of two heterogeneous cell layers; the medial side is a thin monolayer, whereas the lateral side is thicker and contains large compartmental spaces, which are separated by thin septa. Biochemical differences between these two regions have been observed particularly in squid-derived chitinase, which is important for the initiation of symbiosis (Kremer et al., 2013) and which is accumulated along the medial side but not the lateral side of the appendage (Koropatnick et al., 2014).

It should be noted that host factors can affect the cohort of molecules inside the OMVs and the amount that is produced by the bacteria cells (e.g. CFTR inhibitory factor in *P. aeruginosa*; review Orench-Rivera and Kuehn, 2016). Therefore, by using purified OMVs from a bacteria growth culture, I cannot rule out the possibility that it would have affected some of their content and consequently the ¹⁵N-enrichment results inside host cells.

2.4.4 Conclusion and future directions

In summary, the data presented here provide evidence for transfer of soluble bacterial products and OMVs into squid tissues and cells early after the initiation of symbiosis. The fact that differential ¹⁵N-enrichment between tissues was observed, suggests that the squid is selective in their response to bacteria and OMVs. The comparable ¹⁵N-signature that was observed in the squid after the addition of the OMVs and whole bacteria, combined with the results of previous studies showing that OMVs are responsible for inducing the squid phenotype during the development of symbiosis, raises the question of whether squids respond in specific manner to the presence of *V. fischeri*-derived products or whether any bacterial species can induce similar enrichment patterns. In the next Chapter I will discuss how this question was addressed by inoculating juvenile squids with ¹⁵N-labeled non-symbiotic bacterial cells or their OMVs and compared the results with the enrichment patterns that is observed after inoculation with the ¹⁵N-labeled symbionts. Such experiments were designed to elucidate the nature and the specificity of the molecular interactions that induce the ¹⁵N-enrichment patterns.

2.5 Supplementary information

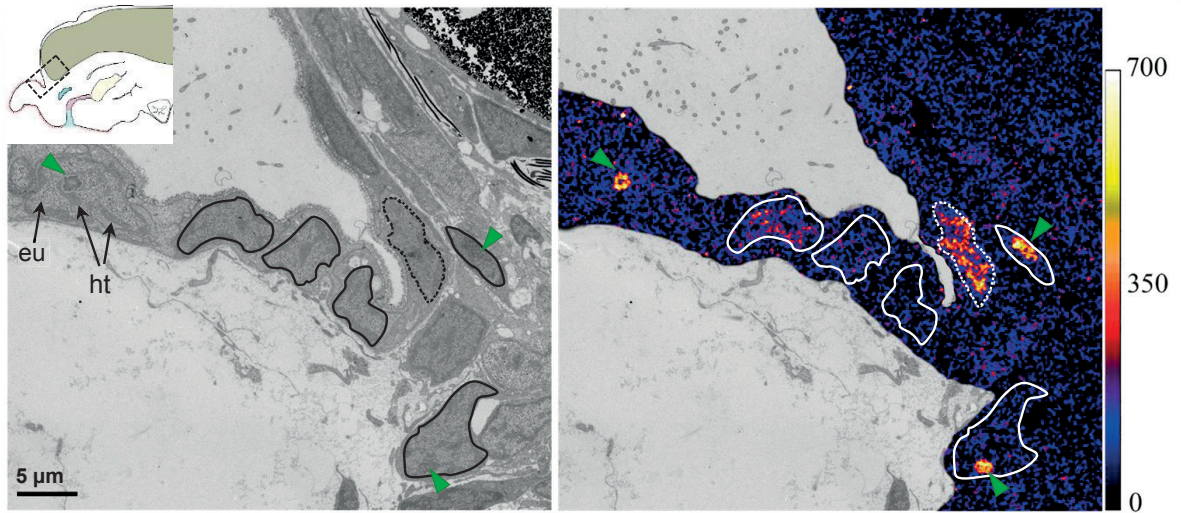


Fig. 2-S1. Differences in ¹⁵N-enrichment in the nuclei of squid epithelial cells that are lining the medial appendage, 2 h post inoculation with ¹⁵N-*V. fischeri* cells. TEM micrograph (left) and the corresponding NanoSIMS ¹⁵N/¹⁴N ratio (right) images. Inset in A illustrates the 'shoulder' area where the images were taken. The nucleolus is shown by the green arrowheads. The black (left) and white (right) outlines are the contour of the cell nuclei. Dashed contour showing a nucleus where the euchromatin regions exhibited high levels of ¹⁵N-enrichment that were comparable to the nucleoli enrichment of the adjacent cells. Values for the NanoSIMS scale are expressed in ‰ (see 'General procedure for NanoSIMS analysis').

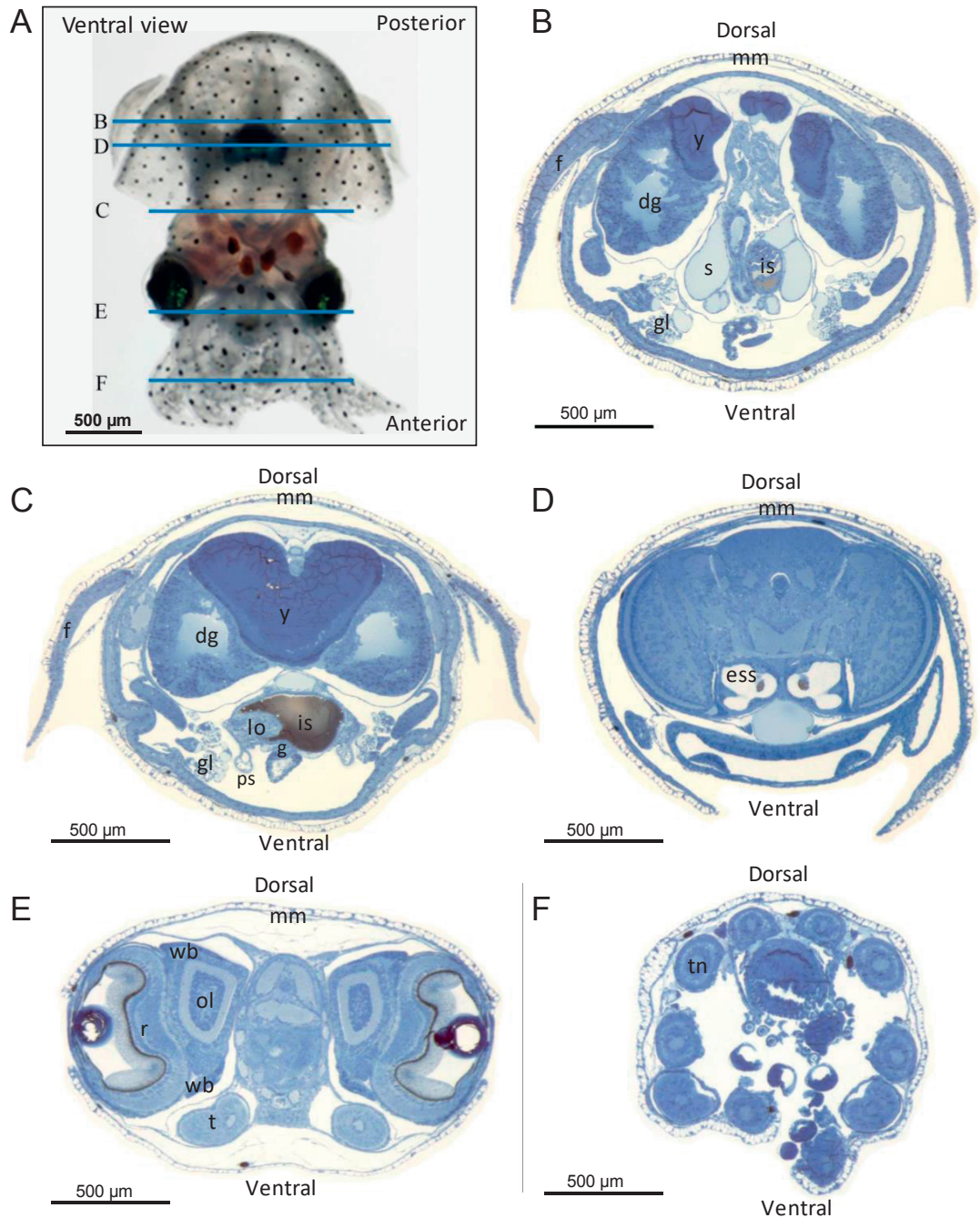


Fig. 2-S2. Light micrographs of histological cross section (0.5 µm thick) of a juvenile *E. scolopes* showing the different organs that were analyzed in this study and their location in the squid. (A) A ventral view of the juvenile squid showing the planes of the images that are presented in (B)-(F). Squids were sectioned from the posterior. The approximate locations of the planes are B-480 µm, C-610 µm, D-1020 µm, E-1560 µm, F-1930 µm. Sections were stained with a mixture of Toluidine-blue and borax. b, brain; dg, digestive gland; ess, epithelium supporting statolites; f, fin; gl, gills; g, gut; is, ink sac; lo, light organ; mm, mantle muscle and mucus cells; ol, optic lobe; pa, posterior appendage; r, retina; s, sinus blood; tn, tentacles y, yolk sac; wb, white body. [The white body is the place in cephalopods where haemocytes are developed (Cowden and Curtis 1981-taken from Nyholm et al.2009)].

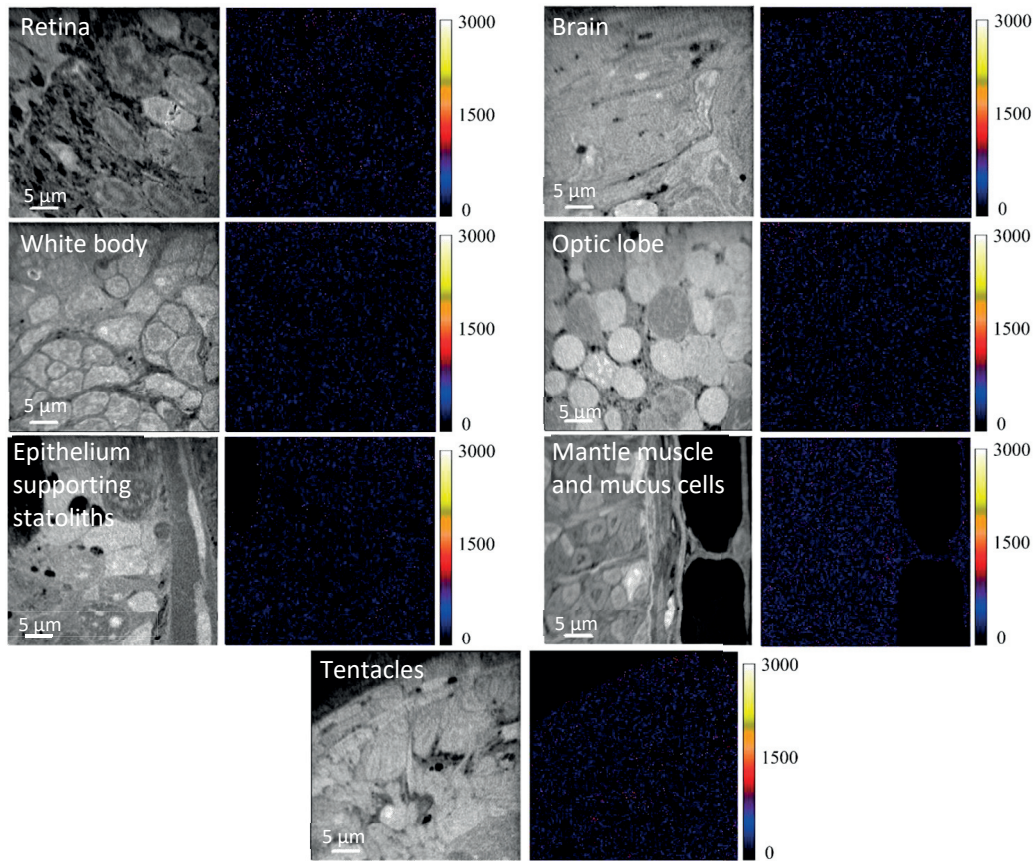


Fig. 2-S3. ^{15}N -enrichment in various epithelial tissues of the juvenile squid, 3.5 h post inoculation with ^{15}N -labelled *V. fischeri* cells. Left panels show tissue structure (NanoSIMS $^{12}\text{C}^{14}\text{N}$ image). Right panels show corresponding, quantified NanoSIMS $^{15}\text{N}/^{14}\text{N}$ ratio image. ^{15}N -enrichment in these organs were similar to the background levels of $^{15}\text{N}/^{14}\text{N}$. Values for the NanoSIMS scale are expressed in ‰ (see ‘General procedure for NanoSIMS analysis’).

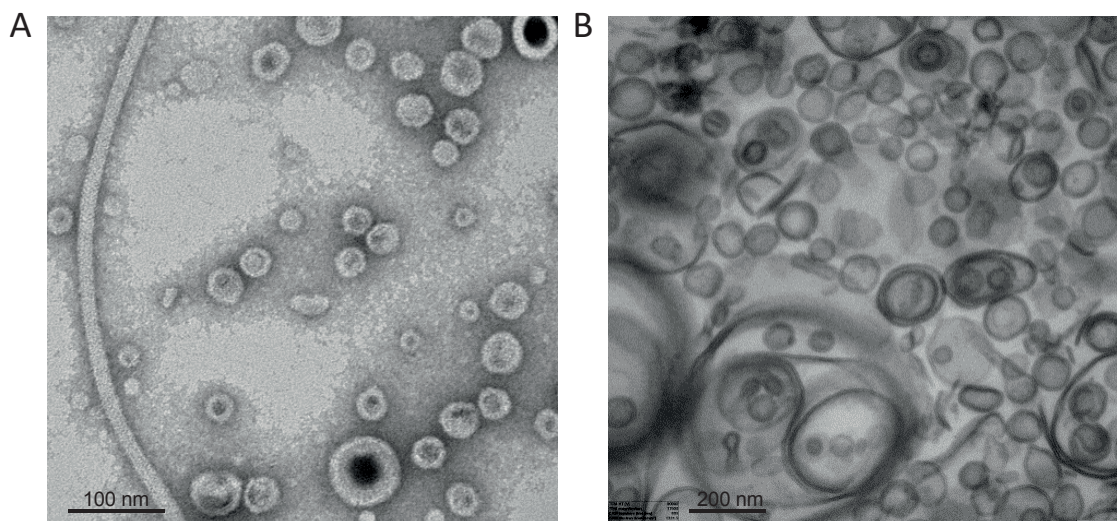


Fig. 2-S4. TEM micrographs of purified OMVs produced by wild-type *V. fischeri* (ES114). (A) Negative-stained OMVs. (B) Resin-embedded OMVs. OMVs were fixed following a similar fixation-infiltration procedure as the used with squid samples.

Fig. 2-S5. ^{15}N -enrichment in the connective tissue (A), gills (B) and reflector (C) after 3.5 h inoculation with ^{15}N -OMVs purified from *V. fischeri* cells. Left panels show TEM micrograph and the right panels show the corresponding NanoSIMS $^{15}\text{N}/^{14}\text{N}$ ratio (right) images. In the gills, ^{15}N -hotspots were also observed on the surface of the epithelial cells. Interestingly, haemocytes cells in the gills were not enriched in ^{15}N in contrast to the haemocytes in the appendage sinus. Values for the NanoSIMS scale are expressed in ‰ (see 'General procedure for NanoSIMS analysis').

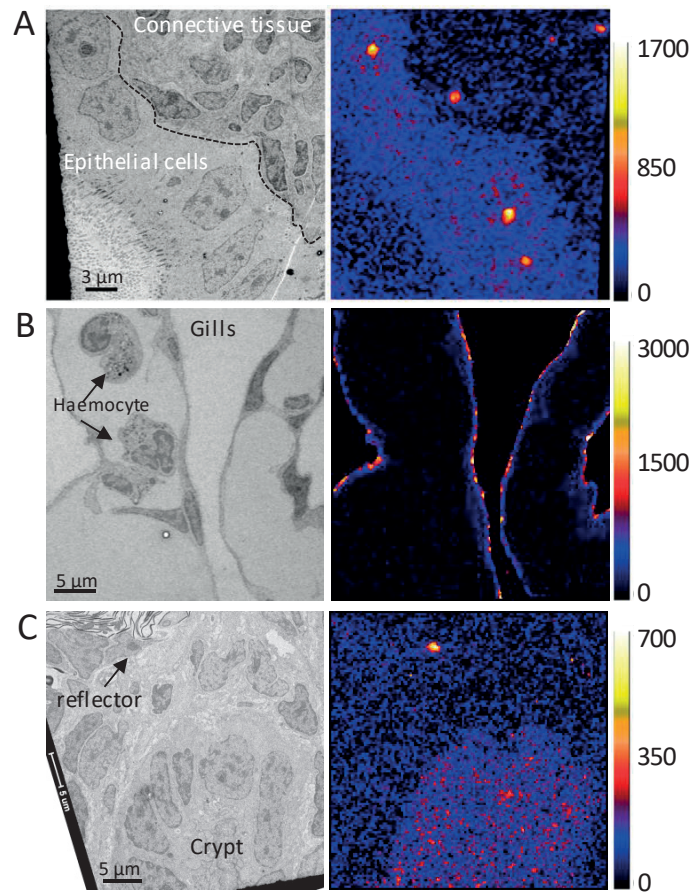


Table S 2-1 Statistical analysis of squids inoculated with *V. fischeri* cells for 2 h (3 animals) and 3.5 h (6 animals) post inoculation. Analysis for (A) and (B) was based on the ¹⁵N-enrichment obtained from high-resolution NanoSIMS mosaics (illustrated in Fig. 2-2B). (A) ¹⁵N-enrichment in the nuclei and compared between the different light-organ compartments (appendage, pore, duct, crypt). (B) ¹⁵N-enrichment in the cytoplasm, nuclei and nucleoli of the light-organ epithelial cells. (C) Comparison of the ¹⁵N-enrichment in the nucleoli of the light-organ epithelial cells were done for all squid animals and compared between time points and compartments (Fig. 2-3B). Mean values, for this analysis, are presented as both δ¹⁵N (‰) and as relative labeling index (RLI= δ¹⁵N of a specific nucleolus/ δ¹⁵N average of all nucleoli per squid). RLI was used for the statistical analysis. (D) Enrichment in other organs, i.e., connective tissue, gills, endothelial cells, gut, and digestive gland were compared to the epithelial cells of the light organ in the 3.5 h experiment (Fig. 2-6 and 2-53). Only ¹⁵N-enriched nuclei at a level of 3 standard deviations above the average ¹⁵N/¹⁴N ratio of nuclei in a control samples, were included in the statistical analyses. CYT, cytoplasm; N, nucleus; Nu, nucleolus; Ap, appendage; Po, pore; Du, duct; Cr, crypt; Dg, digestive gland; Gl, gills; G, gut; CT, connective tissue.

	Variables			N	Mean (‰)	SD (‰)	Mean (RLI)	SD (RLI)	Statistics	P value
	Time	Tissue	Cell organelle							
A	2h	Appendage	Nucleus	56	84	17			Kruskal-Wallis test: χ ² = 114.7, df = 4	<0.0001
		Pore	Nucleus	58	69	9				
		Duct	Nucleus	36	53	9				
		Crypt	Nucleus	142	64	11				
									Nemenyi post-hoc: Ap ≠ Po ≠ Du ≠ Cr	
B	2h	Appendage	Cytoplasm	26	45	6			Kruskal-Wallis test: χ ² = 70.9, df = 2	<0.0001
			Nucleus	56	84	17				
			Nucleolus	14	328	177				
		Pore	Cytoplasm	24	43	7			Kruskal-Wallis test: χ ² = 73.5, df = 2	<0.0001
			Nucleus	58	69	10				
			Nucleolus	18	220	60				
		Duct	Cytoplasm	27	34	6			Kruskal-Wallis test: χ ² = 50.4, df = 2	<0.0001
			Nucleus	36	53	9				
			Nucleolus	6	173	46				
		Crypt	Cytoplasm	27	46	9			Kruskal-Wallis test: χ ² = 156.3, df = 2	<0.0001
			Nucleus	142	64	11				
			Nucleolus	67	176	68				
									Nemenyi post-hoc: CYT ≠ N ≠ Nu	
C	2h	Appendage	Nucleolus	37	350	118	1.33	0.45	Two-way Anova: Main model: F _{5,372} = 20.1 Time: F _{1,372} = 2.10 Compartment: F _{2,372} = 49.8 Time*Compartment: F _{2,372} = 5.28	<0.0001
		Pore	Nucleolus	44	255	87	0.99	0.31		
		Crypt	Nucleolus	80	201	45	0.85	0.17		
	3.5h	Appendage	Nucleolus	90	427	248	1.1	0.27		
		Pore	Nucleolus	54	440	220	0.98	0.21		
		Crypt	Nucleolus	73	313	73	0.89	0.22		

Chapter 2 Tracking *V. fischeri*-derived molecules into squid host tissues during initiation of symbiosis

	Time	Variables		N	Mean (%)	SD (%)	Mean (RLI)	SD (RLI)	Statistics	P value	
		Tissue	Cell organelle								
D	3.5h	Epithelial cells in the light organ	Nucleus	72	81	23			Kruskal-Wallis test: $\chi^2 = 175.1$, df = 5	<0.0001	
		Connective tissue	Nucleus	59	30	18					
		Gills	Nucleus	34	57	26					
		Endothelial cells	Nucleus	48	40	27					
		Gut	Nucleus	100	27	15					
		Digestive gland	Nucleus	31	46	13					
		Brain	Nucleus	16	8	15					Not-labeled
		Retina	Nucleus	11	-7	11					
		Tentacles	Nucleus	29	-1	15					
		White body	Nucleus	27	5	12					
		Epithelium supporting statolith	Nucleus	27	7	11					

Table S 2-2 Statistical analysis of squids inoculated with OMVs from *V. fischeri* cells for 1 h (5 animals) and 3 h (4 animals). (A) ¹⁵N-enrichment in the cytoplasm, nuclei and nucleoli were compared only for the appendage epithelium (Fig. 2-7D). (B) Comparison of the ¹⁵N-enrichment in the nucleoli of the light-organ epithelial cells were compared between time points and compartments (Fig. 2-7E). Mean values are presented as both δ¹⁵N (‰) and as relative labeling index (RLI= δ¹⁵N of a specific nucleolus/ δ¹⁵N average of all nucleoli per squid). RLI was used for the statistical analysis. CYT, cytoplasm; N, nucleus; Nu, nucleolus; Ap, appendage; Po, pore; Cr, crypt.

	Variables			N	Mean (‰)	SD (‰)	Mean (RLI)	SD (RLI)	Statistics	P value
	Time	Tissue	Cell organelle							
A	1h	Appendage	Cytoplasm	47	243	43			Kruskal-Wallis test: χ ² = 67.3, df = 2 Nemenyi post-hoc: CYT = N ≠ Nu Kruskal-Wallis test: χ ² = 79.4, df = 2 Nemenyi post-hoc: CYT ≠ N ≠ Nu	<0.0001
			Nucleus	91	272	63				
			Nucleolus	26	804	300				
	3h	Appendage	Cytoplasm	46	274	96				
			Nucleus	91	349	103				
			Nucleolus	30	1470	545				
B	1h	Appendage	Nucleolus	44	653	232	1.52	0.33	Two-way Anova: Main model: F _{3,294} = 120.5 Time: F _{1,294} = 15 Compartment: F _{2,294} = 178.7 No interactions Tukey post-hoc: 1h: Ap ≠ Po ≠ Cr 3h: Ap ≠ Po ≠ Cr	<0.0001
			Pore	55	381	98	0.96	0.17		
			Crypt	65	271	90	0.68	0.19		
	3h	Appendage	Nucleolus	48	1015	517	1.49	0.72		
			Pore	42	649	281	0.92	0.29		
			Crypt	44	316	123	0.54	0.2		

Table S 2-3 *V. fischeri* ES114 proteins with NLS sequences. Out of total 3,819 protein sequences, 58 proteins were found to carry a putative NLS sequence. Rows in bold refer to proteins found in *V. fischeri* OMVs.

No.	BioCyc protein Id	Name	Predicted NLS sequence	Predicted localization in bacteria
1	G12Y8-2890-MONOMER	RNA helicase	449_KKKRPFSGPKTKGTGENRNGSNFGKSK_477	Cytoplasmic
2	G12Y8-2983-MONOMER	GGDEF/EAL domain-containing protein	554_KRKRKSKK_562	Cytoplasmic Membrane
3	G12Y8-3282-MONOMER	type I restriction-modification system restriction subunit	841_PDPRKIKQ_848	Unknown
4	G12Y8-3296-MONOMER	ATP-dependent RNA helicase	448_PKKKPKQ_454	Cytoplasmic
5	G12Y8-3525-MONOMER	TonB protein	132_RALKRR_137	Unknown
6	G12Y8-3558-MONOMER	4-alpha-glucanotransferase	154_RKRRKAPYEMTLIVTPKACFKQDAMLKGG_182	Cytoplasmic
7	G12Y8-3776-MONOMER	polysaccharide export periplasmic protein	141_RLQLRRSNKV_150	Periplasmic
8	G12Y8-3780-MONOMER	Fis family transcriptional regulator	328_LKKYAKEDHKFKALKR_344	Cytoplasmic
9	G12Y8-3846-MONOMER	CP4-6 prophage; ferric transporter subunit	167_KIRKRLR_173	Cytoplasmic Membrane
10	G12Y8-5-MONOMER	50S ribosomal protein L34	11_KRKRSH_16	Cytoplasmic
11	G12Y8-54-MONOMER	delta-aminolevulinic acid dehydratase	12_RRMRRMR_18	Cytoplasmic
12	G12Y8-55-MONOMER	guanosine pentaphosphate phosphohydrolase	37_KIKRQVR_43	Cytoplasmic
13	G12Y8-67-MONOMER	adenylate cyclase	645_EKRRRF_650	Cytoplasmic
14	G12Y8-79-MONOMER	2-polyprenyl-3-methyl-5-hydroxy-6-methoxy-1, 4-benzoquinol methylase	18_DKRRR_23	Unknown
15	G12Y8-102-MONOMER	ribonuclease BN	127_KKKRRP_132	Cytoplasmic Membrane
16	G12Y8-106-MONOMER	bifunctional (p)ppGpp synthetase II/ guanosine-3',5'-bis pyrophosphate 3'-pyrophosphohydrolase	154_KRRRI_158	Unknown
17	G12Y8-460-MONOMER	ATP-dependent RNA helicase SrmB	397_KKKAALAKKAPKPKK_413	Cytoplasmic
18	G12Y8-471-MONOMER	dinucleoside polyphosphate hydrolase	161_RKFKRKGKK_169	Cytoplasmic
19	G12Y8-501-MONOMER	translation initiation factor IF-2	261_PRRRK_265	Cytoplasmic
20	G12Y8-503-MONOMER	tRNA pseudouridine synthase B	3_RRRKGRPVNGVILIDKPTGITSNDTLQKVK_32	Cytoplasmic
21	G12Y8-575-MONOMER	Signal recognition particle (SRP) component with 4.5S RNA (ffs)	398_RKKRIAAGSGVQVQDVNRMLKFTQMCKMMKMQK_432	Cytoplasmic Membrane
22	G12Y8-683-MONOMER	tRNA-specific adenosine deaminase	153_RRRKEKKE_160	Cytoplasmic
23	G12Y8-735-MONOMER	riboflavin synthase subunit alpha	66_ETLKRT_71	Cytoplasmic
24	G12Y8-845-MONOMER	DNA-binding ATP-dependent protease Lon (La)	304_KRSKVKK_310	Cytoplasmic
25	G12Y8-1336-MONOMER	paraquat-inducible protein A	19_AKVKKKQ_25	Cytoplasmic Membrane
26	G12Y8-1425-MONOMER	formate dehydrogenase subunit delta	251_ARAKGKRFQ_259	Cytoplasmic
27	G12Y8-1435-MONOMER	LamB/YcsF family protein	237_LRKLLKS_243	Unknown
28	G12Y8-1492-MONOMER	acrylsulfatase-like protein	4_KKGTKRRL_11	Unknown
29	G12Y8-1534-MONOMER	superfamily I DNA/RNA helicase	434_KRKT_438	Cytoplasmic
30	G12Y8-1575-MONOMER	methyltransferase	12_DKALRRR_18	Cytoplasmic

Chapter 2 Tracking V. fischeri-derived molecules into squid host tissues during initiation of symbiosis

31	G12Y8-1588-MONOMER	DnaK-like molecular chaperone	684_KKRRRR_689	Cytoplasmic
32	G12Y8-1629-MONOMER	ATP-dependent helicase HrpA	285_RRTHQRN_291	Unknown
33	G12Y8-1772-MONOMER	coniferyl aldehyde dehydrogenase	381_KRPRP_385	Cytoplasmic
34	G12Y8-1911-MONOMER	multifunctional fatty acid oxidation complex subunit alpha	217_KKKAKRKL_224	Cytoplasmic
35	G12Y8-1921-MONOMER	cytochrome c-type biogenesis protein CcmE	3_PRRKKRL_9	Unknown
36	G12Y8-2086-MONOMER	phosphate regulon sensor protein	87_KKRRK_91	Cytoplasmic Membrane
37	G12Y8-2105-MONOMER	phage R protein	6_LKRKART_12	Unknown
38	G12Y8-2196-MONOMER	GTP-binding protein LepA	560_RKKLLKKQKEGKKR_574	Cytoplasmic Membrane
39	G12Y8-2289-MONOMER	poly(A) polymerase	460_KRRSPYRKKKR_470	Cytoplasmic
40	G12Y8-2327-MONOMER	transpeptidase	121_KRKELISKIEKNKRR_136	Cytoplasmic Membrane
41	G12Y8-2459-MONOMER	ribosome-associated GTPase	3_KKKKLTGQVRRVRSNQKKRIEK_25	Cytoplasmic
42	G12Y8-2479-MONOMER	protease with a role in cell division	214_RKRITNESSYLNELQQNEKRLK_235	Outer Membrane
43	G12Y8-2534-MONOMER	DNA-directed RNA polymerase subunit beta'	213_KRKKVTKRLK_222	Cytoplasmic
44	G12Y8-2587-MONOMER	RNA polymerase factor sigma-32	133_RKFFNLRNKKNR_145	Cytoplasmic
45	G12Y8-2593-MONOMER	multiple antibiotic resistance protein MarC	33_KRRRI_37	Cytoplasmic Membrane
46	G12Y8-2704-MONOMER	potassium transporter peripheral membrane protein	105_LREKER_110	Cytoplasmic Membrane
47	G12Y8-3032-MONOMER	hypothetical protein	3_RKKVKDAILKHKRNQTKQSRANKPK_29	Unknown
48	G12Y8-3053-MONOMER	hypothetical protein	58_KKRTH_62	Cytoplasmic Membrane
49	G12Y8-3351-MONOMER	hypothetical protein	13_RKNKLR_20	Unknown
50	G12Y8-3886-MONOMER	hypothetical protein	19_KRKRKFKELIHLHSIVEAENKRPK_44	Unknown
51	G12Y8-80-MONOMER	hypothetical protein	34_KRKRKRK_40	Unknown
52	G12Y8-330-MONOMER	hypothetical protein	16_KKKRR_20	Unknown
53	G12Y8-1058-MONOMER	hypothetical protein	174_LKKRLKS_180	Cytoplasmic
54	G12Y8-1124-MONOMER	hypothetical protein	57_KRPKRRRK_65	Unknown
55	G12Y8-1196-MONOMER	hypothetical protein	26_RKMMKLNLENKRRIRK_45	Unknown
56	G12Y8-1608-MONOMER	hypothetical protein	25_KKKLTIHQQQSSHKSPVVPFDDEADKDK_55	Unknown
57	G12Y8-1846-MONOMER	hypothetical protein	763_RRRRRDRR_770	Cytoplasmic
58	G12Y8-2710-MONOMER	hypothetical protein	145_KRRKQDMKKTPLLRLKTLK_165	Cytoplasmic Membrane

Chapter 3 Tracking molecules from non-symbiotic bacteria into squid host tissues during the early hours after hatching

3.1 Introduction

The establishment of specificity between a host and its symbiotic partner has been an area of great interest among biologists. This phenomenon is most notable in horizontally transmitted symbiosis where the host selects its symbionts anew each generation (Douglas, 1998). Throughout evolution, animals developed anatomical, cellular, and molecular mechanisms to promote successful transmission of specific bacterial symbionts between generations, while discouraging others, and even discriminating between closely related bacteria strains or species (Douglas, 1998; Chaston and Goodrich-Blair, 2010).

The symbiosis between the Hawaiian bobtail squid *Euprymna scolopes* and the marine bioluminescent bacterium *Vibrio fischeri* is highly specific and depends on the strict selection of *V. fischeri* against a background of many other, non-symbiotic bacteria in the seawater (McFall-Ngai and Ruby, 1991). This exclusive relationship is mediated via a series of biomechanical, biochemical, and reciprocal molecular features that ensure the successful selection of *V. fischeri* from the environment and the long-term maintenance of the association (e.g., Nyholm and McFall-Ngai 2004; McFall-Ngai et al. 2012; Stabb and Visick 2014). Extensive work has been carried out to elucidate species-specificity in the squid-*Vibrio* association and the ability of the squid to interact with and respond to non-symbiotic bacteria (Nyholm et al., 2002; Nyholm and McFall-Ngai, 2003; Altura et al., 2013; Aschtgen et al., 2015).

Specificity of the symbiosis starts early in the interaction; the squid and its symbiont must physically contact and recognize one another among the vast array (ca. 10^6 cells/mL) of bacterioplankton that are present in the natural seawater (Nyholm and McFall-Ngai, 2003). However, while the squid specifically responds to a very low number of *V. fischeri* cells in the early stages of symbiosis (Kremer et al., 2013; Altura et al., 2013), studies have demonstrated that the host is also able to sense other bacteria species to some extent (Nyholm and McFall-Ngai, 2003; Nyholm et al., 2009; Altura et al., 2013). For a short period after hatching, the light organ is permissive to any bacteria (Gram-negative or -positive) or particles less than 2 μm in diameter. However, 2 h after hatching all invaders including *V. fischeri* are eliminated from the light organ. During this period *V. fischeri* cells begin to gather along the mucociliary surface of the organ and associate intimately with host cells. Nevertheless, interaction with host cilia is not specific only to *V. fischeri*. In the absence of *V. fischeri*, Gram-negative bacteria can form tight aggregates (Nyholm and McFall-Ngai 2003; Altura et al. 2013; S. Koehler, personal communication) and some can even temporarily reach the light-organ duct (Nyholm and McFall-Ngai, 2003). The main factors

controlling host response to *V. fischeri* are common cell envelope molecules that are widely shared among bacteria (e.g., lipopolysaccharide [LPS], peptidoglycan [PGN]). When co-incubated with the squid, non-symbiotic products, such as outer membrane vesicles (OMVs), PGN, and LPS can trigger light-organ responses similar to *V. fischeri* molecules. For example, shortly after hatching, PGN from both Gram-positive and -negative bacteria induce mucus secretion from the appendage epithelium (Nyholm et al., 2002). Purified *V. fischeri* LPS, as well as LPS from other bacterial species, can attenuate the host enzyme responsible for nitric oxide (NO) production in the light organ (Nitric Oxide Synthase or NOS; Altura et al. 2013) and act synergistically with any PGN to elicit apoptosis of the appendage cells (Foster et al., 2000). More recently, studies have shown that OMVs produced by non-symbiotic environmental bacteria (*V. parahaemolyticus*, *V. harveyi*, and *E. coli*) are capable of inducing characteristics of normal developmental program in the light organ (e.g., haemocyte trafficking) similar to the response caused by symbiont OMVs (Aschtgen et al., 2015). Of note, in the natural seawater environment, none of the non-specific environmental bacteria cells or products, other than PGN-induced mucus shedding, was found to induce these changes in the squid. It is believed that the context in which the molecules are secreted and presented to the host drives this discrepancy and important for the full light-organ response (McFall-Ngai et al., 2012; Aschtgen et al., 2015).

Using a stable isotope-based approach, combined with TEM and quantitative NanoSIMS imaging I showed in Chapter 2 that transfer of ¹⁵N-labeled *V. fischeri*-derived compounds into squid tissues takes place as early as 2 h after exposure to bacteria cells or their OMVs. This transfer was not exclusive to the light-organ epithelial cells, but was also observed in other squid organs, such as gills and gut. These findings demonstrate that, beyond the very specific signaling between symbiont and host with molecules that we cannot image with the NanoSIMS (such as TCT), there is a more general chemical ‘conversation’ taking place between the two partners. These data then bring into question the specificity of this chemical conversation. To attain a deeper understanding of the nature of these molecular transfers of into host cells, in this Chapter, I compared the host responses to several bacteria the host’s uptake and subcellular distribution of ¹⁵N-labeled *V. fischeri*-derived molecules was compared with the uptake and subcellular distribution of ¹⁵N-labeled molecules derived from non-symbiont species. These non-symbiont species included other Vibrionaceae, *Vibrio parahaemolyticus* and *Photobacterium leiognathi*, and *Escherichia coli*.

3.2 Material and Methods

3.2.1 General procedures

Adult *E. scolopes* were collected in Oahu, Hawaii and transported to the Kewalo Marine Laboratory, where breeding animals were maintained in a recirculating seawater system (Doino and

McFall-Ngai, 1995). All experiments were performed in accordance with the relevant regulatory standards established by the University of Hawaii at Manoa.

3.2.2 Bacterial strains and growth conditions

Four bacteria species were used in this study: wild type *Vibrio fischeri* (ES114; Boettcher and Ruby 1990), *Vibrio parahaemolyticus* (KNH1; Nyholm et al. 2000), *Photobacterium leognathi* (KNH6; E. Stabb, personal communication) and *Escherichia coli* (RP437; Zhou et al. 1998). The *Vibrio* strains were grown overnight on LBS agar plates (LB agar containing and additional 2% [wt/vol] NaCl; Graf et al. 1994), while *E. coli* was cultured in LB medium (Bertani, 1951). One colony of bacteria cells was then transferred to a minimal salts media (MSM; Ruby and Nealon 1977), which was supplemented with 11 mM [¹⁵N]-ammonium chloride (NH₄Cl; ¹⁵N, 99%; Cambridge Isotope Laboratories Inc., MA, USA), 40 mM glycerol, 50 mM PIPES buffer (pH 7.2) and 5 g/L of Celtone base powder (¹⁵N, 98%; Cambridge Isotope Laboratories, Inc. MA, USA). Cultures of 100 mL were grown shaking at 28°C and 220 rpm in 125 mL Erlenmeyer flasks to ensure gas exchange occurred between the culture and the air, thereby reducing the possibility of hypoxic conditions. Levels of ¹⁵N-enrichment were maximized by a series sub-culturing the bacteria into fresh labeled-media (initial OD_{600nm} of 0.0025; i.e., 30-40 generations). Cells from the last passage (OD_{600nm} of 0.2-0.5) were thoroughly washed twice in filtered seawater (FSW; 0.2 µm Millipore membrane) by centrifugation (2 min, 8000 rpm) immediately before inoculating the squid. NanoSIMS control samples containing the natural ¹⁵N/¹⁴N isotopic composition analysis were derived following the same protocol, except that bacteria were grown in non-labeled medium.

Before inoculation, it was also important to determine the ¹⁵N-enrichment of bacteria in the culture. To measure this enrichment, a 4-µL aliquot of the washed bacteria was pipetted onto an aluminum stub, and after drying, was analyzed using NanoSIMS (details of this procedure are described in 'General procedure for NanoSIMS analysis'). In the present experiment ¹⁵N-enrichment values in the *Vibrio* strains were about 600-700 fold above the natural ¹⁵N/¹⁴N ratio.

3.2.3 Isolation of outer membrane vesicles (OMVs)

OMVs were purified using a method adapted from Aschtgen et al. (2015). Bacteria were grown to an OD_{600nm} of ~2 in MSM supplemented with ¹⁵N-Celtone base powder, as described before. To obtain a similar amount of OMVs from each strain, *Vibrio* cells were grown in 200 mL while *E. coli* cells were cultured in 1 L (Aschtgen et al., 2016). Bacterial cultures were centrifuged at 4,500 x g for 15 min at 4°C. The resulting supernatant was filtered using 0.45 µm and 0.22 µm pore polyvinylidene difluoride (PVDF) membranes (Millipore Corp., Billerica, MA). The resulting filtrate was then ultracentrifuged at 173,000 x g for 2 h at 4°C in a 90 Ti rotor (Beckman Coulter, Inc., Brea, CA) until a pellet was formed, containing the OMVs. This pellet, was washed 3 times in 15 mL Dulbecco's phosphate buffered saline (dPBS; 0.2 g KCl, 0.2 g KH₂PO₄, 11.7 g NaCl, 1.1 g Na₂HPO₄, 0.1 g MgCl₂*6H₂O, and 0.1 g CaCl₂ per liter deionized water

supplemented with an additional 11.7 g NaCl/L, and filter-sterilized; Aschtgen et al. 2015) and the ultracentrifugation step was repeated after each wash. The vesicle pellet was then resuspended in 1 mL dPBS + NaCl. To determine the protein content of the purified OMVs, the Qubit 2.0 fluorometer was used (Life Technologies, Grand Island, NY) following the manufacturer's protocol. The relative amount of OMV material was also measured using the lipophilic dye FM4-64 (Molecular Probes), as described previously (Aschtgen et al., 2015). For more information regarding the Qubit readings and the lipophilic dye methods, please see Material and Methods in Chapter 2. Purified OMVs were stored at -20°C until animal exposure. Vesicles were visualized by negative staining electron microscopy (see protocol in 'General procedure for NanoSIMS analysis'; Fig 3-S1). OMV concentrations (50 µg protein/mL) for the subsequent experiments were chosen to be similar to previous studies (see Chapter 2).

3.2.4 Squid assays

The goal of this experiment was to compare ¹⁵N-enrichment patterns inside the squid tissues following exposure to either symbiotic or non-symbiotic bacterial cells and/or their OMVs. To achieve this aim, newly hatched *E. scolopes* were placed in FSW from their egg tank, and either ¹⁵N-labeled bacteria cells (*V. fischeri*, *V. parahaemolyticus* and *P. leiognathi*; n=5-7) or ¹⁵N-labeled purified OMVs (50 µg/mL; *V. fischeri*, *V. parahaemolyticus* and *E. coli*; n=3-5) were added. The duration of the incubations lasted for 3.5 h and 3 h for bacteria cells and OMVs, respectively. Control samples consisted of squids inoculated with unlabeled bacteria. Note that the bacterial concentration of the non-symbiotic species was with 10⁷ colony forming units (CFU/mL) 10 times higher than the concentration of *V. fischeri* cells (10⁶ CFU/mL) in the seawater used to inoculate the squids. These concentrations were used because of new evidence showing that *V. parahaemolyticus* are able to form aggregates on the ciliated appendage of the squid host, but they are 10 times smaller than *V. fischeri* aggregates, when presented with the same number of bacterial cells (CFU/mL) in the seawater (S. Koehler, personal communication 2016). Because it was not known whether different sized aggregates would influence enrichment patterns, it was decided to change the concentration of non-specific bacteria cells that were added to the seawater, in order to induce the formation of similar aggregate sizes compared to *V. fischeri*. At the time the study was conducted, there was no information on the aggregate size of *P. leiognathi*. However, recent evidence suggests that *P. leiognathi* forms an aggregate of similar size to *V. fischeri*.

To determine the concentration of bacteria (CFU/mL) in the incubation seawater, 5 µL were plated on LBS medium (LB agar containing 2% [wt/vol] NaCl), and the number of CFU were counted on the next day. Colonization of the symbiotic juvenile squid was confirmed by measuring luminescence output of the juveniles using a TD 20/20 luminometer (Turner Designs, Sunnyvale, CA, USA). After incubation, squids were anesthetized in a solution of 2% ethanol in FSIO containing 0.001% CellTracker

Orange (Molecular Probes, Eugene, OR). The mantle and funnel tissues were then dissected to expose the underlying light organ and the animals were put into fixative solution.

3.2.5 Sample preparation for transmission electron microscopy and NanoSIMS

For details please refer to 'General procedure for NanoSIMS analysis'.

3.2.6 Statistical analysis

Because the data did not meet the assumptions of the parametric test, significance of ^{15}N -enrichment levels among cell organelles and bacteria strains was assessed using the non-parametric Kruskal-Wallis ranked test followed by a Nemenyi *post hoc* test. Correlations between the levels of ^{15}N -enrichment in the nucleus and nucleolus were examined using the non-parametric Spearman's rank correlation. All statistical analyses were performed using the statistical program R (Maxwell and Delaney, 2004), version 3.2.0. Data are expressed as means \pm standard deviation (SD). *P* values of <0.05 were considered as statistically significant for all testing. Table S 3-1 and S 3-2 provide a summary of tests for statistical significance for all experiments presented in this study.

3.3 Results

3.3.1 Juvenile squids inoculated with non-symbiotic bacterial cells

To determine whether non-symbiotic bacteria cells induced host ^{15}N -enrichment patterns similar to those induced by the symbionts (Chapter 2), the results of animals exposed for 3.5 h to ^{15}N -labeled *V. parahaemolyticus* or *P. leiognathi* were compared with the results from 3.5 h exposure to ^{15}N -labeled symbiont cells. In this experiment, however, exposure to *V. fischeri* cells did not induce any measurable ^{15}N -enrichment in the host tissues ($n=4$). Examination of light organs under light microscope showed abnormalities in the structure of some of the light organs, across all treatments. For example, some light organs only had one lobe, while others had irregularly shaped anterior appendages (Fig S 3-2). (Note that although all squids were from the same clutch only some appeared to have irregular light-organ morphology). Together, these observations suggest that the some of the light organs were not fully developed (Montgomery and McFall-Ngai, 1993), a trait often observed in premature squids. Interestingly, squid crypts from these experiments examined for colonization, proved to be fully occupied by *V. fischeri*. While we do not know the reasons why only non-symbiotic cells were able to induce host ^{15}N -enrichment in these experiments, I speculate that if the squids were premature, uptake of bacterial products from the surrounding seawater might be reduced or delayed. On the other hand, the higher inoculum that was used for *V. parahaemolyticus* or *P. leiognathi* (10^7 CFU/mL vs. 10^6 CFU/mL for *V. fischeri*) may have compensated for a potentially weak 'molecular uptake capability' of the squids. In any case, in order to proceed with a comparison with host ^{15}N -enrichment between the non-symbiotic bacteria species and symbiotic *V. fischeri*, results for the latter are used with reference to the experiments described in Chapter 2. It is important to note that despite the high variability in ^{15}N -

enrichment among squid replicates, the ^{15}N -enrichment patterns induced by *V. fischeri* cells and discussed in Chapter 2 were reproducible in two other independent experiments (one experiment is described in the epilogue), suggesting that these findings are robust.

In the presence of non-symbiotic Vibrionaceae cells, *V. parahaemolyticus* and *P. leiognathi*, ^{15}N -enrichment patterns in the epithelial cells of the light organ were comparable to squids inoculated with symbiont cells (Fig. 3-1; Table S 3-1). Specifically, ^{15}N incorporation into subcellular components of the appendage epithelium had similar patterns compared to squids inoculated with *V. fischeri* cells (Fig. 3-1; Table S 3-1); where levels of ^{15}N -enrichment were the strongest in the nucleoli and the lowest in the cytoplasm (cytoplasm < nucleus << nucleolus; Table S 3-1; Fig 3-1C). Systematically, ^{15}N concentrated preferentially in euchromatin regions of the host nucleus (Fig 3-1A; darker area inside the nuclei), as previously observed in squids exposed to *V. fischeri* cells (Chapter 2). However, a greater amount of ^{15}N accumulated inside host cells following exposure to non-symbiotic cells compared to *V. fischeri* cells (Table S 3-1). Preliminary observations also suggested that levels of ^{15}N -enrichment in the appendage epithelium were higher than those in the crypt epithelium (data not shown).

Furthermore, small hotspots were observed along the microvilli lining the cells in the ‘shoulder’ area (indicated with dash box in Fig. 3-1B, top), correlating with fibrous material (Fig. 3-1B) and resembling those observed at 6 h post inoculation with *V. fischeri* cells (Chapter 2). However, as opposed to the results observed in Chapter 2 with *V. fischeri* cells, hotspots were rarely observed along the ciliated fields in squids inoculated with *V. parahaemolyticus*, and were completely absent in squids inoculated with *P. leiognathi* (Fig 2-1A).

The similarities in the enrichment patterns induced by non-symbiotic and symbiotic bacterial cells were not limited to the epithelial cells of the light organ, but were also evident in the connective tissue, gut, and gills (Fig. 3-2). Interestingly, in some tissues, such as the endothelial cells surrounding the blood sinus and the mantle, ^{15}N -enrichment was comparable between the subcellular compartments (Endothelial cells: cytoplasm, $215 \pm 9\%$; Fig. 3-2D; nuclei, $210 \pm 10\%$; Mantle: cytoplasm and nuclei $\sim 55\%$ Fig. 3-2E). In squids inoculated with *V. fischeri* cells no ^{15}N -enrichment was measured in the mantle.

Although squids exposed to ^{15}N -labeled *V. parahaemolyticus* cells incorporated more ^{15}N than squids exposed to *P. leiognathi* (Fig. 3-1C; Table S 3-1), remarkable similarities were observed for the two situations. For example, the average nucleoli-to-nuclei enrichment ratios were about 4.1 in the appendage epithelium of squids exposed to *V. parahaemolyticus* and about 4.9 in *P. leiognathi* (Fig. 3-1C), while levels of ^{15}N -enrichment in the nucleoli were strongly correlated with levels of ^{15}N -enrichment in the nuclei (excluding the nucleoli) (Table S 3-1).

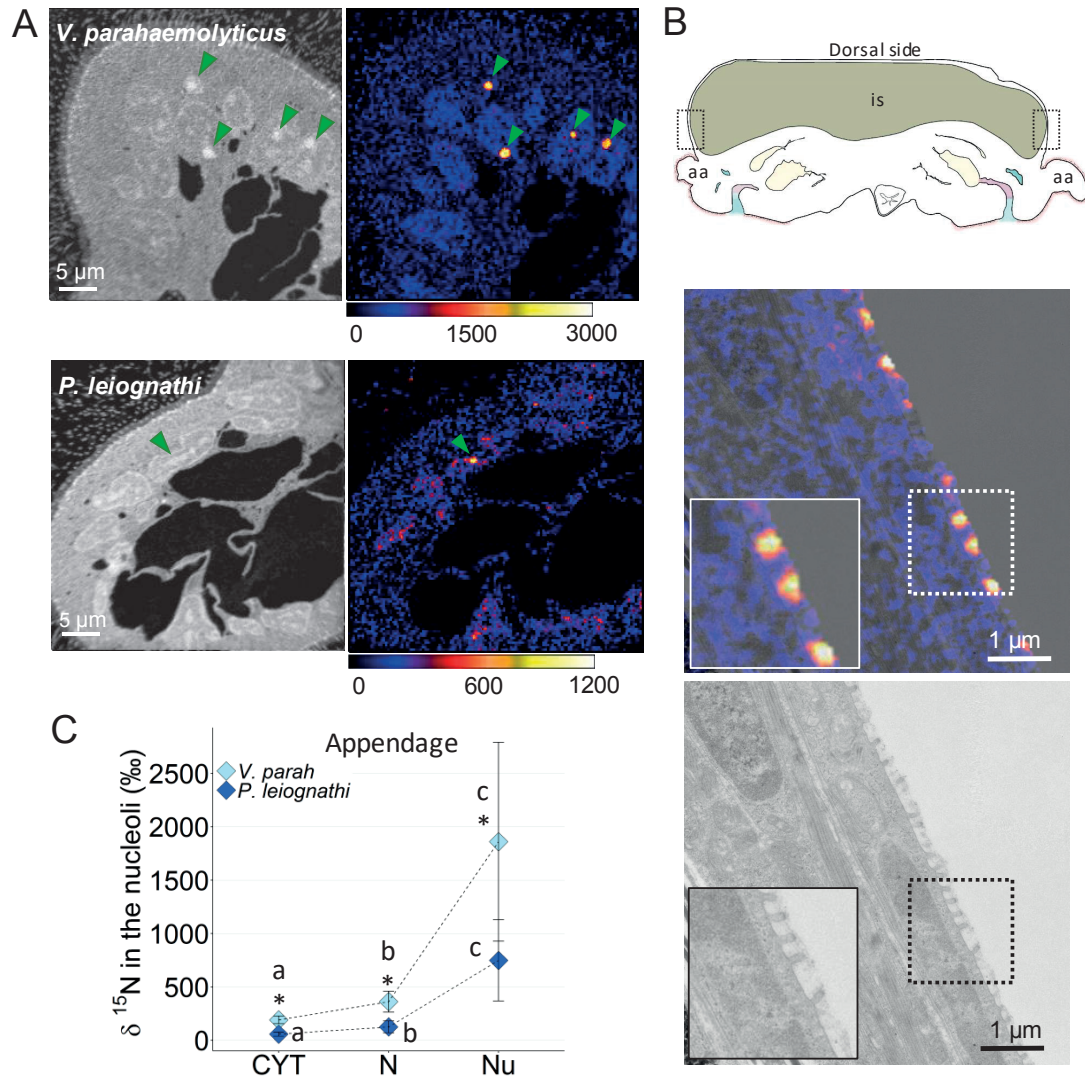


Fig. 3-1. ^{15}N -enrichment (expressed as $\delta^{15}\text{N}$) in the juvenile squid light organ 3.5 h post inoculation with ^{15}N -labeled non-symbiotic *Vibrionaceae* cells. (A) Left panels show tissue structure (NanoSIMS $^{12}\text{C}^{14}\text{N}$ image). Right panels show corresponding, quantified NanoSIMS $^{15}\text{N}/^{14}\text{N}$ ratio image. Nucleoli are indicated by green arrowheads. Values for the NanoSIMS scale are expressed in ‰ (see 'General procedure for NanoSIMS analysis'). (B) ^{15}N - hotspots along the microvilli lining the cells in the 'shoulder' area. Top: Diagram illustrating the light organ with the different compartments. The 'shoulder' region, where the images were obtained, is highlighted in the dash box. aa, anterior appendage; is, ink sac. Middle: a representative high resolution TEM (top) and NanoSIMS ratio image overlay (bottom) of the ^{15}N - hotspots along the microvilli lining the cells in the 'shoulder' area. Inset is high magnification of the region highlighted in the dashed box. Note that most of the hotspots co-localized with fibrous materials that I speculated to be the mucus matrix that is secreted by the squid epithelial cells. (C) ^{15}N -enrichment in the cytoplasm (CYT, n=90-110) nuclei (N, n=200-240) and nucleoli (Nu, 60-70) of the epithelial cells lining the appendage (squids: 5-7 animals; Table S 3-1). Lower case letters indicate statistically significant differences between cell organelles and light-organ compartments (Table S 3-1). Asterisk indicate significant differences between bacteria species (Table S 3-1). Error bars represent 1 standard deviation.

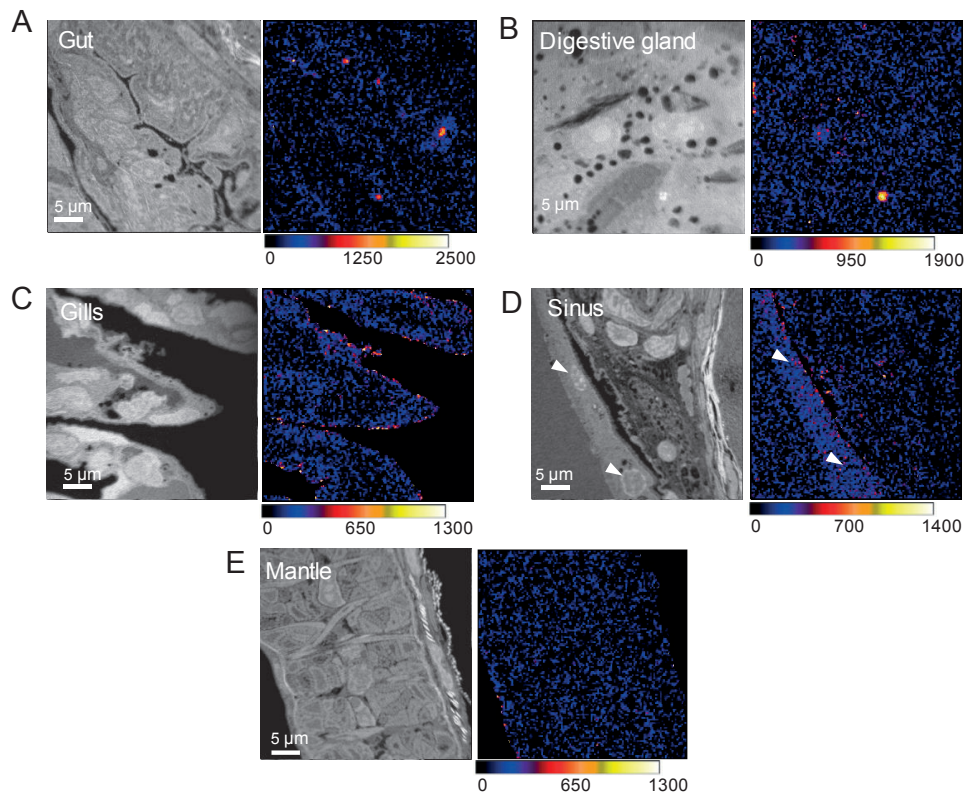


Fig. 3-2. ^{15}N -enrichment in nuclei and nucleoli (hotspots) in epithelial tissues in other squid organs after 3.5 h inoculation with ^{15}N -labelled *V. parahaemolyticus* cells. Left panels show tissue structure (NanoSIMS $^{12}\text{C}^{14}\text{N}$ image). Right panels show corresponding, quantified NanoSIMS $^{15}\text{N}/^{14}\text{N}$ ratio image. Nuclei are indicated by white arrowheads. Values for the NanoSIMS scale are expressed in ‰ (see ‘General procedure for NanoSIMS analysis’).

3.3.2 Juvenile squids inoculated with non-symbiont- derived OMVs

Squids were exposed to the same OMVs concentration (50 μg protein/mL). Irrespective of where the OMVs were derived from (*V. parahaemolyticus*, *V. fischeri*, or *E. coli*), epithelial cells in the appendages and crypts of squids inoculated with OMVs from *V. parahaemolyticus* were generally more enriched in ^{15}N compared to the other two experiments; this observation was most pronounced in the crypt epithelia (Fig. 3-3; Table S 3-2). Significant variation in the level and patterns of ^{15}N -enrichment was observed between host cell organelles in these OMV experiments (Fig. 3-3A and B; Table S 3-2B), with nucleoli recording the highest levels of ^{15}N -enrichment. However, in squids treated with *V. fischeri* as well as *E. coli* OMVs, the three organelles (i.e., cytoplasm, nuclei and nucleoli) were not always enriched at the same time in a given cell and ^{15}N -enrichment was measurable only in 40-70% of these organelles. Despite this, the nucleoli in squid cells exposed to *V. fischeri* OMVs were consistently enriched.

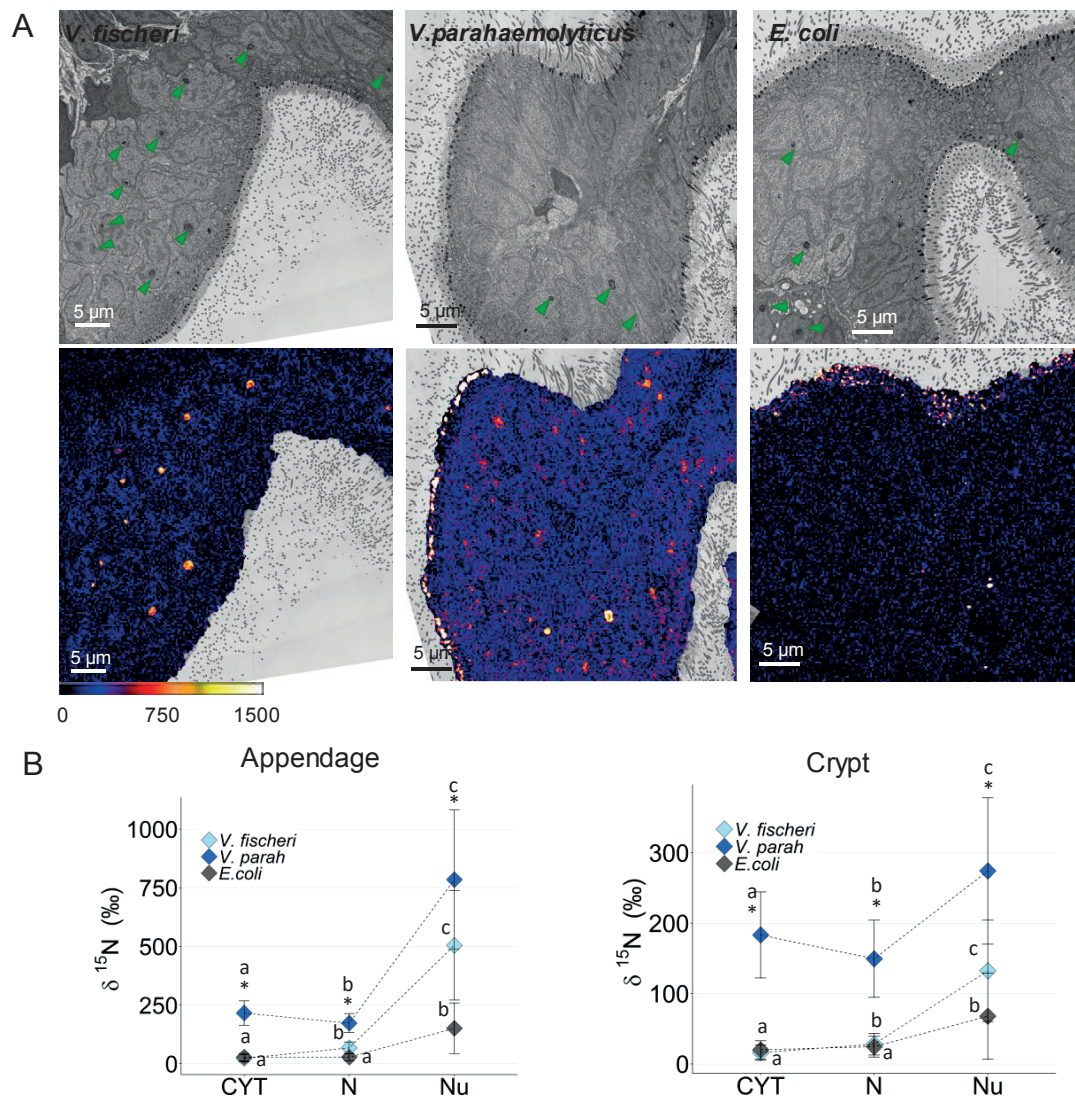


Fig. 3-3. ^{15}N -enrichment in squid epithelial cells exposed for 3 h to ^{15}N -labeled OMVs purified from *V. fischeri*, *V. parahaemolyticus* and *E. coli*, respectively. (A) Mosaic TEM micrographs (top row) and the corresponding NanoSIMS $^{15}\text{N}/^{14}\text{N}$ ratios images (second panel) of cells in the appendage of juvenile squids inoculated with OMVs from the indicated bacteria species. Nucleoli are indicated by green arrowheads on the TEM micrographs. In the NanoSIMS image of the squid exposed to *V. parahaemolyticus* OMVs, ^{15}N hotspots not corresponding to nucleoli were observed. Values for the NanoSIMS scale are expressed in ‰ (see 'General procedure for NanoSIMS analysis'). (B) Distribution of ^{15}N -enrichment in cell organelles cytoplasm (CYT), nucleus (N), and nucleolus (Nu) in the appendage and crypts spaces (squids: 3-5 animals; cell organelles in each squid replicate: CYT: n=10-16; N: n=50-100; Nu: n=8-14; Table S 3-2B). Lower case letters indicate significant differences between the cell organelles; Asterisk indicate significant differences between bacteria species. Error bars represent 1 standard deviation.

Another striking result from the OMV experiments was the difference between the levels of ^{15}N -enrichment in the cytoplasm compared to nuclei and nucleoli in appendage and crypt epithelia (Table S 3-2B). Exposure to *V. fischeri* OMVs led to ^{15}N -labeling in the nucleoli of the epithelial cells that was ~9.4 fold higher than in the surrounding cytoplasm, whereas the difference between the two, following exposure to *V. parahaemolyticus* OMVs, was much lower (1.6 fold; Fig 3-3B). This finding was driven by systematically higher labeling in the cytoplasm in the *V. parahaemolyticus* OMV treatment (Fig. 3-3B;

Table S 3-2B). Interestingly, the cell cytoplasm in squids exposed to *V. parahaemolyticus* OMVs were more highly enriched (17 to 24%) than the nuclei, with visible hotspots in the cytoplasm, while epithelial cells in squids exposed to *V. fischeri* OMVs exhibited the opposite pattern: the cytoplasm was less enriched (42 to 66%, for crypts and appendages, respectively) compared to the nuclei. High-resolution correlative TEM and NanoSIMS images revealed that the ^{15}N -hotspots observed in the appendages in the *V. parahaemolyticus* OMV treatment corresponded with the position of the Golgi apparatus (Fig. 3-4; Table S 3-2A). The Golgi apparatus was also enriched in *V. fischeri* OMVs treatment and in both OMVs treatments, levels of ^{15}N -enrichment in the Golgi were higher than the cell cytoplasm and nuclei (Fig. 3-4B; Table S 3-2A). These results suggest that the OMVs (or their content) from both *Vibrio* species associated with the Golgi apparatus.

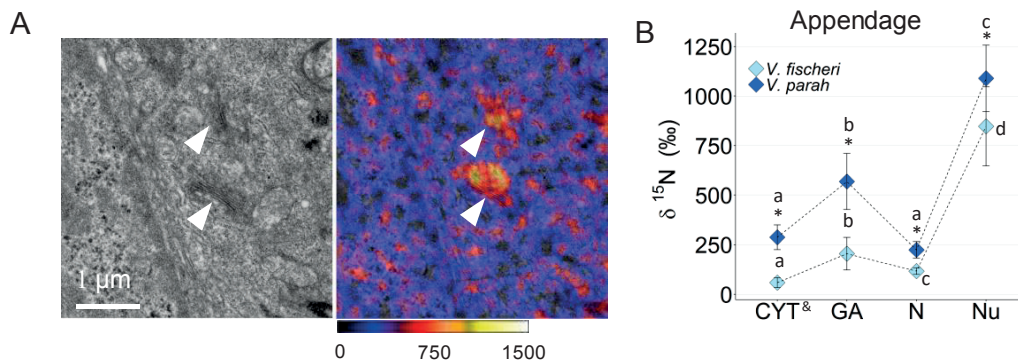


Fig. 3-4. ^{15}N -enrichment in the Golgi of squid epithelial cells exposed for 3 h to ^{15}N -labeled OMVs purified from *V. fischeri* and *V. parahaemolyticus*. To distinguish the Golgi apparatus from the other cytoplasmic organelles (such as mitochondria), high resolution TEM and NanoSIMS images were obtained (1 animal). (A) Representative TEM (left) and NanoSIMS ratio image overlay (right) showing ^{15}N -hotspots correlating with Golgi apparatuses in squid exposed to *V. parahaemolyticus*-OMVs; OMVs from *V. fischeri* did not produce similar Golgi apparatus enrichment and *E. coli* OMVs produced no significant labeling in Golgi apparatuses (data not shown). Values for the NanoSIMS scale are expressed in ‰ (see 'General procedure for NanoSIMS analysis'). (B) Representative distributions of ^{15}N -enrichment in appendage cell organelles after exposure to *V. fischeri* and *V. parahaemolyticus* OMVs (cytoplasm: CYT, n=15-20; Golgi apparatus: GA, n=15; nucleus: N, n=50-60; and nucleolus: Nu, n=11-15; Table S 3-2A) using data from a mosaic that part of it is in Fig. 3-4. $\delta^{15}\text{N}$ in the cytoplasm do not include the Golgi. Lower case letters indicate significant differences between the cell organelles; Asterisk indicate significant differences between bacteria species. Error bars represent 1 standard deviation.

We found a similarity in the correlation coefficient between the ^{15}N -labeling in nucleus and nucleolus in squids exposed to OMVs from either *V. fischeri* or *V. parahaemolyticus* (Fig. 3-5). Finally, the ^{15}N -enrichment on the surface epithelium was investigated. In squids inoculated with *V. parahaemolyticus* OMVs, ^{15}N -hotspots mainly associated with fibrous materials and were observed adjacent to the microvilli and cilia lining these surfaces (Fig. 3-6B). However, in contrast to the experiments with *V. fischeri* OMVs (Chapter 2), hotspots were scarce in squids inoculated with *V. fischeri* OMVs (Fig 3-6A).

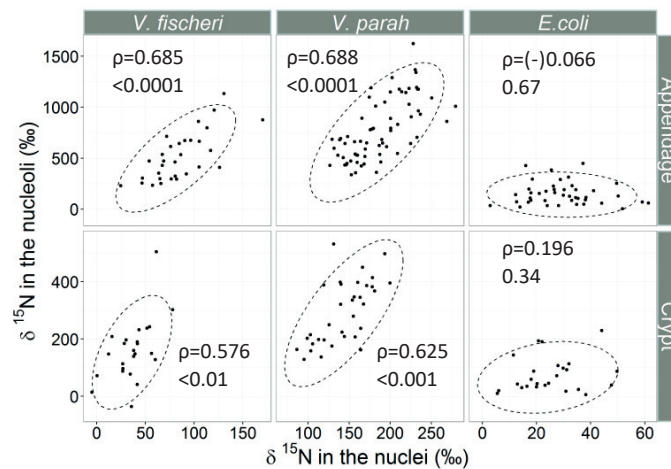


Fig. 3-5. Correlation between the ^{15}N -enrichment in the nuclei and their corresponding nucleoli in squid epithelial cells after 3 h exposure to ^{15}N -labeled OMVs purified from *V. fischeri*, *V. parahaemolyticus* and *E. coli*. The strength of the correlation was examined using Spearman's rank correlation test.

As the exception, squids inoculated with *E. coli* OMVs, presented a clearly different pattern from those observed in squids inoculated with OMV of the *Vibrio* spp.: (i) only very low levels of ^{15}N -enrichment were detected with no differences in the ^{15}N -enrichment levels between the labeling of the cytoplasm of the cells and the nuclei (Fig. 3-3B; Table S 3-2B), (ii) no detectable ^{15}N -enrichment was observed in the Golgi apparatus, (iii) no correlation between the ^{15}N -enrichment in the nuclei and nucleoli was observed (Fig. 3-5), and (iv) ^{15}N -hotspots were highly abundant on the cell surface of the ciliated field (Fig 3-4A and 3-6C). Surprisingly, however, most of the hotspots were associated with vesicle-size spheres (Fig. 3-6C) corresponding to the microvilli (lateral cross section of the microvilli; this study, 93 ± 15 nm in diameter; $n=30$; Montgomery and McFall-Ngai 1993, 70-115 nm in diameter). This finding is in contrast to previous observations across all experiments and treatments (whole bacteria or OMVs; this study and Chapter 2), in which hotspots corresponded predominantly to fibrous structures.

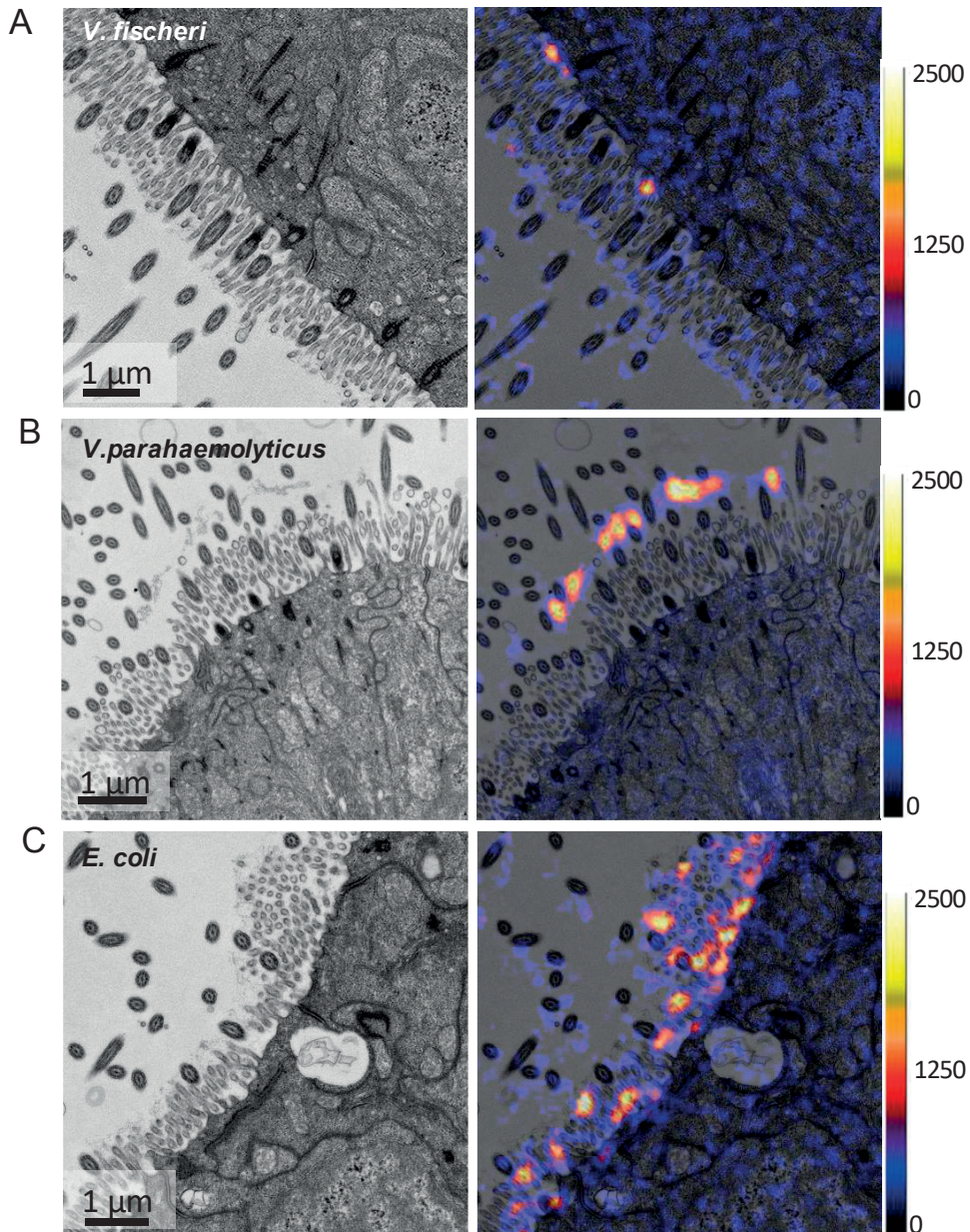


Fig. 3-6. ^{15}N -enrichment on the cell surface of the appendage epithelium in a juvenile squid light organ following 3 h exposure to ^{15}N -labeled OMVs purified from *V. fischeri* (A), *V. parahaemolyticus* (B) and *E. coli* (C). A representative high resolution TEM (left) and NanoSIMS $^{15}\text{N}/^{14}\text{N}$ ratio image overlay (right) of the ^{15}N - hotspots on the cell surface of the epithelial cells. Inset is high magnification of the region highlighted in the dashed box. In squids exposed to *V. fischeri* ^{15}N -hotspots were scarce, in contrast to the highly abundant ^{15}N - hotspots that were observed on the cell surface of the appendage epithelium in previous studies (Chapter 2). Most of the ^{15}N -hotspots co-localized with fibrous materials in squids exposed to *V. parahaemolyticus*-derived OMVs. I speculate that these materials corresponded to be the mucus matrix that is secreted by the squid epithelial cells. Conversely, in animals exposed to *E. coli*-derived OMVs ^{15}N -hotspots mainly ^{15}N -hotspots co-localized to microvilli. Values for the NanoSIMS scale are expressed in ‰ (see ‘General procedure for NanoSIMS analysis’)

3.5 Discussion

Previous studies found that the squid host can incorporate ^{15}N -molecules derived from the symbionts at the early stages of symbiosis into its tissues and cells and that these responses were localized to specific subcellular organelles and specific tissues (Chapter 2). Here, the host response to ^{15}N -labeled bacteria products from Gram-negative, non-symbiotic bacteria species was examined. These data provide evidence that: (i) when juvenile squids were exposed to non-symbiotic *Vibrio* cells, ^{15}N -enrichment was detected in the cytoplasm and nuclei (notably, euchromatin regions), with strong enrichment in the nucleoli of host cells. The ^{15}N -enrichment was most notable in the light organ, but also present in other tissue types, such as gills and gut; (ii) these enrichment patterns were comparable to the patterns induced by the symbiont, although higher levels of ^{15}N -enrichment were recorded in the squids exposed to a non-symbiotic *Vibrio*; (iii) however, when exposed to equal concentration of bacterial OMVs, the light-organ epithelium displayed different intracellular and cell-surface ^{15}N -enrichment patterns that were distinguishable from patterns resulting from exposure to the bacteria cells. These 'OMV patterns' also differ between the bacteria species, specifically between the *Vibrio* spp. and *E. coli*. Together, these findings indicate that the considerable uptake of ^{15}N -labeled bacterial molecules by the squid is not specific to symbiont-derived products. However, the unique ^{15}N -enrichment patterns among the different bacterial OMVs may reflect distinct mechanisms by which the squid detects and internalizes the vesicles. In the following section, I elaborate on these two points, with a focus on the observed differences in ^{15}N -enrichment patterns between bacteria treatments (cells vs. OMVs).

3.5.1 ^{15}N -enrichment patterns are not unique to the symbiotic partner

^{15}N -enrichment recorded in the squid following the incubation with non-symbiotic species (cells, Fig. 3-1 and 3-2; OMVs, Fig. 3-3) revealed that the host is capable of incorporating molecules from other bacterial species, in a seemingly non-specific manner, during the first hours after hatching. Despite the lower levels of ^{15}N -enrichment that were detected inside the host cells after exposure to *E. coli* OMVs, this results support the idea of non-specific interaction between the squid and other bacteria, even with non-*Vibrio* spp. Earlier investigations found that Gram-negative bacteria, such as *V. parahaemolyticus* and *P. leiognathi*, can interact closely with host cilia and form an aggregate on the light-organ surface (Nyholm and McFall-Ngai, 2003; Altura et al., 2013). In addition, purified bacterial cell-envelope molecules (i.e., LPS and PGN) and OMVs from non-symbiotic bacteria (*Vibrio* and non-*Vibrio* spp.) can alter the host response, i.e., haemocyte trafficking and appendage apoptosis, similar to the response induced in symbiotic animals (Aschtgen et al. 2015, 2016). While the presence of biologically relevant concentrations (10^4 CFU/mL) of non-specific bacteria cells failed to induce these responses (Aschtgen et al., 2015), higher concentrations of *V. parahaemolyticus* were able to induce migration of haemocytes to some extent (M.S. Aschtgen, personal communication).

The broad similarities between the ^{15}N -enrichment patterns induced by symbiont and non-symbiont *Vibrio* cells may imply that a shared molecular exchange or similar processing in the squid cells is responsible for these enrichment patterns. This similarity calls into question some of the speculations provided in the previous chapter, including why ^{15}N -enrichment was mostly observed in the subnuclear components. One of the hypothesis raised was that bacteria molecules may specifically target the nucleus by either containing a sorting signal for the nucleus and nucleolus (i.e., NLS, NoLS) or by being small enough to diffuse across the nucleus pores and form a strong interaction with subnuclear components. However, considering the absence of species-specific ^{15}N -enrichment that was observed in the current study, it is perhaps less likely that bacteria molecules from the non-symbiotic *Vibrio* species also had a direct interaction with the subnuclear components. It is then tempting to speculate that the reason a similar ^{15}N -enrichment pattern was found between the *Vibrio* spp. might be related to a more general communication that can occur between the bacteria and the squid during initiation of symbiosis.

3.5.1.1 Stronger response to *V. parahaemolyticus* products

Among the bacteria species tested in this study, *V. parahaemolyticus* cells or OMVs led to the highest ^{15}N -enrichment in host tissues (Fig. 3-1 and 3-3; Table S 3-1 and S 3-2B), with clear enrichment also observed in tissues such as the mantle, in which no ^{15}N -enrichment was observed after exposure to symbiont cells (Fig. 3-2). While the higher inoculum concentration of *V. parahaemolyticus* might partially explain the differences with the *V. fischeri* ^{15}N -enrichment labelling, it cannot account for the differences in enrichment recorded in squids exposed to an equal concentration of bacterial OMVs. Similarly, in another study *V. parahaemolyticus* OMVs tended to induce a higher response of haemocyte trafficking compare to *V. fischeri* OMVs, though not statistically different (M.S. Aschtgen, personal communication). A stronger response to non-symbiotic bacterial products was also observed when squids were co-inoculated with purified LPS from *V. cholerae* compared to symbiont LPS (Foster et al., 2000). It is possible that the molecules that were responsible for the ^{15}N -enrichment in the squid cells were either more biologically active, i.e., interact more with the cells, and/or were delivered at higher quantities (Kulp and Kuehn, 2010; Chutkan and Kuehn, 2011; Collins et al., 2012; Schwechheimer et al., 2013).

3.5.2 The differential response to *E. coli* OMVs might suggest a distinct mechanism of recognition and/or internalization into the host cells

Exposure to *E. coli* OMVs induced either no or relatively low ^{15}N -enrichment inside the squid cells (Fig 3-3; Table S 3-2B). Considerable differences in ^{15}N -enrichment patterns were observed in comparison to the *Vibrio* spp. (no correlation between the ^{15}N -enrichment in the nuclei and nucleoli (Fig. 3-5) and the apparent differences in localization of ^{15}N -hotspots on the cells surface of the appendage epithelia (Fig 3-6C). The inability of *E. coli* OMVs to induce similar ^{15}N -enrichment patterns suggests that these OMVs are

internalized differently, potentially because the *E. coli* OMVs contain different molecules than the OMVs of *Vibrio* spp.

The uptake of diffusible or secreted molecules from non-symbiotic bacteria can occur in a similar fashion to molecular products from symbiont bacteria if these molecules bear shared structural or functional moieties. Unlike these individual molecules, OMVs might need to first bind to the squid or be processed in some way before their contents can be taken up. Bacteria use diverse surface factors such as pili, Outer Membrane Proteins (OMPs), lipoproteins, and adhesins to attach to specific components on the surface of the host cells to facilitate their interaction and binding to the host (Pizarro-Cerdá and Cossart, 2006; Galdiero et al., 2012). Various examples are described in pathogenic associations: the heat-labile enterotoxin (LT) that is associated with OMVs produced by enterotoxigenic *E. coli* is responsible for adherence to host intestinal epithelial cells (Kesty et al., 2004). Cholera cytotoxin (CT) that is associated with *Vibrio cholerae* OMVs binds to cell surface receptor, ganglioside GM1, and aids in internalization into the same type of cells (Chatterjee and Chaudhuri, 2011). Outer surface proteins, OspA and/or OspB, are involved in the attachment of *Borrelia burgdorferi* vesicles to human endothelial cells (Shoberg and Thomas, 1993). However, less is known about the function of surface proteins in binding of OMVs from beneficial bacteria to their host. I suggest two surface molecules that potentially promote recognition of *V. fischeri* OMVs by the squid host.

OMPs, the most abundant and best-described surface proteins, are often important for interactions with various host cells, particularly in pathogenic association (Koebnik et al., 2000; Galdiero et al., 2003; Galdiero et al., 2012). OmpU, the major OMP of *V. fischeri*, is a porin and is essential for colonization of the light organ (Aeckersberg et al., 2001), recognition of *V. fischeri* cells by host haemocytes (Nyholm et al., 2009), and triggering of normal host developmental response (Aschtgen et al., 2016). In some *V. cholerae* strains, OmpU was suggested to play a role in adherence of bacteria cells to human epithelial cells (Sperandio et al., 1995). Although this function has not been described for *V. fischeri* cells, in which a defect in OmpU production did not seem to interfere with *V. fischeri* cells attachment to host cell cilia (Altura et al., 2013), it is possible that the OmpU of *V. fischeri* OMVs is a key determinant in their binding and internalization into the host cells. If this is the case, differences in the OMPs characteristics between *V. fischeri* OMVs and *E. coli* OMVs could provide an explanation for the differences observed in enrichment patterns. Future work should examine whether OmpU is necessary for binding of *V. fischeri* OMVs to the host and investigate whether *V. fischeri* OmpU shares epitopes with one of the major outer membrane proteins: OmpU from *V. parahaemolyticus* (Whitaker et al., 2012) and OmpA, OmpF or OmpC in *E. coli* (Chen et al., 1980; Forst et al., 1988).

V. fischeri LPS may aid in adhesion and recognition of OMVs by the squid host. LPS molecules consists of a core polysaccharide, O-antigen side-chain, and the evolutionarily conserved lipid A. In other

species, the latter two moieties have been reported to play a role in adhesion to various surfaces and human cells (Makin and Beveridge, 1996; Edwards et al., 2000; Munford, 2008) as well as acting as virulence factors. *V. fischeri* lipid A and O-antigen have unique characteristics (Phillips et al., 2011; Post et al., 2012) that distinguish them from other bacterial LPS. Additionally, these moieties are suggested to play a role in colonization (O-antigen; Post et al. 2012) and light-organ morphogenesis (lipid A; Foster et al. 2000; Heath-Heckman et al. 2016). These uncommon chemical structures might serve in the uptake of the *V. fischeri* OMVs by the light-organ epithelia, and would be the cause for the less efficient uptake of *E. coli* OMVs by squid cells. In this context, LPS in *V. parahaemolyticus* OMVs might bear similar moieties to the LPS in *V. fischeri* OMVs resulting in a more comparable levels of ¹⁵N-enrichment between these bacteria OMVs.

Bacteria surface molecules are not always prerequisite for adhesion of the vesicles to their host cells, but their presence can increase the rate of OMVs binding (Parker et al., 2010; Chutkan and Kuehn, 2011). For example, vacuolating cytotoxin VacA, a surface protein of *Helicobacter pylori* OMVs, is not crucial for the OMV binding to gastric epithelial cells. However, VacA-containing OMVs increase their association with the host cells (Parker et al., 2010). In the context of this study, *E. coli* OMVs may lack some surface molecule that promotes uptake by squid cells, reducing their ability to transfer material to the host in this context.

After binding to the cell surface, many of the bacterial OMVs enter the host cells and deliver their cargo via endocytic pathways (reviewed in O'Donoghue and Krachler 2016). There are four major endocytosis pathways: macropinocytosis, clathrin-dependent endocytosis, caveolin-dependent endocytosis, or non-caveolin, non-clathrin dependent endocytosis (Doherty and McMahon, 2009), which have been described to be involved in OMVs internalization to host cells (reviewed in O'Donoghue and Krachler 2016). In the squid, internalization of *V. fischeri* OMVs by both epithelial cells of the light-organ appendages and isolated haemocytes can be blocked by an actin polymerization inhibitor, cytochalasin D, suggesting that *V. fischeri* OMVs enter the cells via micropinocytosis (Aschtgen et al., 2015); care should be taken when interpreting these results as this inhibitor could have affected other endocytosis pathways as well (Fujimoto et al., 2000; Dutta and Donaldson, 2012). If *E. coli* OMVs were directed through a different endocytic pathway compared to OMVs from *V. fischeri* and *V. parahaemolyticus*, the intensity of the ¹⁵N-enrichment inside the host cells could have been affected. Interestingly, some OMVs can use more than one pathway to enter the host cell, each of which are likely to exhibit different efficiency (Parker et al., 2010; Pollak et al., 2012; Thay et al., 2014). For example, uptake of *Aggregatibacter actinomycetemcomitans* OMVs by HeLa cells was reduced to 25% after exposure to an inhibitor of receptor-mediated endocytosis while exposure to filipin, that disrupts lipid rafts (cholesterol-sequester agent), reduced OMVs internalization to 74% (Thay et al., 2014). The presence of specific

molecules inside the OMVs can also influence the delivery mode across the plasma membrane. Internalization of VacA-containing OMVs from *H. pylori* by gastric epithelial cells showed a reduction of 42% in vesicle uptake after the inhibition of the clathrin-mediated endocytosis, whereas only 25% reduction was observed in the uptake of VacA-deficient OMVs (Parker et al., 2010). The partial level of inhibition suggest that OMVs can be delivered via multiple endocytosis pathways and may support the hypothesis that *E. coli* OMVs have used an alternative and less efficient route to enter the squid cells compared to OMVs from *V. fischeri* and *V. parahaemolyticus*. However, it cannot be ruled out that the content of *E. coli* OMVs also contributed to the observed differences in host ^{15}N -enrichment patterns.

The exact mechanism underlying the ^{15}N -enrichment observed on the cell surface of the light-organ appendages remains elusive. Despite the differences that were recorded in the level of ^{15}N -enrichment and in the localization of the ^{15}N -hotspots (fiber-like materials vs. microvilli), in all of these treatments no vesicles were co-localized with the ^{15}N -hotspots. In Chapter 2, I discussed two scenarios for the absence of vesicles from the ^{15}N -enrichment observed on the cell surface: (i) the presence of enzymes that degrade OMVs membranes (e.g., LPS; Weinrauch et al. 1999) before their internalization into the cells and/or (ii) that some of the OMV content is excreted extracellularly via endocytic recycling pathways (Mallard et al., 1998; Grant and Donaldson, 2009). The unique pattern of ^{15}N -enrichment associated with the microvilli in squid exposed to OMVs from *E. coli* might have been affected by the endocytosis route that OMVs use to enter the cells and the molecular content of the OMVs. However, this observation is a preliminary and should be examined further with additional experiments.

3.5.3 OMVs from *V. parahaemolyticus* and *V. fischeri* colocalize with component of the secretory pathways

Squids exposed to *V. fischeri* and *V. parahaemolyticus* OMVs displayed high levels of ^{15}N that co-localized with the Golgi apparatus (Fig. 3-4; Table S 3-2A). Several studies have shown that after OMVs enter eukaryotic cells they associate with compartments of the endocytosis pathway (i.e., secretory pathway), before releasing their cargo into the cytosol. Endocytosed cargo is often transported to early endosome where it can be either recycled back to the plasma membrane, directed to endocytic components, such as late endosome and lysosomes for degradation, or transported to the Golgi and/or endoplasmic reticulum (ER). Additional sorting can occur from the Golgi network: cargo can be transported to other cellular compartments, endosomal-lysosomal system, cell membrane or extracellular milieu. OMVs are associated with endo-lysosomal compartments (Bomberger et al., 2009; Bielaszewska et al., 2013; Vanaja et al., 2016) Golgi apparatus (Guidi et al., 2013; Thay et al., 2014) and/or ER (Kesty et al., 2004; Kuehn and Kesty, 2005; Bauman and Kuehn, 2009; Thay et al., 2014). Interestingly, it has been demonstrated that some OMVs must traffic through the Golgi apparatus before their contents get delivered to the nucleus (Guidi et al., 2013). Manipulation of existing cellular pathways

is a well-known strategy used by pathogens to deliver their toxins into the host (Sandvig and van Deurs, 2005; Blanke, 2006; Hendricks and Bomberger, 2014). By using such a sophisticated mechanism, it was argued that: (i) toxins can have an easier access to the cytosol via the permeable membrane of the ER compared to the plasma membrane; (ii) bacterial factors, such as CTc, can be activated through processes that take place in these organelles (Wernick et al., 2010) and (iii) one of these organelles is the place where they exert their effect (Sandvig and van Deurs, 2005). Some host receptors for bacterial products can be found in these components and aid in detection of bacterial molecules that are trafficked specifically to these organelles, such as the detection of intracellular monomeric LPS by Toll-like receptor 4 that is localized to the Golgi apparatus in some mammalian epithelial cells (Thieblemont and Wright, 1999; Hornef et al., 2002; Latz et al., 2002).

Future studies should involve correlative electron microscopy analysis and immunogold labeling of internalized OMVs (using antibodies for the whole cells of *V. fischeri* or for OmpU) followed by a NanoSIMS analysis to quantify the ^{15}N -enrichment in the compartments along the secretory pathways (i.e., endosomes, lysosomes, ER and Golgi) where OMVs were observed. This approach should be combined with the use of inhibitors for the diverse endocytosis pathways (review in Dutta and Donaldson 2012; O'Donoghue and Krachler 2016) and/or markers of endocytosis components (Bomberger et al., 2009; Furuta et al., 2009) and the retrograde transport, i.e., transport via the Golgi apparatus-ER (Rompikuntal et al., 2012).

Differences in ^{15}N levels of cellular compartments between squids inoculated with OMVs from *V. fischeri* or *V. parahaemolyticus* were mostly apparent in the Golgi apparatus and the cytoplasm (with ~2-4 times higher levels of ^{15}N in squids exposed to *V. parahaemolyticus* OMVs), whereas in the subnuclear compartments it was less pronounced (~less than 1 fold higher levels of ^{15}N in squids exposed for *V. parahaemolyticus* OMVs) (Fig. 3-3B). These results shows that perhaps the type of OMVs mainly determines selective accumulation of ^{15}N in cell cytoplasm and cytoplasmic organelles rather than the subnuclear compartments. This interpretation raises an intriguing question: does some of the molecular cargo from *V. fischeri* and *V. parahaemolyticus* OMVs experience different fates in the host cells? These materials could directly interact with the host cells at these interfaces, or could be processed by the squid before imparting an impact. The reasons for the apparent preferential accumulation of ^{15}N -enrichment in these regions is an attractive and important area for further investigation.

3.5.4 Conclusion and future directions

Collectively, this chapter provides evidence that the ^{15}N -enrichment that was recorded in the squid tissues and cells after exposure to bacterial cells or bacterial products is not symbiont specific. The squid is able to incorporate bacteria-derived molecules also from other bacteria species during the first few hours after hatching, specifically from closely related Gram-negative bacteria. Exposure to non-

symbiotic *Vibrio* species resulted in similar ^{15}N -enrichment patterns as those induced by the symbionts cells. Such an ability of the squid to uptake and respond to molecules that are not unique to the symbiont is not very surprising as it is known that the squids can sense shared cell-envelopes molecules. Interestingly, it was also demonstrated that when squids were exposed to OMVs, the transport of *E. coli* OMVs was less efficient compared to OMVs from *V. fischeri* and *V. parahaemolyticus*. I speculate that the presence of specific surface structures that are associated with the OMVs, and/or the endocytosis pathway by which these OMVs enter the cells, may have actively promoted the uptake of *V. fischeri* and *V. parahaemolyticus* OMVs and hinder the transport of *E. coli* OMVs. It is important to note that while these bacteria cells or OMVs do not reside in the squid's natural habitat at the concentrations that was used in the current study, the squids are ubiquitously exposed to millions different bacteria species (10^6 cells/mL) and their products at their natural environment. As such, there must be mechanisms by which the host maintains a tolerance towards the large pool of bacterial products and modify its response accordingly, specifically in the case of bacterial OMVs that can contain a vast amount of molecules where some can be harmful to the cells.

While the specific nature of the molecules that are causing the ^{15}N -enrichment in these experiments remains undetermined, I propose that not all transferred bacterial molecules have shared features and/or are necessarily related to specific signaling molecules. To gain better insights of the function of these molecules, using bacterial vesicles from distantly related bacteria species, such as MVs (membrane vesicles) from Gram-positive that do not contain LPS and might also have a different molecular cocktail, should be considered.

3.6 Supplementary information

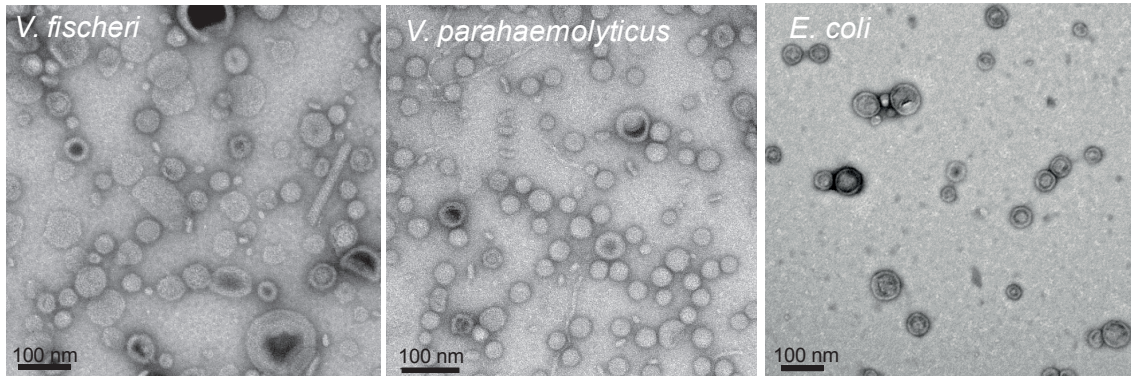


Fig. 3-S1. Negative staining micrographs of OMVs that were isolated from *V. fischeri*, *V. parahaemolyticus* and *E. coli*. Vesicles average size are 43 ± 13 (n=13), 36 ± 10 (n=13) and 62 ± 18 (n=8) in diameter, respectively.

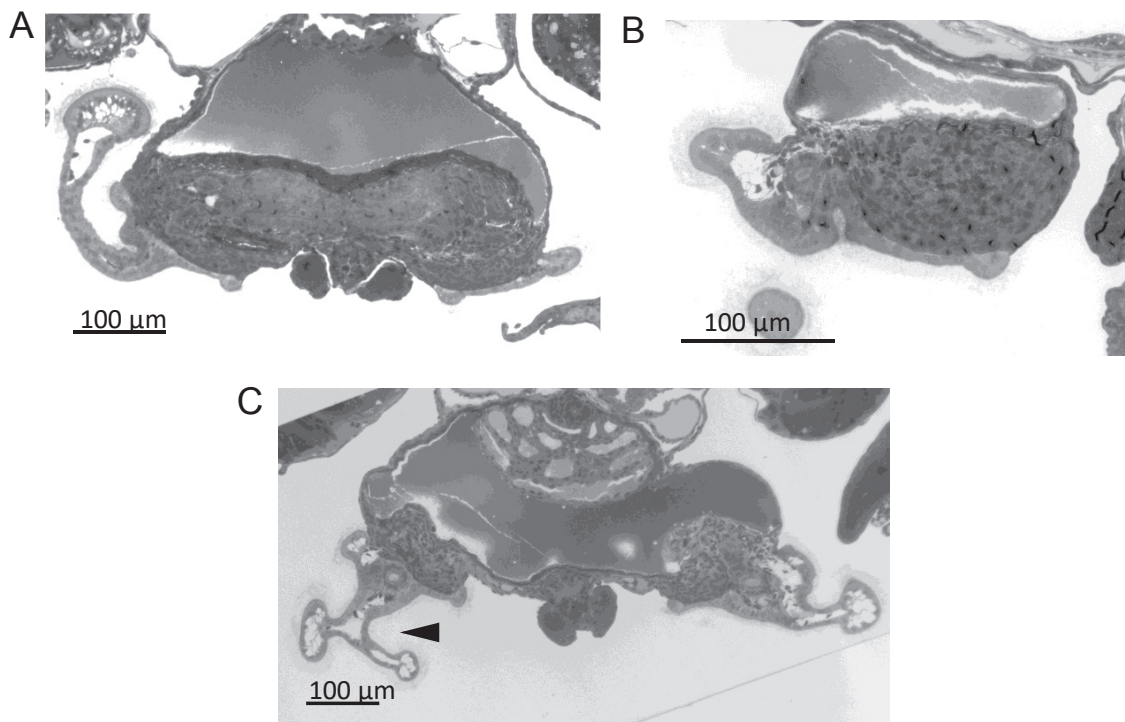


Fig. 3-S2. Light micrographs of histology cross section (0.5 µm thick) of a juvenile *E. scolopes* showing representative light organs that appeared to be abnormal. (A) Elongated appendage. (B) Light organ with only one lobe. (C) irregular structure of appendage (arrowhead). These animals were taken from the same clutch of squids that were used for the experiment comparing ^{15}N -enrichment after exposure to non-symbiotic bacteria cells and symbiotic *V. fischeri*. Although squids with ‘abnormal’ light organs were found in all bacteria treatments, only squids that were exposed to *V. fischeri* were not found ^{15}N -enriched (similar to background levels of $^{15}\text{N}/^{14}\text{N}$). Sections were stained with a mixture of Toluidine-blue and borax and image colors were changed manually to grey colors.

Table S 3-1 Statistical analysis of squids inoculated with nonspecific environmental bacteria cells, *V. parahaemolyticus* (7 animals) and *P. leiognathi* (5 animals) for 3.5 h. ¹⁵N-enrichment in the different cell organelles, cytoplasm, nucleus and nucleolus was compared for each of the bacteria treatments. Data was obtained for the appendages only.

Variables	N	Mean (%)	SD (%)	Statistics	P value	
Bacteria						
	Cell organelle					
<i>V. parahaemolyticus</i>	Cytoplasm	109	191	36	Kruskal-Wallis test: <0.0001 $\chi^2 = 287.8$ df = 2 Nemenyi post-hoc: CYT ≠ GA ≠ N ≠ Nu	
	Nucleus	236	362	98		
	Nucleolus	73	1860	931		
<i>P. leiognathi</i>	Cytoplasm	90	58	19	Kruskal-Wallis test: <0.0001 $\chi^2 = 192.5$ df = 2 Nemenyi post-hoc: CYT ≠ GA ≠ N ≠ Nu	
	Nucleus	196	126	56		
	Nucleolus	57	748	380		
Correlation nucleus-nucleolus				<u><i>V. parah</i></u> Spearman`s: Appendage: $p < 0.0001$ $\rho = 0.828$	<u><i>P. leiognathi</i></u> Spearman`s: Appendage: $p < 0.0001$ $\rho = 0.859$	
Comparing bacteria treatments, for each cell organelle separately				<u>Cell</u> Kruskal-Wallis test: $p < 0.0001$ $\chi^2 = 147.2$ df = 1	<u>Nucleus</u> Kruskal-Wallis test: $p < 0.0001$ $\chi^2 = 310.3$ df = 1	<u>Nucleolus</u> Kruskal-Wallis test: $p < 0.0001$ $\chi^2 = 49.8$ df = 1

Table S 3-2 Statistical analysis of squids inoculated with OMVs from *V. fischeri* (3 animals) and from nonspecific environmental bacteria, *V. parahaemolyticus* (5 animals) and *E. coli* (3 animals) for 3.5 h. (A) and (B) ¹⁵N-enrichment in the different cell organelles, cytoplasm, nucleus and nucleolus was compared for each of the bacteria treatments. (B) Data for the analysis of the Golgi apparatus was obtained from a mosaic high resolution NanoSIMS image that was performed on a representative squid from each bacteria treatment, *V. fischeri* and *V. parahaemolyticus*, and then was compared to the cell organelles: cytoplasm, nucleus and nucleolus. Note that the Golgi apparatus in the *E. coli* treatment was not ¹⁵N-enriched.

	Variables			N	Mean (‰)	SD (‰)	Statistics	P value
	Bacteria	Tissue	Cell organelle					
A	<i>V. fischeri</i>	Appendage	Cytoplasm	20	59	25	Kruskal-Wallis test: $\chi^2 = 80.61$ df = 3	<0.0001
			Golgi apparatus	16	205	82		
			Nucleus	59	117	16		
			Nucleolus	15	848	200		
	<i>V. parah</i>	Appendage	Cytoplasm	14	288	62	Kruskal-Wallis test: $\chi^2 = 58.74$ df = 3	<0.0001
			Golgi apparatus	14	569	142		
			Nucleus	50	222	44		
			Nucleolus	11	1032	248		
B	<i>V. fischeri</i>	Appendage	Cytoplasm	37	23	16	Kruskal-Wallis test: $\chi^2 = 148.4$ df = 2	<0.0001
			Nucleus	202	68	25		
			Nucleolus	34	505	233		
		Crypt	Cytoplasm	33	16	11	Kruskal-Wallis test: $\chi^2 = 44.4$ df = 2	<0.0001
			Nucleus	72	28	16		
			Nucleolus	21	132	72		
	<i>V. parah</i>	Appendage	Cytoplasm	64	216	52	Kruskal-Wallis test: $\chi^2 = 199$ df = 2	<0.0001
			Nucleus	320	174	43		
			Nucleolus	68	785	297		
		Crypt	Cytoplasm	35	182	61	Kruskal-Wallis test: $\chi^2 = 50.6$ df = 2	<0.0001
			Nucleus	109	155	71		
			Nucleolus	35	308	138		
<i>E. coli</i>	Appendage	Cytoplasm	37	28	16	Kruskal-Wallis test: $\chi^2 = 85.1$ df = 2	<0.0001	
		Nucleus	373	28	15			
		Nucleolus	42	151	108			Nemenyi post-hoc: CYT \neq Nu N \neq Nu
	Crypt	Cytoplasm	31	20	13	Kruskal-Wallis test: $\chi^2 = 21.55$ df = 2	<0.0001	
		Nucleus	101	25	15			
		Nucleolus	29	68	61			Nemenyi post-hoc: CYT \neq Nu N \neq Nu

<p>Comparing treatments: <i>V.fischeri</i> vs. <i>V parah</i> vs. <i>E. coli</i> , for each cell organelle separately</p>	<p><u>Cytoplasm</u> Kruskal-Wallis test: Appendage: $p < 0.0001$ $\chi^2 = 103.6$ $df = 2$</p> <p>Crypt: $p < 0.0001$ $\chi^2 = 66.4$ $df = 2$</p>	<p><u>Nucleus</u> Kruskal-Wallis test: Appendage: $p < 0.0001$ $\chi^2 = 727.8$ $df = 2$</p> <p>Crypt: $p < 0.0001$ $\chi^2 = 196.4$ $df = 2$</p>	<p><u>Nucleolus</u> Kruskal-Wallis test: Appendage: $p < 0.0001$ $\chi^2 = 93.4$ $df = 2$</p> <p>Crypt: $p < 0.0001$ $\chi^2 = 103.56$ $df = 2$</p>
<p>Correlation nucleus-nucleolus, for each treatment separately</p>	<p><u><i>V. fischeri</i></u> Spearman's: Appendage: $p < 0.0001$ $\rho = 0.685$</p> <p>Crypt: $p < 0.01$ $\rho = 0.576$</p>	<p><u><i>V. parah</i></u> Spearman's: Appendage: $p < 0.0001$ $\rho = 0.688$</p> <p>Crypt: $p < 0.001$ $\rho = 0.625$</p>	<p><u><i>E. coli</i></u> Spearman's: Appendage: $\rho = 0.67$ $\rho = (-)0.066$</p> <p>Crypt: $\rho = 0.34$ $\rho = 0.196$</p>

General discussion

Animal-microbe symbioses are fundamental to animal physiology, but the nature of the molecular exchange(s) between partners is far from understood. The mutualistic association between *E. scolopes* and *V. fischeri* is a powerful model to investigate interactions between the host and its microbial symbiont. In the present work, TEM and NanoSIMS imaging were combined with stable isotope enrichment experiments to study the transfer and localization of ^{15}N -labeled bacteria-derived molecules into squid host cells during the onset of symbiosis.

Chapter 1 presents an effort to use NanoSIMS imaging to trace ^{15}N -enrichment in the light-organ epithelia of squids exposed to purified ^{15}N -TCT ('tracheal cytotoxin', or peptidoglycan monomer). I found that it is not possible to trace these morphogenesis-inducing signaling molecules within the tissue of the nascent light organ (Fig. 1-1). Most likely these molecules are active at very low concentrations (and perhaps in very specific locations; Alberts et al. 2014), and that their presence in the squid tissues is below the effective detection limit of the NanoSIMS.

This finding led us to investigate the possibility of a more general molecular transfer from the seawater milieu into the host cells, a process that is likely to occur in the squid's natural habitat (e.g., Manahan et al. 1983, 1989; Ben-David-Zaslow and Benayahu 2000). Exposing squids to a mixture of ^{15}N -labeled amino acids yielded subcellular $^{15}\text{N}/^{14}\text{N}$ distribution patterns in squid light-organ tissues, with ^{15}N -enrichment corresponding to cellular organelles/compartments with high protein turnover (e.g., Beatty et al. 2006; Boisvert et al. 2012; Wei et al. 2013) in the following hierarchy: nucleoli > Golgi apparatus > cell cytoplasm > nuclei (Fig 1-2). From these results it was concluded that, while certain specific signaling molecules may not be detectable with the NanoSIMS, the light organ of juvenile squids accumulates other small organic molecules that are easily detected with this technique.

In light of this finding, juvenile squids were inoculated either with strongly ^{15}N -labeled *V. fischeri* cells or with outer membrane vesicles (OMVs) shed by these cells, followed by correlated TEM and NanoSIMS imaging to visualize transfer of symbiont-derived molecules into the squid tissue. This work, described in Chapter 2, revealed that: (i) ^{15}N -enrichment was detected across the entire light organ (Fig. 2-2) and was observed also in other organs and tissue types (such as guts and gills; Fig. 2-6), even in the case of remote interaction between the bacterial cells and the squid cells; (ii) among the different organs analyzed, the light-organ appendages showed the highest ^{15}N -enrichment; (iii) among subcellular organelles, nucleoli had the highest levels of ^{15}N inside host cells, whereas the host cell's cytoplasm had the lowest levels of ^{15}N (Fig. 2-3); (iv) squids exposed to OMVs showed higher levels of ^{15}N compared to squids exposed to *V. fischeri* cells (Fig. 2-7), and (v) small ^{15}N -hotspots on the surface of epithelial cells (in

what is referred to as the 'shoulder' region) were observed after squids were exposed to OMVs (Fig. 2-7), or after a longer exposure (6 h) to the bacterial cells (Fig. 2-5). The hotspots were mainly associated with the cilia and/or microvilli lining these surfaces.

In [Chapter 3](#), the specificity of the observed molecular transfer was investigated. To address this question, the subcellular distribution of ^{15}N -labeled, *V. fischeri*-derived, molecules was compared with the subcellular distribution of ^{15}N -labeled molecules derived from non-symbiont species. When juvenile squids were inoculated with non-symbiotic Vibrionaceae cells (specifically, *V. parahaemolyticus* and *P. leiognathi*), most ^{15}N -enrichment patterns recorded in squid tissues were similar to *V. fischeri*-induced patterns (Fig. 3-1). However, generally higher levels of ^{15}N were detected in squid tissues after exposure to *V. parahaemolyticus* cells.

On the other hand, considerable differences in the ^{15}N -enrichment patterns were observed after inoculation of the squids with ^{15}N -enriched OMVs derived from different bacteria species. In squids exposed to OMVs from *V. parahaemolyticus*, cell cytoplasm had higher levels of ^{15}N -enrichment compared to the nuclei. However, in squids inoculated with *V. fischeri* OMVs, the opposite pattern was observed (Fig. 3-3). Interestingly, in these treatments, high ^{15}N -enrichment were also observed in the Golgi apparatus (Fig. 3-4). In contrast, animals inoculated with *E. coli* OMVs displayed relatively low levels of ^{15}N , but had distinct ^{15}N -enrichment in nuclei and nucleoli as well as a presence of ^{15}N -hotspots on the light-organ surface (Fig. 3-3).

Together our data indicate that: (i) The squid is able to take up and incorporate bacterial products released not only from its natural symbiont *V. fischeri*, but also from other Gram-negative bacteria. (ii) Diffusible or secreted bacterial products are responsible for the ^{15}N -enrichment inside the host. (iii) Variations in the ^{15}N -enrichment patterns between treatments and in distributions of ^{15}N in the squid organs suggest that the uptake of bacterial products is not random; i.e., there is evidence of specificity in the host response to the bacterial-derived materials.

A. The nature of the molecular exchange

These results raise fundamental questions about the nature of the molecular transfer that produces the ^{15}N -enrichment in the squid and, once the bacteria-derived molecules have entered the host tissue, what are their function(s) within the squid cells? The high degree of similarity between the ^{15}N -enrichment patterns induced by the different Vibrionaceae species suggest that at least some of the secreted molecules from the bacteria cells and some molecules carried in their OMVs have shared structural and functional features, and/or that these molecules are processed by similar pathways within the host cells. In [Chapter 2](#), I proposed two hypotheses for the high sub-nuclear ^{15}N -enrichment observed, particularly in the nucleoli. One hypothesis, which suggests a bacteria-specific response, is that

the bacteria-derived ^{15}N -enriched molecules specifically target the subnuclear components by mimicking eukaryotic sequences that destine the molecules to these regions. The second hypothesis, which suggests a non-specific response to the bacteria, is that the bacteria-derived ^{15}N -enriched molecules enter the squid tissue only to become part of the normal cell metabolic processes, i.e., not related to bacteria activity and, as a consequence, organelles with high metabolic activity will more quickly incorporate high levels of ^{15}N .

The widespread distribution of ^{15}N -enrichment in several squid organs, and the fact that ^{15}N -enrichment patterns were not unique to the symbiont, suggest that a large fraction of the observed ^{15}N -enrichment can be attributed to a non-specific chemical transfer from the bacteria into the squid. Highly specific, microbe-associated molecular patterns (MAMPs), such as TCT, LPS and nuclear-targeting molecules, are seemingly undetectable with the NanoSIMS ([Chapter 1](#)), suggesting that their contribution to the ^{15}N -enrichment in the cells is effectively masked by molecules that are part of the more general chemical transfer. Inoculation of squids with a mixture of ^{15}N -enriched amino acids resulted in similar subnuclear patterns (preferential accumulation in the euchromatin regions of the nuclei and hotspots in the nucleoli) to those obtained after inoculation with ^{15}N -enriched bacterial cells or OMVs from *V. fischeri* or phylogenetically related bacteria (but different from those obtained with ^{15}N -enriched *E. coli* OMVs). This similarity was more notable when squids were exposed to *V. parahaemolyticus*-derived OMVs, where the relative difference in ^{15}N -enrichment between cell cytoplasm and the nuclei was very similar to squid exposed to the amino acid mixture. If the results from the exposure to amino acids reflect the pathways and subcellular distribution of metabolized products (e.g., Boisvert et al. 2012), then this similarity suggests that the ^{15}N -bacterial molecules were involved in normal metabolic activity of the host cells. In principle, these ^{15}N -bacterial molecules might themselves be amino acids, byproducts that are broken down into amino acids inside the squid cells, and/or other molecules that are processed via the same metabolic pathways. If one follows this logic to the end, it raises an interesting question, namely: What is the ecological significance for the squid to uptake molecules from the adjacent seawater for metabolic activity? Do juvenile squids take up byproducts from bacteria, and perhaps even other organisms, to satisfy their metabolic demands in a nutrient-limited environment? Addressing this question will be important for future investigations (see below).

Differences in host ^{15}N -enrichment patterns were observed between bacteria/OMVs inoculations compared with the pure amino-acid exposure. Notably, in the amino-acid experiment, the cell cytoplasm was significantly more ^{15}N -enriched compared to the nuclei, whereas the opposite relationship was observed in the bacteria/OMV experiments. Even if metabolic processing is the primary fate of the assimilated bacterial products, this difference in patterns of ^{15}N -enrichment suggests specific pathways for some fraction(s) of the bacterial products. It is hypothesized here that this difference in ^{15}N -

enrichment patterns might be due to the presence of particular molecules of bacterial origin, rather than primary metabolites that participate in normal metabolic processes, and that their processing within the host cell resulted in a higher subnuclear enrichment relative to that in the cytoplasm. Because MAMPs are unlikely to be detected by the NanoSIMS, other bacteria products were possibly involved in producing the differences between these two exposures. Evidence suggests that the highly specific mechanisms induced by MAMPs are not sufficient to shape host response, and that other bacteria-derived small molecules, such as metabolites (e.g., short-chain fatty acids and sugars) and autoinducers or other secondary metabolites, can provide additional information that aid the host in assessing the context in which MAMPs are sensed (Vance et al., 2009; Chang et al., 2014; Sharon et al., 2014; Zargar et al., 2015; Ismail et al., 2016; Cleary et al., 2017). Such small molecules can be critical to understanding host responses to the presence of MAMPs because bacteria cell-wall components (e.g., PGN and LPS) are common molecules produced by many, if not all, bacterial species. Examples of more specific molecules are autoinducers, cyclic-di-GMP, and mRNA that are considered as indicators of live bacteria cells (Zimmermann et al., 2006; Karaolis et al., 2007; Sander et al., 2011; Vanaja et al., 2016). In the squid, the synergistic effects of purified TCT and LPS drive much of the light-organ's morphogenesis but cannot trigger the full host response (e.g., Koropatnick et al. 2007; McFall-Ngai et al. 2012). It is conceivable that some part(s) of the molecular cocktail that is responsible for the ^{15}N -enrichment patterns acts along with the more specific MAMPs, perhaps by inducing specificity in an environment where the squid is continuously exposed to high numbers of bacterial cells and their byproducts. The use in ^{15}N isotopes in this experiment indicates that these molecules must contain nitrogen. As such, short chain fatty acids and sugars like glucose cannot be included. However, D-amino acids, which are PGN derivatives, might be contributing to this enrichment. A recent proteomic analysis revealed abundant protein content in the OMVs (Ruby lab, unpublished data, Chapter 2). As such, although not identifiable by NanoSIMS as proteins, the labeled material could be proteins that are transported into the cells. Indeed, some of these proteins have a nuclear localization signal.

Clear specificity to bacterial products was observed in the ^{15}N -enrichment patterns created by OMVs derived either from different Vibrionaceae species, or from *E. coli*. The cohort of molecules these vesicles contain, may have affected their uptake and processing inside the host cells (e.g., Pizarro-Cerdá and Cossart 2006; Parker et al. 2010; Galdiero et al. 2012). It is reasonable to assume that the squid will exhibit high selectiveness towards the OMVs from different bacterial origins, because in nature some of this cargo might be harmful, i.e., if derived from a pathogen.

To conclude, although the molecules that induce the host ^{15}N -enrichment patterns are not yet known, I hypothesis here that they can be subdivided into two main groups, based on the similarity and the dissimilarity between the squid's responses to exposure to either amino acids or bacterial products

(cells or OMVs), respectively: (i) the molecules that induce the vast majority of the ^{15}N -enrichment inside the host tissues, which conceivably are part of the host cell's general metabolism, and (ii) the molecules that induced a more specific ^{15}N -enrichment response in the host, which are bacterial-species specific. The latter molecule(s) conceivably act along with MAMPs, providing the host with additional chemical 'information' to distinguish non-harmful bacteria from pathogens.

B. OMVs colocalize with the Golgi apparatus: a specific pathway for OMVs delivery?

The ^{15}N -enrichment observed in the Golgi apparatus after OMVs exposure raise the possibility that the molecular content of bacterial OMVs takes advantage of the existing cell endocytosis pathways to deliver important information into the host. Translocation of molecules between membrane-bound compartments of the endocytosis pathways, such as endosome, Golgi apparatus, ER, can provide protection from cytosolic proteases and ensure successful delivery of the proteins into the host (Kulp and Kuehn, 2010; Vanaja et al., 2016). Various studies have colocalized OMVs in compartments along these pathways (e.g., Bomberger et al. 2009; Thay et al. 2014). OMVs that are being trafficked can either use the Golgi apparatus as a sorting station for the internalized cargo or as the place where they exert their biological activity. While little evidence exists to support which of these scenarios is likely to occur, I believe that further studies will deepen our understanding of the role of OMVs in the squid-*Vibrio* symbiosis.

C. Permissiveness of the light organ

Across all experiments, the light-organ epithelia had the highest levels of ^{15}N suggesting that it is the most sensitive organ to external bacterial products. This result is perhaps not surprising considering that the squid hatches from the egg in a state of readiness to 'accept' *V. fischeri* cells and their products (Kremer et al., 2013). However, the ^{15}N -signature in the light-organ duct was distinct (Fig. 2-2), suggesting that the duct epithelium senses and responds differently to the bacterial cells compared with the response of other regions of light-organ epithelia. The dramatic changes in gene expression induced in light-organ tissues by *V. fischeri* cells aggregated on the appendages (Kremer et al., 2013) might indicate an increase in the metabolic activity and protein turnover in these cells. Therefore, high ^{15}N -enrichment in the light-organ tissue may also correspond to cell organelles that exhibit a relatively high metabolic rate, such as the nuclei and nucleoli, as discussed above. Although these robust transcriptional changes were not observed in squids exposed to environmental bacteria (10^6 CFU/ mL, but devoid of *V. fischeri*; Kremer et al. 2013), it is not known whether high concentrations of non-symbiotic *Vibrio* species, similar to those used in the experiments here, can also induce similar transcriptional changes.

Interestingly, no ^{15}N -enrichment was detected in the light organ of squids continuously exposed to symbiont cells for 14 h. It is possible that at this time point, after successful colonization of the light-

organ crypts by *V. fischeri* cells, metabolite transfer from bacterial species in the external seawater is diminished, and the squid light organ switches to a hyposensitive state towards the products of external bacteria. Exposure of squids to ^{15}N -labeled compounds for more extended times, before and after colonization, will provide important insights about the permissiveness of the light organ, and should be further examined.

D. Concluding remarks and future perspective

This thesis work revealed that the uptake of bacterial materials by the juvenile squid is more significant than believed in the past. The broad similarity in the response of squids exposed to bacterial cells and OMVs suggests that the OMVs are biologically relevant to this molecular transfer. While no clear conclusion can be drawn from these studies regarding the specific role of the bacterial products that induce the ^{15}N -enrichment within the host cells, the results open new perspectives on interactions between the squid and the bacteria that reside in its natural marine habitat. To better understand the extent to which this uptake is ubiquitous (metabolic-driven) or specific (i.e., depending on the bacterial species), future experiments should examine ^{15}N -enrichment patterns in squids exposed to, for example: (i) distantly related bacterial species and their OMVs, such as non-*Vibrio* species and even Gram-positive bacteria; (ii) degraded OMVs vs. intact OMVs; (iii) OMVs that are produced by *V. fischeri* cells with a defect in surface-bound molecules, such as OmpU or lipid A; and (iv) ^{15}N -labeled amino acids, with or without non-labeled *V. fischeri* cells. The latter experiment will elucidate whether the presence of *V. fischeri* cells in the seawater has an effect on host metabolism of external nutrients.

Although tracking of highly specific signaling molecules in the whole animal was not possible with the NanoSIMS, experiments in which cell cultures are exposed directly to such molecule(s), could avoid the confounding effects of dilution that occur in whole-animal studies, as well as induce a stronger (and perhaps NanoSIMS detectable) effect. In addition, the NanoSIMS technique should be combined with other imaging (e.g., fluorescent microscopy or MALDI), molecular and proteomics approaches that can provide a more comprehensive insight about the molecules that are involved, as well as the mechanism(s) that underlie these ^{15}N -enrichment patterns. This thesis also raises the importance of investigating bacteria-host interaction in their native context, such as the observation of ^{15}N -hotspots on the cell surface of light-organ epithelia associated with microvilli and/or cilia. The vast majority of the published OMVs studies are done in epithelial cell cultures, which might bias or hinder such observations because typical epithelial-cell characteristics, such as microvilli and cilia, are generally absent in cell culture.

In a broader perspective, does the observed bacteria-derived molecular transfer exist in other symbiotic systems in which host tissues experience a similar bacteria-rich environment, i.e., seawater, or in the human intestine? Do pathogens have a similar capability of contributing to or influencing

molecular transfer? If these parallels exist in other systems, it will open new horizons for biologists to explore host-microbe interactions. In any case it seems clear that the NanoSIMS technique, with its high spatial resolution and relatively high sensitivity, combined with the ability to correlate isotopic images with other sub-cellular or ultrastructure level imaging approaches, represents a powerful tool to investigate subcellular processes that govern animal-bacteria association.

References

- A -

- Aeckersberg, F., Lupp, C., Feliciano, B., and Ruby, E. (2001) *Vibrio fischeri* outer membrane protein OmpU plays a role in normal symbiotic colonization. *J Bacteriol* **183**: 6590–6597.
- Ahmad, Y., Boisvert, F.-M., Gregor, P., Cobley, A., and Lamond, A.I. (2009) NOPdb: nucleolar proteome database—2008 update. *Nucleic Acids Res* **37**: D181–D184.
- Ahmad-Nejad, P., Häcker, H., Rutz, M., Bauer, S., Vabulas, R.M., and Wagner, H. (2002) Bacterial CpG-DNA and lipopolysaccharides activate Toll-like receptors at distinct cellular compartments. *Eur J Immunol* **32**: 1958–1968.
- Akira, S., Uematsu, S., and Takeuchi, O. (2006) Pathogen recognition and innate immunity. *Cell* **124**: 783–801.
- Alberts, B., A, J., Lewis, J., Raff, M., Roberts, K., and Walter, P. (2015) *Molecular biology of the cell*. 6th edition. New York Garland Science.
- Allemand, D., De Renzis, G., Maistre, C., Girard, J.-P., and Payan, P. (1985) Uptake of valine and alanine by a neutral amino-acid carrier in sea urchin eggs: cyclic variations in the early cleavage stage. *J Membr Biol* **87**: 217–224.
- Altura, M.A., Heath-Heckman, E.A.C., Gillette, A., Kremer, N., Krachler, A.-M., Brennan, C., et al. (2013) The first engagement of partners in the *Euprymna scolopes-Vibrio fischeri* symbiosis is a two-step process initiated by a few environmental symbiont cells. *Environ Microbiol* **15**: 2937–2950.
- Altura, M.A., Stabb, E., Goldman, W., Apicella, M., and McFall-Ngai, M.J. (2011) Attenuation of host NO production by MAMPs potentiates development of the host in the squid–vibrio symbiosis. *Cell Microbiol* **13**: 527–537.
- Alvarez-Venegas, R. (2014) Bacterial SET domain proteins and their role in eukaryotic chromatin modification. *Front Genet* **5**: 65.
- Amano, A., Takeuchi, H., and Furuta, N. (2010) Outer membrane vesicles function as offensive weapons in host-parasite interactions. *Microbes Infect* **12**: 791–798.
- Andersen, J.S., Lam, Y.W., Leung, A.K., Ong, S.-E., Lyon, C.E., Lamond, A.I., and Mann, M. (2005) Nucleolar proteome dynamics. *Nature* **433**: 77–83.

- Applebaum, S.L., Ginsburg, D.W., Capron, C.S., and Manahan, D.T. (2013) Expression of amino acid transporter genes in developmental stages and adult tissues of Antarctic echinoderms. *Polar Biol* **36**: 1257–1267.
- Aschtgen, M., Wetzel, K., Goldman, W., McFall-Ngai, M., and Ruby, E. (2015) *Vibrio fischeri*-derived outer membrane vesicles trigger host development. *Cell Microbiol*.
- Aschtgen, M.-S., Lynch, J.B., Koch, E., Schwartzman, J., McFall-Ngai, M., and Ruby, E. (2016) Rotation of *Vibrio fischeri* flagella produces outer membrane vesicles that induce host development. *J Bacteriol* **198**: 2156–2165.
- Audas, T.E., Jacob, M.D., and Lee, S. (2012a) The nucleolar detention pathway: a cellular strategy for regulating molecular networks. *Cell Cycle* **11**: 2059–2062.
- Audas, T.E., Jacob, M.D., and Lee, S. (2012b) Immobilization of proteins in the nucleolus by ribosomal intergenic spacer noncoding RNA. *Mol Cell* **45**: 147–157.

- B -

- Baboo, S., Bhushan, B., Jiang, H., Grovenor, C.R., Pierre, P., Davis, B.G., and Cook, P.R. (2014) Most human proteins made in both nucleus and cytoplasm turn over within minutes. *PLoS ONE* **9**: e99346.
- Backert, S., and Meyer, T.F. (2006) Type IV secretion systems and their effectors in bacterial pathogenesis. *Curr Opin Microbiol* **9**: 207–217.
- Bäckhed, F., Ley, R.E., Sonnenburg, J.L., Peterson, D.A., and Gordon, J.I. (2005) Host-bacterial mutualism in the human intestine. *Science* **307**: 1915–1920.
- Bauman, S.J., and Kuehn, M.J. (2009) *Pseudomonas aeruginosa* vesicles associate with and are internalized by human lung epithelial cells. *BMC Microbiol* **9**: 26.
- Bayne, C. (1973) Internal defense mechanisms of *Octopus dofleini*. *Malacol Rev* **6**: 13–17.
- Beatty, K.E., Liu, J.C., Xie, F., Dieterich, D.C., Schuman, E.M., Wang, Q., and Tirrell, D.A. (2006) Fluorescence visualization of newly synthesized proteins in mammalian cells. *Angew Chem* **118**: 7524–7527.
- Ben-David-Zaslow, R., and Benayahu, Y. (2000) Biochemical composition, metabolism, and amino acid transport in planula-larvae of the soft coral *Heteroxenia fuscescens*. *J Exp Zool* **287**: 401–412.
- Berry, D., Stecher, B., Schintlmeister, A., Reichert, J., Brugiroux, S., Wild, B., et al. (2013) Host-compound foraging by intestinal microbiota revealed by single-cell stable isotope probing. *Proc Natl Acad Sci* **110**: 4720–4725.

- Berry, S.S. (1912) The cephalopoda of the Hawaiian Islands. *Bull US Bur Fish* **32**: 255–362.
- Bertani, G. (1951) Studies on lysogenesis .1. The mode of phage liberation by lysogenic *Escherichia coli*. *J Bacteriol* **62**: 293–300.
- Bickmore, W.A., and Sutherland, H.G. (2002) Addressing protein localization within the nucleus. *EMBO J* **21**: 1248–1254.
- Bielaszewska, M., Rüter, C., Kunsmann, L., Greune, L., Bauwens, A., Zhang, W., et al. (2013) Enterohemorrhagic *Escherichia coli* hemolysin employs outer membrane vesicles to target mitochondria and cause endothelial and epithelial apoptosis. *PLoS Pathog* **9**: e1003797.
- Bierne, H., and Cossart, P. (2012) When bacteria target the nucleus: the emerging family of nucleomodulins. *Cell Microbiol* **14**: 622–633.
- Birnstiel, M. (1967) The nucleolus in cell metabolism. *Annu Rev Plant Physiol* **18**: 25–58.
- Blanke, S.R. (2006) Portals and pathways: principles of bacterial toxin entry into host cells. *Microbe* **1**: 26.
- Boettcher, K.J., and Ruby, E.G. (1990) Depressed light emission by symbiotic *Vibrio fischeri* of the Sepiolid squid *Euprymna scolopes*. *J Bacteriol* **172**: 3701–3706.
- Boettcher, K.J., Ruby, E.G., and McFall-Ngai, M.J. (1996) Bioluminescence in the symbiotic squid *Euprymna scolopes* is controlled by daily biological rhythm. *J Comp Physiol A* **179**: 65–73.
- Boisvert, F.-M., Ahmad, Y., Gierliński, M., Charrière, F., Lamont, D., Scott, M., et al. (2012) A quantitative spatial proteomics analysis of proteome turnover in human cells. *Mol Cell Proteomics* **11**: M111. 011429.
- Bomberger, J.M., MacEachran, D.P., Coutermarsh, B.A., Ye, S., O'Toole, G.A., and Stanton, B.A. (2009) Long-distance delivery of bacterial virulence factors by *Pseudomonas aeruginosa* outer membrane vesicles. *PLoS Pathog* **5**: e1000382.
- Boulikas, T. (1992) Nuclear localization signals (NLS). *Crit Rev Eukaryot Gene Expr* **3**: 193–227.
- Boulon, S., Westman, B.J., Hutten, S., Boisvert, F.-M., and Lamond, A.I. (2010) The nucleolus under stress. *Mol Cell* **40**: 216–227.
- Brooks, J.F., Gyllborg, M.C., Cronin, D.C., Quillin, S.J., Mallama, C.A., Foxall, R., et al. (2014) Global discovery of colonization determinants in the squid symbiont *Vibrio fischeri*. *Proc Natl Acad Sci* **111**: 17284–17289.
- Brosnan, J.T. (2001) Amino acids, then and now--a reflection on sir hans krebs' contribution to nitrogen metabolism. *IUBMB Life* **52**: 265–270.

- Carpenter, K.J., Weber, P.K., Davisson, M.L., Pett-Ridge, J., Haverty, M.I., and Keeling, P.J. (2013) Correlated SEM, FIB-SEM, TEM, and NanoSIMS imaging of microbes from the hindgut of a lower termite: methods for in situ functional and ecological studies of uncultivable microbes. *Microsc Microanal* **19**: 1490–1501.
- Casadevall, A., and Pirofski, L. (2015) What is a host? Incorporating the microbiota into the damage-response framework. *Infect Immun* **83**: 2–7.
- Cerf-Bensussan, N., and Gaboriau-Routhiau, V. (2010) The immune system and the gut microbiota: friends or foes? *Nat Rev Immunol* **10**: 735–744.
- Chang, P.V., Hao, L., Offermanns, S., and Medzhitov, R. (2014) The microbial metabolite butyrate regulates intestinal macrophage function via histone deacetylase inhibition. *Proc Natl Acad Sci* **111**: 2247–2252.
- Chaston, J., and Goodrich-Blair, H. (2010) Common trends in mutualism revealed by model associations between invertebrates and bacteria. *FEMS Microbiol Rev* **34**: 41–58.
- Chatterjee, D., and Chaudhuri, K. (2011) Association of cholera toxin with *Vibrio cholerae* outer membrane vesicles which are internalized by human intestinal epithelial cells. *FEBS Lett* **585**: 1357–1362.
- Chen, R., Schmidmayr, W., Krämer, C., Chen-Schmeisser, U., and Henning, U. (1980) Primary structure of major outer membrane protein II (OmpA protein) of *Escherichia coli* K-12. *Proc Natl Acad Sci* **77**: 4592–4596.
- Chia, F. (1974) Classification and adaptive significance of developmental patterns in marine invertebrates. *Thalass Jugosl* **10**: 121–130.
- Christophe-Hobertus, C., Duquesne, V., Pichon, B., Roger, P.P., and Christophe, D. (1999) Critical residues of the homeodomain involved in contacting DNA bases also specify the nuclear accumulation of thyroid transcription factor-1. *FEBS J* **265**: 491–497.
- Chu, H., and Mazmanian, S.K. (2013) Innate immune recognition of the microbiota promotes host-microbial symbiosis. *Nat Immunol* **14**: 668–675.
- Chun, C.K., Troll, J.V., Koroleva, I., Brown, B., Manzella, L., Snir, E., et al. (2008) Effects of colonization, luminescence, and autoinducer on host transcription during development of the squid-vibrio association. *Proc Natl Acad Sci U S A* **105**: 11323–11328.
- Chutkan, H., and Kuehn, M.J. (2011) Context-dependent activation kinetics elicited by soluble versus outer membrane vesicle-associated heat-labile enterotoxin. *Infect Immun* **79**: 3760–3769.

Cleary, J.L., Condren, A.R., Zink, K.E., and Sanchez, L.M. (2017) Calling all hosts: bacterial communication in situ. *Chem* **2**: 334–358.

Cloud-Hansen, K.A., Peterson, S.B., Stabb, E.V., Goldman, W.E., McFall-Ngai, M.J., and Handelsman, J. (2006) Breaching the great wall: peptidoglycan and microbial interactions. *Nat Rev Microbiol* **4**: 710–716.

Cokol, M., Nair, R., and Rost, B. (2000) Finding nuclear localization signals. *EMBO Rep* **1**: 411–415.

Collins, A.J., Schleicher, T.R., Rader, B.A., and Nyholm, S.V. (2012) Understanding the role of host hemocytes in a squid/*Vibrio* symbiosis using transcriptomics and proteomics. *Front Immunol* **3**: 91.

Cookson, B.T., Tyler, A.N., and Goldman, W.E. (1989) Primary structure of the peptidoglycan-derived tracheal cytotoxin of *Bordetella pertussis*. *Biochemistry (Mosc)* **28**: 1744–1749.

Crivat, G., and Taraska, J.W. (2012) Imaging proteins inside cells with fluorescent tags. *Trends Biotechnol* **30**: 8–16.

- D -

Dang, C.V., and Lee, W. (1989) Nuclear and nucleolar targeting sequences of *c-erb-A*, *c-myb*, *N-myc*, p53, HSP70, and HIV *tat* proteins. *J Biol Chem* **264**: 18019–18023.

Daniel, R.A., and Errington, J. (2003) Control of cell morphogenesis in bacteria: two distinct ways to make a rod-shaped cell. *Cell* **113**: 767–776.

Davidson, S.K., Koropatnick, T.A., Kossmehl, R., Sycuro, L., and McFall-Ngai, M.J. (2004) NO means “yes” in the squid-vibrio symbiosis: nitric oxide (NO) during the initial stages of a beneficial association. *Cell Microbiol* **6**: 1139–1151.

Davis, J.P., and Stephens, G.C. (1984) Regulation of net amino acid exchange in sea urchin larvae. *Am J Physiol-Regul Integr Comp Physiol* **247**: R1029–R1037.

DeLoney-Marino, C.R., Wolfe, A.J., and Visick, K.L. (2003) Chemoattraction of *Vibrio fischeri* to serine, nucleosides, and N-acetylneuraminic acid, a component of squid light-organ mucus. *Appl Environ Microbiol* **69**: 7527–7530.

Dieterich, D.C., Link, A.J., Graumann, J., Tirrell, D.A., and Schuman, E.M. (2006) Selective identification of newly synthesized proteins in mammalian cells using bioorthogonal noncanonical amino acid tagging (BONCAT). *Proc Natl Acad Sci* **103**: 9482–9487.

Dillon, S.C., Zhang, X., Trievel, R.C., and Cheng, X. (2005) The SET-domain protein superfamily: protein lysine methyltransferases. *Genome Biol* **6**: 227.

Dingwall, C., and Laskey, R.A. (1991) Nuclear targeting sequences—a consensus? *Trends Biochem Sci* **16**: 478–481.

Doherty, G.J., and McMahon, H.T. (2009) Mechanisms of endocytosis. *Annu Rev Biochem* **78**: 857–902.

Doino, J.A., and McFall-Ngai, M.J. (1995) A transient exposure to symbiosis-competent bacteria induces light organ morphogenesis in the host squid. *Biol Bull* **189**: 347–355.

Douglas, A. (1998) Host benefit and the evolution of specialization in symbiosis. *Heredity* **81**: 599–603.

Dunn, A.K. (2012) *Vibrio fischeri* metabolism: symbiosis and beyond. *Adv Microb Physiol* **61**: 37.

Dutta, D., and Donaldson, J.G. (2012) Search for inhibitors of endocytosis: intended specificity and unintended consequences. *Cell Logist* **2**: 203–208.

- E -

Edwards, N.J., Monteiro, M.A., Faller, G., Walsh, E.J., Moran, A.P., Roberts, I.S., and High, N.J. (2000) Lewis X structures in the O antigen side-chain promote adhesion of *Helicobacter pylori* to the gastric epithelium. *Mol Microbiol* **35**: 1530–1539.

Elhenawy, W., Debelyy, M.O., and Feldman, M.F. (2014) Preferential packing of acidic glycosidases and proteases into *Bacteroides* outer membrane vesicles. *MBio* **5**: e00909-14.

Ellis, T.N., and Kuehn, M.J. (2010) Virulence and immunomodulatory roles of bacterial outer membrane vesicles. *Microbiol Mol Biol Rev* **74**: 81–94.

Escoll, P., Mondino, S., Rolando, M., and Buchrieser, C. (2016) Targeting of host organelles by pathogenic bacteria: a sophisticated subversion strategy. *Nat Rev Microbiol* **14**: 5–19.

- F -

Ferrier, M.D. (1991) Net uptake of dissolved free amino acids by four scleractinian corals. *Coral Reefs* **10**: 183–187.

Fidopiastis, P.M., Von Boletzky, S., and Ruby, E.G. (1998) A new niche for *Vibrio logei*, the predominant light organ symbiont of squids in the genus *Sepiola*. *J Bacteriol* **180**: 59–64.

Floss, C., Stadermann, F.J., Bradley, J.P., Dai, Z.R., Bajt, S., Graham, G., and Lea, A.S. (2006) Identification of isotopically primitive interplanetary dust particles: a NanoSIMS isotopic imaging study. *Geochim Cosmochim Acta* **70**: 2371–2399.

Fontes, M.R., Trazel, T., Gabor, T., Anna, J., Imre, P., and Bostjan, K. (2003) Role of flanking sequences and phosphorylation in the recognition of the simian-virus-40 large T-antigen nuclear localization sequences by importin- α . *Biochem J* **375**: 339–349.

Forst, S., Delgado, J., Ramakrishnan, G., and Inouye, M. (1988) Regulation of *ompC* and *ompF* expression in *Escherichia coli* in the absence of *envZ*. *J Bacteriol* **170**: 5080–5085.

Foster, J.S., Apicella, M.A., and McFall-Ngai, M.J. (2000) *Vibrio fischeri* lipopolysaccharide induces developmental apoptosis, but not complete morphogenesis, of the *Euprymna scolopes* symbiotic light organ. *Dev Biol* **226**: 242–254.

Foster, J.S., and McFall-Ngai, M.J. (1998) Induction of apoptosis by cooperative bacteria in the morphogenesis of host epithelial tissues. *Dev Genes Evol* **208**: 295–303.

Frisz, J.F., Lou, K., Klitzing, H.A., Hanafin, W.P., Lizunov, V., Wilson, R.L., et al. (2013) Direct chemical evidence for sphingolipid domains in the plasma membranes of fibroblasts. *Proc Natl Acad Sci* **110**: E613–E622.

Fujimoto, L.M., Roth, R., Heuser, J.E., and Schmid, S.L. (2000) Actin assembly plays a variable, but not obligatory role in receptor-mediated endocytosis. *Traffic* **1**: 161–171.

Furuta, N., Tsuda, K., Omori, H., Yoshimori, T., Yoshimura, F., and Amano, A. (2009) *Porphyromonas gingivalis* outer membrane vesicles enter human epithelial cells via an endocytic pathway and are sorted to lysosomal compartments. *Infect Immun* **77**: 4187–4196.

- G -

Galán, J.E., and Wolf-Watz, H. (2006) Protein delivery into eukaryotic cells by type III secretion machines. *Nature* **444**: 567–573.

Galdiero, M., Vitiello, M., and Galdiero, S. (2003) Eukaryotic cell signaling and transcriptional activation induced by bacterial porins. *FEMS Microbiol Lett* **226**: 57–64.

Galdiero, S., Falanga, A., Cantisani, M., Tarallo, R., Elena Della Pepa, M., D’Orlando, V., and Galdiero, M. (2012) Microbe-host interactions: structure and role of Gram-negative bacterial porins. *Curr Protein Pept Sci* **13**: 843–854.

Gama-Carvalho, M., and Carmo-Fonseca, M. (2001) The rules and roles of nucleocytoplasmic shuttling proteins. *FEBS Lett* **498**: 157–163.

Gardner, K.E., Allis, C.D., and Strahl, B.D. (2011) Operating on chromatin, a colorful language where context matters. *J Mol Biol* **409**: 36–46.

Gomme, J. (2001) Transport of exogenous organic substances by invertebrate integuments: the field revisited. *J Exp Zool Part Ecol Genet Physiol* **289**: 254–265.

- González, J.F., and Venturi, V. (2013) A novel widespread interkingdom signaling circuit. *Trends Plant Sci* **18**: 167–174.
- Goodell, E. (1985) Recycling of murein by *Escherichia coli*. *J Bacteriol* **163**: 305–310.
- Goodson, M.S., Kojadinovic, M., Troll, J.V., Scheetz, T.E., Casavant, T.L., Soares, M.B., and McFall-Ngai, M.J. (2005) Identifying components of the NF- κ B pathway in the beneficial *Euprymna scolopes-Vibrio fischeri* light organ symbiosis. *Appl Environ Microbiol* **71**: 6934–6946.
- Gori, A., Grover, R., Orejas, C., Sikorski, S., and Ferrier-Pagès, C. (2014) Uptake of dissolved free amino acids by four cold-water coral species from the Mediterranean Sea. *Deep Sea Res Part II Top Stud Oceanogr* **99**: 42–50.
- Gorski, S.A., Dundr, M., and Misteli, T. (2006) The road much traveled: trafficking in the cell nucleus. *Curr Opin Cell Biol* **18**: 284–290.
- Graf, J., Dunlap, P.V., and Ruby, E.G. (1994) Effect of transposon-induced motility mutations on colonization of the host light organ by *Vibrio fischeri*. *J Bacteriol* **176**: 6986–6991.
- Graf, J., and Ruby, E.G. (1998) Host-derived amino acids support the proliferation of symbiotic bacteria. *Proc Natl Acad Sci U S A* **95**: 1818–1822.
- Grant, B.D., and Donaldson, J.G. (2009) Pathways and mechanisms of endocytic recycling. *Nat Rev Mol Cell Biol* **10**: 597–608.
- Green, E.R., and Meccas, J. (2016) Bacterial secretion systems—an overview. *Microbiol Spectr* **4**.
- Grignon, N., Halpern, S., Jeusset, J., Briancon, C., and Fragu, P. (1997) Localization of chemical elements and isotopes in the leaf of soybean (*Glycine max*) by secondary ion mass spectrometry microscopy: critical choice of sample preparation procedure. *J Microsc* **186**: 51–66.
- Grovenor, C., Smart, K., Kilburn, M., Shore, B., Dilworth, J., Martin, B., et al. (2006) Specimen preparation for NanoSIMS analysis of biological materials. *Appl Surf Sci* **252**: 6917–6924.
- Grover, R., Maguer, J.-F., Allemand, D., and Ferrier-Pagès, C. (2008) Uptake of dissolved free amino acids by the scleractinian coral *Stylophora pistillata*. *J Exp Biol* **211**: 860–865.
- Grünwald, D., Martin, R.M., Buschmann, V., Bazett-Jones, D.P., Leonhardt, H., Kubitscheck, U., and Cardoso, M.C. (2008) Probing intranuclear environments at the single-molecule level. *Biophys J* **94**: 2847–2858.
- Guidi, R., Levi, L., Rouf, S.F., Puiac, S., Rhen, M., and Frisan, T. (2013) *Salmonella enterica* delivers its genotoxin through outer membrane vesicles secreted from infected cells. *Cell Microbiol* **15**: 2034–2050.

- H -

- Hamilton, H.L., and Dillard, J.P. (2006) Natural transformation of *Neisseria gonorrhoeae*: from DNA donation to homologous recombination. *Mol Microbiol* **59**: 376–385.
- Hamon, M.A., and Cossart, P. (2008) Histone modifications and chromatin remodeling during bacterial infections. *Cell Host Microbe* **4**: 100–109.
- Harouz, H., Rachez, C., Meijer, B.M., Marteyn, B., Donnadieu, F., Cammas, F., et al. (2014) *Shigella flexneri* targets the HP1 γ subcode through the phosphothreonine lyase OspF. *EMBO J* e201489244.
- Hatanaka, M. (1990) My favourite molecule: discovery of the nucleolar targeting signal. *Bioessays* **12**: 143–148.
- Hayat, M.A. (1981) Principles and techniques of electron microscopy. Biological applications. 4th edition., Edward Arnold, London.
- Heath-Heckman, E.A., Foster, J., Apicella, M.A., Goldman, W.E., and McFall-Ngai, M. (2016) Environmental cues and symbiont microbe-associated molecular patterns function in concert to drive the daily remodelling of the crypt-cell brush border of the *Euprymna scolopes* light organ. *Cell Microbiol* **18**: 1642–1652.
- Heath-Heckman, E.A., Peyer, S.M., Whistler, C.A., Apicella, M.A., Goldman, W.E., and McFall-Ngai, M.J. (2013) Bacterial bioluminescence regulates expression of a host cryptochrome gene in the squid-vibrio symbiosis. *MBio* **4**: e00167-13.
- Hendricks, M.R., and Bomberger, J.M. (2014) Who's really in control: microbial regulation of protein trafficking in the epithelium. *Am J Physiol-Cell Physiol* **306**: C187–C197.
- Hentschel, U., Steinert, M., and Hacker, J. (2000) Common molecular mechanisms of symbiosis and pathogenesis. *Trends Microbiol* **8**: 226–231.
- Hickey, C.A., Kuhn, K.A., Donermeyer, D.L., Porter, N.T., Jin, C., Cameron, E.A., et al. (2015) Colitogenic *Bacteroides thetaiotaomicron* antigens access host immune cells in a sulfatase-dependent manner via outer membrane vesicles. *Cell Host Microbe* **17**: 672–680.
- Hoegh-Guldberg, O. (1999) Net uptake of dissolved free amino acids by the giant clam, *Tridacna maxima*: alternative sources of energy and nitrogen?. *Coral Reefs* **18**: 91–96.
- Hoegh-Guldberg, O., Dove, S.G., and Siggaard, D. (1997) Dissolved free amino acid (DFAA) concentrations in Great Barrier Reef waters: the implications for the role of DFAA transport by *Acanthaster planci*. *Proc 8th Int Coral Reef Symp, Panama City* **2**: 1237–1241.

- Hoppe, P. (2006) NanoSIMS: a new tool in cosmochemistry. *Appl Surf Sci* **252**: 7102–7106.
- Hoppe, P., Cohen, S., and Meibom, A. (2013) NanoSIMS: technical aspects and applications in cosmochemistry and biological geochemistry. *Geostand Geoanalytical Res* **37**: 111–154.
- Hornef, M.W., Frisan, T., Vandewalle, A., Normark, S., and Richter-Dahlfors, A. (2002) Toll-like receptor 4 resides in the Golgi apparatus and colocalizes with internalized lipopolysaccharide in intestinal epithelial cells. *J Exp Med* **195**: 559–570.
- Hughes, D.T., and Sperandio, V. (2008) Inter-kingdom signalling: communication between bacteria and their hosts. *Nat Rev Microbiol* **6**: 111–120.
- Huisinga, K.L., Brower-Toland, B., and Elgin, S.C. (2006) The contradictory definitions of heterochromatin: transcription and silencing. *Chromosoma* **115**: 110–122.

- I -

- Ismail, A.S., Valastyan, J.S., and Bassler, B.L. (2016) A host-produced autoinducer-2 mimic activates bacterial quorum sensing. *Cell Host Microbe* **19**: 470–480.
- Itoh, N., and Takahashi, K.G. (2008) Distribution of multiple peptidoglycan recognition proteins in the tissues of Pacific oyster, *Crassostrea gigas*. *Comp Biochem Physiol B Biochem Mol Biol* **150**: 409–417.
- Iversen, T.-G., Skretting, G., Llorente, A., Nicoziani, P., Van Deurs, B., and Sandvig, K. (2001) Endosome to Golgi transport of ricin is independent of clathrin and of the Rab9-and Rab11-GTPases. *Mol Biol Vell* **12**: 2099–2107.

- J -

- Jacobs, C., Huang, L., Bartowsky, E., Normark, S., and Park, J. (1994) Bacterial cell wall recycling provides cytosolic muropeptides as effectors for beta-lactamase induction. *EMBO J* **13**: 4684.
- Jaekle, W.B., and Manahan, D.T. (1992) Experimental manipulations of the organic compositions of seawater: implications for studies of energy budgets in marine invertebrate larvae. *J Exp Mar Biol Ecol* **156**: 273–284.
- Jiang, H., Favaro, E., Goulbourne, C., Rakowska, P., Hughes, G., Ryadnov, M., et al. (2014) Stable isotope imaging of biological samples with high resolution secondary ion mass spectrometry and complementary techniques. *Methods* **68**: 317–324.
- Jones, B.W., and Nishiguchi, M.K. (2004) Counterillumination in the hawaiian bobtail squid, *Euprymna scolopes* Berry (Mollusca : Cephalopoda). *Mar Biol* **144**: 1151–1155.

- K -

- Kaiser, C., Kilburn, M.R., Clode, P.L., Fuchslueger, L., Koranda, M., Cliff, J.B., et al. (2015) Exploring the transfer of recent plant photosynthates to soil microbes: mycorrhizal pathway vs direct root exudation. *New Phytol* **205**: 1537–1551.
- Kaparakis-Liaskos, M., and Ferrero, R.L. (2015) Immune modulation by bacterial outer membrane vesicles. *Nat Rev Immunol* **15**: 375–387.
- Karaolis, D.K., Means, T.K., Yang, D., Takahashi, M., Yoshimura, T., Muraille, E., et al. (2007) Bacterial c-di-GMP is an immunostimulatory molecule. *J Immunol* **178**: 2171–2181.
- Kawai, T., and Akira, S. (2007) Signaling to NF- κ B by Toll-like receptors. *Trends Mol Med* **13**: 460–469.
- Kendall, M.M., and Sperandio, V. (2016) What a dinner party! Mechanisms and functions of interkingdom signaling in host-pathogen associations. *MBio* **7**: e01748-15.
- Kesty, N.C., Mason, K.M., Reedy, M., Miller, S.E., and Kuehn, M.J. (2004) Enterotoxigenic *Escherichia coli* vesicles target toxin delivery into mammalian cells. *EMBO J* **23**: 4538–4549.
- Kilberg, M.S., Pan, Y.X., Chen, H., and Leung-Pineda, V. (2005) Nutritional control of gene expression: how mammalian cells respond to amino acid limitation. *Annu Rev Nutr* **25**: 59–85.
- Kimbell, J.R., and McFall-Ngai, M.J. (2004) Symbiont-induced changes in host actin during the onset of a beneficial animal-bacterial association. *Appl Environ Microbiol* **70**: 1434–1441.
- Koebnik, R., Locher, K.P., and Van Gelder, P. (2000) Structure and function of bacterial outer membrane proteins: barrels in a nutshell. *Mol Microbiol* **37**: 239–253.
- Kopp, C., Domart-Coulon, I., Escrig, S., Humbel, B.M., Hignette, M., and Meibom, A. (2015) Subcellular investigation of photosynthesis-driven carbon assimilation in the symbiotic reef coral *Pocillopora damicornis*. *MBio* **6**: e02299-14.
- Kopp, C., Pernice, M., Domart-Coulon, I., Djediat, C., Spangenberg, J., Alexander, D., et al. (2013) Highly dynamic cellular-level response of symbiotic coral to a sudden increase in environmental nitrogen. *MBio* **4**: e00052-13.
- Koropatnick, T., Goodson, M.S., Heath-Heckman, E.A., and McFall-Ngai, M. (2014) Identifying the cellular mechanisms of symbiont-induced epithelial morphogenesis in the squid-vibrio association. *Biol Bull* **226**: 56–68.
- Koropatnick, T.A., Engle, J.T., Apicella, M.A., Stabb, E.V., Goldman, W.E., and McFall-Ngai, M.J. (2004) Microbial factor-mediated development in a host-bacterial mutualism. *Science* **306**: 1186–1188.
- Koropatnick, T.A., Kimbell, J.R., and McFall-Ngai, M.J. (2007) Responses of host hemocytes during the initiation of the squid-vibrio symbiosis. *Biol Bull* **212**: 29–39.

Krasity, B.C., Troll, J.V., Lehnert, E.M., Hackett, K.T., Dillard, J.P., Apicella, M.A., et al. (2015) Structural and functional features of a developmentally regulated lipopolysaccharide-binding protein. *mBio* **6**: e01193-15.

Krasity, B.C., Troll, J.V., Weiss, J.P., and McFall-Ngai, M.J. (2011) LBP/BPI proteins and their relatives: conservation over evolution and roles in mutualism. *Biochem Soc Trans* **4**:1039-1044.

Kremer, N., Philipp, E.E., Carpentier, M.-C., Brennan, C.A., Kraemer, L., Altura, M.A., et al. (2013) Initial symbiont contact orchestrates host-organ-wide transcriptional changes that prime tissue colonization. *Cell Host Microbe* **14**: 183–194.

Kremer, N., Schwartzman, J., Augustin, R., Zhou, L., Ruby, E.G., Hourdez, S., and McFall-Ngai, M.J. (2014) The dual nature of haemocyanin in the establishment and persistence of the squid–vibrio symbiosis. *Proc R Soc Lond B Biol Sci* **281**: 20140504.

Kuehn, M.J., and Kesty, N.C. (2005) Bacterial outer membrane vesicles and the host–pathogen interaction. *Genes Dev* **19**: 2645–2655.

Kulp, A., and Kuehn, M.J. (2010) Biological functions and biogenesis of secreted bacterial outer membrane vesicles. *Annu Rev Microbiol* **64**: 163–184.

Kuru, E., Hughes, H., Brown, P.J., Hall, E., Tekkam, S., Cava, F., et al. (2012) In situ probing of newly synthesized peptidoglycan in live bacteria with fluorescent D-amino acids. *Angew Chem Int Ed* **51**: 12519–12523.

- L -

Lamarcq, L.H., and McFall-Ngai, M.J. (1998) Induction of a gradual, reversible morphogenesis of its host's epithelial brush border by *Vibrio fischeri*. *Infect Immun* **66**: 777–785.

Lange, A., Mills, R.E., Lange, C.J., Stewart, M., Devine, S.E., and Corbett, A.H. (2007) Classical nuclear localization signals: definition, function, and interaction with importin α . *J Biol Chem* **282**: 5101–5105.

Latz, E., Visintin, A., Lien, E., Fitzgerald, K.A., Monks, B.G., Kurt-Jones, E.A., et al. (2002) Lipopolysaccharide rapidly traffics to and from the Golgi apparatus with the toll-like receptor 4-MD-2-CD14 complex in a process that is distinct from the initiation of signal transduction. *J Biol Chem* **277**: 47834–47843.

Lau, K., Christlieb, M., Schröder, M., Sheldon, H., Harris, A., and Grovenor, C. (2010) Development of a new bimodal imaging methodology: a combination of fluorescence microscopy and high-resolution secondary ion mass spectrometry. *J Microsc* **240**: 21–31.

- Lebreton, A., Lakisic, G., Job, V., Fritsch, L., Tham, T.N., Camejo, A., et al. (2011) A bacterial protein targets the BAHD1 chromatin complex to stimulate type III interferon response. *Science* **331**: 1319–1321.
- Lechene, C., Hillion, F., McMahon, G., Benson, D., Kleinfeld, A.M., Kampf, J.P., et al. (2006) High-resolution quantitative imaging of mammalian and bacterial cells using stable isotope mass spectrometry. *J Biol* **5**: 20.
- Lechene, C.P., Luyten, Y., McMahon, G., and Distel, D.L. (2007) Quantitative imaging of nitrogen fixation by individual bacteria within animal cells. *Science* **317**: 1563–1566.
- Lee, B.J., Cansizoglu, A.E., Süel, K.E., Louis, T.H., Zhang, Z., and Chook, Y.M. (2006) Rules for nuclear localization sequence recognition by karyopherin β 2. *Cell* **126**: 543–558.
- Lee, C., Wakeham, S., and Arnosti, C. (2004) Particulate organic matter in the sea: the composition conundrum. *AMBIO J Hum Environ* **33**: 565–575.
- Lee, K.-H., and Ruby, E.G. (1994) Effect of the squid host on the abundance and distribution of symbiotic *Vibrio fischeri* in nature. *Appl Environ Microbiol* **60**: 1565–1571.
- Lema, K.A., Clode, P.L., Kilburn, M.R., Thornton, R., Willis, B.L., and Bourne, D.G. (2015) Imaging the uptake of nitrogen-fixing bacteria into larvae of the coral *Acropora millepora*. *ISME J* **10**: 1804–1808.
- Leulier, F., and Lemaitre, B. (2008) Toll-like receptors—taking an evolutionary approach. *Nat Rev Genet* **9**: 165–178.
- Li, D., Shao, L., Chen, B.-C., Zhang, X., Zhang, M., Moses, B., et al. (2015) Extended-resolution structured illumination imaging of endocytic and cytoskeletal dynamics. *Science* **349**: aab3500.
- Li, T., Lu, Q., Wang, G., Xu, H., Huang, H., Cai, T., et al. (2013) SET-domain bacterial effectors target heterochromatin protein 1 to activate host rDNA transcription. *EMBO Rep* **14**: 733–740.
- Liu, J., Xu, Y., Stoleru, D., and Salic, A. (2012) Imaging protein synthesis in cells and tissues with an alkyne analog of puromycin. *Proc Natl Acad Sci* **109**: 413–418.
- Lu, H., Motley, S.T., and Lory, S. (1997) Interactions of the components of the general secretion pathway: role of *Pseudomonas aeruginosa* type IV pilin subunits in complex formation and extracellular protein secretion. *Mol Microbiol* **25**: 247–259.
- Lusk, C.P., Blobel, G., and King, M.C. (2007) Highway to the inner nuclear membrane: rules for the road. *Nat Rev Mol Cell Biol* **8**: 414–420.

- MacDonald, I.A., and Kuehn, M.J. (2012) Offense and defense: microbial membrane vesicles play both ways. *Res Microbiol* **163**: 607–618.
- Mackey, D., and McFall, A.J. (2006) MAMPs and MIMPs: proposed classifications for inducers of innate immunity. *Mol Microbiol* **61**: 1365–1371.
- Magalhaes, J.G., Philpott, D.J., Nahori, M., Jéhanno, M., Fritz, J., Bourhis, L., et al. (2005) Murine Nod1 but not its human orthologue mediates innate immune detection of tracheal cytotoxin. *EMBO Rep* **6**: 1201–1207.
- Makin, S.A., and Beveridge, T.J. (1996) The influence of A-band and B-band lipopolysaccharide on the surface characteristics and adhesion of *Pseudomonas aeruginosa* to surfaces. *Microbiology* **142**: 299–307.
- Mallard, F., Antony, C., Tenza, D., Salamero, J., Goud, B., and Johannes, L. (1998) Direct pathway from early/recycling endosomes to the Golgi apparatus revealed through the study of shiga toxin B-fragment transport. *J Cell Biol* **143**: 973–990.
- Manahan, D.T. (1990) Adaptations by invertebrate larvae for nutrient acquisition from seawater. *Am Zool* **30**: 147–160.
- Manahan, D.T., Davis, J.P., and Stephens, G.C. (1983) Bacteria-free sea urchin larvae: selective uptake of neutral amino acids from seawater. *Science* **220**: 204–206.
- Manahan, D.T., Jaeckle, W.B., and Nourizadeh, S.D. (1989) Ontogenic changes in the rates of amino acid transport from seawater by marine invertebrate larvae (Echinodermata, Echiura, Mollusca). *Biol Bull* **176**: 161–168.
- Manahan, D.T., Wright, S.H., Stephens, G.C., and Rice, M.A. (1982) Transport of dissolved amino acids by the mussel, *Mytilus edulis*: demonstration of net uptake from natural seawater. *Science* **215**: 1253–1255.
- Mandel, M.J., Schaefer, A.L., Brennan, C.A., Heath-Heckman, E.A.C., DeLoney-Marino, C.R., McFall-Ngai, M.J., and Ruby, E.G. (2012) Squid-derived chitin oligosaccharides are a chemotactic signal during colonization by *Vibrio fischeri*. *Appl Environ Microbiol* **78**: 4620–4626.
- Mandel, M.J., Wollenberg, M.S., Stabb, E.V., Visick, K.L., and Ruby, E.G. (2009) A single regulatory gene is sufficient to alter bacterial host range. *Nature* **458**: 215–218.
- Marfori, M., Mynott, A., Ellis, J.J., Mehdi, A.M., Saunders, N.F., Curmi, P.M., et al. (2011) Molecular basis for specificity of nuclear import and prediction of nuclear localization. *Biochim Biophys Acta BBA-Mol Cell Res* **1813**: 1562–1577.

- Martin, R.M., Ter-Avetisyan, G., Herce, H.D., Ludwig, A.K., Lättig-Tünnemann, G., and Cardoso, M.C. (2015) Principles of protein targeting to the nucleolus. *Nucleus* **6**: 314–325.
- Maxwell, S.E., and Delaney, H.D. (2004) *Designing experiments and analyzing data*. Mahwah, N.J: Lawrence Erlbaum Associates.
- McAnulty, S.J., and Nyholm, S.V. (2017) The role of hemocytes in the hawaiian bobtail squid, *Euprymna scolopes*: a model organism for studying beneficial host–microbe interactions. *Front Microbiol* **7**: 2013.
- McFall-Ngai, M. (2008) Are biologists in “future shock”? Symbiosis integrates biology across domains. *Nat Rev Microbiol* **6**: 789–792.
- McFall-Ngai, M., Hadfield, M.G., Bosch, T.C., Carey, H.V., Domazet-Lošo, T., Douglas, A.E., et al. (2013) Animals in a bacterial world, a new imperative for the life sciences. *Proc Natl Acad Sci* **110**: 3229–3236.
- McFall-Ngai, M., Heath-Heckman, E.A., Gillette, A.A., Peyer, S.M., and Harvie, E.A. (2012) The secret language of coevolved symbioses: Insights from the *Euprymna scolopes-Vibrio fischeri* symbiosis. *Semin Immunol* **24**: 3–8.
- McFall-Ngai, M., and Montgomery, M.K. (1990) The anatomy and morphology of the adult bacterial light organ of *Euprymna scolopes* Berry (Cephalopoda: Sepiolidae). *Biol Bull* **179**: 332–339.
- McFall-Ngai, M., Nyholm, S.V., and Castillo, M.G. (2010) The role of the immune system in the initiation and persistence of the *Euprymna scolopes-Vibrio fischeri* symbiosis. *Semin Immunol* **22**: 48–53.
- McFall-Ngai, M.J., and Ruby, E.G. (1991) Symbiont recognition and subsequent morphogenesis as early events in an animal-bacterial mutualism. *Science* **254**: 1491–1493.
- McFall-Ngai, M.J., and Ruby, E.G. (1998) Sepiolids and vibrios: when first they meet-reciprocal interactions between host and symbiont lead to the creation of a complex light-emitting organ. *Bioscience* **48**: 257–265.
- Medzhitov, R. (2007) Recognition of microorganisms and activation of the immune response. *Nature* **449**: 819–826.
- Meijer, A.J. (2003) Amino acids as regulators and components of nonproteinogenic pathways. *J Nutr* **133**: 2057S–2062S.
- Mellman, I., and Warren, G. (2000) The road taken: past and future foundations of membrane traffic. *Cell* **100**: 99–112.
- Meyer, E., and Manahan, D.T. (2009) Nutrient uptake by marine invertebrates: cloning and functional analysis of amino acid transporter genes in developing sea urchins (*Strongylocentrotus purpuratus*). *Biol Bull* **217**: 6–24.

- Millikan, D.S., and Ruby, E.G. (2002) Alterations in *Vibrio fischeri* motility correlate with a delay in symbiosis initiation and are associated with additional symbiotic colonization defects. *Appl Environ Microbiol* **68**: 2519–2528.
- Montgomery, M.K., and McFall-Ngai, M. (1993) Embryonic development of the light organ of the sepiolid squid *Euprymna scolopes* Berry. *Biol Bull* **184**: 296–308.
- Montgomery, M.K., and McFall-Ngai, M. (1994) Bacterial symbionts induce host organ morphogenesis during early postembryonic development of the squid *Euprymna scolopes*. *Development* **120**: 1719–1729.
- Munford, R., and Hunter, J.P. (1992) Acyloxyacyl hydrolase, a leukocyte enzyme that deacylates bacterial lipopolysaccharides, has phospholipase, lysophospholipase, diacylglycerollipase, and acyltransferase activities in vitro. *J Biol Chem* **267**: 10116–10121.
- Munford, R.S. (2008) Sensing gram-negative bacterial lipopolysaccharides: a human disease determinant? *Infect Immun* **76**: 454–465.
- Musat, N., Stryhanyuk, H., Bombach, P., Adrian, L., Audinot, J.-N., and Richnow, H.H. (2014) The effect of FISH and CARD-FISH on the isotopic composition of ¹³C- and ¹⁵N-labeled *Pseudomonas putida* cells measured by NanoSIMS. *Syst Appl Microbiol* **37**: 267–276.

- N -

- Nealson, K., and Hastings, J. (1991) The luminous bacteria. In A. Balows, H. G. Trüper, M. Dworkin, W. Harder, and K.-H. Schleifer (ed.), *The prokaryotes: a handbook for the biology of bacteria. Ecophysiology, isolation, identification, applications*, 2nd ed., vol. 1. Springer-Verlag, Berlin, Germany, p. 625–639.
- Neyen, C., Poidevin, M., Roussel, A., and Lemaitre, B. (2012) Tissue- and ligand-specific sensing of gram-negative infection in drosophila by PGRP-LC isoforms and PGRP-LE. *J Immunol* **189**: 1886–1897.
- Ng, W.-L., and Bassler, B.L. (2009) Bacterial quorum-sensing network architectures. *Annu Rev Genet* **43**: 197–222.
- Nikolakakis, K., Lehnert, E., McFall-Ngai, M., and Ruby, E. (2015) Use of hybridization chain reaction-fluorescent in situ hybridization to track gene expression by both partners during initiation of symbiosis. *Appl Environ Microbiol* **81**: 4728–4735.
- Nyholm, S.V., Deplancke, B., Gaskins, H.R., Apicella, M.A., and McFall-Ngai, M.J. (2002) Roles of *Vibrio fischeri* and nonsymbiotic bacteria in the dynamics of mucus secretion during symbiont colonization of the *Euprymna scolopes* light organ. *Appl Environ Microbiol* **68**: 5113–5122.
- Nyholm, S.V., and Graf, J. (2012) Knowing your friends: invertebrate innate immunity fosters beneficial bacterial symbioses. *Nat Rev Microbiol* **10**: 815–827.

Nyholm, S.V., and McFall-Ngai, M.J. (1998) Sampling the light-organ microenvironment of *Euprymna scolopes*: description of a population of host cells in association with the bacterial symbiont *Vibrio fischeri*. *Biol Bull* **195**: 89–97.

Nyholm, S.V., and McFall-Ngai, M.J. (2003) Dominance of *Vibrio fischeri* in secreted mucus outside the light organ of *Euprymna scolopes*: The first site of symbiont specificity. *Appl Environ Microbiol* **69**: 3932–3937.

Nyholm, S.V., and McFall-Ngai, M.J. (2004) The winnowing: establishing the squid-Vibrio symbiosis. *Nat Rev Microbiol* **2**: 632–642.

Nyholm, S.V., Stabb, E.V., Ruby, E.G., and McFall-Ngai, M.J. (2000) Establishment of an animal-bacterial association: recruiting symbiotic vibrios from the environment. *Proc Natl Acad Sci U S A* **97**: 10231–10235.

Nyholm, S.V., Stewart, J.J., Ruby, E.G., and McFall-Ngai, M.J. (2009) Recognition between symbiotic *Vibrio fischeri* and the haemocytes of *Euprymna scolopes*. *Environ Microbiol* **11**: 483–493.

- O -

O'Dell, S.J., and Stephens, G.C. (1986) Uptake of amino acids by *Pareurythoe californica*: substrate interaction modifies net influx from the environment. *Biol Bull* **171**: 682–693.

O'Donoghue, E.J., and Krachler, A.M. (2016) Mechanisms of outer membrane vesicle entry into host cells. *Cell Microbiol* **18**: 1508–1517.

Olricks, N.K., Aarsman, M.E., Verheul, J., Arnusch, C.J., Martin, N.I., Hervé, M., et al. (2011) A novel in vivo cell-wall labeling approach sheds new light on peptidoglycan synthesis in *Escherichia coli*. *ChemBioChem* **12**: 1124–1133.

Olson, M. (2004) Sensing cellular stress: another new function for the nucleolus. *Sci Signal* **2004**: pe10.

Orench-Rivera, N., and Kuehn, M.J. (2016) Environmentally controlled bacterial vesicle-mediated export. *Cell Microbiol* **18**: 1525–1536.

Ou, D., Li, D., Cao, Y., Li, X., Yin, J., Qiao, S., and Wu, G. (2007) Dietary supplementation with zinc oxide decreases expression of the stem cell factor in the small intestine of weanling pigs. *J Nutr Biochem* **18**: 820–826.

- P -

Pabst, M.J., Beranova-Giorgianni, S., and Krueger, J.M. (1999) Effects of muramyl peptides on macrophages, monokines, and sleep. *Neuroimmunomodulation* **6**: 261–283.

- Paine, P.L., Moore, L.C., and Horowitz, S.B. (1975) Nuclear envelope permeability. *Nature* **254**: 109–114.
- Parker, H., Chitcholtan, K., Hampton, M.B., and Keenan, J.I. (2010) Uptake of *Helicobacter pylori* outer membrane vesicles by gastric epithelial cells. *Infect Immun* **78**: 5054–5061.
- Pederson, T., and Tsai, R.Y. (2009) In search of nonribosomal nucleolar protein function and regulation. *J Cell Biol* **184**: 771–776.
- Phair, R.D., and Misteli, T. (2000) High mobility of proteins in the mammalian cell nucleus. *Nature* **404**: 604–609.
- Phillips, N.J., Adin, D.M., Stabb, E.V., McFall-Ngai, M.J., Apicella, M.A., and Gibson, B.W. (2011) The lipid A from *Vibrio fischeri* lipopolysaccharide a unique structure bearing a phosphoglycerol moiety. *J Biol Chem* **286**: 21203–21219.
- Pizarro-Cerdá, J., and Cossart, P. (2006) Bacterial adhesion and entry into host cells. *Cell* **124**: 715–727.
- Pollak, C.N., Delpino, M.V., Fossati, C.A., and Baldi, P.C. (2012) Outer membrane vesicles from *Brucella abortus* promote bacterial internalization by human monocytes and modulate their innate immune response. *PLoS ONE* **7**: e50214.
- Post, D.M.B., Yu, L., Krasity, B.C., Choudhury, B., Mandel, M.J., Brennan, C.A., et al. (2012) O-antigen and core carbohydrate of *Vibrio fischeri* lipopolysaccharide: composition and analysis of their role in *Euprymna scolopes* light organ colonization. *J Biol Chem* **287**: 8515–8530.
- Psort, I. (1997) PSORT: a program for detecting sorting signals in proteins and predicting their subcellular localization. *J Mol Biol* **266**: 594–600.
- Puckett, C.A., and Barton, J.K. (2009) Fluorescein redirects a ruthenium-octaarginine conjugate to the nucleus. *J Am Chem Soc* **131**: 8738.
- Pütter, A. (1909) *Die Ernährung der Wassertiere und der Stoffhaushalt der Gewässer*. Verlag von Gustav Fischer in Jena.

- R -

- Rakowska, P.D., Jiang, H., Ray, S., Pyne, A., Lamarre, B., Carr, M., et al. (2013) Nanoscale imaging reveals laterally expanding antimicrobial pores in lipid bilayers. *Proc Natl Acad Sci* **110**: 8918–8923.
- Rath, C.M., and Dorrestein, P.C. (2012) The bacterial chemical repertoire mediates metabolic exchange within gut microbiomes. *Curr Opin Microbiol* **15**: 147–154.
- Relman, D.A. (2008) “Til death do us part”: coming to terms with symbiotic relationships. *Nat Rev Microbiol* **6**: 721–724.

- Rice, P., Longden, I., and Bleasby, A. (2000) EMBOSS: the European molecular biology open software suite. *Trends Genet* **16**: 276-277.
- Roberts, B.L., Richardson, W.D., and Smith, A.E. (1987) The effect of protein context on nuclear location signal function. *Cell* **50**: 465-475.
- Rompikuntal, P.K., Thay, B., Khan, M.K., Alanko, J., Penttinen, A.-M., Asikainen, S., et al. (2012) Perinuclear localization of internalized outer membrane vesicles carrying active cytolethal distending toxin from *Aggregatibacter actinomycetemcomitans*. *Infect Immun* **80**: 31-42.
- Rosenthal, R.S., Nogami, W., Cookson, B.T., Goldman, W.E., and Folkening, W.J. (1987) Major fragment of soluble peptidoglycan released from growing *Bordetella pertussis* in tracheal cytotoxin. *Infect Immun* **55**: 2117-2120.
- Royet, J., Gupta, D., and Dziarski, R. (2011) Peptidoglycan recognition proteins: modulators of the microbiome and inflammation. *Nat Rev Immunol* **11**: 837-851.
- Ruby, E.G., and Asato, L.M. (1993) Growth and flagellation of *Vibrio fischeri* during initiation of the sepiolid squid light organ symbiosis. *Arch Microbiol* **159**: 160-167.
- Ruby, E.G., and McFall-Ngai, M.J. (1999) Oxygen-utilizing reactions and symbiotic colonization of the squid light organ by *Vibrio fischeri*. *Trends Microbiol* **7**: 414-420.
- Ruby, E.G., and Nealson, K.H. (1977) Pyruvate production and excretion by luminous marine-bacteria. *Appl Environ Microbiol* **34**: 164-169.
- Ruby, E.G., Urbanowski, M., Campbell, J., Dunn, A., Faini, M., Gunsalus, R., et al. (2005) Complete genome sequence of *Vibrio fischeri*: a symbiotic bacterium with pathogenic congeners. *Proc Natl Acad Sci U S A* **102**: 3004-3009.

- S -

- Sander, L.E., Davis, M.J., Boekschoten, M.V., Amsen, D., Dascher, C.C., Ryffel, B., et al. (2011) Detection of prokaryotic mRNA signifies microbial viability and promotes immunity. *Nature* **474**: 385-389.
- Sandvig, K., and Deurs, B. van (2005) Delivery into cells: lessons learned from plant and bacterial toxins. *Gene Ther* **12**: 865-872.
- Schleicher, T.R., and Nyholm, S.V. (2011) Characterizing the host and symbiont proteomes in the association between the Bobtail squid, *Euprymna scolopes*, and the bacterium, *Vibrio fischeri*. *PLoS ONE* **6**: e25649.

- Schleicher, T.R., VerBerkmoes, N.C., Shah, M., and Nyholm, S.V. (2014) Colonization state influences the hemocyte proteome in a beneficial squid–vibrio symbiosis. *Mol Cell Proteomics* **13**: 2673–2686.
- Schlichter, D., and Liebezeit, G. (1991) The natural release of amino acids from the symbiotic coral *Heteroxenia fuscescens* (Ehrb.) as a function of photosynthesis. *J Exp Mar Biol Ecol* **150**: 83–90.
- Schubert, U., Anton, L.C., Gibbs, J., Norbury, C.C., Yewdell, J.W., and Bennink, J.R. (2000) Rapid degradation of a large fraction of newly synthesized proteins by proteasomes. *Nature* **404**: 770–774.
- Schwartzman, J.A., Koch, E., Heath-Heckman, E.A., Zhou, L., Kremer, N., McFall-Ngai, M.J., and Ruby, E.G. (2015) The chemistry of negotiation: rhythmic, glycan-driven acidification in a symbiotic conversation. *Proc Natl Acad Sci* **112**: 566–571.
- Schwartzman, J.A., and Ruby, E.G. (2016) A conserved chemical dialog of mutualism: lessons from squid and vibrio. *Microbes Infect* **18**: 1–10.
- Schwechheimer, C., and Kuehn, M.J. (2015) Outer-membrane vesicles from Gram-negative bacteria: biogenesis and functions. *Nat Rev Microbiol* **13**: 605–619.
- Schwechheimer, C., Sullivan, C.J., and Kuehn, M.J. (2013) Envelope control of outer membrane vesicle production in Gram-negative bacteria. *Biochemistry (Mosc)* **52**: 3031.
- Scott, M.S., Boisvert, F.-M., McDowall, M.D., Lamond, A.I., and Barton, G.J. (2010) Characterization and prediction of protein nucleolar localization sequences. *Nucleic Acids Res* **38**: 7388–7399.
- Senyo, S.E., Steinhauser, M.L., Pizzimenti, C.L., Yang, V.K., Cai, L., Wang, M., et al. (2013) Mammalian heart renewal by pre-existing cardiomyocytes. *Nature* **493**: 433–436.
- Shames, S.R., Bhavsar, A.P., Croxen, M.A., Law, R.J., Mak, S.H., Deng, W., et al. (2011) The pathogenic *Escherichia coli* type III secreted protease NleC degrades the host acetyltransferase p300. *Cell Microbiol* **13**: 1542–1557.
- Sharon, G., Garg, N., Debelius, J., Knight, R., Dorrestein, P.C., and Mazmanian, S.K. (2014) Specialized metabolites from the microbiome in health and disease. *Cell Metab* **20**: 719–730.
- Shen, Y., Torchia, M.L.G., Lawson, G.W., Karp, C.L., Ashwell, J.D., and Mazmanian, S.K. (2012) Outer membrane vesicles of a human commensal mediate immune regulation and disease protection. *Cell Host Microbe* **12**: 509–520.
- Shibata, S., and Visick, K.L. (2012) Sensor kinase RscS induces the production of antigenically distinct outer membrane vesicles that depend on the symbiosis polysaccharide locus in *Vibrio fischeri*. *J Bacteriol* **194**: 185–194.

- Shick, J.M. (1975) Uptake and utilization of dissolved glycine by *Aurelia aurita* scyphistomae: temperature effects on the uptake process; nutritional role of dissolved amino acids. *Biol Bull* **148**: 117–140.
- Shimizu, N., and Hart, S. (1982) Isotope fractionation in secondary ion mass spectrometry. *J Appl Phys* **53**: 1303–1311.
- Shoberg, R.J., and Thomas, D.D. (1993) Specific adherence of *Borrelia burgdorferi* extracellular vesicles to human endothelial cells in culture. *Infect Immun* **61**: 3892–3900.
- Singley, C. (1982) Histochemistry and fine-structure of the ectodermal epithelium of the sepiolid squid *Euprymna scolopes*. *Malacologia* **23**: 177–192.
- Sinha, R.K., and Rosenthal, R.S. (1980) Release of soluble peptidoglycan from growing gonococci: demonstration of anhydro-muramyl- containing fragments. *Infect Immun* **29**: 914–925.
- Small, A.L., and McFall-Ngai, M.J. (1999) Halide peroxidase in tissues that interact with bacteria in the host squid *Euprymna scolopes*. *J Cell Biochem* **72**: 445–457.
- Sperandio, V., Giron, J.A., Silveira, W.D., and Kaper, J.B. (1995) The OmpU outer membrane protein, a potential adherence factor of *Vibrio cholerae*. *Infect Immun* **63**: 4433–4438.
- Sperandio, V., Torres, A.G., Jarvis, B., Nataro, J.P., and Kaper, J.B. (2003) Bacteria–host communication: the language of hormones. *Proc Natl Acad Sci* **100**: 8951–8956.
- Stabb, E.V., and Visick, K.L. (2014) *Chapter 20 – Vibrio fischeri: a bioluminescent light organ symbiont of the bobtail squid Euprymna scolopes*. 4th ed., Springer-Verlag, Berlin.
- Stephens, G.C. (1988) Epidermal amino acid transport in marine invertebrates. *Biochim Biophys Acta BBA-Rev Biomembr* **947**: 113–138.
- Stern, R.A., Fletcher, I.R., Rasmussen, B., McNaughton, N.J., and Griffin, B.J. (2005) Ion microprobe (NanoSIMS 50) Pb-isotope geochronology at < 5 μm scale. *Int J Mass Spectrom* **244**: 125–134.
- Strahl, B.D., and Allis, C.D. (2000) The language of covalent histone modifications. *Nature* **403**: 41–45.
- Sycuro, L.K., Ruby, E.G., and McFall-Ngai, M. (2006) Confocal microscopy of the light organ crypts in juvenile *Euprymna scolopes* reveals their morphological complexity and dynamic function in symbiosis. *J Morphol* **267**: 555–568.

- T -

- Talcott, B., and Moore, M.S. (1999) Getting across the nuclear pore complex. *Trends Cell Biol* **9**: 312–318.

- Thay, B., Damm, A., Kufer, T.A., Wai, S.N., and Oscarsson, J. (2014) *Aggregatibacter actinomycetemcomitans* outer membrane vesicles are internalized in human host cells and trigger NOD1- and NOD2-dependent NF- κ B activation. *Infect Immun* **82**: 4034–4046.
- Thieblemont, N., and Wright, S.D. (1999) Transport of bacterial lipopolysaccharide to the Golgi apparatus. *J Exp Med* **190**: 523–534.
- Thompson, R., and Bayne, B. (1972) Active metabolism associated with feeding in the mussel *Mytilus edulis* L. *J Exp Mar Biol Ecol* **9**: 111–124.
- Thomson, C.W. (1874) The depths of the sea. an account of the general results of the dredging cruises of H.M. SS. 'Porcupine' and 'Lightning' during the summers of 1868, 1869 and 1870, under the scientific direction of Dr. Carpenter, J. Gwyn Jeffreys, and Dr. Wyville Thomson. Macmillian and Co., London.
- Thorson, G. (1946) Reproductive and larval development of Danish marine bottom invertebrates, with special reference to planktonic larvae in the Sound (Oresund). Danmarks fiskeri havundersogelser, Ser. Plankton.
- Tremethick, D.J. (2007) Higher-order structures of chromatin: the elusive 30 nm fiber. *Cell* **128**: 651–654.
- Troll, J.V., Adin, D.M., Wier, A.M., Paquette, N., Silverman, N., Goldman, W.E., et al. (2009) Peptidoglycan induces loss of a nuclear peptidoglycan recognition protein during host tissue development in a beneficial animal-bacterial symbiosis. *Cell Microbiol* **11**: 1114–1127.
- Troll, J.V., Bent, E.H., Paquette, N., Wier, A.M., Goldman, W.E., Silverman, N., and McFall-Ngai, M.J. (2010) Taming the symbiont for coexistence: a host PGRP neutralizes a bacterial symbiont toxin. *Environ Microbiol* **12**: 2190–2203.
- Tseng, T.-T., Tyler, B.M., and Setubal, J.C. (2009) Protein secretion systems in bacterial-host associations, and their description in the Gene Ontology. *BMC Microbiol* **9**: S2.

- V -

- Valle, N., Drillet, J., Pic, A., and Migeon, H. (2011) Nano-SIMS investigation of boron distribution in steels. *Surf Interface Anal* **43**: 573–575.
- Vanaja, S.K., Russo, A.J., Behl, B., Banerjee, I., Yankova, M., Deshmukh, S.D., and Rathinam, V.A. (2016) Bacterial outer membrane vesicles mediate cytosolic localization of LPS and caspase-11 activation. *Cell* **165**: 1106–1119.
- Vance, R.E., Isberg, R.R., and Portnoy, D.A. (2009) Patterns of pathogenesis: discrimination of pathogenic and nonpathogenic microbes by the innate immune system. *Cell Host Microbe* **6**: 10–21.

Vautier, D., Chesné, P., Cunha, C., Calado, A., Renard, J.-P., and Carmo-Fonseca, M. (2001) Transcription-dependent nucleocytoplasmic distribution of hnRNP A1 protein in early mouse embryos. *J Cell Sci* **114**: 1521–1531.

Vázquez-Martínez, R., Díaz-Ruiz, A., Almabouada, F., Rabanal-Ruiz, Y., Gracia-Navarro, F., and Malagón, M.M. (2012) Revisiting the regulated secretory pathway: from frogs to human. *Gen Comp Endocrinol* **175**: 1–9.

Viala, J., Chaput, C., Boneca, I.G., Cardona, A., Girardin, S.E., Moran, A.P., et al. (2004) Nod1 responds to peptidoglycan delivered by the *Helicobacter pylori* cag pathogenicity island. *Nat Immunol* **5**: 1166–1174.

Visick, K.L., Foster, J., Doino, J., McFall-Ngai, M., and Ruby, E.G. (2000) *Vibrio fischeri* lux genes play an important role in colonization and development of the host light organ. *J Bacteriol* **182**: 4578–4586.

- W -

Wacey, D., Saunders, M., Brasier, M.D., and Kilburn, M.R. (2011) Earliest microbially mediated pyrite oxidation in ~3.4 billion-year-old sediments. *Earth Planet Sci Lett* **301**: 393–402.

Wai, S.N., Lindmark, B., Söderblom, T., Takade, A., Westermark, M., Oscarsson, J., et al. (2003) Vesicle-mediated export and assembly of pore-forming oligomers of the enterobacterial ClyA cytotoxin. *Cell* **115**: 25–35.

Wang, D.-Z., Kong, L.-F., Li, Y.-Y., and Xie, Z.-X. (2016) Environmental microbial community proteomics: status, challenges and perspectives. *Int J Mol Sci* **17**: 1275.

Wang, Y., Dufour, Y.S., Carlson, H.K., Donohue, T.J., Marletta, M.A., and Ruby, E.G. (2010) H-NOX-mediated nitric oxide sensing modulates symbiotic colonization by *Vibrio fischeri*. *Proc Natl Acad Sci* **107**: 8375–8380.

Wei, L., Yu, Y., Shen, Y., Wang, M.C., and Min, W. (2013) Vibrational imaging of newly synthesized proteins in live cells by stimulated Raman scattering microscopy. *Proc Natl Acad Sci* **110**: 11226–11231.

Weinrauch, Y., Katz, S.S., Munford, R.S., Elsbach, P., and Weiss, J. (1999) Deacylation of purified lipopolysaccharides by cellular and extracellular components of a sterile rabbit peritoneal inflammatory exudate. *Infect Immun* **67**: 3376–3382.

Wells, J.M., Loonen, L.M., and Karczewski, J.M. (2010) The role of innate signaling in the homeostasis of tolerance and immunity in the intestine. *Int J Med Microbiol* **300**: 41–48.

Wernick, N.L., Chinnapen, D.J.-F., Cho, J.A., and Lencer, W.I. (2010) Cholera toxin: an intracellular journey into the cytosol by way of the endoplasmic reticulum. *Toxins* **2**: 310–325.

Whitaker, W.B., Parent, M.A., Boyd, A., Richards, G.P., and Boyd, E.F. (2012) The *Vibrio parahaemolyticus* ToxRS regulator is required for stress tolerance and colonization in a novel orogastric streptomycin-induced adult murine model. *Infect Immun* **80**: 1834–1845.

Wier, A.M., Nyholm, S.V., Mandel, M.J., Massengo-Tiasse, R.P., Schaefer, A.L., Koroleva, I., et al. (2010) Transcriptional patterns in both host and bacterium underlie a daily rhythm of anatomical and metabolic change in a beneficial symbiosis. *Proc Natl Acad Sci U S A* **107**: 2259–2264.

Wobken, D., Burow, L.C., Behnam, F., Mayali, X., Schintlmeister, A., Fleming, E.D., et al. (2015) Revisiting N₂ fixation in Guerrero Negro intertidal microbial mats with a functional single-cell approach. *ISME J* **9**: 485–496.

Wright, S.H., and Manahan, D.T. (1989) Integumental nutrient uptake by aquatic organisms. *Annu Rev Physiol* **51**: 585–600.

Wu, G. (2009) Amino acids: metabolism, functions, and nutrition. *Amino Acids* **37**: 1–17.

- X -

Xu, D., Farmer, A., and Chook, Y.M. (2010) Recognition of nuclear targeting signals by Karyopherin- β proteins. *Curr Opin Struct Biol* **20**: 782–790.

- Y -

Yip, E.S., Geszvain, K., DeLoney-Marino, C.R., and Visick, K.L. (2006) The symbiosis regulator RscS controls the *syp* gene locus, biofilm formation and symbiotic aggregation by *Vibrio fischeri*. *Mol Microbiol* **62**: 1586–1600.

- Z -

Zargar, A., Quan, D.N., Carter, K.K., Guo, M., Sintim, H.O., Payne, G.F., and Bentley, W.E. (2015) Bacterial secretions of nonpathogenic *Escherichia coli* elicit inflammatory pathways: a closer investigation of interkingdom signaling. *MBio* **6**: e00025-15.

Zhang, D.-S., Piazza, V., Perrin, B.J., Rzdzinska, A.K., Poczatek, J.C., Wang, M., et al. (2012) Multi-isotope imaging mass spectrometry reveals slow protein turnover in hair-cell stereocilia. *Nature* **481**: 520–524.

Zhou, J., Sharp, L.L., Tang, H.L., Lloyd, S.A., Billings, S., Braun, T.F., and Blair, D.F. (1998) Function of protonatable residues in the flagellar motor of *Escherichia coli*: a critical role for Asp 32 of MotB. *J Bacteriol* **180**: 2729–2735.

References

Zimmermann, M., Escrig, S., Hübschmann, T., Kirf, M.K., Brand, A., Inglis, R.F., et al. (2015) Phenotypic heterogeneity in metabolic traits among single cells of a rare bacterial species in its natural environment quantified with a combination of flow cell sorting and NanoSIMS. *Front Microbiol* **6**: 243.

Zimmermann, S., Wagner, C., Müller, W., Brenner-Weiss, G., Hug, F., Prior, B., et al. (2006) Induction of neutrophil chemotaxis by the quorum-sensing molecule N-(3-oxododecanoyl)-L-homoserine lactone. *Infect Immun* **74**: 5687–5692.

Epilogue

An experiment to examine potential carry-over effects from the washing of the bacteria cells grown in ^{15}N -labeled Celtone medium was carried out. Across all bacterial experiments presented in this thesis work, cells from the last sub-culture were washed twice in filtered seawater (FSW; $0.2\ \mu\text{m}$ Millipore membrane) by centrifugation (2 min, 8000 rpm), before inoculating the squids. Carry-over may have occurred if some leftover labeled medium remained in the washing tubes and would have been transferred into the seawater used to inoculate the squid with the bacteria cells. In turn, this carry-over could have induced ^{15}N -enrichment inside the squid cells in addition to the enrichment induced by the bacteria cells. To determine the degree of ^{15}N -enrichment inside squid cells due to such potential carry-over, levels of ^{15}N were compared between juvenile squids that were inoculated with either non-labeled or ^{15}N -labeled *V. fischeri* cells (Fig. 1).

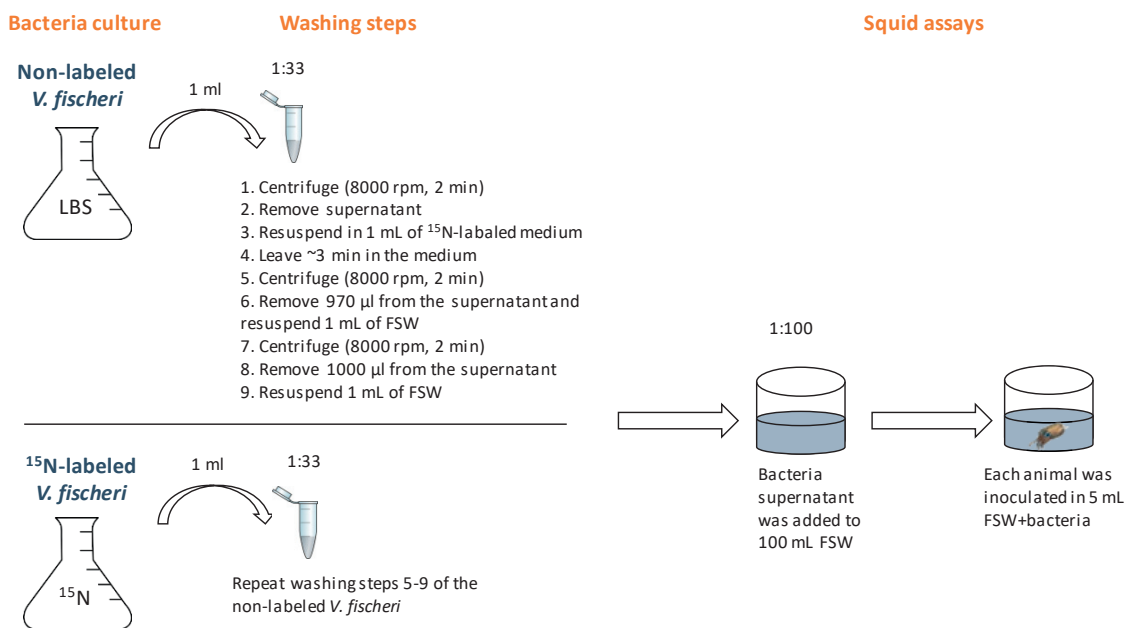


Fig. 1. Experimental design

Non-labeled *V. fischeri* cells were grown on LBS (LB medium containing 2% [wt/vol] NaCl; Graf et al. 1994). Bacteria cells (1 mL containing 108 CFU) were then transferred to 1.5 mL tubes, centrifuged (2 min, 8000 rpm) and the pellet was re-suspended in 1 mL of ^{15}N -labeled Celtone medium. The re-suspended bacteria were left for 3 mins in the labeled medium before they were washed twice in 1 mL FSW by centrifugation (Fig. 1, step 4). The motivation for leaving bacteria cells in suspension was that they might absorb compounds from the labeled medium to their cell surface, which could contribute to

the carry-over effect(s). Because it was not possible to estimate how much medium was left between each washing step in the experiments presented in this thesis work, the ‘carry over’ effect of leaving 30 μL (1:33 dilution) labeled medium in the 1.5 mL tubes was investigated (Fig. 1, step 6). Following the second wash, bacteria cells were resuspended and diluted in 100 mL of FSW (1:100 dilution), the seawater used for the squid assays. Control samples included *V. fischeri* cells (in the same concentration as used for non-labeled cells) that were grown in ^{15}N -labeled Celtone medium and subsequently washed following the same procedure as the non-labeled *V. fischeri* cells (Fig. 1). Juvenile *E. scolopes* were inoculated with either ^{15}N -labeled *V. fischeri* cells or non-labeled cells, in 5 mL FSW for 3.5 h. At the end of the incubation, animals were fixed and prepared for stable isotopes imaging in the NanoSIMS according to the protocol described in ‘General procedure for NanoSIMS analysis’. NanoSIMS analysis was performed only on the light-organ appendages.

Results of ^{15}N -enrichment are presented in Table 1. The assumption was that if ^{15}N -enrichment patterns were observed in the squids exposed to non-labeled bacteria due to carry-over, such enrichment was predicted to be similar to the patterns induced in squid exposed to Celtone medium (the amino acids experiment described in Chapter 1). However, due to the much lower concentration of Celtone medium in the current experiment, levels of ^{15}N -enrichment were anticipated to be correspondingly low, if detectable.

In both treatments, no ^{15}N -enrichment was detected in the cell cytoplasm, therefore, percentage enrichment was compared only for the nuclei and nucleoli. Based on this experiment it is concluded that a maximum of 16% and 11% of the enrichment that was observed inside the nuclei and nucleoli, respectively, in squids exposed to ^{15}N -labeled *V. fischeri* can be attributed to a carry-over of ^{15}N -enriched growth medium

Table 1. ^{15}N -enrichment values of squids inoculated with either ^{15}N -labeled *V. fischeri* or non-labeled *V. fischeri* for 3.5 h (3 animals). Note that all nucleoli in squid exposed to ^{15}N -labeled *V. fischeri* were significantly labeled (> 3 sigma above the natural $^{15}\text{N}/^{14}\text{N}$ ratio) whereas in squid exposed to non-labeled *V. fischeri*, only 46% (n=10) were labeled.

Variables		N	Mean (%)	SD (%)
Treatment	Cell organelle			
^{15}N - <i>V. fischeri</i>	Cytoplasm	36	-1.7	16
	Nucleus	86	44	20
	Nucleolus	20	527	183
Non-labeled <i>V. fischeri</i>	Cytoplasm	33	5.9	12
	Nucleus	77	8	16
	Nucleolus	22	61	46

Curriculum Vitae

Stephanie Cohen

+41-78-6235403– stephanie.cohen@epfl.ch

Date of birth: October 22, 1978

Place of birth: Sweden

Nationality: French and Israeli

EDUCATION

- | | |
|-----------------------|---|
| 2012 – present | PhD candidate
“Visualizing chemical transport from extracellular symbionts into squid host tissues using NanoSIMS”
ENAC, EPFL, Switzerland. Collaborations with University of Wisconsin, Madison (2013-2015) and University of Hawaii (2016-2017).
Thesis Director: Prof. Anders Meibom
Thesis Co-Director: Prof. Margaret McFall-Ngai |
| 2007-2011 | MSc
“Coral calcification under reduced pH conditions”
Faculty of life science, Bar-Ilan University and The Interuniversity Institute for Marine Sciences in Eilat.
Supervisor: Prof. Maoz Fine
With distinction, <i>Magna Cum Laude</i> |
| 2003-2006 | BSc
Marine Sciences
School of Marine Sciences and Marine Environment, Ruppin Academic Center.
With distinction, <i>Magna Cum Laude</i> |

MILITARY SERVICE

- | | |
|------------------|---|
| 1999-2001 | Lieutenant of IT. Led a team of soldiers that were responsible for technical support and users' guidance. |
| 1997-1998 | Computer operator. |

AWARDS AND HONORS

- | | |
|------------------|---|
| 2005 | Mobility Award, to encourage PhDs students to go for an academic visit to an external research institution. Doctoral program in Civil and Environmental Engineering (EDCE), EPFL, Lausanne, Switzerland |
| 2012 | Travelling fellowships for 3 months research in Paris, France. The French scientific office for cooperation –Israel, Embassy of France, Israel. |
| 2011 | "Chen Efrat" scholarship for excellence as a teaching assistance. The Interuniversity Institute for Marine Sciences in Eilat. |
| 2007-2008 | Keren Kayemeth LeIsrael – Jewish National Fund Scholarships. |

PROFESSIONAL EXPERIENCE

Research experience

- 2012** Three months internship on methods for establishing primary cultures of scleractinian coral cells. The Museum National d'Histoire Naturelle in Paris, France. Supervisor: Dr. Isabel Domart-Coulon and Dr. Maoz Fine.
- 2011-2012** Establishing primary culture of scleractinian coral cells. Faculty of life science, Bar-Ilan University and The Interuniversity Institute for Marine Sciences in Eilat. Supervisor: Dr. Maoz Fine.
- 2006-2007** Research assistant and laboratory technician. Focus: coral reefs ecology and molecular approach studying mollusk population dynamics. Employer: Prof. Avigdor Abelson at Tel-Aviv University.

Teaching experience

- 2013-2016** Teaching assistant for "Environmental monitoring laboratory". ENAC, EPFL.
- 2010** Teaching assistant for "Ecosystem of the Mediterranean Sea". The Marine Sciences and Marine Environment, Ruppin Academic Center.
- 2007-2012** Teaching assistant for "Biogeochemistry of coral reefs", "Marine photosynthesis", "Corals biology" (twice), "The nano-injections system of Cnidaria" (twice) and "Marine venoms and defense systems". The Interuniversity Institute for Marine Sciences in Eilat.
- 2003-2012** Tutor for students from premier and high schools on different subjects in the marine biology field at the Interuniversity Institute for Marine Sciences in Eilat.
- 2007-2009** Teaching assistant for "Biological aspects of the Red Sea" (twice), "Advanced laboratory" and "Ecological aspects of the Mediterranean Sea". Bar-Ilan University.

PUBLICATIONS

Cohen S, Kruger T and Fine M. Gross and Net calcification of *Stylophora pistillata* under OA conditions-methodological approach. (*submitted*)

Fine M, Tsadok R, Meron D, **Cohen S** and Milazzo M. 2016. Environmental sensitivity of *Neogoniolithon brassica-florida* associated with vermetid reefs in the Mediterranean Sea. ICES Journal of Marine Science: Journal du Conseil. p. 167

Lecoite A, **Cohen S**, Geze M, Djediat C, Meibom A and Domart-Coulon I. 2013. Scleractinian coral cell proliferation is reduced in primary culture of suspended multicellular aggregates compared to polyps. Cytotechnology 65 (5): 705-724.

Hoppe P, **Cohen S** and Meibom A. 2013. NanoSIMS: Technical Aspects and Applications in Cosmochemistry and Biological Geochemistry. Geostandards and Geoanalytical research 37 (2): 111-154.

Mass T, Kline D I, Roopin M, Veal C J, **Cohen S**, Iluz D and Levy O. 2010. The spectral quality of light is a key driver of photosynthesis and photoadaptation in *Stylophora pistillata* colonies from different depths. Journal of Experimental Biology 213: 4084-4091.

PRESENTATIONS

- 2016** 'My Thesis in 3 min' contest, finalist, EPFL, Switzerland
- 2016** 6th ASM Conference on Beneficial Microbes, poster presentation, "Visualizing chemical transport from extracellular symbionts into squid host tissues using NanoSIMS"

- 2016** International Coral Reef Symposium (ICRS), oral presentation “Visualizing chemical transport from extracellular symbionts into squid host tissues using NanoSIMS”
- 2016** Seminar at Assaf Vardi’s lab, Department of Plant and Environmental Sciences, Weizman Institute of Science, Israel
- 2015** Seminar at the Kewalo marine lab, University of Hawaii, US.
- 2014** GHI seminar, SV, EPFL, Lausanne, Switzerland.
- 2011** Seminar at the Interuniversity Institute for Marine Sciences of Eilat, Israel.

QUALIFICATIONS

Diving certificates – Dive master, nitrox and rescue diver
Skipper license (30)
First Aid

LANGUAGES

Hebrew (mother tongue), English (fluent), French (moderate)

"The end of one journey,

the beginning of another..."

